Refining the estimates of subsurface nitrate attenuation in New Zealand agricultural landscapes

A thesis presented in partial fulfilment of the requirements for the degree of

Doctor of Philosophy

in

Soil Science

at Massey University, Palmerston North, New Zealand

TE KUNENGA KI PŪREHUROA | MASSEY UNIVERSITY

UNIVERSITY OF NEW ZEALAND

Stephen Brian Collins

2025

Abstract

Nutrient losses from intensive land use are degrading freshwater quality in agricultural catchments. A robust understanding of nutrient sources, pathways and their potential attenuation is needed to design effective water quality mitigation measures. However, estimates of subsurface nitrate attenuation dynamics have typically relied on sub-catchment-scale mass balance investigations, inferred from the difference between the observed (attenuated) river nitrogen loads and the estimated (unattenuated) root zone nitrogen losses from different land use typologies in a catchment. These nitrogen mass balance calculations yield the nitrogen attenuation factor (AF_N), representing the proportion of nitrogen removed during transport processes from the root zone to receiving waters, with estimates often ranging from 0.1 to 0.9 at sub-catchment scales. While the mass balance approach highlights spatial variability in subsurface nitrate attenuation capacities at sub-catchment scale, it obscures modelling and mapping of finer-scale variability of subsurface nitrate attenuation dynamics within a sub-catchment and catchment.

This study developed the Landscape Subsurface Nitrate-Attenuation Index (*LSNAI*), a novel approach for modelling and mapping spatially variable subsurface nitrate attenuation capacity at landscape unit scale across the Horizons region. The *LSNAI* refines AF_N estimation from sub-catchments to landscape units, a more realistic scale for representing subsurface nitrate attenuation in agricultural landscapes. The study compiled and analysed a national data set for assessment of spatial and temporal variability of groundwater redox conditions across New Zealand landscapes, and an XGBoost machine learning model was trained to predict subsurface redox probabilities for each landscape unit in the Horizons region. The subsurface redox probability predictions, combined with the rock type and soil drainage information, were classified into five *LSNAI* categories (from *Very low* to *Very high*) representing subsurface nitrate attenuation of different landscape units across the region. This *LSNAI* classification was validated with a data set of independent groundwater redox and denitrification measurements in shallow groundwater, and with continuous soil redox probe measurements in a hill country farm, which confirmed that the *LSNAI* classification reflected the observed spatial variability in subsurface redox conditions in the study area.

The *LSNAI* categories were then integrated into sub-catchment scale nitrogen export coefficient modelling (ECM) to parameterise the *LSANI's* five categories into a set of calibrated values of AF_N for the Horizons region's ~11,000 landscape units. The sub-catchment scale ECM modelling accounted for the root zone nitrogen losses from different land use typologies, any point-source (wastewater) nitrogen discharges, and estimates of river instream nitrogen uptake/attenuation in the study region. The initially assigned AF_N for the *LSANI's* categories (from *Very low* to *Very high*) were calibrated by comparing the predicted with the observed average annual loads of soluble inorganic nitrogen (*SIN*) at 38 river monitoring sites. The calibrated AF_N values successfully predicted average annual river *SIN* loads in larger sub-catchments (> 500 t *SIN* yr^{-1}), although the errors between the observed and predicted the average annual river *SIN* loads were higher in smaller sub-catchments (< 500 t *SIN* yr^{-1}). The ECM modelling performance improved slightly when the AF_N values were calibrated for individual catchments, as compared to the whole region. Further research is recommended to improve calibration of AF_N for the *LSANI's* categories in the study region and other similar catchments.

Compared with traditional nitrogen mass balance approaches, the *LSNAI* provided a more consistent framework that better captured underlying spatial heterogeneity and aligned more closely with observed subsurface redox characteristics and landscape attributes across the study region. This research demonstrates that the newly develop approach of *LSNAI* can refine estimates of subsurface nitrate attenuation from sub-catchment to landscape unit scale, improving how spatially variable subsurface nitrate attenuation dynamics are represented when predicting average annual river nitrogen loads. With further refinement, this approach offers a promising basis for targeted and effective evaluation of land use, on-farm and edge-of-field mitigations, and regulatory scenarios, supporting efforts to reduce river nitrogen loads and improve water quality in agricultural catchments.

Acknowledgements

There are many people I must acknowledge and thank, because getting to this stage would not have been possible without the help and involvement of so many people. First and foremost, my main supervisor, Prof Ranvir Singh. A dedicated teacher and supervisor, thank you for providing the guidance, ideas, support and constructive criticism I needed to succeed. To my co-supervisors, Dr Stuart Mead and Prof Dave Horne, thank you for the help and advice I received when I needed it.

From Horizons Regional Council, I need to thank Dr Jon Roygard in particular, for his assistance early in my PhD in helping me set the direction of this research. I also need to thank Sean Hodges for his help in accessing regional council data. Horizons is also thanked for co-funding my PhD research.

From the School of Agriculture and Environment, I'd like to thank Bob Toes, Dr Mike Bretherton, Dr Alan Palmer, Dr Anja Moebis and Eduadro Sandoval for their help in the field, in the lab and in the office. Their help was much appreciated.

I would like to thank Massey University's Farmed Landscapes Research Centre for my PhD scholarship, making it possible for me to undertake this research. I also need to acknowledge the Johannes August Anderson PhD Scholarship; Leonard Condell Farming PhD Scholarship; Hurley Fraser Postgraduate Scholarship; and the John Hodgson Pastoral Science Scholarship for additional funding.

To my office friends, Fernando and Tamsin, thank you for providing such light-hearted and often much needed relief from the general grind of PhD study.

And last, but not least, thanks to James, for helping to keep everything in perspective for me.

Table of Contents

List of Figures

List of Tables

List of Abbreviations

AFDM	Ash free dry mass
AF_N	Nitrogen attenuation factor
APSIM	Agricultural Production Systems SIMulator
AUC-ROC	Area under the receiver operating characteristic curve
Ca^{2+}	Calcium
CEC	Cation exchange capacity
Cl^-	Chloride
DEA	Denitrification enzyme activity
DIN	Dissolved inorganic nitrogen
DO	Dissolved oxygen
DRP	Dissolved reactive phosphorus
ECM	Export coefficient model
$Fe(III)/Fe^{3+}$	Iron (III)/Ferric iron
Fe^{2+}	Dissolved iron/Ferrous iron
FMU	Freshwater Management Unit
FSL	Fundamental Soil Layer
GNS Science	Institute of Geological and Nuclear Sciences
HRC	Horizons Regional Council
HRU	Hydrologic response unit
IGF	Inter-catchment groundwater flow
K^+	Potassium
LSNAI	Landscape Subsurface Nitrate-Attenuation Index
MAE	Mean absolute error
MAPE	Mean absolute percentage error
MdAPE	Median absolute percentage error
Mg^{2+}	Magnesium
$Mn(IV)/Mn^{4+}$	Manganese (IV)
Mn^{2+}	Dissolved manganese
MRT	Mean residence time
N	Nitrogen
N_2	Dinitrogen/Atmospheric nitrogen
N_2O	Nitrous oxide
Na^+	Sodium
Nar	Nitrate reductase

NF	No facies
NH_3	Ammonia
NH_4^+	Ammonium
Nir	Nitrite reductase
NO	Nitric oxide
NO_2^-	Nitrite
NO_3^-	Nitrate
NO_3^--N	Nitrate-Nitrogen
Nor	Nitric oxide reductase
Nos	Nitrous oxide reductase
NLES5	Nitrate Leaching Simulation model version 5
NPS-FM	National Policy Statement for Freshwater Management
NZ	New Zealand
NZLRI	New Zealand Land Resource Inventory
ORP	Oxidation Reduction Potential
PAW	Profile available water
PET	Potential evapotranspiration
R	Transmission coefficient
R^2	Coefficient of determination
REC	River environments classification
RMSE	Root mean square error
ROTAN	Rotorua and Taupo Nitrogen model
SCAMP	Simplified Contaminant Allocation Model Platform
SEM	Standard error of the mean
SIN	Soluble inorganic nitrogen
SO_4^{2-}	Sulphate
SPARROW	Spatially-Referenced Regression on Watershed attributes
SPASMO	Soil Plant Atmosphere Systems Model
SWAT+	Soil and Water Assessment Tool
TN	Total nitrogen
XGBoost	Extreme gradient boosting

Chapter 1: Introduction

1.1 Background

Freshwater quality has come under increasing pressure from agricultural activities globally, including in New Zealand (Bell et al., 2021; Fraser, 2023; Scarsbrook and Melland, 2015; Withers et al., 2014). Elevated nutrient losses to New Zealand freshwaters and many other countries have been driven largely by the expansion of dairy farming on to land previously used for sheep and beef farming, alongside growth in irrigated agriculture (MacLeod and Moller, 2006; Wilcock et al., 2011; Wright, 2015). To address declining water quality, The National Policy Statement for Freshwater Management 2020 (NPS-FM; Ministry for the Environment, 2024) requires New Zealand regional councils to set enforceable water quality limits for freshwater bodies, known as freshwater management units (FMUs). Within this framework, the National Objectives Framework guides the process of defining values (such as ecosystem health) for each FMU and setting measurable attributes (e.g. nitrate toxicity levels) (Ministry for the Environment, 2024). The National Objectives Framework specifies the desired condition (e.g. national bottom lines) for several key water quality attribute states (e.g. an in-river concentration of 2.4 mg/L NO_3^--N annual median), which guides resource use limits (e.g. nitrogen loads in kg/ha/year) in FMUs.

In the Manawatū-Whanganui region of New Zealand, where water quality is under the governance of the Horizons Regional Council, meeting these target water quality attribute states requires a substantial reduction of up to 64 % for total nitrogen and up to 70 % for total phosphorus on average, across the entire region (Snelder, 2024). Because point-source inputs generally make up only a minority of instream contaminant loads (Roygard et al., 2012), water quality improvements will need to come from changes to the way diffuse nutrient losses are managed across agricultural FMUs in the region. But for nitrogen, which primarily moves through subsurface pathways as nitrate, effective management must consider its transport and transformation (attenuation) processes in the subsurface environment.

One key subsurface nitrate attenuation process is denitrification – the microbially-mediated reduction of nitrate to gaseous forms of nitrogen. Denitrification requires specific conditions such as available electron donors (e.g. dissolved organic carbon); low oxygen or anoxic environments; and the presence of denitrifying microbes (Korom, 1992; Rivett et al., 2008). Where these conditions are met, substantial nitrate reduction can occur in the subsurface environment; but where they are absent, nitrate may remain mobile. Given the heterogeneity of soil-hydrobiogeological conditions across landscapes, the potential for subsurface denitrification varies spatially (Seitzinger et al., 2006). Therefore, assessing this spatial variability in subsurface nitrate attenuation capacity is essential to the design and implementation of targeted nitrogen management practices in agricultural landscapes (Hansen et al., 2024; Singh & Horne, 2019). The challenge lies in representing subsurface nitrate attenuation at scales that reflect landscape heterogeneity, enabling better predictions of how land use decisions impact on nitrogen losses of surface water bodies and how freshwater quality targets can be achieved in sensitive FMUs in agricultural catchments.

During the development of the One Plan, the Horizons Regional Council's resource management plan (Horizons Regional Council, 2014), a range of land use scenarios were used to assess the impacts of different farming practices on instream nitrogen loads. At the time (c. ~2007), this modelling exercise required estimates of subsurface nitrate attenuation (Clothier et al., 2007). These authors defined the 'transmission coefficient (R)', which is based on a comparison between the landscape yield (kg-N ha^{-1} yr^{-1}) (i.e., modelled leaching rate from soil profile) and the catchment yield (kg-N ha^{-1} yr^{-1}) (based on the river water flows and concentrations). In this nutrient mass balance analysis for the Upper Manawatū catchment, Clothier et al. (2007) estimated R to be 0.5, meaning only 50 % of the nitrogen lost from land uses was estimated to be transferred to the river. This transmission coefficient (0.5) was subsequently used as a uniform nitrogen transmission factor for other 'priority' catchments in the Horizons region for the development of key components of the One Plan (Clothier et al., 2007).

The estimates of nitrogen transmission coefficient in Tararua and Rangitīkei catchments were later revised and expressed as the nitrogen attenuation factors (AF_N; where $R = 1 - AF_N$) to map greater spatial variability in nitrogen attenuation dynamics in different hydrogeological settings across those catchments (Elwan, 2018; Elwan et al., 2015; Singh et al., 2017a, 2017b). However, like the calculations of R, estimates of AF_N are based on a mass balance approach which compares the soluble inorganic nitrogen (SIN) in the river at water quality monitoring sites, and estimates of inorganic nitrogen leaching rates under different land uses in the catchments. This revised analysis identified AF_N values ranging from 0.14 to 0.77 in Tararua/Upper Manawatū and 0.67 to 0.94 in the Rangitīkei catchments (Elwan, 2018), demonstrating the spatial variability of nitrogen attenuation at the sub-catchment scale. But as subsurface nitrate attenuation varies due to heterogeneous soil-hydrobiogeological conditions (Seitzinger et al., 2006), AF_N refined at the sub-catchment scale is unable to deliver fine-scale mapping of subsurface nitrate attenuation capacity of different land units or landscapes.

Therefore, AF_N needs to be refined to the landscape scale to reflect the natural spatial variability of subsurface nitrate attenuation across diverse land units in agricultural catchments. Achieving this will improve the accuracy of nitrogen transport models and enable a more targeted approach to land use and nutrient management decisions. This is critical for supporting regulatory frameworks like the NPS-FM, which require catchment-scale land use decisions to be linked to measurable water quality improvements. Unless the variable nature of subsurface nitrogen attenuation at the landscape scale is incorporated into the design and implementation of land use and land management policies, their ability to achieve target attribute states, especially for nitrate, will be limited.

1.2 Rationale for this study

Despite the recognised importance of the influence of subsurface nitrate attenuation on nitrogen loads to rivers, current approaches for estimating subsurface attenuation, such as AF_N, are often based on nitrogen mass balance calculations. While these methods demonstrate spatial nitrate attenuation variability at sub-catchment scales, they do not explicitly account for landscape scale variability of subsurface nitrate attenuation which plays a key role in determining where and to what extent subsurface denitrification occurs in agricultural catchments. This limits the ability of catchment-scale modelling to prioritise interventions such as land use changes or edge-of-field mitigations in areas where they will be most effective and constrains the effective implementation of regulatory frameworks like the NPS-FM.

To address this gap, there is a need for an approach that incorporates the influences of landscape heterogeneity in mapping and modelling subsurface nitrate attenuation at catchment scale. Specifically, this study refines estimates of subsurface nitrate attenuation by integrating, at a finer scale, key landscape characteristics known to influence subsurface denitrification, such as subsurface redox conditions, soil drainage and rock type. Given the nature of the denitrification process, subsurface redox conditions are likely to be a key determinant of the magnitude of nitrate attenuation and a good starting point in the development of the Landscape Subsurface Nitrate-Attenuation Index (*LSNAI*). Furthermore, given the paucity of surface and subsurface data for hill country, some challenges are anticipated in validating the *LSNAI* in these landscapes. This research develops the *LSNAI* and classifies the Horizons region into five subsurface nitrate attenuation categories, ranging from *Very low* to *Very high*. This approach provides a more spatially explicit understanding of subsurface nitrate attenuation dynamics within the landscape and supports more targeted management of diffuse nitrogen losses.

1.3 Research aim and high-level objectives

The aim of this thesis is to refine the estimates of subsurface nitrate attenuation in the Horizons region. To achieve this aim, the following high-level objectives will be addressed:

i) Improve understanding of the spatial variability of subsurface redox conditions relevant to nitrate attenuation in New Zealand;
ii) Develop a spatial framework for representing subsurface nitrate attenuation at a finer resolution consistent with landscape variability;
iii) Evaluate the performance of this framework by using field-based observations; and
iv) Apply the framework within a catchment modelling context to assess its effectiveness for predicting nitrogen loads.

1.4 Study area

While the focus of this thesis is primarily on the Horizons region, research took place across three spatial scales – national, regional and farm-scale. At the national scale, an assessment of the spatial variability and temporal stability of groundwater redox conditions was undertaken for all of New Zealand. Acquiring a groundwater redox data set for all of New Zealand was necessary to model subsurface redox conditions in the Horizons region, as existing groundwater data within the region are unevenly distributed and strongly biased toward certain landscape types, particularly Late Quaternary deposits (Zarour, 2008).

The Horizons region, located in the central North Island of New Zealand, covers 22,215 km^2 (2,221,500 ha) and features several large river catchments that discharge into the Tasman Sea on the west coast of the island. Local geology includes Mesozoic-age basement greywacke exposed in the southern part of the region; unconsolidated Plio-Pleistocene deposits throughout; and volcanic deposits in the north (Begg et al., 2005). Dominant land uses across the region include pasture grazed by sheep/beef/deer (44 %); native forest on non-agricultural land (18 %); pasture grazed by dairy cows (8 %); native forest on agricultural land (6 %); and commercial forestry (4 %) (Herzig et al., 2020). Native forest, conservation land and low intensity farming are primarily located in steep and hill country areas, while intensive agriculture, such as dairy farming and cropping, is concentrated on river plains, uplifted terraces and coastal areas. It is for this region that the *LSNAI* was developed.

At farm-scale, Tuapaka Farm, a hill country sheep and beef farm, is used as a case study site to validate some *LSNAI* categories for hill country landscape. Tuapaka is a typical hill country farm in the Horizons region and provides a practical setting for validating the *LSNAI* in hill country land units. Soil redox probes were deployed in three different soil types to characterise subsurface redox conditions and temporal trends in these landscapes.

1.5 Thesis structure

This thesis is divided into seven chapters with chapters 3 to 6 aligning with the research objectives of this thesis. Chapters 3, 4 and 6 have been formatted as manuscripts for submission to peer-reviewed journals.

Chapter 1 (this chapter) outlines the background and rationale for this thesis in addition to the research objectives and the structure of the thesis.

Chapter 2 provides a literature review on subsurface nitrate attenuation, how it is currently modelled or characterised, current research gaps, and how this thesis demonstrates an alternative approach to quantifying subsurface nitrate attenuation at landscape unit scale.

Chapter 3 collates a national groundwater redox data set from New Zealand regional councils. Understanding the distribution and spatial variability of subsurface redox conditions is vital for interpreting potential nitrate attenuation dynamics in agricultural catchments. This chapter compares the frequency and distribution of subsurface redox data against various soil-hydrobiogeological attribute data available for landscape units in New Zealand. This data set is subsequently used in Chapter 4 to make predictions about landscape unit subsurface redox conditions. This chapter fulfils objective i and has been published in *Environmental Monitoring and Assessment*.

Chapter 4 develops a spatial framework known as the Landscape Subsurface Nitrate-Attenuation Index (*LSNAI*) for the Horizons region. This chapter uses the data collated in Chapter 3 to make predictions about landscape unit subsurface redox conditions. These predictions together with the rock type and drainage class attributes are integrated to model and map five *LSNAI* categories based on their subsurface nitrate attenuation potential, ranging from *Very low* to *Very high*. The *LSNAI*'s spatial framework is underpinned by the landscape unit, with independent shallow groundwater (piezometer) observations used to validate the *LSNAI* mapping. This chapter fulfils objective ii and has been published in the *Journal of Environmental Management*.

Chapter 5 validates the *LSNAI* in hill country landscapes. Due to the constraints within the national redox data set (Chapter 3), there is a lack of representative data about typical subsurface redox conditions in hill country landscapes, making predictions about them uncertain and challenging to validate. A set of soil redox sensors were deployed to characterise subsurface redox conditions and validate *LSNAI* categories at Tuapaka Farm, (i.e. at farm-scale) a hill country sheep and beef farm located near Palmerton North in the Horizons region. This chapter fulfils objective iii.

Chapter 6 parameterises the *LSNAI* categories with calibrated values of AF_N. The *LSNAI* is developed to classify landscape units based on their subsurface nitrate attenuation potential (categories ranging from *Very low* to *Very high*) but require conversion to factors (a numeric value between 0 and 1) so they can be used in catchment nitrogen modelling. An export coefficient modelling approach is used to calibrate the AF_N values. This chapter fulfils objective iv and is prepared as a manuscript for publication in a scientific journal.

Chapter 7 summarises and provides a synthesis of the main findings of this thesis. It also recommends potential avenues for future research to continue reducing the uncertainty of these estimates.

Chapter 2: Literature review

This chapter provides a review of nitrate dynamics and subsurface nitrate attenuation, focusing on nitrate transport and denitrification dynamics in subsurface environment, and how these processes are currently represented in catchment-scale water quality models. It then considers methods for upscaling point-scale subsurface denitrification and groundwater redox data using spatial landscape proxies, and the refinement of subsurface nitrate attenuation factors at landscape-unit scale. This provides a robust basis to inform the focus and methodological approaches developed and applied in this thesis.

2.1 Nitrate dynamics and subsurface nitrate attenuation

While nitrate attenuation can occur in a range of terrestrial and aquatic environments including streams; riparian zones; wetlands; soil root zone; lakes; and estuaries, this thesis focuses specifically on subsurface nitrate attenuation, defined as attenuation occurring below the root zone. The phenomenon has been described in the literature using terms such as accumulation (Rosenstock et al., 2014); retention (Blicher-Mathiesen et al., 2014); and attenuation (Rivett et al., 2007). These terms broadly refer to the difference in nitrate lost from below the root zone, and the nitrate subsequently transferred to receiving waters. Conceptually, subsurface nitrate attenuation occurs in the zone between the root zone and discharge points to surface waters, with transport processes acting between these two endpoints. Denitrification is generally considered to be the main mechanism involved in subsurface nitrate attenuation (Korom, 1992; Rivett et al., 2008).

2.1.1 The nitrogen cycle

Nitrogen is critical for meeting current and future global food demand (Tilman et al., 2011; Zhang et al., 2015). Although atmospheric nitrogen (N_2) is the most abundant form it is biologically unavailable to plants until fixed, such as by nitrogen fixing legumes (Herridge et al., 2008). In addition, most nitrogen in the soil environment is unavailable to plants as it is part of the soil organic matter fraction (McLaren and Cameron, 1990). Soil organic matter requires conversion to available forms of nitrogen, such as NO_3^- and ammonium (NH_4^+), so that it can be taken up by plants. This cycling of nitrogen from one form to another is referred to as the nitrogen cycle (Figure 2.1). Compared with other nutrient cycles (such as the carbon cycle), the nitrogen cycle is relatively complex, featuring a number of different oxidation states of nitrogen, each with different bio-availability and reactivity potentials (Robertson, 1997).

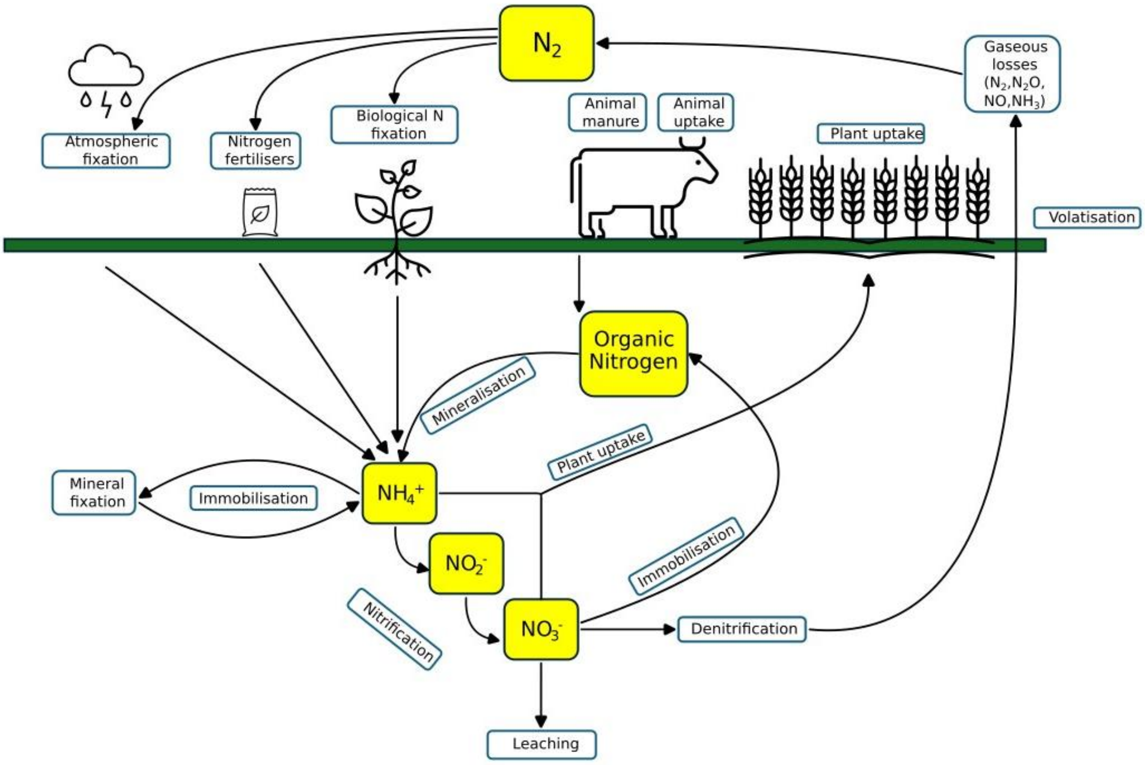

Figure 2.1: The soil/plant nitrogen cycle (adapted from Cameron et al., 2013).

Nitrogen fixation, mediated by soil micro-organisms or in the root nodules of legumes, involves the reduction of atmospheric N_2 to ammonia (NH_3), which rapidly converts to ammonium (NH_4^+) in soil. Soil organic matter, including plant material and animal wastes, is also mineralised to NH_4^+ through ammonification. NH_4^+ is available for plant uptake but can also be immobilised again when converted back to organic nitrogen compounds or adsorbed to clay minerals in the soil. NH_4^+ may also be converted again to nitrite (NO_2^-) and nitrate (NO_3^-) via nitrification. While NO_3^- is available for plant uptake, it is also highly mobile due to its negative charge, making it vulnerable to leaching from the root zone and soil profile under wet conditions. Leached NO_3^- can be transported via subsurface flow pathways beyond its source, potentially contributing to downstream, or down gradient, water quality impacts. However, NO_3^- can also be removed from the soil-water system, either by immobilisation back into soil organic matter, or by denitrification.

Denitrification reduces NO_3^- to gaseous nitrogen forms, typically under anaerobic conditions, returning nitrogen to the atmosphere and completing the cycle (Figure 2.1).

In addition to denitrification, other nitrogen attenuation processes exist, including plant and microbial uptake or immobilisation; dissimilatory nitrate reduction to ammonium; assimilatory nitrate reduction; non-respiratory denitrification; and anaerobic ammonium oxidation (anammox) (Robertson and Groffman, 2015). These processes may play a role in attenuating nitrogen in the subsurface environment, but the extent to which they do is uncertain (Burbery, 2018). Meanwhile, denitrification is generally regarded as the main nitrogen attenuation process within the saturated zone (Korom, 1992; Rivett et al., 2008).

2.1.2 Nitrate sources, losses and transport dynamics

Agriculture is a major source of diffuse nitrogen loading to freshwater and marine systems around the world, with NO_3^- identified as the dominant nitrogen species contributing to water quality degradation (Ballantine and Davies-Colley, 2014; Chan et al., 2024; Wang et al., 2016). The negative charge of the NO_3^- ion coupled with the predominantly negative charge of soils prevents NO_3^- from being adsorbed to soil particles, creating an inherent leaching risk. In agricultural landscapes, NO_3^- originates primarily from synthetic fertilisers, animal manure from pastoral farming and biological nitrogen fixation by leguminous crops (Anas et al., 2020; Fowler et al., 2013; Ju et al., 2009, 2006). Nitrate losses from these sources typically occur by leaching below the root zone, but is also influenced by factors such as climate, soil type, land use intensity and management practices (Bibi et al., 2016; Cameron et al., 2013; Peña-Haro et al., 2014).

In New Zealand, pastoral livestock farming is the main contributor to NO_3^- leaching, with cow urine patches representing the main pathway for losses to occur (Di and Cameron, 2002; Selbie et al., 2015). The nitrogen loading from a single urine patch is approximately equivalent to 1,000 kg N ha^{-1}, exceeding the capacity of the plant or crop to take up the nitrogen (Di and Cameron, 2002). Following deposition, urea in urine is hydrolised to NH_4^+, and subsequently nitrified to NO_3^-. Where soils are saturated and draining beyond field capacity, surplus NO_3^- is leached beyond the root zone into the vadose and saturated zones (Huang et al., 2018; Zhu et al., 2024).

Nitrate leaching in pastoral systems is strongly seasonal. During dry periods, NO_3^- can accumulate in the soil profile and is prevented from leaching within the soil profile due to limited drainage, but when rainfall resumes, or irrigation commences, the accumulated nitrate is mobilised with percolating pore water (Jiménez-de-Santiago et al., 2019; Klaus et al., 2020; Zhou et al., 2010). In New Zealand, this leads to a characteristic seasonal pattern, with the majority of leaching occurring in autumn and early winter when drainage occurs (Selbie et al., 2015). This seasonality has important implications for farm and livestock management, as targeted mitigation practices are often most effective when timed to coincide with periods of high leaching risk (Buckthought et al., 2015).

The risk of nitrate losses can be further exacerbated under irrigated pasture, particularly for soils that are free-draining, or have high infiltration rates (Arauzo and Valladolid, 2013; Magesan et al., 1999). When irrigation rates or volumes are poorly matched to soil type, crop demand, or the irrigation system is poorly managed or timed, nitrate present in the root zone is more likely to be transported below the root zone (Bibi et al., 2016; Costa et al., 2002). In some New Zealand regions, such as Canterbury, irrigated dairy farming on free-draining soils has been identified as a significant driver of elevated groundwater nitrate concentrations (Jenkins, 2019; White, 2001).

Natural drainage dynamics can be further modified where artificial drainage systems, such as mole and tile drains, have been installed in agricultural landscapes (Dinnes et al., 2002; McLaren and Cameron, 1990). While artificial drainage improves the productivity of agricultural land by removing excess water from the soil profile, they also change the natural flow paths of leached nitrate. Instead of percolating through the vadose zone and into groundwater, nitrified drainage water is diverted to drains and surface water bodies via the artificial drainage network (Chan et al., 2024; Jaynes and Isenhart, 2019; Tiemeyer et al., 2006). Not only is a shortcut created for leached nitrate to enter surface water bodies, but the drained soil profile environment may increase N mineralisation leading to more nitrate leaching (Di and Cameron, 2002).

Where nitrate has leached through the soil profile and the vadose zone, its subsequent transport dynamics are determined by regional groundwater flow patterns (Daniel et al., 2023; Molénat and Gascuel-Odoux, 2002; Paradis et al., 2018). In unconfined aquifers, nitrate enters shallow groundwater systems once it reaches the water table, where it is transported laterally along hydraulic gradients towards surface water bodies such as streams, rivers, lakes or estuaries (McLarin et al., 1999; Tesoriero et al., 2005). However, conceptualising exact groundwater pathways, particularly in heterogeneous or structurally complex geo-hydrological settings, can be challenging. It requires integration of geological and hydrogeological data such as aquifer stratigraphy, hydraulic parameters and groundwater head measurements, often supplemented by numerical or conceptual groundwater modelling (Musacchio et al., 2021; Schäfer et al., 2024; Wriedt and Rode, 2006).

To complement, or substitute for, detailed pathway mapping, groundwater mean residence times (MRT) are frequently used as an indicator of flow dynamics (Hofmann et al., 2020; Montcoudiol et al., 2018; Morgenstern et al., 2015). MRT can be described as "the average time water spends in a subsurface system before it arrives at a designated point" (Kuo et al., 2022). Depending on the regional hydrogeology, MRT can range from years in shallow unconfined conditions, to decades or centuries in deeper, confined systems (Morgenstern et al., 2017). Where nitrate is present, MRTs help provide details about the likely duration that nitrate has remained in the system, and the lag times between changes in land use or land management and observed impacts on environmental receptors (Stewart et al., 2011). MRTs can help characterise pollution vulnerability, where short MRTs indicate that groundwater is at risk from pollution (Kralik, 2015), whereas longer MRTs may provide opportunity for nitrate attenuation through processes such as denitrification, particularly when aquifer conditions are favourable (Kaown et al., 2018).

2.1.3 Subsurface denitrification and its measurements

Leached nitrate from agricultural lands could be further transformed by various biogeochemical process in the subsurface environment. Denitrification is a microbially mediated reduction process whereby NO_3^- is reduced to NO_2^- and then to gaseous nitrogen species including nitric oxide (NO), nitrous oxide (N_2O), and finally N_2 (Korom, 1992). Complete denitrification results in the release of inert N_2 gas to the atmosphere, effectively removing nitrogen from the soil-water system. Four key requirements must be met for denitrification to occur: the presence of NO_3^- as a terminal electron acceptor; denitrifying microorganisms, typically facultative anaerobes; the presence of electron donors, usually organic carbon, but in some cases reduced inorganic compounds; and anaerobic conditions, where oxygen availability is restricted favouring the use of NO_3^- as an alternative electron acceptor (Korom, 1992; Rivett et al., 2008). This process can happen in both the unsaturated zone and the saturated zone within the subsurface when these conditions are met (Clague et al., 2019; Lenhart et al., 2021; Rivas et al., 2020; Singleton et al., 2007; Tesoriero et al., 2000).

Denitrification is catalysed by a wide range of microbes (Groffman et al., 2006) and a range of enzymes from these microbes are required for reduction from NO_3^- to N_2: nitrate reductase (*Nar*) reduces NO_3^- to NO_2^-; nitrite reductase (*Nir*) reduces NO_2^- to NO; nitric oxide reductase (*Nor*) reduces NO to N_2O; and finally, nitrous oxide reductase (*Nos*) reduces N_2O to N_2, completing the process (Lycus et al., 2018; Robertson and Groffman, 2015). A wide variety of subsurface bacteria are said to express *Nar*, but a narrower range of bacterial species possess *Nir*, considered the 'true' denitrification step as it is irreversible (Burbery, 2018). Incomplete denitrification, where N_2O is not further reduced to N_2, contributes to global climate change as N_2O is a potent greenhouse gas (Fernandes et al., 2010; Graf et al., 2016; Palta et al., 2013).

Denitrification can be measured in numerous ways, though there are challenges associated with each method (Groffman et al., 2006; Rivas, 2018). The acetylene inhibition method was an early development in denitrification studies. It is based on the ability of acetylene to prevent the reduction of N_2O to N_2, which has high background concentrations, and N_2O being relatively easy to measure in the laboratory (Groffman et al., 2006). The method has been used extensively in both terrestrial and aquatic environments (Dodla et al., 2008; Rivas et al., 2014; Saggar et al., 2013; Seitzinger et al., 1993; Yoshinari et al., 1977; Yuan et al., 2024). In terrestrial environments, denitrification enzyme activity (DEA) assays are used to estimate denitrification potential. DEA provides a snapshot of the activity of the denitrifying enzymes present in the soil at the time of sampling, under conditions of non-limiting nitrate and carbon supply (Rivas et al., 2014).

In aquatic environments the 'push-pull' method has been widely used to understand denitrification in shallow groundwater conditions (Istok, 2013; Istok et al., 1997). The single-well push-pull method is an *in situ* site characterisation method to determine denitrification from a piezometer that is both used to inject nitrate and a conservative tracer (often bromide) into and sampled from periodically (Addy et al., 2002; Anderson et al., 2014b; Collins et al., 2017; Kim et al., 2005; Rivas et al., 2020, 2025).

The use of stable isotopes has also been a common method for denitrification assessment. This involves measuring the natural abundances of nitrogen ($\delta^{15}N$) and oxygen ($\delta^{18}O$) isotopes in NO_3^- to identify source and transformation dynamics (Cao et al., 2025; J.C. Clague et al., 2015; Zhu et al., 2019). During denitrification, microbes preferentially use the lighter isotopes, causing the remaining nitrate to become enriched in ^{15}N and ^{18}O, providing evidence of denitrification (Kendall, 1998; Kendall et al., 2008). The main disadvantage of this method is that the isotopic signature disappears once denitrification has progressed to a point where all NO_3^- has been removed from the system (Martindale et al., 2019). The various sources of nitrogen also have a distinct isotopic composition, allowing for their identification and tracking (Nikolenko et al., 2018; Sacchi et al., 2013). Related to this is the ^{15}N tracer method which involves adding ^{15}N-labelled NO_3^- to soil and measuring the production of ^{15}N-labelled N_2 or N_2O gases (Groffman et al., 2006). This is primarily used in soil/terrestrial environments but may be used in combination with push-pull tests for groundwater assessments (Eschenbach et al., 2015; Schürmann et al., 2003).

The 'excess' N_2 method measures dissolved nitrogen gas in aquatic and terrestrial environments (either *in situ* or in the laboratory), with concentrations above atmospheric equilibrium interpreted as a byproduct of denitrification (Groffman et al., 2006; Martindale et al., 2019). The main benefit of this method is that it is able to quantify actual rates of denitrification (Martindale et al., 2019).

Other approaches to measuring denitrification include mass balance approaches, stoichiometric approaches, *in situ* gradients of environmental tracers, and molecular approaches (Groffman et al., 2006). In mass balance approaches, denitrification is estimated by direct measurement or estimates of all other N fluxes and changes in storage at a range of scales (See Nutrient budget models). Related to mass balance approaches, stoichiometric methods estimate denitrification by comparing the expected amount of dissolved inorganic nitrogen (*DIN*) during organic matter decomposition (based on known elemental ratios) with what is observed in the environment. Denitrification is inferred from the difference between expected and observed *DIN*. For *in situ* gradients of environmental tracers, the approach estimates denitrification rates in groundwater by combining NO_3^- concentration gradients with data about the age of the water. Environmental tracers such as tritium, SF_6 and ^{14}C are used to date groundwater, thereby enabling the calculation of a rate of denitrification. Finally, molecular approaches assess the number, diversity and role of denitrifying enzymes in the environment (Groffman et al., 2006).

Despite the availability of these methods to measure subsurface denitrification, distinct challenges remain. A key source of uncertainty lies in the quantification of denitrification rates, which are influenced by the underlying reaction kinetics (Rivas et al., 2025). Denitrification is a biologically mediated process governed by complex, non-linear kinetics and is best described by Michaelis-Menten models (Ghane et al., 2015; Kouanda and Hua, 2021). However, due to practical limitations of parameterising such models, denitrification is often simplified using either zero-order or first-order kinetics (Boisson et al., 2013; Shah and Coulman, 1978). These simplifications can affect the estimated rates of reduction and contribute to uncertainty in interpreting the magnitude and spatial variability of denitrification in groundwater (Rivas et al., 2025).

A further challenge is the limited range of soil-hydrobiogeological conditions from which denitrification data have been collected, particularly in New Zealand (Burbery, 2018). Given the critical role of denitrification in subsurface nitrate attenuation, this lack of representative data limits our ability to characterise spatially variable denitrification dynamics and to apply denitrification rate estimates across different environmental settings with confidence.

2.2 Modelling subsurface nitrate attenuation

A number of methods are available to model subsurface nitrate attenuation and these are based on the three main types of catchment nutrient models; budget, statistical and mechanistic (Snelder et al., 2018). Budget models, also known as nutrient budget models or mass-balance models, account for inputs and outputs of nutrients at scales ranging from farm-scale to catchment-scale. Rather than simulating processes at fine spatial and temporal scales, they typically rely on average annual estimates of parameters to simulate these processes (Johnes, 1996). Statistical models, also known as data-driven models, use empirical relationships between observed nutrient yields (i.e. kg ha^{-1} yr^{-1}) and landscape variables to make predictions about nutrient loads (Snelder et al., 2018). Mechanistic models simulate physical, chemical and biological processes that represent nutrient transport and transformation in a catchment (Beven, 2012). They simulate processes like runoff, leaching, plant uptake and transport dynamics and are therefore also known as process-based or physically based models. Data needs are typically highest for mechanistic models, followed by statistical models and then budget models. These model types are not mutually exclusive and various models can have elements of each of them, essentially creating hybrid models.

2.2.1 Nutrient budget models

Nitrogen budget models are a method of tracking nutrient inputs, the internal cycling of nutrients, and outputs from farming systems. At farm scale, examples include Overseer® Nutrient Budgets used in New Zealand (Overseer; Wheeler, 2022), and the Nitrate Leaching Simulation model version 5 used in Denmark (NLES5; Børgesen et al., 2022). Both models require input data such as climate, soil, land use, fertiliser use, irrigation and general management practice information, but are designed to reflect the main farming system type in each country. Overseer is designed for New Zealand's pastoral farming systems (sheep, beef, dairy, deer etc.) and a range of vegetable, arable and horticultural crops (Shepherd and Wheeler, 2010), while NLES5 was designed for Denmark's arable farming systems such as cropping (Børgesen et al., 2022). Overseer is more comprehensive in describing nutrient outputs and losses (such as including runoff, phosphorus and greenhouse gas emissions) (Watkins and Selbie, 2015), but both provide comprehensive budgets for root zone nitrate losses (60 cm for Overseer and 1 m for NLES5). Results are reported at block (Overseer; areas of a farm with the same biophysical attributes such as soil type or topography) or field (NLES5) scale in kg N ha^{-1} (or kg N ha^{-1} yr^{-1}) with nitrate being the form of N that is reported (Børgesen et al., 2022; Robertson et al., 2025).

While these nutrient budget models consider nutrient inputs and cycling within the farm boundary, what occurs below the root zone (the vertical farm boundary) is not accounted for. Therefore, these models do not consider nitrate attenuation below the root zone.

However, the outputs of these models can be considered export coefficients (kg N ha^{-1} yr^{-1}) and have been used to track nutrient inputs and outputs at catchment-scale within an export coefficient model (ECM; Johnes, 1996; Johnes & Heathwaite, 1997). The ECM approach was developed to calculate the total nitrogen (and total phosphorus) load delivered to a surface water body as the sum of all the individual loads exported from each source in the catchment (Johnes, 1996). The concept was subsequently modified to account for lateral shallow subsurface flow by incorporating a distance-decay component in the export coefficient (Johnes and Heathwaite, 1997).

The ECM modelling concept can also be used to estimate the fraction of N attenuated in a catchment by comparing root zone losses with the observed load measured at a surface water monitoring site (Monaghan et al., 2007). The AF_N is an example of this, where a value of 0 implies no subsurface N attenuation occurring, whereas a value of 1 implies complete removal of N. This method has been tested in two catchments in the Manawatū-Whanganui region of New Zealand, in the Rangitīkei River catchment (Singh et al., 2017b) and the Tararua catchment (Elwan, 2018). Nitrogen leaching rates were estimated with Overseer and reference N-loss values were used for non-agricultural sources. AF_N values ranged from 0.67 to 0.94 in Rangitīkei and from 0.14 to 0.77 in Tararua. Similarly, in the Odense Fjord catchment in Denmark, where N-loss rates were estimated with N-LES (an earlier version of NLES5) nitrate attenuation varied between < 40 % and up to 70-80 % of the root zone N losses (Blicher-Mathiesen et al., 2014). In Flanders, Belgium, the average attenuation factor was 78 % with a range of 28-98 % was reported (D'Haene et al., 2022). However, this approach also makes it possible to report negative attenuation rates, where root zone losses are less than instream loads, this may result from underestimation of export coefficients or inaccurate instream load assessment (McDowell et al., 2021; Snelder et al., 2023).

These studies demonstrate the high degree of spatial variability of subsurface nitrate attenuation, especially within catchments. It also suggests that some sub-catchments are contributing more of the overall nutrient load than other areas. However, the scale of this variability relates to the location of surface water monitoring sites, not necessarily the natural variability that exists in the soil-hydrobiogeological setting of the catchment or sub-catchment. As landscape variability, with particular reference to hot spots and shallow pathways, is determined by natural processes such as deposition and erosion

(Pinay et al., 2015; Seitzinger et al., 2006) but also anthropogenic causes such as artificial drainage (Billy et al., 2013; David et al., 2015), it can be expected that nitrate attenuation dynamics occur at a much larger scale i.e. at farm scale.

The Rotorua and Taupō Nitrogen (ROTAN) model is a GIS-based rainfall-runoff-groundwater model designed to predict water flows and nitrogen concentrations on a daily or weekly timescale (Upton, 2024). When used at catchment-scale, it can also be used to predict nitrogen loads to the Rotorua and Taupo lakes from historical and future land use changes (Rutherford et al., 2019). ROTAN is based on a rainfall-runoff model known as HBV-N that has been modified to route water and nitrogen from land to lake along three pathways: quickflow, groundwater and streamflow (Rutherford et al., 2019). Overseer was integrated into the model, and two nitrogen attenuation scenarios were tested: spatially homogeneous attenuation; and spatially variable attenuation. In the spatially variable attenuation scenario, nitrogen attenuation was estimated with ten monitoring sites in the lake catchment, similar to the method outlined above. Attenuation was assumed to vary between monitoring sites but be spatially homogeneous across the area draining to the same monitoring site.

2.2.2 Statistical models

Statistical models fit observed values, such as nutrient concentrations or loads (e.g. kg N $yr^{-1,}$) to catchment-scale predictor variables. Because these models predict concentrations or loads directly from observed data, they do not require export coefficients as inputs, unlike the budget models described above. Instead, yields (e.g. kg N ha^{-1} yr^{-1}) are inferred from the statistical relationships between observed water quality data and the model's predictor variables. This bypasses the need to explicitly characterise subsurface nitrate attenuation because the combined effect of attenuation and other catchment processes is captured in the observed (and predicted) values. As such, nitrate attenuation is implicitly accounted for, rather than explicitly parameterised.

An example of this is a new type of empirical model that statistically estimates parameters for each land use *type* within a typology (Snelder et al., 2023). A typology is a classification system that groups land areas with similar characteristics (e.g. land use, soil moisture, slope), and a *type* is one of the classes within that system (e.g. dairy on wet soils, steep native forest etc.). In these empirical models, parameters are estimated for each *type* directly from observed water quality data. These parameters represent the combined effect of diffuse source losses and attenuation, meaning that attenuation is incorporated into the land use classification, rather than represented as a separate coefficient. While this approach helps avoid some of the uncertainty associated with export and attenuation coefficient parameters (Snelder et al., 2023) and can be applied over large spatial areas (McDowell et al., 2017), it does not explicitly provide spatially refined estimates of subsurface nitrate attenuation.

This class of models includes regression-based approaches (McDowell et al., 2021, 2017), machine learning models such as random forest (Snelder et al., 2018), and hybrid approaches such as the Spatially-Referenced Regression on Watershed attributes (SPARROW; Alexander et al., 2002; Elliott et al., 2005).

2.2.3 Mechanistic models

Mechanistic models simulate the physical, chemical and biological processes that relate to the movement and transport of solutes through soil and water (Beven, 2012; Upton, 2024). Also called process-based models, they simulate processes like runoff, leaching, plant uptake and transport in the soil-water biophysical environment. The application scale of these models ranges from field-scale to catchment-scale, and sometimes both. Mechanistic models that estimate leaching losses (field-scale) include the Agricultural Production Systems SIMulator (APSIM; Holzworth et al., 2018), the Soil Plant Atmosphere Systems Model (SPASMO; Clothier & Green, 2017) and Daisy (Abrahamsen and Hansen, 2000). Unlike Overseer and NLES5, which provide average annual estimates of losses, APSIM, SPASMO and Daisy provide losses as daily time-steps (Børgesen et al., 2022; Cichota and Snow, 2009). But like Overseer and NLES5, they simulate nitrogen leaching losses from the root zone and do not take account of attenuation thereafter. Whether the root zone model is empirical (e.g. Overseer) or process-based (e.g. APSIM), these are often combined with mechanistic transport models to simulate the loss and subsequent movement of nutrients from their source to environmental receptor.

At the catchment-scale, a range of mechanistic models can simulate nitrogen (and other contaminant and hydrological) flows. One model commonly used in contaminant transport studies is the Soil and Water Assessment Tool (SWAT+; Bieger et al., 2017), a process-based model that simulates contaminant and hydrological flows in both surface water and groundwater. SWAT+ operates at multiple spatial scales (hydrologic response unit (HRU), sub-catchment, reach, catchment) and temporal scales ranging from daily to yearly (Upton, 2018). The HRU is the basic modelling unit in SWAT+, representing a unique combination of land use, soil type and slope, and it is where all hydrological and biogeochemical processes are simulated (Bieger et al., 2017). As SWAT+ also simulates root zone losses, it can be used independently of root zone models (Yulianti et al., 2025) or be used in combination with them (Becker et al., 2023). Nitrate attenuation in SWAT+ is represented through a denitrification routine that depends on three key input variables: SOL_CBN, the fraction of organic carbon in the soil layer (%); CDN, the denitrification rate coefficient (day^{-1}); and SDNCO, the threshold value of nutrient cycling water factor above which denitrification occurs[1]. These parameters can be left at the software's default values, adjusted based on local knowledge or conditions (Avendaño Veas, 2023), or calibrated against observed data (Me et al., 2015), including from isotopic evidence (Yulianti et al., 2025).

In Denmark, a National Nitrogen Model has been developed by integrating three sub-models: NLES5 for nitrate leaching estimates and disaggregated to daily values using Daisy; a national hydrological model known as the DK-model and is constructed in the physically-based and fully distributed catchment modelling system MIKE SHE; and statistical models to calculate nitrate retention in streams, wetlands and lakes (Hansen et al., 2017; Højberg, 2018). In this model, nitrate attenuation is simulated when N particles cross a redox interface and are assumed to be completely reduced (Hansen et al., 2017). The main source of uncertainty in these models is therefore the determination of the flow paths, which is derived from geological models, and the depth of the redox interface (Hansen et al., 2017).

Another catchment modelling platform is eWater Source, a model developed for water resource management in Australia but also used within New Zealand. To test various

[1] https://swatplus.gitbook.io/io-docs

scenarios with varying rates of AF_N, Overseer was integrated with Source to model nitrate loads to rivers in the Manawatū catchment of New Zealand (Legarth et al., 2022a). Four different scenarios were defined based on their nitrate attenuation potential: no nitrate attenuation; uniform nitrate attenuation; spatially variable nitrate attenuation; and spatially variable nitrate attenuation applied to different flow pathways. Spatially variable nitrate attenuation was classified based on soil texture, soil drainage and geological permeability properties after Elwan (2018) and Singh et al. (2017b). The study found that when spatially variable nitrogen attenuation is considered, and when applied to both quick flow and slow flow pathways from different functional units, the model more accurately predicted dissolved inorganic nitrogen loads both on an annual and monthly basis.

Models may also be a hybrid between two types of models. For example, the Simplified Contaminant Allocation Model Platform (SCAMP) combines statistical features (regression) with some mechanistic applications for contaminant transport (Cox et al., 2023, 2022). SCAMP is a spreadsheet-based method to assess the effects of different land use and contaminant scenarios (from both point and diffuse sources) on water quality (Upton, 2024). Nitrogen attenuation coefficients are calibrated to water quality monitoring sites (Snelder et al., 2020).

These various modelling methodologies outlined here highlight that subsurface nitrate attenuation can be represented in different ways depending on the modelling approach. A key distinction lies in the spatial scale at which subsurface nitrate attenuation is currently applied: at sub-catchments in nutrient budget or statistical models (Elwan, 2018; Singh et al., 2017b; Snelder et al., 2020), and at HRUs in mechanistic models (Avendaño Veas, 2023; Me et al., 2015),. This raises the challenge of how best to represent subsurface nitrate attenuation at scales that reflect natural landscape variability while remaining useful for catchment management. To address this challenge, it is necessary to identify suitable landscape proxies that can capture the environmental controls on subsurface nitrate attenuation (via denitrification) across landscapes.

2.3 Proxies for landscape-scale subsurface nitrate attenuation

While subsurface denitrification is typically quantified through point-scale measurements (Section 2.1.3), estimating subsurface nitrate attenuation across a landscape requires accounting for spatial variability in key environmental factors. Upscaling mapping and modelling of subsurface nitrate attenuation from point measurements to landscape scale relies on integrating spatial datasets with information on the main landscape influences on subsurface nitrate attenuation (via denitrification process) across landscapes. Two important proxies are i) soil-hydrobiogeological properties and ii) subsurface redox conditions. These are discussed below.

2.3.1 Soil-hydrobiogeological properties

Although measurements of subsurface denitrification are relatively sparse, studies provide insight into how soil-hydrobiogeological properties influence nitrate attenuation in subsurface environment. Factors that control the movement and residence time of water through subsurface materials, such as permeability and soil drainage, have consistently been linked to subsurface denitrification potential, alongside broader lithological influences (Jahangir et al., 2013a; Rivas et al., 2020; Wu et al., 2018).

Wu et al. (2018) tested the denitrification potential of a low permeability layer within a Beijing aquifer composed primarily of silty clay and compared this with the overlying layer composed of primarily medium sand. Using a dual isotope approach coupled with an analysis of denitrifier genetic analyses, it was found the low permeability sediments attenuated nitrate at about twice the rate of the high permeability sediments. Jahangir et al. 2013a) quantified *in situ* groundwater denitrification beneath two contrasting sites: a poorly drained, intensively managed grassland and a well-drained arable system in Ireland. Denitrification rates were highest at the bedrock interface under the poorly drained grassland, highlighting that low drainage conditions with low dissolved oxygen and high organic carbon created hotspots for subsurface nitrate removal. In contrast, the well-drained arable site showed generally low denitrification rates, reflecting the influence of high dissolved oxygen in limiting nitrate attenuation.

Rivas et al. (2020) examined the denitrification rate among various hydrogeological settings in the Manawatū catchment, located in the lower North Island of New Zealand. Two of the sites were characterised by stony silt loam or silt loam underlain by loess over gravel; and two further sites were characterised by silt and clay loam or sandy loam underlain by alluvium. Through single-well push-pull tests and examining denitrifying enzyme activity, the sites characterised by loess over gravels were found to have less denitrification potential than those sites underlain by alluvium. Similarly, the drainage status of soils within the unsaturated zone may be a predictor for denitrification potential in groundwaters. Using a transect of shallow groundwater piezometers in Reporoa Basin, located in the Waikato region of New Zealand, Clague et al. (2019) examined groundwater denitrification potential and the redox status of the various soil drainage characteristics. They found generally reduced groundwater conditions indicating higher denitrification potential under imperfectly/poorly drained soils, compared to well-drained soils resulting in oxic groundwater with low denitrification potential in the study piezometers.

While denitrification has been shown to be an effective process for nitrate removal in a range of hydrogeological settings, it is also known not to occur ubiquitously across landscapes (Pinay et al., 2015; Seitzinger et al., 2006). To explore the potential relationship between certain landscape attributes and nitrate attenuation, comparative studies between catchments have been undertaken to demonstrate and highlight the influence of underlying soil and rock types (Deakin et al., 2016; McAleer et al., 2017; Mellander et al., 2014; Orr et al., 2016).

Deakin et al. (2016) compared the nutrient pathways for two contrasting Irish catchments: the Mattock catchment, underlain by poorly drained soils, subsoils and bedrock; and the Nuenna catchment, underlain by freely draining soils and subsoils and highly karstified limestone. The poorly drained setting of the Mattock catchment resulted in higher phosphorus losses per hectare than those in the Nuenna catchment. However, nitrogen losses per hectare were approximately 3.5 times greater in Nuenna than in the Mattock catchment. Orr et al. (2016) also contrasted the Nuenna catchment with another poorly drained Irish catchment, the Glen burn. Here, similar to Deakin et al. (2016), the contrasting hydrogeological settings influenced the biogeochemical fate and transport processes for nitrogen in a similar way. Nitrification is the dominant process influencing nitrogen mobility in the Nuenna catchment, where aquifer transmissivity values are higher, whereas denitrification is the dominant process in the lower transmissivity Glen Burn catchment (Orr et al., 2016).

McAleer et al. (2017) and Mellander et al. (2014) also examined two contrasting Irish catchments, an arable catchment primarily characterised by continuous arable crop production underlain by slate and silt geology; and a grassland catchment characterised by dairy production underlain by sandstone and mudstone geology. Within each catchment, hillslopes were instrumented and investigated for their capacity to naturally attenuate agriculturally derived nitrate. In this case, the sandstone catchment had significantly lower mean groundwater and stream nitrate concentrations than the slate catchment despite a higher nitrogen loading rate. The sandstone catchment showed a 43 % reduction in nitrate from groundwater to stream compared with a 7 % reduction in the slate catchment (McAleer et al., 2017). It was thought that the heterogeneity of the sandstone, and low permeability at depth, may encourage a longer residence time promoting denitrification and reducing nitrate concentrations in near stream zones. It suggests there exists a hierarchy of environmental factors (including agronomy, water table elevation and permeability) that combine to determine hydrochemical outcomes (McAleer et al., 2017). This highlights that there are a range of potential factors, some more significant than others, that will determine nitrogen fate.

At the time the nitrogen attenuation factor (AF_N) was being developed for the Horizons region, the influence of catchment characteristics on the spatial variability of AF_N was investigated in the Tararua and Rangitīkei catchments (Elwan, 2018). AF_N varied spatially from 0.14 to 0.94 across the wider catchments' major sub-catchments. AF_N was higher in poorly drained soils and mudstones and lower in well-drained soils and gravels. A hydrogeologic-based model incorporating soil and rock indices improved predictions of river nitrate loads, demonstrating that effective water quality management must consider both land use and the subsurface nitrate attenuation capacity of catchments. These results, and those outlined above, suggest that denitrification, and subsurface nitrate attenuation, are strongly influenced by soil-hydrobiogeological properties. However, another important but related factor is subsurface redox conditions.

2.3.2 Subsurface redox conditions

Redox reactions, or reduction-oxidation reactions, involve the transfer of electrons between chemical species. In these reactions, one compound is reduced (electrons are gained), while another is oxidised (electrons are lost). Denitrification is a key redox reaction in subsurface environments, but is only one step in a sequence of redox reactions that can occur as conditions become increasingly reduced (Korom, 1992; Rivett et al., 2008). Because dissolved oxygen (DO) is thermodynamically favoured over NO_3^- as a terminal electron acceptor, denitrification typically occurs after DO is depleted. Therefore, a lack of DO becomes an indicator of denitrification potential in the subsurface environment. In this thermodynamic sequence, NO_3^- reduction is followed by the reduction of manganese (IV) (Mn(IV)), ferric iron (Fe(III)) and sulphate (SO_4^{2-}), reflecting a progression towards more reducing conditions (Rivett et al., 2008).

Using observations of redox sensitive species, McMahon & Chapelle (2008) developed a criteria to assess redox status and processes occurring in groundwater systems. This assessment requires commonly analysed water quality parameters to determine whether a groundwater sample is oxidised, mixed or reduced. It uses a decision tree-type approach to classify groundwater redox status and processes depending on the concentration of several parameters, including DO, NO_3^--N, dissolved manganese (Mn^{2+}), dissolved iron (Fe^{2+}) and SO_4^{2-}. This classification criteria has been widely used (Clague et al., 2019; Close et al., 2016; Rivas et al., 2020, 2017; Rosecrans et al., 2017; Stenger et al., 2018) and is seen as a valuable method of assigning redox status to groundwater samples. It has also been adapted for New Zealand groundwater conditions (Close et al., 2016).

Subsurface redox conditions have also been cited in denitrification studies, drawing a link between reduced subsurface conditions and nitrate reduction (Clague et al., 2019; Collins et al., 2017; Jahangir et al., 2013a; Rivas et al., 2017, 2020; Stenger et al., 2018). This connection has led to recent efforts to map and model subsurface redox conditions in both New Zealand and around the world using machine learning methods. Within New Zealand, Close et al. (2016) and Wilson et al. (2018) used linear discriminant analysis to predict groundwater redox status with a range of predictor variables, including geology, topography and soil characteristics in the Waikato, Canterbury and Southland regions. This was extended by Wilson et al. (2020) to cover all of New Zealand with redox status predictions made for depths of 15 m and 50 m. Elsewhere, similar approaches have been undertaken to map and model subsurface redox conditions in Germany (Knoll et al., 2020), the United States (Rosecrans et al., 2017; Tesoriero et al., 2024, 2015) and Denmark (Hansen et al., 2014; Kim et al., 2019; Koch et al., 2019, 2024; Madsen et al., 2021).

Water quality data has mostly been used to model subsurface redox conditions (McMahon and Chapelle, 2008), though Kim et al. (2019) points out that upscaling point measurement-based redox assessments to catchment-scale is challenging because of geological heterogeneity, particularly in the glacial till environments of Denmark. In response to this, a 3D 'redox architecture' was developed based on geophysical data provided by transient electromagnetic resistivity measurements integrated with sediment and water chemistry data (Kim et al., 2021, 2019; Madsen et al., 2021). Sediment colour was previously used as a binary classification predictor in redox models (Koch et al., 2019), but subsequently developed into a probabilistic framework for sediment colour-based redox classification (Kim et al., 2025; Koch et al., 2024). This approach divided subsurface redox conditions into three zones (1) an oxic zone with no nitrate reduction; (2) an anoxic nitrate-reducing zone; and (3) a reduced zone. These zones will be used in a spatially targeted approach to regulating nitrate losses at farm scale in Denmark (Hansen et al., 2017; Hansen et al., 2024; Hashemi, et al., 2018).

2.4 Refining landscape-scale subsurface nitrate attenuation

The aim of this research is to refine estimates of AF_N – currently assessed at sub-catchment scales with limited connection to landscape variability – so they can be applied at larger scales that better capture the natural spatial variability of subsurface nitrate attenuation. However, considering landscape influences on subsurface redox (dentification, as reviewed above), modelling and mapping of subsurface nitrate attenuation potential could be potentially refined by adopting landscape units as the spatial modelling framework for upscaling proxies of subsurface denitrification potential.

2.4.1 Landscape units

A landscape unit is broadly defined as a spatial area that exhibits relatively homogeneous physical and geographic characteristics (Campos-Campos et al., 2018). In New Zealand, no single nationally consistent data set exists that was explicitly designed to represent hydrogeological landscape units. Therefore, this study adopts polygons from the New Zealand Land Resource Inventory (NZLRI) as a pragmatic spatial framework. The NZLRI is a national spatial database developed to support land use planning and erosion management in New Zealand. The Land Resource Inventory (LRI) is a method for recording five key land characteristics relating to soils, rock type, slope, presence and severity of erosion, and vegetation at a scale of 1:50,000 (Lynn et al., 2009). These five physical factors are integrated within the NZLRI alongside derived Land Use Capability (LUC) classifications for land management purposes. NZLRI polygons therefore represent areas of relatively consistent combinations of those attributes, but were originally delineated primarily to support assessments of land use limitations and versatility, with a strong emphasis on erosion-related limitations.

NZLRI units are not strictly landform or hydrogeological units, and their delineation reflects the requirements of LUC classification rather than the representation of subsurface processes such as nutrient attenuation. Furthermore, the information within the NZLRI is variable in quality, reflecting the availability of soil surveys at the time of mapping. The NZLRI is further supplemented by 16 additional soil properties collectively known as the Fundamental Soil Layer (FSL; Barringer et al., 1998; Newsome et al., 2008). However, it is a derived product that incorporates modelled estimates of soil properties and therefore introduces additional uncertainty.

Despite these limitations, NZLRI polygons provide a nationally consistent spatial framework that integrates some of the key controls on subsurface processes including lithology and soil characteristics. In the absence of an alternative spatial framework, NZLRI units are adopted as a practical basis for delineating landscape units that represent a generalised approach to subsurface heterogeneity.

Across New Zealand, the NZLRI defines approximately 100,000 polygons, including approximately 11,000 in the Horizons region. In this study, these polygons provide the spatial framework for upscaling proxies for denitrification potential, specifically soil-hydrobiogeological properties and subsurface redox conditions.

2.4.2 Linking landscape subsurface nitrate attenuation to targeted regulation

Defining subsurface nitrogen attenuation at the scale of landscape units enables more accurate mapping and modelling of spatially variable nitrate attenuation in catchment models and freshwater accounting. Landscape-unit-scale estimates not only improve future modelling prospects but also highlight where water quality interventions could be most effective, targeting ‘hot spots’ and ‘hot moments’ of nutrient loss. The potential for such a spatially targeted approach to regulating agricultural activities is a growing area of research in New Zealand (Rissmann et al., 2018; Sarris et al., 2019; Singh and Horne, 2019; Vogeler et al., 2014) and internationally (David et al., 2015; Hansen et al., 2017, 2024; Hashemi et al., 2018a, 2018b; Højberg, 2018; Jacobsen and Hansen, 2016; Zimmerman et al., 2019). Such detail is not yet available for many sensitive agricultural catchments in New Zealand, but adopting a landscape unit approach provides a practical framework for targeting mitigation activities based on improved knowledge of nitrogen transport and fate dynamics.

2.5 Summary

Achieving freshwater quality targets will require substantial reductions in nitrogen loads. While some progress can be made through improved management of point-source discharges, the greatest reductions will come from addressing diffuse nitrogen losses, which dominate nutrient inputs in the Horizons region. However, diffuse nitrogen is particularly challenging to model because subsurface transport and transformation processes vary spatially across catchments.

Denitrification is the primary mechanism for subsurface nitrate attenuation, but it occurs unevenly across landscapes due to heterogeneous soil-hydrobiogeological and subsurface redox conditions. Although the environmental controls on denitrification are reasonably well understood, their spatial and temporal expression remains highly uncertain. Measurement challenges and limited representative data sets add to this uncertainty. As a result, current estimates of subsurface nitrate attenuation remain coarse and do not adequately reflect underlying environmental heterogeneity. While process-based and statistical models offer useful insights, they are often constrained by high data requirements and limitations in resolving spatial variability at catchment scales.

A potential alternative involves upscaling point-scale understanding of denitrification using environmental proxies that better capture spatial variability. Soil-hydrobiogeological properties and subsurface redox conditions are two particularly important controls on denitrification potential and are more widely available than direct measurements of surface denitrification. Integrating these proxies within a landscape unit framework provides a practical means of refining subsurface nitrate attenuation estimates at a scale that better reflects natural spatial variability, rather than relying on sub-catchment scale averages derived from nutrient mass balance approaches.

Such an approach has the potential to improve the representation of subsurface nitrate attenuation dynamics within catchment-scale water quality models, support more robust testing of land use scenarios, and enable more targeted management of diffuse nitrogen losses. Linking subsurface nitrate attenuation to landscape units provides an opportunity to target regulation at scales consistent with natural processes, potentially improving both scientific accuracy and management outcomes.

2.6 Detailed research objectives

The literature highlights the need for improved representation of spatial variability in subsurface nitrate attenuation, particularly through the integration of landscape-scale controls such as soil properties, lithology and subsurface redox conditions. While process-based catchment models (e.g. SWAT+, MIKE SHE, eWater Source) provide detailed representations of nitrogen transport and transformation, they are typically highly data intensive, requiring extensive information on hydrological processes, subsurface properties and land management across large spatial extents. Such data are often unavailable or uncertain at the scale required for regional nitrogen modelling. Consequently, there is a need for alternative approaches that can represent subsurface nitrogen attenuation processes at appropriate spatial scales using available data.

To address this gap, this thesis addresses the following detailed research objectives:

i) Compile and analyse a national groundwater redox data set to assess the distribution and representativeness of subsurface redox conditions across landscape attributes;

ii) Develop a predictive modelling approach for landscape unit subsurface redox conditions using landscape-scale variables;

iii) Integrate landscape unit subsurface redox predictions with soil and lithological information to develop a Landscape Subsurface Nitrate-Attenuation Index (*LSNAI*);

iv) Evaluate *LSNAI* classifications using field-based observations of soil redox conditions across selected sites; and

v) Parameterise *LSNAI* categories for use within an export coefficient modelling framework and assess its effectiveness for predicting instream nitrogen loads.

Chapter 3: Assessment of spatial variability and temporal stability of groundwater redox conditions in New Zealand

Brief introduction for thesis

This chapter collates a national groundwater redox dataset from New Zealand regional councils and evaluates its frequency and distribution in relation to soil-hydrogeological attributes. Understanding the spatial variability of subsurface redox conditions is essential for interpreting subsurface nitrate attenuation dynamics in agricultural catchments. The resulting dataset provides the foundation for predicting landscape unit scale subsurface redox conditions in the Horizons region (Chapter 4).

This chapter has been published as:

Collins, S.B., Singh, R., Mead, S.R., Horne, D.J., Roygard, J.K.F., 2025b. Assessment of spatial variability and temporal stability of groundwater redox conditions in New Zealand. Environ. Monit. Assess. 197, 58. https://doi.org/10.1007/s10661-024-13427-y

3.1 Abstract

Mitigating the impacts of agricultural nutrients (nitrogen and phosphorus) on water quality requires a clear understanding of their transport pathways and transformation processes from land to receiving waters. For nitrate, which is subject to subsurface denitrification, it is therefore important to assess the spatial variability and temporal stability of groundwater redox conditions, as nitrate reduction typically occurs in reducing conditions. This paper presents a robust assessment of a large groundwater quality data set collected across New Zealand landscapes; develops methods to impute missing groundwater redox-sensitive variables; and characterises the spatial variability and temporal stability of groundwater redox conditions against relevant landscape hydrogeochemical characteristics. Random forest and extreme gradient boosting (XGBoost) outperformed linear regression in predicting missing Mn^{2+} values, achieving higher accuracy ($R^2 > 0.8$) and lower error ($RMSE < 0.2$ mg/L). Analysis of groundwater redox conditions highlights considerable spatial variability, particularly influenced by subsurface geology (rock types) and soil characteristics such as soil carbon and drainage across various hydrogeological settings. Our findings also reveal a higher prevalence of oxidised redox status in shallower groundwater and greater temporal stability in oxidised conditions across New Zealand landscapes. These insights have significant implications for targeted management strategies to reduce nitrate losses from farming activities, particularly in oxidised, shallow groundwater across different hydrogeological land units.

3.2 Introduction

The robust management of freshwater quality requires an accurate assessment of nutrient losses and their critical source areas in a catchment (Anderson et al., 2014a; Guo et al., 2022; Wang et al., 2018). However, quantification of catchment nitrogen loads, necessary for freshwater accounting under New Zealand's National Policy Statement for Freshwater Management 2020 (Ministry for the Environment, 2024), is generally compromised by the poor quantification of, and uncertainty in, subsurface nitrate reduction, or 'attenuation' (Destouni et al., 2006; Hasler et al., 2019; Keller et al., 2014; Snelder et al., 2020). As nitrate is leached from the root zone, it is exposed to a range of biogeochemical conditions that may cause it to be attenuated *in situ* along groundwater flow paths (Welch et al., 2011; Zhu et al., 2019). To overcome this challenge, rates of subsurface nitrate attenuation need to be refined at landscape scale, due to the variability at which nitrate attenuation is typically observed (Blicher-Mathiesen et al., 2014; Elwan et al., 2015).

The primary pathway for subsurface nitrate attenuation is denitrification, the microbially-mediated removal of nitrate to gaseous forms of nitrogen (Korom, 1992; Rivett et al., 2008). Evidence of denitrification in New Zealand groundwaters has been reported in various studies (Burbery, 2018), however, direct measurements of it are sparse. In addition, direct measurements of subsurface denitrification tend to be complicated and time-consuming to perform and discrete measurements may not reflect the pattern of nitrate attenuation across different hydrogeological settings in agricultural landscapes (Pinay et al., 2015; Seitzinger et al., 2006; Vidon et al., 2010). This leads to the challenge of matching discrete direct observations of subsurface denitrification to wider water quality considerations at catchment-scale (Seitzinger et al., 2006).

As groundwater redox conditions have a strong connection to denitrification in groundwater, they can be used as a proxy to map and model nitrate attenuation potential at the catchment-scale (Clague et al., 2019; Collins et al., 2017; Rivas et al., 2020, 2017, p. 201; Stenger et al., 2018). The reduction of nitrate (NO_3^-) to gaseous forms of nitrogen (predominately dinitrogen; N_2) only occurs in favourable redox conditions in groundwaters (Rivett et al., 2008). Within this context, dissolved oxygen (DO; O_2) is preferentially oxidised with dissolved organic carbon as it is the most energetically favourable to aerobic bacteria (Rivett et al., 2008). However, once DO is depleted, nitrate becomes energetically favourable to a range of anaerobic bacteria. Several studies have demonstrated the connection between reduced groundwater conditions and denitrification in New Zealand (Clague et al., 2019; Collins et al., 2017; Rivas et al., 2020, 2017; Stenger et al., 2018), and internationally (Böhlke et al., 2002; Højberg et al., 2017; Jahangir et al., 2013b; Puckett and Cowdery, 2002; Stuart, 2018; Welch et al., 2011). In addition, there is growing evidence that subsurface denitrification and redox conditions are strongly influenced by landscape characteristics such as soil drainage (Clague et al., 2019; Rivas et al., 2020; Wu et al., 2018) but comparatively little is known about the temporal stability of redox conditions in groundwater and so it will be important to identify any variability with time before using redox as a proxy for denitrification in groundwaters. Therefore, a robust assessment of the spatial variability and temporal stability of groundwater redox conditions and their relationships with landscape characteristics have the potential to inform mapping and modelling of subsurface denitrification, and therefore nitrate attenuation potential, across agricultural catchments.

The spatial variability and temporal stability of groundwater redox conditions with respect to key hydrogeochemical characteristics across New Zealand landscapes was investigated. The existing groundwater data obtained from 15 regions of New Zealand was collated and analysed. Groundwater redox is assessed based on groundwater water quality data, using a combination of key redox species parameters including DO, nitrate-nitrogen (NO_3^--N), dissolved manganese (Mn^{2+}), dissolved iron (Fe^{2+}) and sulphate (SO_4^{2-}) (McMahon and Chapelle, 2008). However, groundwater quality data often feature missing observations of redox species data, conceding the ability to make groundwater redox assessments for some groundwater quality data. To help increase the utility of existing groundwater data, we developed and applied a novel data imputation method to fill the data gaps and increase the number of groundwater redox assessments able to be made. The aims of this study were to develop and evaluate new data imputation methods to help increase the number of groundwater redox assessments; assess the spatial variability of groundwater redox conditions across a wide variety of landscape types; and assess the temporal stability of groundwater redox conditions.

3.3 Data and methods

3.3.1 Study area

New Zealand is a geologically and volcanically active archipelago, consisting of two main islands (the North Island and the South Island) and hundreds of others. Its geologically active nature is due to its position on the boundary between the Pacific and Australian tectonic plates, causing high rates of uplift and exposing basement geology in many regions (King, 2000; Mortimer, 2004). Related tectonic processes such as erosion, subsidence, deposition, volcanism and climate fluctuations have all contributed to shaping New Zealand's groundwater resources. These groundwater resources have been mapped as hydrogeological units at 1:250,000 scale, based on geological and hydrogeological data, and classified as aquifer, aquitard, aquiclude or basement (Figure 3.1; White et al., 2019). The 'aquifer' units are generally of Quaternary age and are derived from sediments associated with alluvial fans rising from the axial ranges in both the North and South islands (White et al., 2019). Extensive ignimbrite deposits in the central North Island associated with Quaternary volcanism have also formed important aquifers (White et al., 2019). These areas typically host the most intensive land uses in New Zealand, such as dairy farming, cropping and vegetable production. Complex groundwater flow pathways and recharge dynamics in New Zealand aquifers complicate our understanding of nutrient transport and attenuation, including groundwater redox conditions (Collins et al., 2017; Morgenstern et al., 2019, 2017; Singh et al., 2019; Wells et al., 2016).

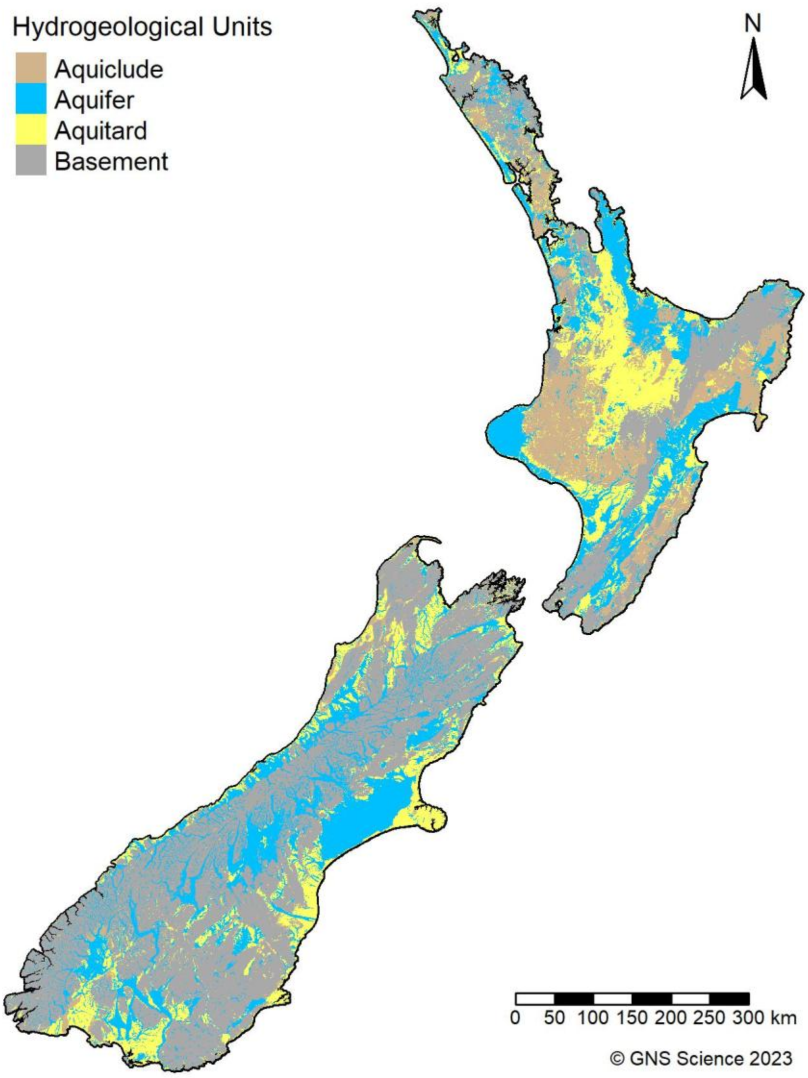

Figure 3.1: The main hydrogeological units of New Zealand, ranging from aquifers, aquitard, aquiclude and basement (White et al., 2019). Reproduced with permission from Springer Nature.

3.3.2 Data provenance and summary

Regional councils in New Zealand undertake environmental monitoring, including quarterly groundwater monitoring, across their regions. To compile a data set for this study, groundwater quality (hydrochemical) data was obtained from all 15 regional councils for the dates between 1 January 1990 and 31 December 2019. Because of this long period of time, and the involvement of 15 different regional councils, it is expected that some aspects of groundwater monitoring programmes would be different from council to council or would have changed over time. While a degree of consistency has been achieved in recent years, including the implementation of a quality coding system for environmental data (Milne, 2019), the legacy of different agencies collecting environmental data means different laboratory analysis methods have been employed, as well as different sampling methods, field equipment, sampling protocols, and the suite of parameters analysed. We have made no effort to verify consistency in the data collection methods/protocols used or summarise differences in data collection methods or assess their comparability over time. There are therefore some limitations to this data set. However, we have implemented data pre-processing measures, as follows, and in the following order:

- Any negative DO values converted to zero;
- zeros replaced with the most common censored value for that parameter (e.g. < 0.005 mg/L);
- censored data assigned a value of $1/\sqrt{2}$ of the detection limit (Finkelstein and Verma, 2001); and
- values greater than the 99th percentile for each parameter were removed as outliers.

These pre-processing measures resulted in a collation of 85,162 groundwater data points (individual rows/samples) with measurements of a range of groundwater quality parameters, including redox species, for more than 30 years in diverse hydrogeological settings across New Zealand landscapes (Table 3.1). Nitrate-N is the most common parameter represented in the data set. Nitrate-N has been of particular interest to regional councils and water resource managers in recent decades as a signal of land use effects on water quality (Bekesi, 1999; McLarin et al., 1999). The other common variables observed are chloride, sulphate and ammoniacal-N (Table 3.1). Only 25% of the collated data points had records of all five redox relevant observations of DO, NO_3^--N, Mn^{2+}, Fe^{2+} and SO_4^{2-}. Of these, measurements of DO, Mn^{2+} and Fe^{2+} had the most missing values, as they were absent in over half of the records.

Table 3.1: Summary of hydrochemistry data collected by New Zealand regional councils as part of their groundwater monitoring programmes 1990-2019. Outliers are those above the 99th percentile (p99) and have been removed from the data set. Reproduced with permission from Springer Nature.

Measurement	Unit	n	Max	p99	Median	Min	n Outliers
Nitrate-N	mg/L	66,996	520.00	25.00	2.10	<0.01	639
Chloride	mg/L	64,764	16,500.00	370.00	14.00	0.04	638
Sulphate	mg/L	58,398	8211.00	100.00	7.40	<0.01	582
Ammoniacal-N	mg/L	53,876	2,100.00	7.70	0.01	<0.01	535
Dissolved Na	mg/L	45,311	7,000.00	340.00	14.00	0.07	443
Dissolved Ca	mg/L	44,266	2,300.00	134.00	16.20	0.01	436
Dissolved Mg	mg/L	43,605	900.00	39.60	5.10	<0.01	437
Dissolved K	mg/L	42,730	610.00	24.00	1.50	0.01	427
Total Alkalinity	mg/L $CaCO_3$	42,588	6,600.00	882.00	54.00	<0.01	425
Dissolved Fe	mg/L	40,041	450.59	15.00	0.02	<0.01	391
Dissolved Mn	mg/L	38,278	23.00	1.70	0.01	<0.01	371
Dissolved Oxygen	mg/L	37,115	665.00	11.85	5.60	0.01	371
Dissolved Reactive Phosphorus	mg/L	35,777	1,840.00	1.74	0.02	<0.01	357
Dissolved Silica	mg/L SiO_2	33,845	472.00	92.00	18.40	0.01	322

3.3.3 Imputation of missing Mn^{2+} variables

Assessing groundwater redox conditions requires a range of hydrochemistry data. McMahon and Chapelle (2008) first devised a classification scheme to describe the redox status of principal aquifers in the United States: their scheme requires values of DO, NO_3^--N, Mn^{2+}, Fe^{2+} and SO_4^{2-}. In New Zealand, McMahon and Chapelle's (2008) classification was modified for local conditions by Close et al. (2016) using only measurements of DO, NO_3^--N, Mn^{2+}. Both classifications are vulnerable to missing data. In this case, a sample may be classified as 'Indeterminate'. Due to the differences among regional councils as to collected data, missing values are a feature of this collated groundwater quality data set, limiting the potential number of groundwater monitoring sites that could be classified. Mn^{2+} was the focus for imputation because it more strongly reflects background soil and geological conditions, rather than those that are more directly influenced by land use (NO_3^--N) or processes highest in the redox sequence (DO).

A three-step process was undertaken to impute missing Mn^{2+} values. First, a subset of the data was identified that would be used for imputation. While there were many missing

Mn^{2+} values in the data set (Table 3.1), it was not possible to attempt to impute them all. Machine learning models are themselves vulnerable to missing data and require appropriate strategies to handle them. There are several methods available to do this, but a common strategy is to simply remove rows or columns with missing data. Therefore, it was necessary to identify a subset from the data set with as many non-missing variables as possible for which to train a model to predict missing Mn^{2+} values. This subset was known as the imputation data set.

Second, the imputation data set was grouped into six clusters, referred to as hydrochemical facies, to reflect the natural variation in New Zealand's groundwater (Daughney and Reeves, 2005). We applied k-means clustering (Kanungo et al., 2002) to the predictor variables to identify the six facies.

Third, we trained and evaluated three different models – linear regression, random forest (Breiman, 2001) and extreme gradient boosting (XGBoost; Chen and Guestrin, 2016) – for each hydrochemical facies identified in the imputation data set. In addition, we created a single group with no facies (i.e. the entire imputation data set) to compare with the six facies. Data in each facies was split into training and testing sets (50/50 split) with 10 cross-validation folds generated from the training data sets for model training purposes. R^2 and root mean square error (*RMSE*) results were observed and compared between the trained model results before selecting the model with the best scores. Finally, the testing data set was used to compare the R^2 results for each facies of the selected model. Only facies with $R^2 > 0.8$ were used for Mn^{2+} imputation.

All data analysis was carried out in R (R Core Team, 2022; v. 4.2.2) with predictive analysis undertaken with Tidymodels (Kuhn and Wickham, 2020; v. 1.1.1).

3.3.4 Groundwater redox classification

As described, after imputing missing Mn^{2+} values, the redox classification scheme by Close et al. (2016) was used to classify New Zealand's groundwater data. This classification, developed for New Zealand conditions, classifies groundwater data based on certain thresholds (DO < 1.0 mg/L; NO_3^--N < 0.5 mg/L; Mn^{2+} > 0.05 mg/L), into one of three redox states: 'Oxidised', 'Mixed', or 'Reduced'. If a sample is out of the range of these thresholds, or does not contain the necessary variables, it is classified as 'Indeterminate'.

3.3.5 Spatial variability of groundwater redox conditions

A geographical dataset of landscape attributes and landscape unit boundaries is obtained from the New Zealand Land Resource Inventory (NZLRI; Newsome et al., 2008). The NZLRI is an inventory of five physical factors, mapped at a scale of 1:50,000, that are understood to characterise land use capability in New Zealand. In addition, the NZLRI is supplemented with an interpreted data set known as the Fundamental Soils Layer (FSL), containing data on additional soil attributes. Together, these geographical data sets provide around 100,000 polygons (landscape units) across New Zealand. Fourteen attributes have been selected from the NZLRI and the FSL to represent the landscape characteristics that are potentially related to redox processes in the subsurface environment (e.g. Clague et al., 2019; Rivas et al., 2020; Wu et al., 2018). These include top rock; base rock; slope; carbon content; gravel content; soil drainage; permeability; profile available water (PAW); pH; cation exchange capacity (CEC); phosphate retention; plant rooting depth; flood class; and macroporosity (Newsome et al., 2008).

Top rock and base rock are derivations of rock type in the NZLRI. Top rock is the first-named entire rock type, irrespective of any succeeding stratigraphy and can have several lithology expressions depending on the dominance of the rock types in a single polygon unit. Base rock is the single value that identifies the principal basement lithology (Newsome et al., 2008). In this study, these have been merged as 'top rock over base rock' and reclassified as 'Rock type'. Where top rock and base rock are the same, just the single attribute is described (e.g. 'Greywacke over Greywacke' becomes 'Greywacke') and where they are distinct both attributes have been retained (e.g. 'Loess over Alluvium'). In addition, for both top rock and base rock, the various ash deposits have been reclassified as 'volcanic ash', and along with other kinds of volcanic deposits, these have been reclassified as 'volcanic deposits'. This helped reduce and simplify the number of geographical variables for rock type.

Slope refers to a physiographic area of relatively homogeneous average relief and includes eight classes. It is derived from stereo aerial photograph interpretation and field verification and allows up to two slope expressions within a single polygon (Newsome et al., 2008). In this study, just the first/dominant named slope attribute class has been retained (e.g. 'Flat to gently undulating'). The eight classes have also been collapsed into four classes: Flat (Flat to gently undulating, Undulating); Rolling; Easy hill (Strongly rolling, Moderately steep); and Steep hill (Steep, Very steep, Precipitous). Descriptions of slope are not necessarily uniform across the polygon/landscape unit e.g. there may be areas of flatter relief such as a toe slope in a steep slope class. Permeability refers to the rate at which water moves through saturated soil and includes three classes, 'Slow', 'Medium' and 'Rapid', of which multiple combinations are possible in layered soils (Clayden and Webb, 1994). In this study, just the first named permeability attribute class has been retained (e.g. 'Slow'). The remaining attributes of carbon content; gravel; soil drainage; PAW; pH; CEC; phosphate retention; plant rooting depth; flood class; and macroporosity have been retained as they were outlined in (Newsome et al., 2008) and are further described there. In all cases, unrelated classifications within these attributes e.g., lakes, estuaries, towns/cities, have been classified as 'Not specified'.

3.3.6 Temporal stability of groundwater redox conditions

While landscape characteristics, such as those outlined above, do not generally change, seasonal variation in groundwater recharge and flow rates could affect the supply of redox-sensitive variables such as DO as could the leaching of NO_3^--N and dissolved organic carbon from the soil profile (Ki et al., 2015; Zhu et al., 2019). Fluctuations in these inputs could affect the temporal stability of groundwater redox conditions in the subsurface environment. To investigate this further, groundwater sites with more than ten redox assessments were categorised according to their dominant redox status, as follows:

- Groundwater redox stable ≥ 90 % of the time
- Groundwater redox stable 80-89 % of the time
- Groundwater redox stable 70-79 % of the time
- Groundwater redox stable 60-69 % of the time
- Groundwater redox stable 50-69 % of the time

For example, if a site had 25 redox assessments and 21 of them are oxidised, then groundwater redox is stable 80-89 % of the time.

3.4 Results and discussion

3.4.1 Imputation of missing Mn^{2+} variables

The imputation data set consisted of 38,182 rows containing Ca^{2+}, Mg^{2+}, K^+, Na^+ and Cl^- and 8,634 missing Mn^{2+} values (Figure 3.2). This filtered data set was used to impute the missing Mn^{2+} values, using the associated hydrochemistry variables as predictors. Correlation plots of these predictor variables are found in Appendix A.

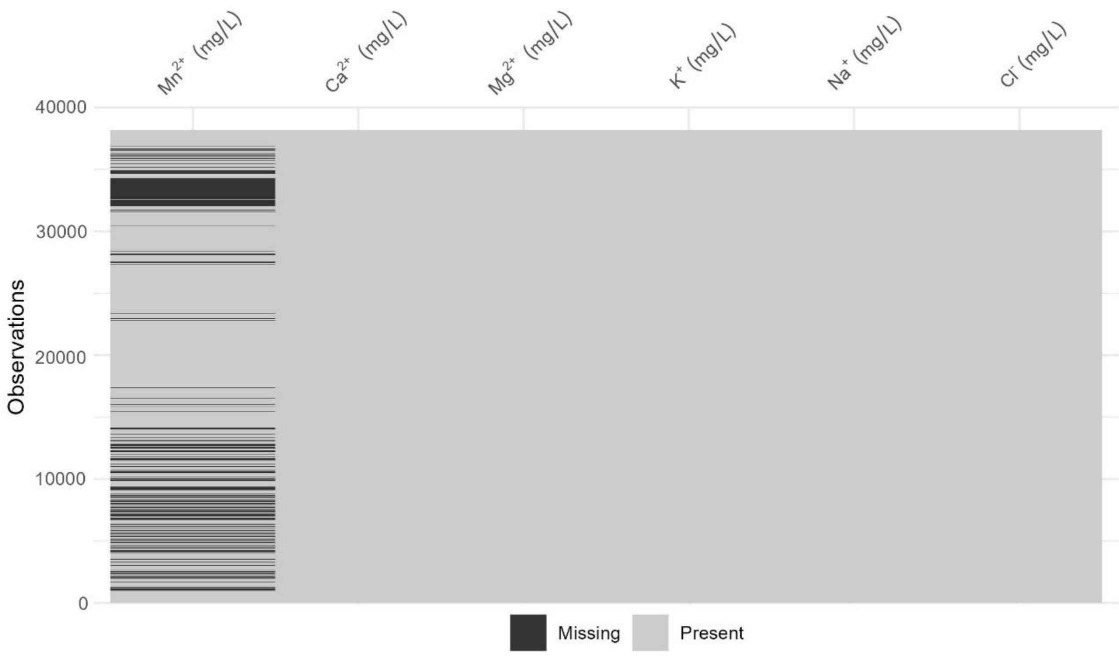

Figure 3.2: Imputation data set featuring a subset of 38,182 rows containing 8,634 missing Mn^{2+} values and non-missing predictor variables consisting of Ca^{2+}, Mg^{2+}, K^+, Na^+ and Cl^-. Reproduced with permission from Springer Nature.

Clustering the imputation data set into six hydrochemical facies (based only on the predictor variables of Ca^{2+}, Mg^{2+}, K^+, Na^+ and Cl^-), created distinct groups with a range of Mn^{2+} concentrations (Table 3.2). Facies 2, 3, 4 and 6 have higher mean concentrations of Mn^{2+}, potentially indicating that these represent more reduced groundwater, while facies 1 and 5 may represent more oxidising groundwater because of their lower mean Mn^{2+} concentrations (McMahon and Chapelle, 2008). These two facies are notably larger and represent more than 80% of the imputation data set (Table 3.2).

Table 3.2: Facies generated from the imputation data set by k-means clustering. Mean concentrations are shown for each variable. Reproduced with permission from Springer Nature.

Facies	Mn^{2+} (mg/L)	Ca^{2+} (mg/L)	Mg^{2+} (mg/L)	K^{+} (mg/L)	Na^{+} (mg/L)	Cl^{-} (mg/L)	n	n Mn^{2+} missing
1	0.03	12.66	3.79	1.53	9.44	7.67	19,589	4,772
2	0.34	38.31	19.45	5.09	157.56	220.03	382	94
3	0.25	72.00	11.33	3.46	32.25	40.67	2,175	346
4	0.37	38.78	11.82	3.86	83.74	108.73	1,175	182
5	0.10	22.80	7.45	2.39	18.52	19.76	11,715	2,736
6	0.29	19.98	8.16	3.03	42.95	45.63	3,146	504
Total	•	•	•	•	•	•	38,182	8,634

For each model, the cross-validation folds were used for training and evaluation of each facies, including a ‘no facies’ group. Figure 3.3 and Figure 3.4 outline the mean R^2 and mean *RMSE* scores, respectively, for each model. Mean here refers to the average across the 10 cross-validation folds. R^2 and *RMSE* results were generally better for random forest and XGBoost compared to linear regression. The linear regression R^2 scores were consistently lower than the other models and did not achieve more than 0.5, except for facies 2. In addition, the *RMSE* scores were consistently higher for the linear model than those obtained by the other models. The performance of random forest was slightly better than XGBoost and has therefore been used for imputation of Mn^{2+} missing values.

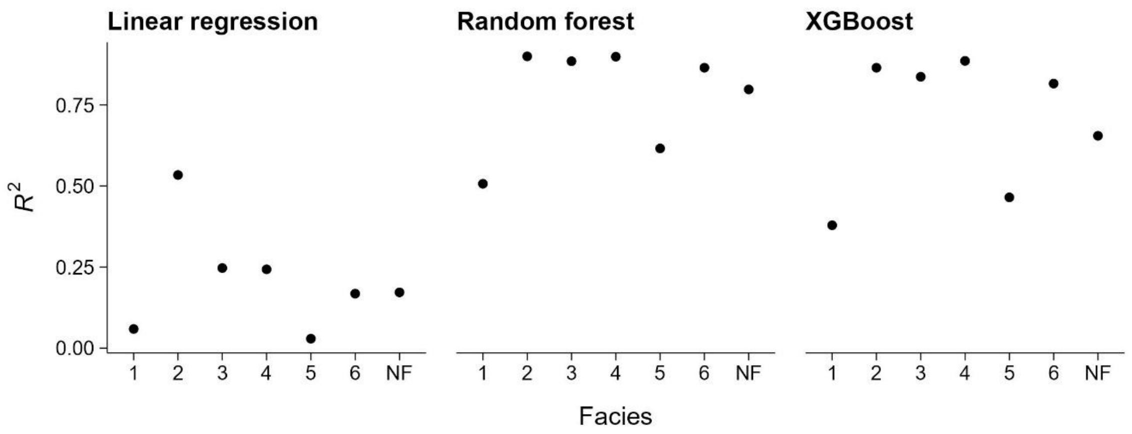

Figure 3.3: R^2 scores for each facies for the prediction of Mn^{2+} by linear regression, random forest and XGBoost models. NF refers to 'no facies'. Resampled data from the training data set has been used. Reproduced with permission from Springer Nature.

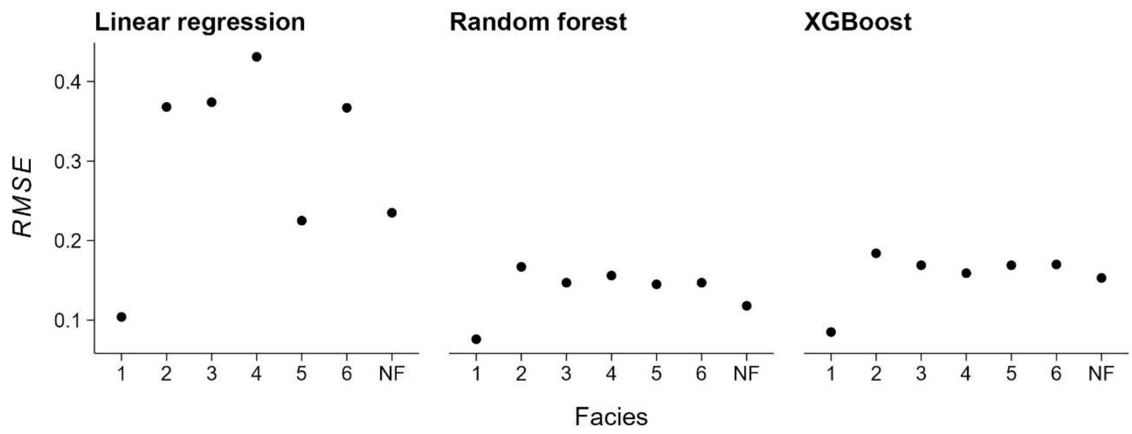

Figure 3.4: *RMSE* scores for each facies for the prediction of Mn^{2+} by linear regression, random forest and XGBoost models. NF refers to 'no facies'. Resampled data from the training data set has been used. Reproduced with permission from Springer Nature.

With random forest selected as the imputation algorithm, the model is fit to the testing data to compare observed Mn^{2+} with predicted Mn^{2+}. Some of the models performed better than others, with facies 3, 4 and 6 achieving R^2 scores of > 0.8 (Figure 3.5). These facies had a relatively higher concentration of mean Mn^{2+}, indicating they are likely from zones of reduced groundwater (Table 3.2). For the remaining facies, particularly 1 and 5, the models seemed to under-predict Mn^{2+}. These are relatively large facies (Table 3.2) and had a lower mean Mn^{2+} concentration, potentially indicating they are from more oxidised groundwater zones. In the absence of any hydrochemical facies (Figure 3.6), R^2 is > 0.8 overall, but under-predictions of Mn^{2+} are more likely compared to facies 3, 4 and 6. In all, the 1,032 missing Mn^{2+} values from facies with R^2 > 0.8 (3, 4 and 6) were able to be reliably imputed from the imputation data set out of a possible 8,634 (Figure 3.2, Table 3.2). Imputed data from these facies had a *RMSE* of < 0.2 mg/L (Figure 3.4). The mean Mn^{2+} concentration of facies 3, 4 and 6 is above the redox threshold for Mn^{2+} even with this error (Table 3.2), indicating errors in imputation will have little effect on redox classification.

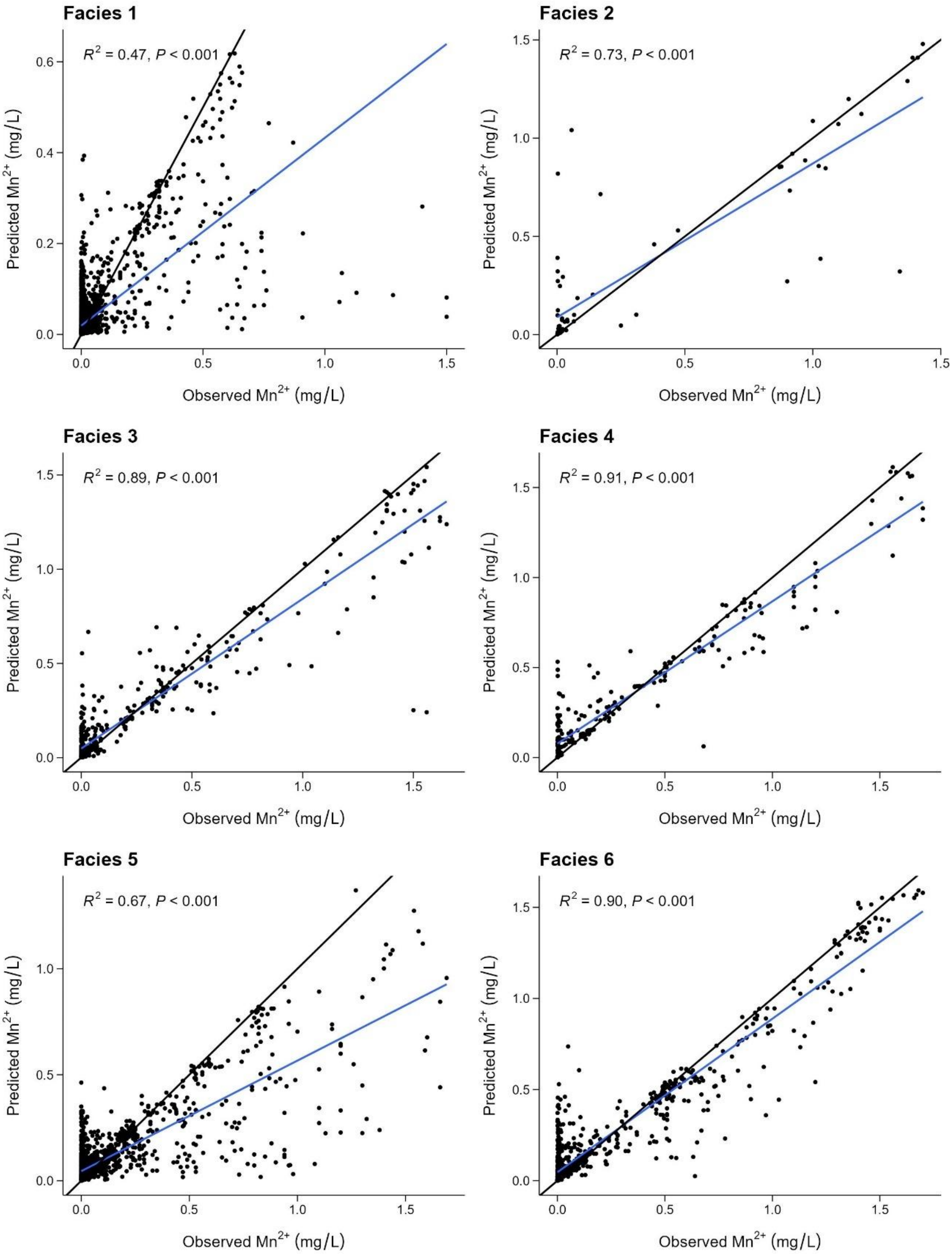

Figure 3.5: ***R^2*** **results for each random forest facies. Testing data has been used. The black line is the 1:1 line and the blue line is the regression line. Reproduced with permission from Springer Nature.**

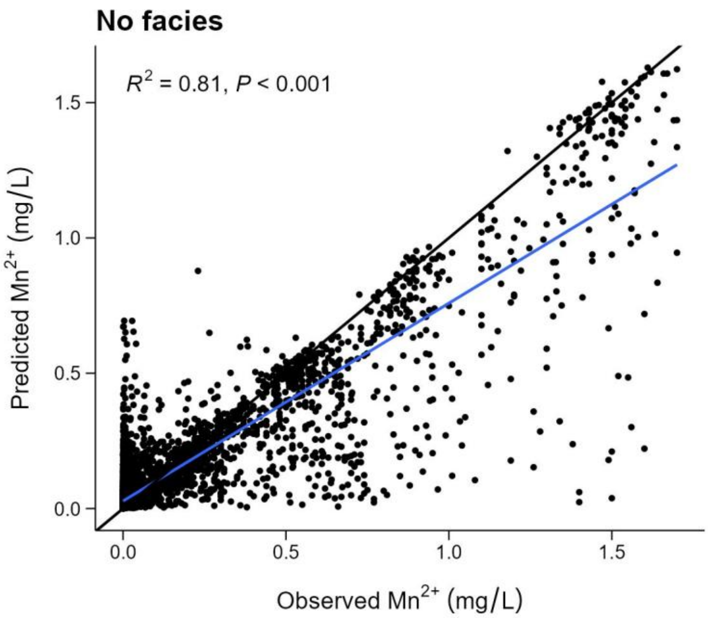

Figure 3.6: R^2 results for random forest where facies were not defined. Testing data has been used. The black line is the 1:1 line and the blue line is the regression line. Reproduced with permission from Springer Nature.

3.4.2 Groundwater redox classification

Table 3.3 summarises the redox assignments, made using the collated data set, with Close et al.'s (2016) classification criteria, and those made with the addition of imputed Mn^{2+} values. Most of the redox assignments are oxidised, followed by reduced and mixed. However, by including imputed Mn^{2+} values, the number of oxidised assignments slightly decreases while the number of mixed and reduced assignments increased by approximately 5 %. This is primarily because hydrochemical facies that had a higher mean Mn^{2+} concentration (Table 3.2) had a higher R^2 result and were therefore included for imputation. The imputation of missing Mn^{2+} values in the collated data set has helped classify otherwise indeterminate groundwater quality data, increasing the number of reduced samples in the data set. The physical distribution of these data demonstrates a strong bias towards the 'Aquifer' and 'Aquitard' hydrogeological units across New Zealand (Figure 3.7).

Table 3.3: Number of groundwater redox classifications determined with Close et al.'s (2016) redox classification before and after the inclusion of imputed Mn^{2+} values. Reproduced with permission from Springer Nature.

Redox status	n with Close et al. (2016)	n with Close et al. (2016) and imputed Mn^{2+}
Oxidised	23,628	23,507

Mixed	3,943	4,169
Reduced	6,102	6,429
Indeterminate	51,489	51,057
Total	85,162	85,162

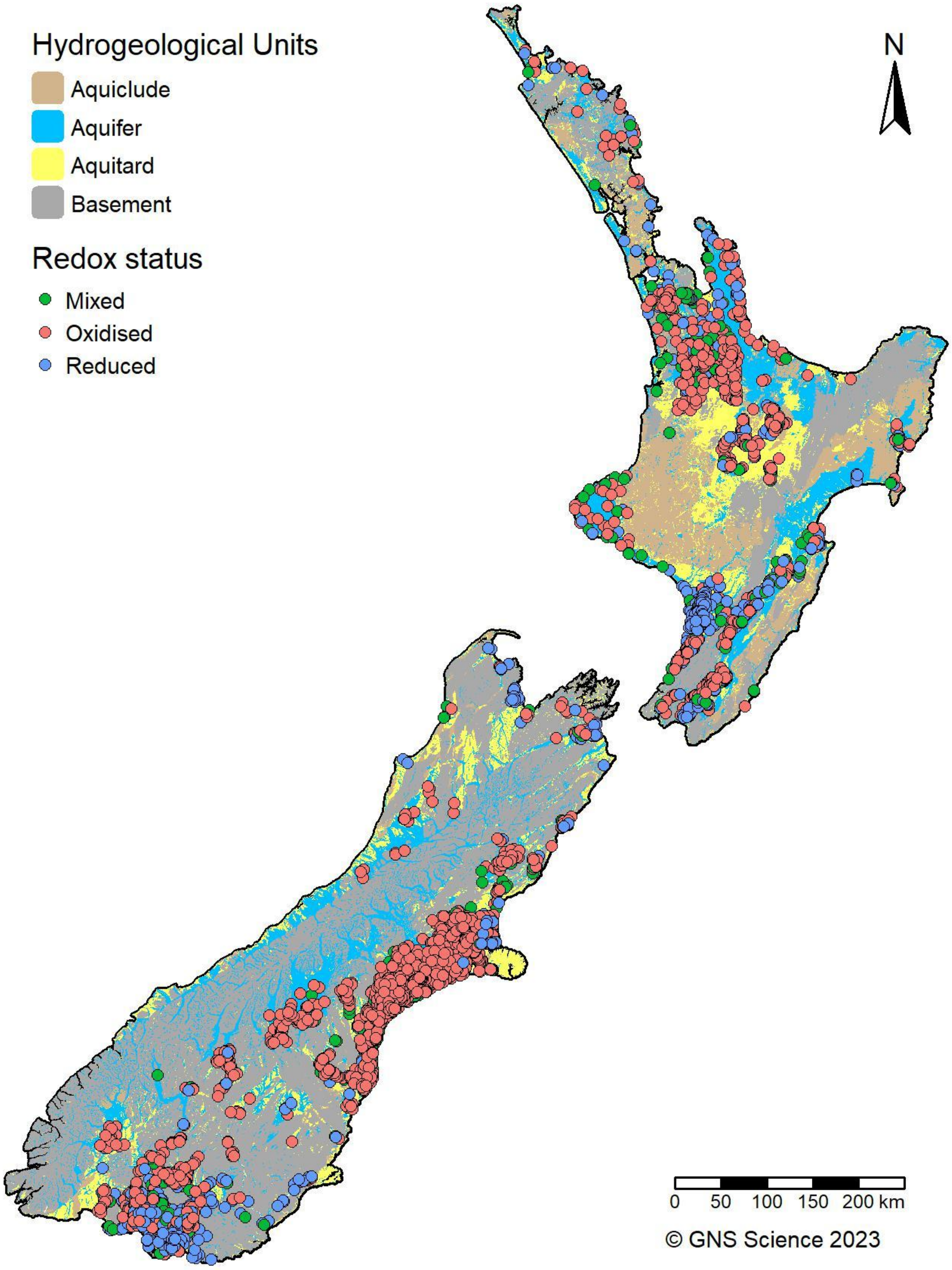

Figure 3.7: Physical location of groundwater redox classifications (derived from groundwater quality samples) across New Zealand.

The number of bores available for classification has increased steadily over the 30-year period from 1990 to 2019 (Figure 3.8), particularly since 2000. Although this growth has occurred over all three groundwater redox classes, oxidised groundwater has seen the largest growth in the New Zealand data set. This may reflect the fact that most groundwater in New Zealand aquifers is of a more oxidised nature, or it could reflect a bias in the location of bores in New Zealand (Figure 3.7). Existing groundwater production wells are installed in porous aquifer materials (such as gravels) that allow for higher rates of land surface recharge and groundwater flows, generally found in oxidised groundwater conditions. Furthermore, the existing groundwater data is sourced from wells that are in flat (78%), alluvial (60%) areas, which represent only 15% and 14% of agricultural landscapes across New Zealand (Section 3.4.3).

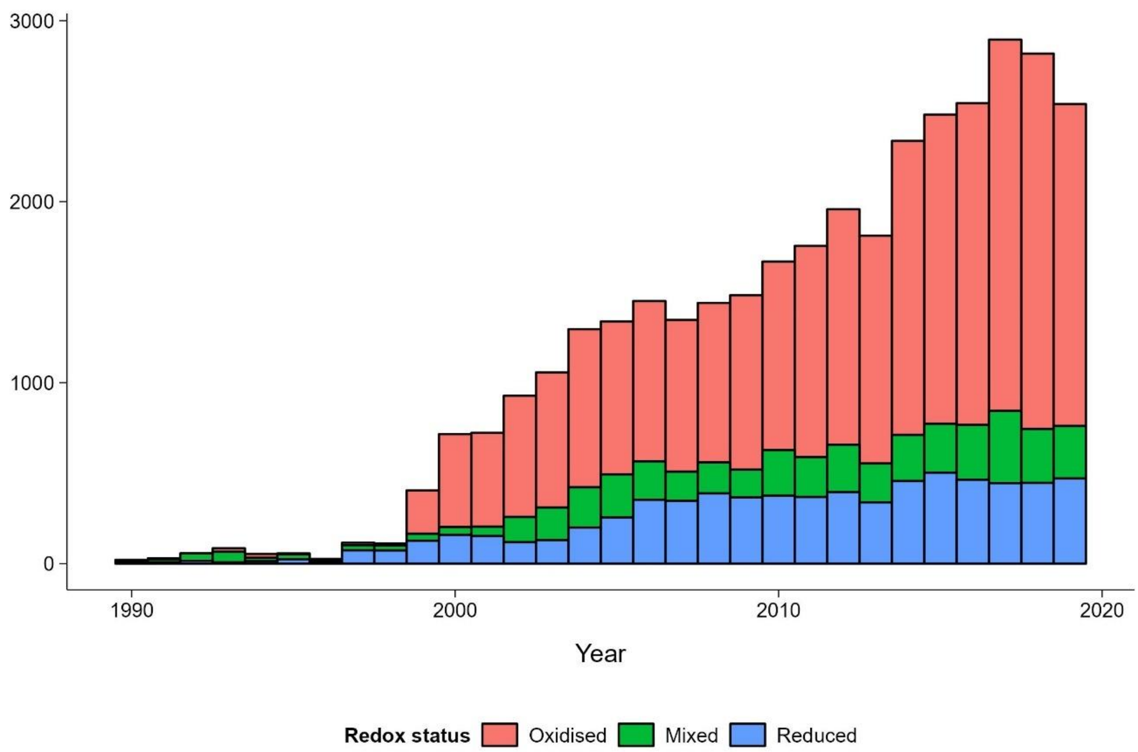

Figure 3.8: Number of groundwater redox classifications (derived from groundwater quality samples) made over a period of 30 years (1990-2019) across New Zealand. Reproduced with permission from Springer Nature.

Most of the available redox data has been sourced from bores < 50 m deep, with comparatively very few data points beyond 100 m (Figure 3.9). This limitation in available data notwithstanding, it appears that groundwater less than approximately 40 m deep is typically oxidised, highlighting the vulnerability of shallow groundwater to land use effects and the leaching of nitrate from the root zone. This depth of 40 m is arbitrary and is based on the relative distribution of redox status across depth (Figure 3.9). At depths beyond 40 m, the proportion of reduced groundwater increases, though not consistently, likely due to low sample numbers at these depths (Figure 3.9). The proportion of reduced groundwater increases in deeper bores, to around 50 %. Where groundwater is reduced, it is thought that deeper groundwater may provide the opportunity for denitrification to occur in aquifers because of the longer residence time (Severe et al., 2023).

Figure 3.9: Relative distribution of groundwater redox status (derived from groundwater quality samples) per depth across New Zealand. The number of samples is shown at the top of each bin. Reproduced with permission from Springer Nature.

3.4.3 Spatial variability of groundwater redox conditions

The national distribution of each attribute (e.g. mudstone) from each landscape characteristic (e.g. Rock type) was compared with the proportion of redox data that has been observed for those attributes (Table 3.4). This illustrates how representative an attribute is among the entire New Zealand redox data set. The relative distribution of each attribute was also shown for each redox status, i.e. oxidised, mixed, reduced, demonstrating how the mix of landscape attributes changes with redox status.

For Rock type (Table 3.4), groundwater redox data was under-represented for greywacke; metamorphic rocks; sandstone; mudstone; igneous rocks; volcanic ash over greywacke; argillite; volcanic ash over sandstone; conglomerate; loess over sandstone; alluvium over greywacke; and volcanic ash over mudstone across New Zealand landscapes. However, together, these rock type areas make up around 60 % of the total area nationally but were represented by only about 1 % of the groundwater redox data. Alternatively, the groundwater redox data was well- or over-represented for alluvium; volcanic deposits; volcanic ash; loess over alluvium; unconsolidated sediments; windblown sands; gravels; and loess over gravels. These rock types make up about 26 % of the total area nationally but were represented by 87 % of the groundwater redox data. Among the different rock types, differences in the distribution of redox status can also be observed. Some rock types are strongly oxidising, such as alluvium, volcanic/igneous deposits, and volcanic ash deposits, while others are more strongly reducing such as mudstone or windblown sands. Sandstone also offers a useful example of how redox status can change depending on what overlies it. Where Loess over Sandstone occurs, it was typically strongly reducing, however where Volcanic ash over Sandstone occurs it was rather more oxidising (Table 3.4). These findings may reflect the impact that geology has on groundwater residence times and the promotion of reducing conditions (Fenton et al., 2011, 2009; McAleer et al., 2017).

Gravel class is broadly split between those landscape units characterised as non-gravelly and those having some degree of gravel within them, ranging from slightly gravelly to extremely gravelly (Table 3.4). The groundwater redox data was roughly in proportion to the gravel classes at a national scale, with non-gravelly areas having a smaller proportion of the oxidised groundwater data and a larger proportion of the reduced groundwater redox data, as compared with all other sites with a gravel content.

Table 3.4: Distribution of groundwater redox data among rock types and gravel classes in New Zealand. Reproduced with permission from Springer Nature.

	NZ distribution (%)	Redox data (%)	Oxidised (%)	Mixed (%)	Reduced (%)
Rock type (Top rock over Base rock)					
Greywacke	17.4	0.2	23.6	70.9	5.5
Metamorphic rocks	14.2	0.0	NA	NA	NA
Alluvium	14.1	59.4	72.4	11.5	16
Sandstone	9.0	0.4	40.6	12	47.4
Other	5.3	0.3	44.6	18.8	36.6
Mudstone	4.9	0.1	45.3	3.8	50.9
Volcanic deposits	4.3	6.1	74.0	14.6	11.4
Igneous rocks	3.7	0.1	88.0	4.0	8.0
Not specified	3.6	6.0	54.1	15.1	30.8
Volcanic ash over Volcanic deposits	3.1	0.9	90.6	5.2	4.2
Volcanic ash	2.5	3.3	71.1	12.8	16.1
Argillite	2.3	0.0	NA	NA	NA
Volcanic ash over Greywacke	1.9	0.1	73.9	21.7	4.3
Loess over Alluvium	1.8	3.8	69.6	13.5	16.9
Volcanic ash over Sandstone	1.6	0.1	84.8	15.2	NA
Unconsolidated sediments	1.5	3.3	58.8	12.1	29.1
Conglomerate	1.3	0.0	NA	NA	NA
Loess over Sandstone	1.0	0.1	4.4	22.2	73.3
Windblown sands	1.0	5.0	39.6	15.9	44.5
Alluvium over Greywacke	0.9	0.0	NA	NA	NA
Volcanic ash over Mudstone	0.9	0.0	NA	NA	NA
Loess over Greywacke	0.8	0.1	51.7	31	17.2
Limestone	0.7	0.1	93.3	3.3	3.3
Gravels	0.6	5.2	57.3	15.7	27.0
Volcanic ash over Unconsolidated sediments	0.6	0.2	48.1	22.2	29.6
Loess	0.5	0.9	76.1	6.7	17.3
Loess over Gravels	0.5	1.3	41.7	29.0	29.2
Total	100.0	97.0	•	•	•
Gravel Class					
Non-gravelly	66.0	67.4	61.4	15	23.5
Slightly gravelly	18.7	7.6	81.6	7.9	10.5
Moderately gravelly	8.3	9.9	86.0	8.2	5.8
Very gravelly	1.2	9.1	84.5	6.0	9.5
Not specified	5.6	6.0	54.1	15.1	30.8
Extremely gravelly	0.2	NA	NA	NA	NA
Total	100.0	100.0	•	•	•

The New Zealand LRI Slope class includes eight primary classifications that have here been reclassed into four categories, ranging from flat and rolling to easy hill and steep hill (Table 3.5). In New Zealand, hill country has been defined as those slopes > 15°

(Kemp and Lopez, 2016) covering the easy hill and steep hill classes. The groundwater redox data was primarily concentrated on flat reliefs (87.1 %) compared to its national coverage of only 22.4 % of New Zealand's landscapes. This is due to groundwater being more accessible in these areas. The rolling slope category makes up a further 4.2 % of the groundwater redox data against its national coverage of around 8.5 %. The remaining slope classes (Easy hill and Steep hill) make up around 65 % of the national area coverage but were represented by only 3 % of the groundwater redox data. Interestingly, between the Flat and the Rolling classes, where most the redox data is contained, there was a decrease in the incidence of oxidised groundwater and an increase in reduced, however this trend reverses in hill country (Easy hill) where oxidised becomes the majority class again.

Table 3.5: Distribution of groundwater redox data among slope classes in New Zealand. Reproduced with permission from Springer Nature.

	NZ distribution (%)	Redox data (%)	Oxidised (%)	Mixed (%)	Reduced (%)
Slope class					
Flat (0-7°)	22.4	87.1	69.5	12.5	18
Rolling (8-15°)	8.5	4.2	40.8	17.4	41.8
Easy hill (16-25°)	26.8	2.5	61.6	12.4	26.0
Steep hill (>25°)	38.7	0.3	39.2	43.3	17.5
Not specified	3.6	6.0	54.1	15.1	30.8
Total	100.0	100.1	•	•	•

Flood class relates to the exposure a landscape unit has to flooding events with categories ranging from Nil to Very severe (Table 3.6). Those flood classes with some flood exposure risk (Slight to Very severe) had a higher proportion of redox data than their New Zealand distribution. A trend was apparent where the proportion of oxidised groundwater decreases, while the proportion of reduced groundwater increases, as flood class moves from Nil to Very severe. As riparian zones are hotspots for denitrification (Hill, 1990; McPhillips et al., 2015; Vidon and Hill, 2004), this could explain why the Severe and Very severe flood classes had the highest incidence of reduced groundwater.

Table 3.6: Distribution of groundwater redox data among flood class intervals in New Zealand. Reproduced with permission from Springer Nature.

	NZ distribution (%)	Redox data (%)	Oxidised (%)	Mixed (%)	Reduced (%)
Flood class					
Nil	87.2	67.0	73.1	10.9	16.0
Slight	4.2	17.1	68.3	16.3	15.4
Moderate	1.3	5.7	27.1	23.1	49.8
Moderately severe	1.1	1.9	69.9	11.3	18.8
Severe	0.3	1.1	19.2	15.0	65.8
Very severe	0.3	1.1	6.9	23.9	69.2
Not specified	5.6	6.0	54.1	15.1	30.8
Total	100.0	99.9	•	•	•

The soil chemical attributes of carbon class, phosphate retention, CEC class and pH class were reasonably well represented in the groundwater redox data (Table 3.7; Appendix B). Soil carbon content is considered to be an important requirement for subsurface denitrification, acting as the electron donor in heterotrophic denitrification (Rivett et al., 2008). Interestingly, between the low and very high soil carbon classes, the proportion of the oxidised groundwater redox samples decreased, while the proportion of reduced groundwater redox samples increased, reinforcing the importance of soil carbon to denitrification processes in the subsurface environment (Korom, 1992; Rivett et al., 2008; Xu and Li, 2024). The very low category, however, reversed this trend and was potentially an outlier. Similarly, the CEC class exhibited the same trend with an increase in the incidence of oxidised groundwater as the CEC class moves from Very high to Low. The Very low category was also an exception to the general trend and may be an outlier. The opposite trend emerged for phosphate retention where the proportion of oxidised groundwater decreases as the phosphate retention class moves from very high to very low, though the high class appeared also to be an outlier to this trend. Phosphorus losses have been found to be higher under reducing conditions than oxidising conditions (Shaheen et al., 2021), a trend which was observed in the phosphate retention data if the high class was considered an outlier (Appendix B). pH class does not exhibit any trend over the entire range, however, as pH class moves from Moderately low to Very low the incidence of oxidised groundwater decreases while reduced groundwater increased.

Table 3.7: Distribution of groundwater redox data among soil chemical and physical attributes in New Zealand. Reproduced with permission from Springer Nature.

	NZ distribution (%)	Redox data (%)	Oxidised (%)	Mixed (%)	Reduced (%)
Carbon class					
Very high	1.4	0.7	30.4	16.2	53.5
High	7.0	2.3	50.7	20.7	28.6
Medium	46.7	38.1	65.4	13.0	21.7
Low	35.2	47.3	74.2	11.3	14.5
Very low	4.1	5.5	43.3	21.8	34.9
Not specified	5.6	6.0	54.1	15.1	30.8
Total	100.0	99.9	•	•	•
pH class					
High	0.2	0.2	76.7	11.7	11.7
Moderately high	2.9	7.6	49.7	17.6	32.6
Near neutral	18.4	31.4	70.2	13.9	15.9
Moderately low	29.5	39.6	74.9	11.7	13.4
Low	26.5	13.5	55.4	11.4	33.2
Very low	16.9	1.8	43.4	9.7	46.9
Not specified	5.6	6.0	54.1	15.1	30.8
Total	100.0	100.1	•	•	•
Drainage class					
Very poor	1.3	1.5	44.0	15.0	41.0
Poor	4.8	14.5	33.2	19.6	47.2
Imperfect	14.5	9.1	63.1	15.6	21.3
Moderately well	20.3	17.0	77.4	9.7	13.0
Well	53.5	52.0	76.0	11.4	12.6
Not specified	5.6	6.0	54.1	15.1	30.8
Total	100.0	100.1	•	•	•
Permeability class					
Slow	3.3	6.4	23.9	22.4	53.7
Moderate	78.9	67.9	73.8	11.8	14.4
Rapid	11.2	18.8	63.0	13.3	23.7
Not specified	6.5	6.9	51.6	15.1	33.3
Total	99.9	100.0	•	•	•

Groundwater redox data was also reasonably well spread among soil physical attributes including soil drainage, plant rooting depth, permeability, profile available water and macroporosity (Table 3.7; Appendix B). At a national scale, most landscape units in New Zealand were characterised as well-drained soils and the groundwater redox data was highly associated with drainage class. The highest proportion of oxidised groundwater redox samples were associated with moderately well and well-drained soil classes, and the highest proportion of reduced groundwater redox samples were associated with the very poor and poor soil drainage classes. Drainage class is thought to be important to denitrification due to how dissolved oxygen diffuses through the soil profile (Burbery, 2018; Clague et al., 2019; Wu et al., 2018). Infiltration and recharge occur at a faster rate in well-drained soils, such as those underlain by gravel and coarse alluvium, which leads to oxidised conditions (Deakin et al., 2016; Orr et al., 2016). Some exceptions may exist such as coastal sandy soils with shallow groundwater levels upwelling from regional groundwater flow (Thomas, 2017). Similar associations appeared for soil permeability in the data where the slow permeability class was dominated by reduced groundwater; and for soil macroporosity where the proportion of oxidised samples reduced from high to low classes (Table 3.7). Drainage class, soil permeability and macroporosity may also reflect the dynamics explored in the rock type discussion, perhaps lengthening residence times and promoting reducing conditions. The Slow permeability class exhibited the lowest incidence of oxidised groundwater, and the highest incidence of reduced groundwater, compared to the Moderate and Rapid classes. Similarly, for macroporosity, as the classes move from High to Low, the incidence of oxidised groundwater decreased while the incidence of reduced groundwater increased. Similar trends were not able to be identified for plant rooting depth or profile available water (Appendix B).

3.4.4 Temporal stability of groundwater redox conditions

The redox assessment for individual monitoring sites with ten or more groundwater quality sample results was categorised according to the stability of redox status over time (Table 3.8). Most of the oxidised sites remained stable ≥ 90 % of the time, and only 4 % of the sites were stable for 50 % to 70 % of the time. There were fewer sites overall assessed as being mixed or reduced (Table 3.3), however, compared with the oxidised sites there was less stability for the mixed and reduced data overall. Only a minority of the mixed and reduced redox sites were stable ≥ 90 % of the time, compared with the other classes. As reflected in Figure 3.9, the oxidised sites are, on average, shallower depth bores than the reduced sites. Redox stability reduced at increasing depth for oxidised groundwater, while no such trend was apparent for reduced groundwater, showing a reasonably consistent depth with reducing redox stability (Table 3.8).

Table 3.8: Groundwater redox stability over time. Groundwater sites with more than 10 redox results have been categorised based on their stability over time. Mean and median bore depths are also shown. Reproduced with permission from Springer Nature.

Redox stability	n	Bore depth (m)	
		Mean	Median
Oxidised ≥ 90%	552	27.6	17.0
Oxidised 80-89%	63	19.3	9.4
Oxidised 70-79%	31	28.1	23.0
Oxidised 60-69%	15	23.7	10.0
Oxidised 50-59%	10	88.1	44.1
Mixed ≥ 90%	21	12.6	10.5
Mixed 80-89%	11	21.2	15.0
Mixed 70-79%	14	31.3	17.4
Mixed 60-69%	23	33.7	18.0
Mixed 50-59%	15	16.8	12.0
Reduced ≥ 90%	51	52.3	44.6
Reduced 80-89%	42	43.8	32.8
Reduced 70-79%	35	46.1	31.8
Reduced 60-69%	25	60.1	48.5
Reduced 50-59%	24	46.9	43.5

These findings may reflect groundwater recharge dynamics, where oxygenated sources of recharge displaces or mixes with groundwater as it moves through the unsaturated zone. Due to contact with the atmosphere, oxygen is supplied to groundwater via river losses or by precipitation (Morgenstern et al., 2017; Rosen and White, 2001; Scott, 2015). Studies in managed aquifer recharge demonstrate how redox conditions can cause a change in water quality and the overall redox status of groundwater depending on the state of the existing water and the recharge water (Barbieri et al., 2011; Seibert et al., 2016). Where oxygenated recharge water comes into contact with already oxidised groundwater there may be no change to the overall chemistry of the receiving water, however where the groundwater is reduced the oxygenated recharge water may cause the precipitation of solids due to redox changes (Barbieri et al., 2011; Hübner et al., 2022; Seibert et al., 2016). The results of this study (Table 3.8) suggest that the mixed and reduced groundwaters were less stable groundwater types compared to the oxidised groundwater. However, it is unknown what accounts for this difference but could be due to groundwater recharge dynamics specific in individual catchments.

3.5 Conclusion

This study presents an assessment of the spatial variability and temporal stability of groundwater redox conditions across New Zealand. Groundwater redox status was highly spatially variable among landscape characteristics. While the redox data were primarily sourced from a few rock types, variations in redox status distribution were observed. Rock types such as alluvium, limestone, volcanic/igneous deposits, and volcanic ash deposits were primarily associated with oxidising groundwaters, whereas rock types such as mudstone or windblown sands were more often associated with reducing conditions. Coarse-textured, free-draining soils over gravels with low soil carbon content were mostly found in flat landscapes with rapid soil drainage, where groundwater redox status was predominantly oxidised. Although these areas represent a small proportion of New Zealand's total area, they are hugely important to agriculture. In contrast, soil types with poor drainage, slow permeability and low microporosity were more likely to exhibit reduced groundwater redox status. Moreover, most the oxidised redox sites demonstrated stability ≥ 90 % of the time, whereas only a minority of the mixed and reduced sites exhibited this level of stability. While oxidised sites were, on average, shallower than reduced sites, redox stability decreased with depth for oxidised groundwater, a trend not observed in reduced groundwater. This spatial and temporal variability in subsurface redox conditions may significantly influence the transformation and transfer of nitrate from farming activities across different hydrogeological land units, impacting water quality in receiving waters.

Chapter 4: Modelling and mapping of subsurface nitrate-attenuation index in agricultural landscapes

Brief introduction for thesis

This chapter develops a spatial framework known as the Landscape Subsurface Nitrate-Attenuation Index (*LSNAI*). Building on the dataset from Chapter 3, a machine learning model is trained to predict landscape unit subsurface redox conditions. These predictions are then combined with rock type and soil drainage attributes in an unsupervised classification to map five *LSNAI* categories, ranging from *Very Low* to *Very High* subsurface nitrate attenuation potential.

This chapter has been published as:

Collins, S.B., Singh, R., Mead, S.R., Horne, D.J., 2025a. Modelling and mapping of subsurface nitrate-attenuation index in agricultural landscapes. J. Environ. Manage. 384, 125628. https://doi.org/10.1016/j.jenvman.2025.125628

This graphical abstract was also published with the article:

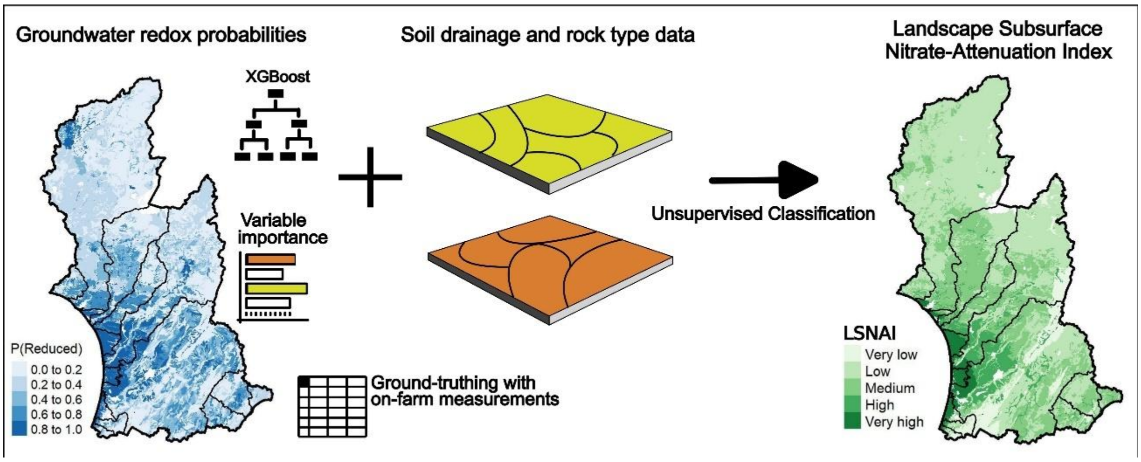

4.1 Abstract

Environmental management of nutrient losses from agricultural lands is required to reduce their potential impacts on the quality of groundwater and eutrophication of surface waters in agricultural landscapes. However, accurate accounting and management of nitrogen losses relies on a robust modelling of nitrogen leaching and its potential attenuation – specifically, the reduction of nitrate to gaseous forms of nitrogen – in subsurface flow pathways. Subsurface denitrification is a key process in potential nitrate attenuation, but the spatial and temporal dynamics of where and when it occurs remain poorly understood, especially at catchment-scale. In this paper, a novel Landscape Subsurface Nitrate-Attenuation Index (*LSNAI*) is developed to map spatially variable subsurface nitrate attenuation potential of diverse landscape units across the Manawatū-Whanganui region of New Zealand. A large dataset of groundwater quality across New Zealand was collated and analysed to assess spatial and temporal variability of groundwater redox status (based on dissolved oxygen, nitrate and dissolved manganese) across different hydrogeological settings. The Extreme Gradient Boosting algorithm was used to predict landscape unit subsurface redox status by integrating the nationwide groundwater redox status data set with various landscape characteristics. Applying the hierarchical clustering analysis and unsupervised classification techniques, the *LSNAI* was then developed to identify and map five landscape subsurface nitrate attenuation potential classes, varying from very low to very high potential, based on the predicted groundwater redox status probabilities and identified soil drainage and rock type as key influencing landscape characteristics. Accuracy of the *LSNAI* mapping was further investigated and validated using a set of independent observations of groundwater quality and redox assessments in shallow groundwaters in the study area. This highlights the potential for further research in up-scaling mapping and modelling of landscape subsurface nitrate attenuation index to accurately account for spatial variability in subsurface nitrate attenuation potential in modelling and assessment of water quality management measures at catchment-scale in agricultural landscapes.

4.2 Introduction

Around the world, the need to provide food and fibre to growing populations has led to the intensification of agricultural land (Alexander et al., 2015; Fróna et al., 2019; Godfray and Garnett, 2014; Tscharntke et al., 2012). This has subsequently led to an increase in the leaching and runoff of agriculturally-sourced nutrients to receiving waters, causing eutrophication and related environmental and human-health issues (Keatley et al., 2011; Savage et al., 2010; Withers et al., 2014). Inorganic nitrogen is a readily available nutrient for algae/periphyton growth in streams and rivers, posing potential toxicity effects to aquatic life, and degrading drinking water quality supplies posing risks to human health. Nitrate is generally the main form of inorganic nitrogen leached to groundwaters and in streams and rivers (Dymond et al., 2013; Mcdowell et al., 2009). In New Zealand, the National Policy Statement for Freshwater Management has been developed to reduce nutrient losses and meet water quality objectives on a regional basis (Ministry for the Environment, 2024). As a response, various good management practices and land use scenarios need to be modelled to help assess where and how nitrate losses from agricultural lands are to be reduced or managed at catchment-scale. However, due to varying rates of potential nitrate attenuation 'reduction' in subsurface environments, it is difficult to accurately model these scenarios (Elwan, 2018; Singh et al., 2017b; Snelder et al., 2020). To overcome these challenges, new knowledge and tools to map and model spatially variable subsurface nitrate attenuation capacities at landscape unit scale are required for the development of targeted and effective mitigation strategies for nitrate losses from agricultural lands.

Nitrate's transport and fate in the subsurface is strongly influenced by landscape characteristics such as soil type, underlying geology and groundwater chemistry (Elwan, 2018; Jahangir et al., 2012; McAleer et al., 2017; Orr et al., 2016; Rivas et al., 2017). In this study, these landscape characteristics are referred to as landscape factors, which can be mapped to assess their potential influence on nitrate attenuation in the subsurface environment. Denitrification, where nitrate is transformed to gaseous forms of nitrogen under favourable conditions (Korom, 1992; Rivett et al., 2008), is usually the primary pathway for nitrate attenuation in subsurface flow pathways (Clague et al., 2019; Clague et al., 2015; Collins et al., 2017; Jahangir et al., 2013a; Rivas et al., 2020, 2017). However, field-based measurements of subsurface denitrification are complicated, conducted infrequently, and limited to only a few regions with a narrow range of soil and rock type combinations (Burbery, 2018). This lack of relevant data makes it difficult to correlate subsurface denitrification potential with the natural variability of landscape characteristics, posing a practical challenge for predicting and mapping landscape subsurface nitrate attenuation potential.

To gain the spatial reach that subsurface denitrification data lacks, groundwater redox conditions have been used as a proxy for nitrate attenuation potential because of observations of subsurface dentification in reduced groundwater conditions (Clague et al., 2019; Collins et al., 2017; Rivas et al., 2020, 2017; Stenger et al., 2018). With the availability of extensive data sets including those for groundwater quality, soil, and geology, variability of groundwater redox conditions have been mapped in New Zealand and elsewhere (Close et al., 2016; Knoll et al., 2020; Koch et al., 2024, 2019; Rosecrans et al., 2017; Sarris et al., 2019; Tesoriero et al., 2024, 2015; Wilson et al., 2020, 2018). While the international research effort has been focused on identifying the depth of the subsurface redox interface (Hansen et al., 2014; Koch et al., 2019; Tesoriero et al., 2015), the focus in New Zealand has been on assessment of spatial variability of groundwater redox states and the depth at which they occur (Close et al., 2016; Wilson et al., 2020, 2018). In particular, efforts have been focused on reducing selection bias in the groundwater data (Wilson et al., 2020) and reducing uncertainty in assessment of groundwater redox status across different landscapes (Sarris et al., 2024).

However, a robust management of water quality measures require tools to estimate and reduce nitrate fluxes in different flow pathways from agricultural lands at catchment-scale. While methods have been developed and refined to estimate catchment-scale nitrogen loads (Fraser, 2021; Snelder et al., 2020, 2017), the gap that currently exists is a robust assessment and effective accounting of subsurface nitrate attenuation in New Zealand catchments (Singh et al., 2017a; Snelder et al., 2020). Accounting of subsurface nitrate attenuation can inform both farm- and catchment-scale land use decisions and implementation of targeted water quality measures. However, further research is required to develop practical tools for a robust assessment and accounting of subsurface nitrate attenuation potential at catchment-scale that can accurately represent estimation and reduction of nitrate loads to streams and rivers in agricultural landscapes.

This paper aimed to review and further develop a Landscape Subsurface Nitrate-Attenuation Index (*LSNAI*) to map subsurface nitrate attenuation potential of diverse hydrogeological settings across the Manawatū-Whanganui region, located in the lower North Island of New Zealand. It defines *LSNAI* and presents a novel methodology for analysing and integrating landscape hydrogeological variability, groundwater redox assessments, and on-farm shallow groundwater observations to predict and validate a regional-scale *LSNAI* map of different landscape units across the study area. Whereas previous studies predicting New Zealand groundwater redox conditions have employed linear discriminant analysis (Close et al., 2016; Wilson et al., 2018), or tested a range of machine learning algorithms (Friedel et al., 2020), this study evaluates and applies extreme gradient boosting (XGBoost) to predict groundwater redox status (Chen and Guestrin, 2016). XGBoost is a flexible algorithm which is increasingly being used in hydrological studies (Niazkar et al., 2024; Ransom et al., 2022). This study develops a novel modelling approach, integrating applications of machine learning (XGBoost) and unsupervised classification techniques, to classify and map spatially variable subsurface nitrate attenuation potential of different landscape units. A robust approach is taken to validating predictions by using field-scale measurements of shallow groundwater denitrification and redox data to independently verify landscape unit subsurface redox classifications. Finally, the landscape unit subsurface redox predictions and key landscape factors learned from the model training process are used to classify and map landscape units into groups of relatively high to low subsurface nitrate attenuation potential classes. The study provides new insights into the spatial variability of landscape factors' potential influences on subsurface nitrate attenuation and its transport pathways from agricultural lands to receiving waters in diverse hydrogeological landscapes. It generates new information and knowledge to further develop accurate catchment-scale water quality models to robustly quantify potential impacts of various land use scenarios and management practices for targeted and effective water quality measures across agricultural landscapes.

4.3 Data and methods

4.3.1 Study area

This study focused as a case study on the Manawatū-Whanganui region of New Zealand, also known as the Horizons region (Figure 4.1). The region covers 22,215 km^2 (2,221,500 ha) and is characterised by several large river catchments that discharge into the Tasman Sea on the west coast (Figure 4.1a). Local geology ranges from Mesozoic-age basement greywacke exposed in the southern part of the region; an abundance of unconsolidated Plio-Pleistocene-age deposits throughout; and volcanic deposits in the north (Figure 4.1b; Begg et al., 2005). The Manawatū catchment is divided by two mountain ranges, known as the Ruahine and Tararua ranges, with the river flowing east to west through a narrow gorge, known as the Manawatū Gorge (Figure 4.1a, Figure 4.1b). These two mountain ranges are formed by greywacke bedrock, shown in Figure 4.1b, with Ruahine in the north and Tararua in the south.

Groundwater resources are limited to two distinct basins that have developed either side of the Ruahine and Tararua ranges (Figure 4.1c). On the eastern side, unconsolidated gravel and sand within the main river valleys, which rest on Tertiary-age mudstone, forms the main groundwater resource across Tararua valleys in the Manawatū catchment (Zarour, 2008). The groundwater resources on the western side are part of the Whanganui Basin, a deep sedimentary basin characterised by marine and alluvial deposits (Carter and Naish, 1998). Groundwater recharge and discharge dynamics also differ between these basins. On the eastern side, rainfall recharge infiltrates quickly into the shallow aquifer and discharges into the local rivers making for relatively short groundwater mean residence times (Morgenstern et al., 2017). Groundwater recharge is thought to reach much deeper depths on the western side, with groundwater discharging at the coastal margin into shallower groundwater and springs due to an upwards vertical hydraulic gradient (Thomas, 2017). Groundwater mean residence times are also significantly longer on the western side (Morgenstern et al., 2017). However, in most cases, groundwater abstraction is associated with Late Quaternary deposits (Zarour, 2008).

Land use ranges from native forest/conservation land and low intensity farming in steep and hill country areas, to intensive agriculture such as dairy farming and cropping on the river plains and coastal areas (Figure 4.1d). Soils in the region are primarily considered well-drained (Newsome et al., 2008), though drainage characteristics are highly dependent on a soil's landscape position (Cowie et al., 1967; Cowie and Rijkse, 1977). A unique feature of the region is the sand dune formations on the region's west coast that have developed over the late Holocene. A major component of these dune formations is the titanomagnetite-rich ironsands that have been deposited along the coast by onshore winds, the source of which is erosion of andesitic volcanic rocks of nearby Taranaki volcanoes, located north-west of the Horizons region (Brathwaite et al., 2017).

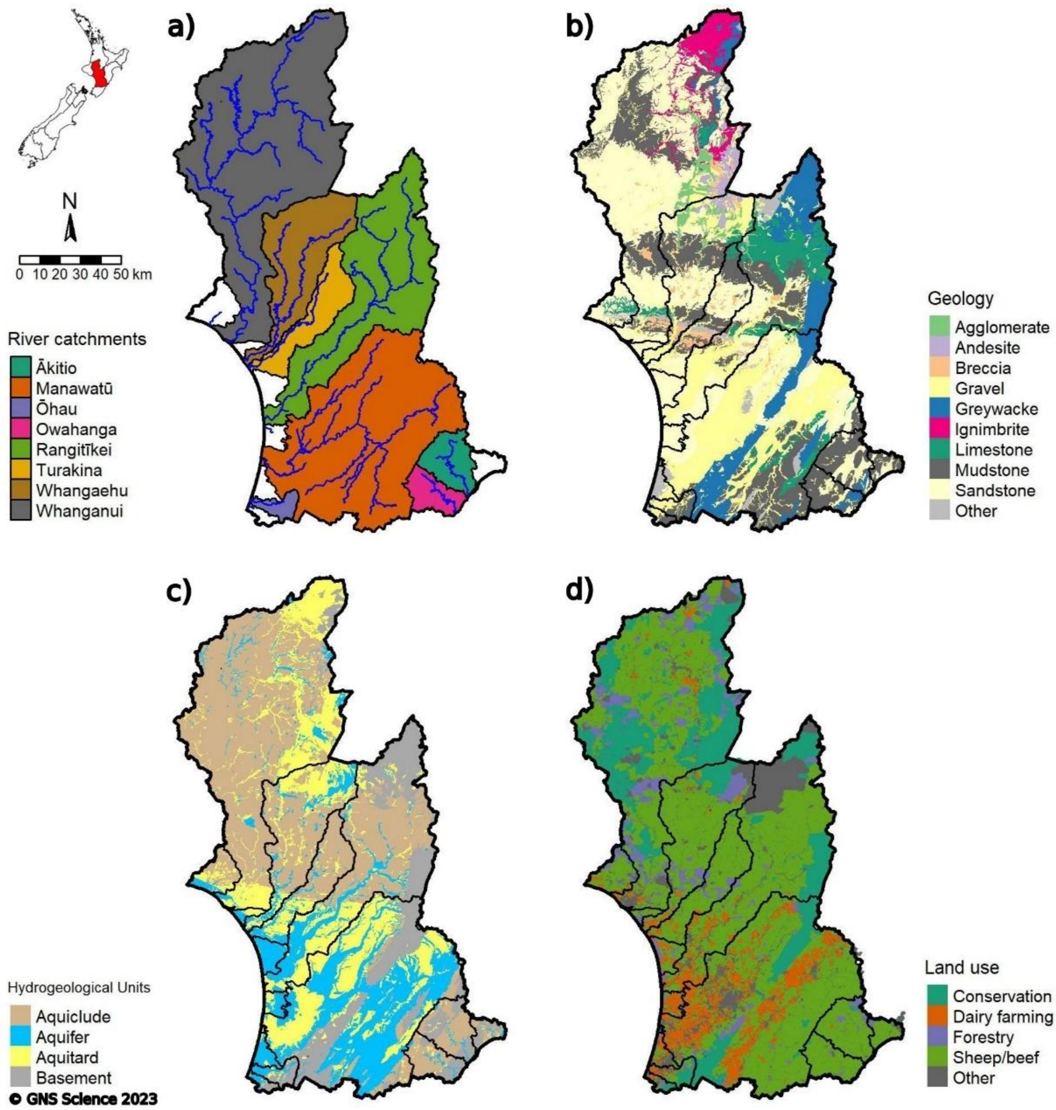

Figure 4.1: Maps of a) the main river catchments, b) geological types (GNS Science, 2012), c) hydrogeological units (White et al., 2019) and d) land uses (Herzig et al., 2020) across the Manawatū-Whanganui region of New Zealand, also known as the Horizons region.

4.3.2 Groundwater redox assessments and landscape characteristics

Collins et al. (2025) collated and analysed a comprehensive groundwater data set collected over the 30-year period from 1990 to 2019 across 15 regions of New Zealand. These data were collected primarily from domestic/drinking water wells, farm supply and irrigation wells, or monitoring wells. The groundwater samples were sourced from a range of depths, with most groundwater samples taken from depths of 50 m or less (Collins et al., 2025b). The groundwater quality data were classified into groundwater redox status as per the groundwater redox classification by Close et al. (2016), which was modified from McMahon and Chapelle (2008) for New Zealand conditions. It classifies groundwater redox status based on the thresholds of dissolved oxygen (DO) < 1.0 mg/L; nitrate-nitrogen (NO_3^--N) < 0.5 mg/L; and dissolved manganese (Mn^{2+}) > 0.05 mg/L (Close et al., 2016; Collins et al., 2025b). The collated groundwater dataset included some missing Mn^{2+} values (an important redox variable), which were imputed using locally-developed random forest regression models between observations of Mn^{2+} and Ca^{2+}, Mg^{2+}, K^+, Na^+ and Cl^- values in the groundwater dataset (Collins et al., 2025b). Across the study area, shallow groundwater was classified predominantly oxidised, whereas the reduced groundwater conditions were assessed more frequently at greater depths (Collins et al., 2025b). Refer to Collins et al. (2025b; Chapter 3) for further details on the assessment of the collated groundwater quality dataset and its application for assessing the spatial variability and temporal stability of groundwater redox conditions across New Zealand regions. The collated national-scale groundwater data set resulted in 34,098 individual groundwater redox assessments from 3,764 wells across New Zealand, of which 1,242 groundwater redox assessments were located across the Horizons region from 227 wells. Table 4.1 summarises the basic statistics associated with the classification of the national-scale groundwater data set into either an oxidised, mixed or reduced category (Collins et al., 2025b). Oxidised groundwater is the majority category and typically has higher mean and median DO and NO_3^--N concentrations, while reduced groundwater has higher mean and median dissolved Mn^{2+} and Fe^{2+} concentrations. This pattern conforms to the general understanding of subsurface redox conditions (Rivett et al., 2008).

Table 4.1: A summary of New Zealand groundwater quality data as per their redox status.

Redox Status	n	Parameter	Mean	Median	Min	Max	Standard deviation
Oxidised	23,504	DO (mg/L)	6.58	6.90	1.00	11.85	2.42
		NO_3^--N (mg/L)	4.90	3.80	<0.01	25.00	4.47
		Mn^{2+} (mg/L)	0.01	<0.01	<0.01	0.05	0.01
		Fe^{2+} (mg/L)	0.05	0.01	<0.01	8.20	0.18
		SO_4^{2-} (mg/L)	12.13	9.20	0.01	100.00	11.00
Mixed	4171	DO (mg/L)	2.27	1.15	0.01	11.64	2.50
		NO_3^--N (mg/L)	1.79	0.20	<0.01	25.00	3.49
		Mn^{2+} (mg/L)	0.26	0.10	<0.01	1.70	0.35
		Fe^{2+} (mg/L)	1.01	0.11	<0.01	15.00	2.20
		SO_4^{2-} (mg/L)	14.09	8.00	0.01	100.00	18.73

		DO (mg/L)	0.21	0.15	0.01	0.99	0.20
		NO_3^--N (mg/L)	0.04	0.01	<0.01	0.50	0.08
Reduced	6423	Mn^{2+} (mg/L)	0.44	0.27	0.05	1.70	0.41
		Fe^{2+} (mg/L)	2.53	1.20	<0.01	15.00	3.16
		SO_4^{2-} (mg/L)	7.53	2.60	0.01	99.90	12.96

Within the Horizons region, groundwater redox data was sourced from a depth of 2 m to 235 m (Table 4.2). Like the national data set, these data were collected from groundwater wells primarily used for domestic/drinking water, farm or industrial use. The groundwater data were collected from 1990, though particularly from 2000 when the frequency and coverage of groundwater monitoring increased in the study region. Oxidised groundwater was, on average, assessed at shallower depths, compared to more mixed or reduced groundwater assessed at relatively deeper groundwater depths (Table 4.2).

Table 4.2: A summary of depth of groundwater wells, in metres below ground level, from which groundwater redox data was sourced from within the Horizons region. p25 and p75 refer to the 25th and 75th percentile.

Redox Status	n	Min (m)	p25 (m)	Median (m)	Mean (m)	p75 (m)	Max (m)
Oxidised	548	2.0	10.5	17.0	19.3	22.3	135
Mixed	134	2.0	10.6	27.0	45.9	68.6	134
Reduced	560	2.6	18.0	30.3	49.5	68.6	235

A geographical dataset of landscape attributes and landscape unit boundaries was obtained from the New Zealand Land Resource Inventory (NZLRI; Newsome et al., 2008). The NZLRI is an inventory of five physical factors, soil, rock type, slope, presence and severity of erosion, and vegetation, mapped at a scale of 1:50,000, that drive land use capability mapping in New Zealand (Lynn et al., 2009). In addition, the NZLRI is supplemented with 16 additional soil properties collectively known as the Fundamental Soil Layers (FSL; Barringer et al., 1998; Newsome et al., 2008). Together, these geographical data sets provide around 100,000 polygons (landscape units) across New Zealand featuring a range of landscape attributes.

In this study, a total of fourteen attributes were selected from the NZLRI and the FSL to represent landscape characteristics, potentially related to redox processes in the subsurface environment (Collins et al., 2025b). These include top rock, base rock, slope, carbon content, gravel content, soil drainage, permeability, profile available water

(PAW), pH, cation exchange capacity (CEC), phosphorus retention, plant rooting depth, flood class, and macroporosity. Each groundwater observation was spatially linked to the landscape polygon (i.e. landscape unit) in which the well was located, and the values of the corresponding landscape attributes were assigned accordingly. A complete list of these variables and their categories can be found in the supplementary data file.

In the NZLRI (Newsome et al., 2008), the top rock and base rock are derivations of rock type mapped across the landscape. Top rock is the first-named entire rock type, irrespective of any underlying stratigraphy and can have several lithology expressions depending on the dominance of the rock types in a single polygon unit. Base rock is the single value that identifies the principal basement lithology (Newsome et al., 2008). In this study, these have been merged as 'top rock over base rock' and reclassified as 'Rock type'. Where top rock and base rock are the same, just the single attribute is described (e.g. 'Greywacke over Greywacke' becomes 'Greywacke') and where they are distinct, both attributes have been retained (e.g. 'Loess over Alluvium'). In addition, for both top rock and base rock types, the various ash deposits have been reclassified as 'volcanic ash'. Other kinds of volcanic deposits that are not ash have been reclassified as 'volcanic deposits'. This helped reduce and simplify the number of variables for rock type.

Slope, which has eight classes, refers to a physiographic area of relatively homogeneous average relief. It is derived from stereo aerial photograph interpretation and field verification and allows up to two slope expressions within a single polygon (Newsome et al., 2008). In this study, just the first/dominant named slope attribute class has been retained (e.g. 'Moderately steep + Steep' becomes 'Moderately steep'). Permeability refers to the rate at which water moves through saturated soil and includes three classes, 'Slow', 'Medium' and 'Rapid', of which multiple combinations are possible in layered soils (Clayden and Webb, 1994). In this study, just the first named permeability attribute class has been retained (e.g. 'Moderate/Rapid' becomes 'Moderate'). The remaining attributes of carbon content; gravel; soil drainage; PAW; pH; CEC; phosphorus retention; potential rooting depth; flood class; and macroporosity have been retained as they are described in (Newsome et al., 2008). In all cases, unrelated categories within these variables e.g., lakes, estuaries, towns/cities, have been classified as 'Not specified'.

New Zealand’s groundwater redox data is unevenly distributed among some landscape variables (Collins et al., 2025; Chapter 3). For example, groundwater redox data was reasonably well distributed among the different categories of carbon class, soil drainage class and permeability class. However, it was somewhat more unevenly distributed among some rock type categories. Alluvium, gravels and windblown sands were over-represented in the groundwater redox data set (relative to their New Zealand distribution), while sandstone and mudstone were under-represented. This tends to reflect the hydrogeological conditions where groundwater can be accessed, primarily those areas characterised by alluvium, gravels and windblown sands (Zarour, 2008).

4.3.3 Prediction of landscape unit subsurface redox status

The collated groundwater redox status and landscape factors were modelled to predict and map the subsurface nitrate attenuation potential of landscape units across the study area. The model predictions do not consider any potential for nitrate attenuation in the soil profile, unsaturated zone, riparian or in-stream environments of the landscape. However, the groundwater redox status is used as a proxy of the landscape subsurface redox status and nitrate attenuation potential, as observed by field studies in New Zealand landscapes and elsewhere (Clague et al., 2019; Collins et al., 2017; Jahangir et al., 2013a; Kruisdijk et al., 2022; Rivas et al., 2020, 2017; Steiness et al., 2021; Yang et al., 2023).

The groundwater redox classification by Close et al. (2016) included a ‘mixed’ status, however in this study only the probability of a landscape unit being classified as either ‘oxidised’ or ‘reduced’ in its subsurface environment was predicted for classification and mapping. The mixed groundwater redox status is characterised by relatively high values across all the redox-related hydrochemistry variables (Table 4.1), making its implication somewhat unclear for assessment of landscape subsurface nitrate attenuation potential of a landscape unit.

The collated national-scale groundwater redox data set (Collins et al., 2025b; Chapter 3) and associated landscape attributes were used to train and test an XGBoost model that predicted a landscape unit’s subsurface redox status probability as either oxidised or reduced. The XGBoost model training data set consisted of point-level groundwater redox status observations distributed across New Zealand (classified as oxidised or reduced)

(Collins et al., 2025b), which were used as the response variable alongside landscape-level predictors such as rock type, soil drainage and carbon classes. While only areas with groundwater redox observations available were included in the training data set, the trained model was applied to predict the subsurface redox status of all ~11,000 landscape units within the Horizons region, including those without direct groundwater redox data. This approach uses the relationships learned by the XGBoost model in the training datasets to generate robust predictions of subsurface redox status in areas lacking direct groundwater observations.

The XGBoost algorithm was used to predict landscape unit redox status probabilities for the Horizons region, i.e. P(Oxidised) and P(Reduced). The XGBoost algorithm is an ensemble tree-based machine learning method that is widely used for supervised learning tasks such as regression and classification (Niazkar et al., 2024). It is based on gradient boosting, whereby subsequent trees are trained to correct the errors of their predecessors. However, XGBoost incorporates several additional features such as regularisation and tree pruning to mitigate overfitting (Niazkar et al., 2024). XGBoost has been used in a number of groundwater and water quality studies, from predicting river nitrate concentrations (Dorado-Guerra et al., 2022; Xie et al., 2024), groundwater nitrate and manganese concentrations (Bedi et al., 2020; Collins et al., 2025b; DeSimone and Ransom, 2021; Ransom et al., 2022), to assessing the occurrence of edge of field runoff (Hu et al., 2021). Although boosted regression trees have been used to predict groundwater redox conditions previously (DeSimone et al., 2020), using XGBoost for such a task is a recent development (Koch et al., 2024).

The national data set were first partitioned into training and testing data sets (75/25 split) with groundwater redox status stratified to ensure an even spread between the two data sets. A 10-fold cross-validation data set was created from the training data set for the model's hyperparameter tuning. Several data pre-processing steps were necessary prior to training. First, infrequent categories were collapsed for the Rock type variable, as there were dozens of individual attributes within this variable. Attributes that featured less than 0.5% of the total number of landscape units were collapsed to 'other'. The remaining landscape variables (e.g. Soil drainage class, CEC class) had relatively few individual categories that did not require collapsing (Table 3.4; Table 3.5; Table 3.6; Table 3.7; and Table B.1). Second, as XGBoost requires the creation of dummy variables (Kuhn and

Silge, 2022), all categorical variables were converted into numerical data with one-hot encoding. Finally, predictor variables with zero variance were removed and the now-numeric data was also centred and scaled.

The model's performance was evaluated using sensitivity, specificity, accuracy, kappa (Viera and Garrett, 2005) and area under the receiver operating characteristic curve (*AUC-ROC*; Fawcett, 2006). Sensitivity (true positive rate) measures the proportion of cases that were correctly identified as an oxidised land unit by the model. Specificity (true negative rate) measures the proportion of cases that were correctly identified as a reduced land unit by the model. Accuracy measures the overall correctness of predictions made by the model across both oxidised and reduced land unit classes, while kappa accounts for chance agreement, offering a more robust metric for class imbalance (Viera and Garrett, 2005). The *AUC-ROC* evaluates the performance of a binary classification model across different threshold values. The *AUC-ROC* curve assesses sensitivity against 1-specificity at various threshold values. A higher value indicates better model performance.

The hyperparameters of the XGBoost model were also tuned to optimise its performance. These are settings applied to the model but are not learned during the training process (Niazkar et al., 2024). To achieve a tuned model, Latin hypercube sampling, featuring a range of 30 possible hyperparameter configurations, was used. The cross-validation folds were used to evaluate the performance of different configurations generated by the Latin hypercube. Mean *AUC-ROC* (across the 10 cross-validation folds) was used to select the optimal combination of hyperparameters for the model. These were then used to train the model.

All data analysis was carried out in R (R Core Team, 2022; v. 4.2.2) with predictive analysis undertaken with Tidymodels (Kuhn and Wickham, 2020; v. 1.1.1).

4.3.3.1 Ground-truthing landscape subsurface redox predictions

A number of local studies have been recently undertaken in the Horizons region to better understand groundwater redox conditions and the potential for denitrification in the subsurface environment (Collins et al., 2017; Collins, 2015; Gonzalez Moreno, 2019; Rivas et al., 2020, 2017, 2014; Smith et al., 2017). A range of field measurement methods were employed in these studies, including the installation of shallow groundwater piezometers; sampling and analysis of shallow groundwater quality; and single-well push-pull tests. The push-pull test is an *in situ* method for a site characterisation (Istok, 2013; Istok et al., 1997) and identifying subsurface biogeochemical processes including denitrification (Addy et al., 2002; Anderson et al., 2014a; Jahangir et al., 2013b; Rivas et al., 2014). The observations and results of these existing local studies in the Horizons region were collated and used to provide independent validation of the XGBoost model's predictions of landscape unit subsurface redox status across the study area.

4.3.4 Development of the Landscape Subsurface Nitrate-Attenuation Index

The *LSNAI* was developed by classifying the Horizons region's ~11,000 landscape units into five distinct clusters using hierarchical clustering (Everitt et al., 2011). A landscape unit was defined as a spatial area, or unit of territory, that shares similar physical and geographic characteristics (Campos-Campos et al., 2018). The classification was achieved by integrating the XGBoost model's landscape subsurface redox status predictions and associated key influencing landscape characteristics of rock type and soil drainage. Rock type and soil drainage were chosen due to their significant roles observed in nitrate attenuation in the subsurface environment (Elwan, 2018; Jahangir et al., 2012; McAleer et al., 2017; Orr et al., 2016; Rivas et al., 2017) and their high variable importance scores in the XGBoost model.

A hierarchical (agglomerative) clustering analysis was applied for its interpretability and ability to provide meaningful clusters of similar landscape units. The number of *LSNAI* clusters was determined to achieve a distinct range of mean subsurface redox status probabilities (P(Oxidised) and P(Reduced)). This classification approach resulted in hierarchical clusters ranging from Very low nitrate attenuation potential, characterised by a high P(Oxidised) and low P(Reduced) redox status, to Very high nitrate attenuation potential, characterised by a high P(Reduced) and low P(Oxidised) redox status. These classes represent the relative potential of subsurface nitrate attenuation assessed for different landscape units in the Horizons region, forming the basis of the development of the *LSNAI* for classification and mapping of landscape units and their subsurface nitrate attenuation potential in agricultural landscapes.

4.4 Results and discussion

4.4.1 Prediction of landscape unit subsurface redox status

The pre-processing steps outlined above resulted in a total of 73 features to train the XGBoost model. The 10 cross-validation folds were used to optimise the model's hyperparameters, with a range of values tested during the tuning process (Table 4.3). The combination of values that yielded the highest mean *AUC-ROC* result across the 10 cross-validation folds was selected to train the final model.

Table 4.3: Hyperparameter values used to tune the XGBoost model, and the optimised values used to train the model.

Hyperparameter name (Tidymodels alias)	Description[2]	Hypercube range	Optimal value
Learning rate (learn_rate)	The rate at which the boosting algorithm adapts from iteration to iteration.	1.35e-10 – 7.15e-02	0.07
Number of rounds (trees)	The number of trees contained in the ensemble.	7 – 1796	296
Maximum tree depth (tree_depth)	The maximum depth of the tree i.e. number of splits.	1 – 15	7
Minimum child weight (min_n)	The minimum number of data points in a node that is required for the node to be split further.	2 – 40	4
Gamma (loss_reduction)	The reduction in the loss function required to split further.	2.37e-10 – 18.17	5.74e-10
Subsample (sample_size)	The proportion of data that is exposed to the fitting routine.	0.13 – 1.00	0.74
Column sample by node (mtry)	The proportion of predictors that will be randomly sampled at each split when creating the tree models.	0.12 – 0.98	0.34
Early stopping (stop_iter)	The number of iterations without improvement before stopping.	3 – 20	18

Model performance was evaluated using the held-out testing data set, which was not used during model training. The testing data set results showed a sensitivity (the true positive rate for oxidised conditions) of 0.96 and a specificity (the true negative rate for reduced conditions) of 0.80. This implies the model is more effective at identifying oxidised conditions than reduced. The relatively higher sensitivity compared to specificity is likely a result of class imbalance in the data set, where oxidised conditions were more prevalent. The overall rate of accuracy on the testing data was 0.93, with a kappa statistic of 0.78

[2] Kuhn & Vaughan (n.d.) *Boosted trees*. Retrieved August 8, 2024, from https://parsnip.tidymodels.org/reference/boost_tree.html

and an *AUC-ROC* of 0.97. The lower kappa value, compared to the higher accuracy, is also consistent with class imbalance.

As the model was trained on the national data set, but only applied to the Horizons region, these metrics have also been calculated for training and testing data within the study area (Table 4.4). The model's performance for training and testing data within the study area was similar for the model trained using the national data set (Table 4.4), except for a slightly higher specificity and kappa, demonstrating a slight improvement on the model's ability to predict reduced conditions in the study region, compared to nationally.

Table 4.4: The XGBoost model performance metrics calculated for the training and testing data for prediction of landscape subsurface (groundwater) redox status. The number of data points in each testing and training data set are in parentheses.

	National data set		Horizons data set	
Metric	**Training (21,029)**	**Testing (7011)**	**Training (815)**	**Testing (285)**
Sensitivity	0.97	0.96	0.96	0.98
Specificity	0.80	0.80	0.88	0.82
Accuracy	0.94	0.93	0.92	0.90
Kappa	0.79	0.78	0.84	0.81
ROC-AUC	0.97	0.97	0.96	0.96

The trained XGBoost model was used to predict the subsurface redox status probability for each landscape unit in the Horizons region (Figure 4.2). The results demonstrate widely variable landscape subsurface redox conditions throughout the region, with some areas likely to be more strongly oxidising and other areas likely to be more strongly reducing. While no subsurface redox assessment has been completed specifically for the Horizons region, Wilson et al. (2020) produced a national-scale groundwater redox assessment for New Zealand, exempting the mountainous and steep areas of the country. Wilson et al.'s (2020) assessment predicted groundwater (subsurface) redox conditions at various depths (15 m, 50 m and 80 m) with a vertical redox gradient apparent in some areas over this range. There are broad similarities between the predictions in this study (Figure 4.2) and those of Wilson et al. (2020), but specific subsurface redox depth was not examined here, due to this study's focus on predicting the probability of a landscape unit's subsurface redox status. The results of this study (Figure 4.2) and those of Wilson et al. (2020), both indicate a greater likelihood of oxidising subsurface conditions in the northern part of the region and reducing subsurface conditions in the south-west coastal area. The northern part of the region features volcanic deposits in addition to various sedimentary marine deposits such as sandstone and mudstone (Figure 4.1b). Significantly older basement greywacke also outcrops in the north-east of the region (Figure 4.1b). In the south, the western coast is characterised by alluvial and marine sedimentary deposits including sands and gravel. Iron-rich windblown sands form a thin veneer across this area with sand dunes aligned with the predominant north-west wind direction. The axial ranges, dividing the south-east of the region with the south-west, were unmodelled by Wilson et al. (2020), but were predicted as being strongly oxidising landscapes in this analysis (Figure 4.1b, Figure 4.2a).

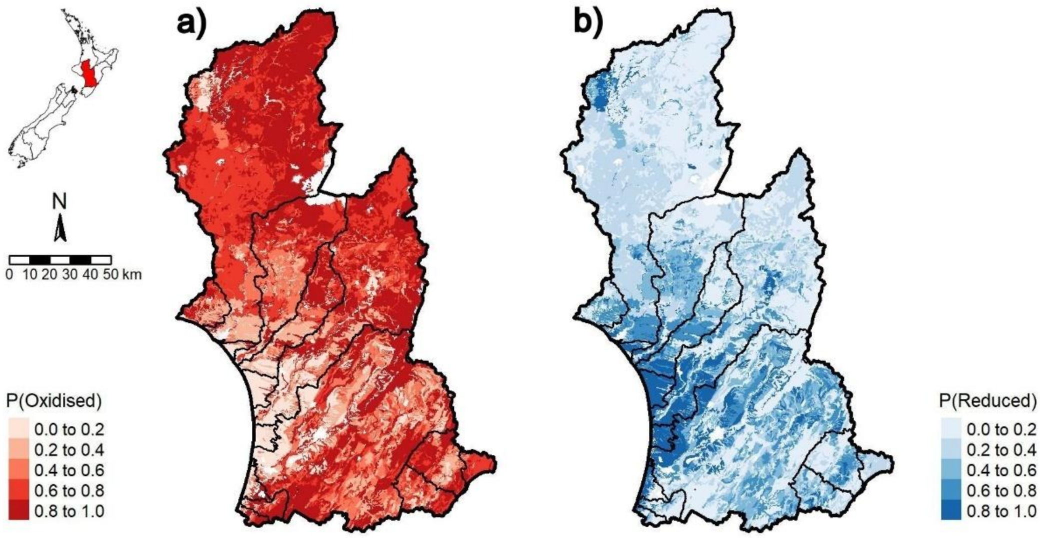

Figure 4.2: Predicted landscape subsurface redox status determined by the XGBoost model: a) probability that landscape units are oxidised; b) probability that landscape units are reduced. A higher probability value indicates a greater level of confidence in the prediction.

Figure 4.3 plots the variable importance scores calculated from the trained XGBoost model. The most important variables in assessing landscape subsurface redox conditions were scored as poorly drained soils and alluvium rock type. In this context, soil drainage characteristics are based on the depth and duration of water tables inferred from soil colours and mottles; while alluvium refers to undifferentiated floodplain alluvium, colluvium and glacial drift (Newsome et al., 2008). Soil drainage and sediment type have previously been associated with denitrification and reducing conditions in groundwater (Clague et al., 2019; Clague et al., 2015; Collins et al., 2017; Rivas et al., 2017; Wu et al., 2018). Wu et al. (2018) found that a low permeability silty clay layer within a Beijing aquifer attenuated nitrate at about twice the rate of an overlying medium grain sand layer. In New Zealand, Clague et al. (2019) observed higher denitrification potential under imperfectly/poorly drained soils compared to well-drained soils in the Reporoa Basin, Waikato; while Rivas et al. (2020) noted that sites underlain by alluvium had greater subsurface denitrification potential than those with loess over gravel. Similarly, Collins et al. (2017) observed denitrification occurring in shallow groundwaters at three sites characterised by poorly-drained coastal soil types.

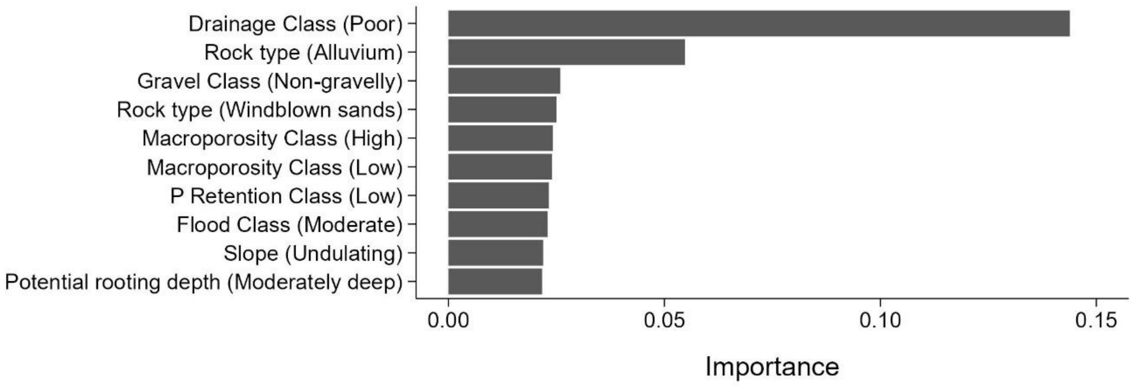

Figure 4.3: Top ten variable importance scores calculated from the trained XGBoost model to predict landscape redox status in the Horizons region.

4.4.1.1 Ground-truthing of landscape subsurface redox predictions

Ground-truthing the results of the XGBoost model involved comparing the predicted landscape subsurface redox status, as P(Oxidised) or P(Reduced), with the shallow groundwater redox status established though field techniques from previous studies within the Horizons region (Figure 4.4 and Table 4.5). The redox status at each of these sites has been established either through shallow groundwater monitoring (Gonzalez Moreno, 2019; Smith et al., 2017) using McMahon and Chapelle's (2008) classification (incorporating DO, NO_3^--N, Mn^{2+}, Fe^{3+} and SO_4^{2-}), and/or through the single-well push-pull tests by observing the concentration of NO_3^--N against a conservative tracer (Collins et al., 2017; Gonzalez Moreno, 2019; Rivas et al., 2020). At each location, the individual piezometers were generally within several metres of each other, though the Pahiatua sites were up to 1 km apart. No data from these studies were used in the training of the XGBoost model.

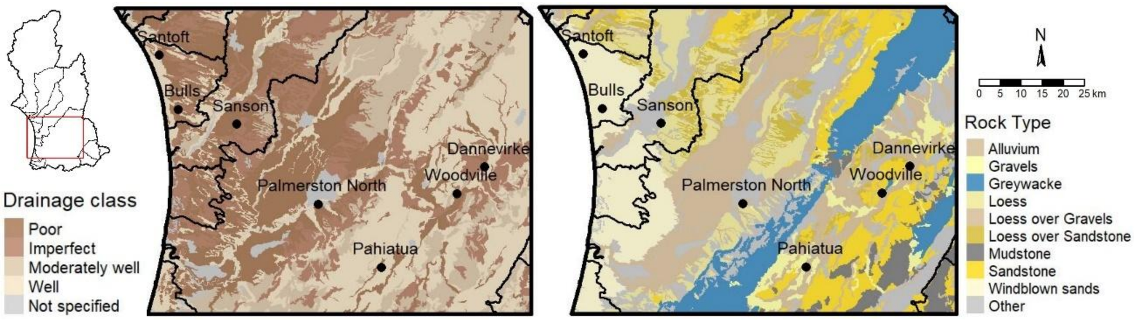

Figure 4.4: Location of ground-truthing studies in the southern Horizons region showing both soil drainage class and rock type categories. Site locations do not necessarily reflect the exact locations of places they are named for.

Table 4.5: Shallow groundwater redox and denitrification studies, compared with the XGBoost predictions of landscape subsurface redox status in the Horizons region. Depth is m below ground level.

Reference	Piezo depth (m)	Redox status	P(Oxidised)	P(Reduced)
		Santoft sites		
Collins et al. (2017)	3.00	Reduced	0.05	0.95
Smith (2017)	2.40	Reduced	0.02	0.98
Smith (2017)	5.00	Reduced	0.02	0.98
Smith (2017)	3.40	Reduced	0.01	0.99
Smith (2017)	5.00	Reduced	0.01	0.99
Gonzalez Moreno (2019)	3.00	Reduced	0.01	0.99
Smith (2017)	3.00	Reduced	0.01	0.99
Gonzalez Moreno (2019)	6.00	Reduced	0.01	0.99
Smith (2017)	6.00	Reduced	0.01	0.99
Gonzalez Moreno (2019)	6.00	Mixed	0.01	0.99
Smith (2017)	3.00	Reduced	0.01	0.99
Smith (2017)	3.50	Reduced	0.01	0.99
		Bulls sites		
Collins et al. (2017)	3.00	Reduced	0.05	0.95
Collins et al. (2017)	6.00	Reduced	0.05	0.95
		Sanson sites		
Collins et al. (2017)	3.00	Reduced	0.01	0.99
Collins et al. (2017)	6.00	Reduced	0.01	0.99
		Woodville sites		
Gonzalez Moreno (2019)	5.00	Reduced	0.37	0.63
Rivas et al. (2020)	5.00	Reduced	0.37	0.63
Gonzalez Moreno (2019)	6.00	Reduced	0.37	0.63
Rivas et al. (2020)	6.00	Reduced	0.37	0.63
Gonzalez Moreno (2019)	7.50	Reduced	0.37	0.63
Rivas et al. (2020)	7.50	Reduced	0.37	0.63
		Pahiatua sites		
Gonzalez Moreno (2019)	3.60	Oxidised	0.70	0.30

Gonzalez Moreno (2019)	4.51	Oxidised	0.85	0.15
Gonzalez Moreno (2019)	6.40	Oxidised	0.85	0.15
Gonzalez Moreno (2019)	4.40	Oxidised	0.97	0.03
Rivas et al. (2020)	4.40	Oxidised	0.97	0.03
Gonzalez Moreno (2019)	5.40	Oxidised	0.97	0.03
Rivas et al. (2020)	5.40	Oxidised	0.97	0.03
Gonzalez Moreno (2019)	6.40	Oxidised	0.97	0.03
Rivas et al. (2020)	6.40	Oxidised	0.97	0.03
		Palmerston North sites		
Gonzalez Moreno (2019)	5.50	Oxidised	0.20	0.80
Rivas et al. (2020)	7.50	Reduced	0.20	0.80
Gonzalez Moreno (2019)	7.50	Reduced	0.20	0.80
Gonzalez Moreno (2019)	8.70	Reduced	0.20	0.80
		Dannevirke sites		
Gonzalez Moreno (2019)	4.50	Mixed	0.70	0.30
Rivas et al. (2020)	4.50	Oxidised	0.70	0.30
Gonzalez Moreno (2019)	7.50	Reduced	0.70	0.30
Rivas et al. (2020)	7.50	Reduced	0.70	0.30

The Santoft and Bulls sites (Table 4.5) were both located in the Rangitīkei catchment's sand country on a sand dune complex classified geologically as windblown sand. Soils here are described in associations, where the landscape is made up of repeating phases of dune ridge, sand plain and peaty swamp (Cowie et al., 1967). Soil drainage characteristics can vary depending on the soil type and its position in the repeating phases. The studies identified in Table 4.5 used a combination of shallow groundwater monitoring and various push-pull tests carried out in shallow piezometers both of which suggest widespread subsurface (groundwater) reducing conditions (Collins et al., 2017; Gonzalez Moreno, 2019; Smith et al., 2017). The area is known to have strongly reducing groundwater conditions, possibly due to it being a regional discharge zone for older, more hydrochemically evolved groundwater (Morgenstern et al., 2017; Thomas, 2017), and groundwater redox conditions influenced by the high levels of iron in the sand dune deposits of volcanic origin (Brathwaite et al., 2017). The Sanson site was located further inland than the sand country, with surficial geology characterised by alluvium over gravels. The soil, Ohakea silt loam, is imperfectly-to-poorly-drained at the Sanson site. Across these three locations (Santoft, Bulls and Sanson), the local studies have determined the shallow groundwater to be largely reduced (Collins et al., 2017; Gonzalez Moreno, 2019; Smith et al., 2017). This validates the XGBoost model's prediction of a strong likelihood of reducing landscape subsurface (groundwater) conditions in this area (Table 4.5).

The Woodville and Pahiatua sites, which were located on the eastern side of the Manawatū catchment (Figure 4.4), are more closely associated with alluvial and river deposits. The Woodville site was underlain by alluvium with soils described as silt loam and clay loam. At all three depths (5 m, 6 m, 7.5 m below ground level) reducing groundwater conditions were measured in these field studies (Table 4.5), which validates the XGBoost model's prediction of 0.63 probability suggesting high likelihood of reducing subsurface conditions at the Woodville site. At Pahiatua sites, some piezometers were installed in alluvium, while others were installed in gravels with soils described at each site as a stony silt loam. Local studies here identified oxidised groundwater conditions at the various depths tested (3.6 m – 6.4 m below ground level). Likewise, the XGBoost model also predicted a high likelihood of Pahiatua sites being oxidised (0.70 – 0.97) in their subsurface environment.

The remaining two sites, at Palmerston North and Dannevirke (also in the Manawatū catchment), demonstrates the challenge of predicting landscape subsurface redox status where, potentially, a redox interface occurs at shallow depths (Table 4.5). In both cases, the shallowest piezometers were measured as oxidised (or mixed) groundwaters, and slightly deeper piezometers measured as reduced groundwaters (Table 4.5). However, the XGBoost model predicted Palmerston North as a higher probability (0.80) of reduced subsurface redox conditions (i.e. below the redox interface), while at the Dannevirke sites it predicted a greater probability (0.70) of oxidised subsurface redox (i.e. above the redox interface). While a redox interface has been observed in various subsurface environments (Böhlke et al., 2002; Hansen et al., 2014; Koch et al., 2024, 2019; Kolbe et al., 2019; Refsgaard et al., 2014), it may not be a widespread occurrence throughout the Horizons region with reducing conditions found at very shallow depths in places (Table 4.5).

However, a high degree of correspondence between the field measurements and the predicted oxidised or reduced probabilities (Table 4.5) demonstrates independent validation of the trained XGBoost model's performance in modelling and mapping of subsurface redox status probabilities of different landscape units across the Horizons region.

4.4.2 Mapping of Landscape Subsurface Nitrate-Attenuation Index

A total of five clusters were selected for the *LSNAI* based on their interpretability (Table 4.6), with each group exhibiting distinct mean values of P(Oxidised) and P(Reduced) across different land units. These clusters were then categorised into *LSNAI* classes ranging from 'Very low' to 'Very high', resulting in distinct distributions of soil drainage class and rock type classes (Figure 4.5), as well as a spatially distributed range of *LSNAI* categories across the major catchments of the Horizons region (Figure 4.6).

Table 4.6: Classification of *LSNAI* developed for the Horizons region. Shown are the total number of landscape units within each cluster (n); the mean probability of oxidised and reduced predictions for each cluster; the standard deviation; and the total area for each *LSNAI* class.

***LSNAI* categories**	**Landscape units (n)**	**Mean P(Oxidised)**	**Mean P(Reduced)**	**Standard deviation**	**Area (km^2)**
Very low	737	0.89	0.11	0.14	1,802
Low	6,033	0.78	0.22	0.20	12,422
Medium	3,330	0.56	0.44	0.26	6,168
High	988	0.31	0.69	0.25	1,841
Very high	531	0.13	0.87	0.20	774

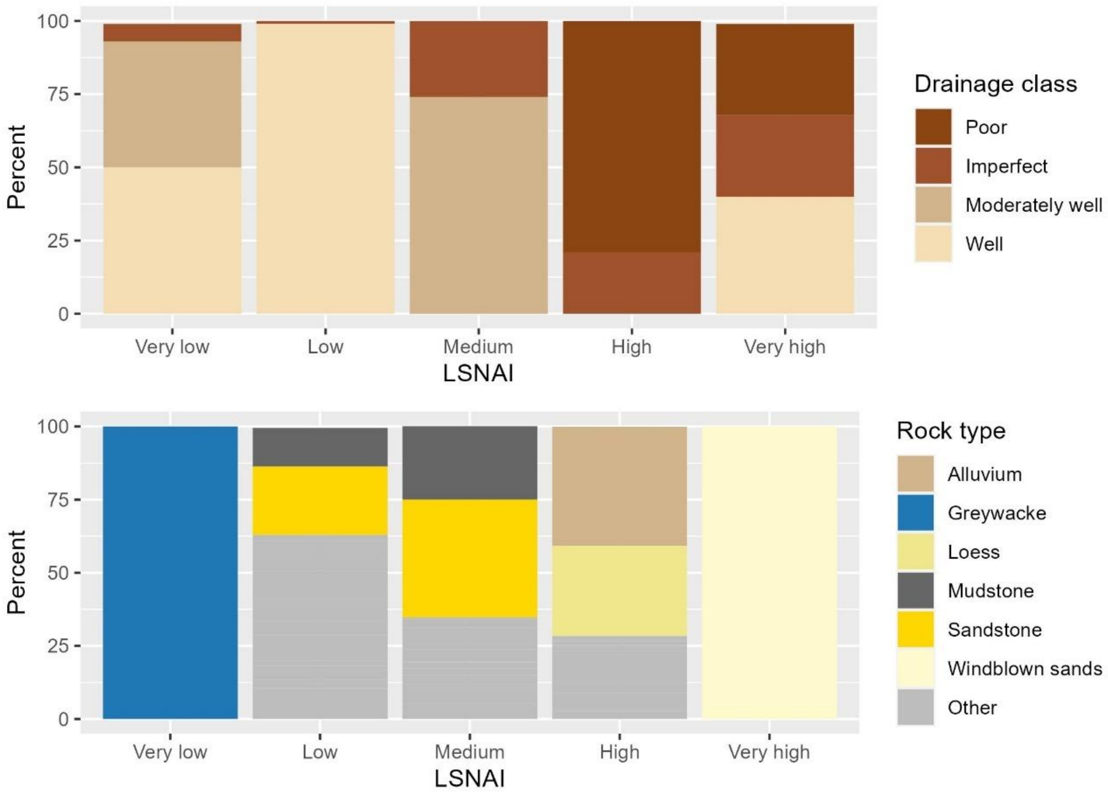

Figure 4.5: Distribution of soil drainage class and rock type groupings of each *LSNAI* class predicted and mapped in the Horizons region.

The *Very low LSNAI* landscape class is composed of 737 land units, with a mean P(Oxidised) value of 0.89, i.e. highly oxidised subsurface redox conditions with very low nitrate attenuation potential, covering about 1802 km^2 of the study area. This class is characterised entirely by greywacke rock type (100 %), but with a range of soil drainage classes, primarily well drained (50 %) and moderately well drained (43 %) (Figure 4.5).

The *Low LSNAI* category, which is composed of 6,033 land units, has a mean P(Oxidised) value of 0.78. There is a wider range of rock types but the soil drainage class is almost entirely well drained (99 %). Rock types primarily include mudstone (13 %) and sandstone (23 %) but also includes a range of volcanic deposits (Figure 4.5). This category is the largest *LSNAI* class mapped in the region (Table 4.6).

The *Medium LSNAI* class is comprised of a balance between P(Oxidised) and P(Reduced) redox status (Table 4.6). Rock types in this class comprise a greater share of mudstone (25 %) and sandstone (40 %) with soil drainage class split between moderately well drained (74 %) and imperfectly drained (26 %) (Figure 4.5).

The *High LSNAI* class, comprising 988 landscape units, has a mean P(Oxidised) value of 0.31 or a mean P(Reduced) value of 0.69 (Table 4.6). These landscape units are primarily composed of poorly drained soils (79 %), with loess (31 %) and alluvium (41 %) making up the dominant rock types (Figure 4.5), which covers about 1841 km^2 of the study area. Loess over gravels and loess over sandstone also make up minor portions of the *High LSNAI* class.

Finally, the *Very high LSNAI* class features a range of soil drainage classes but is exclusively composed of windblown sands (100 %) (Figure 4.5), located along the western coast of the region (Figure 4.6 and Figure 4.1). It has a mean P(Oxidised) of only 0.13, or mean P(Reduced) of 0.87, covering 774 km^2 of the study area.

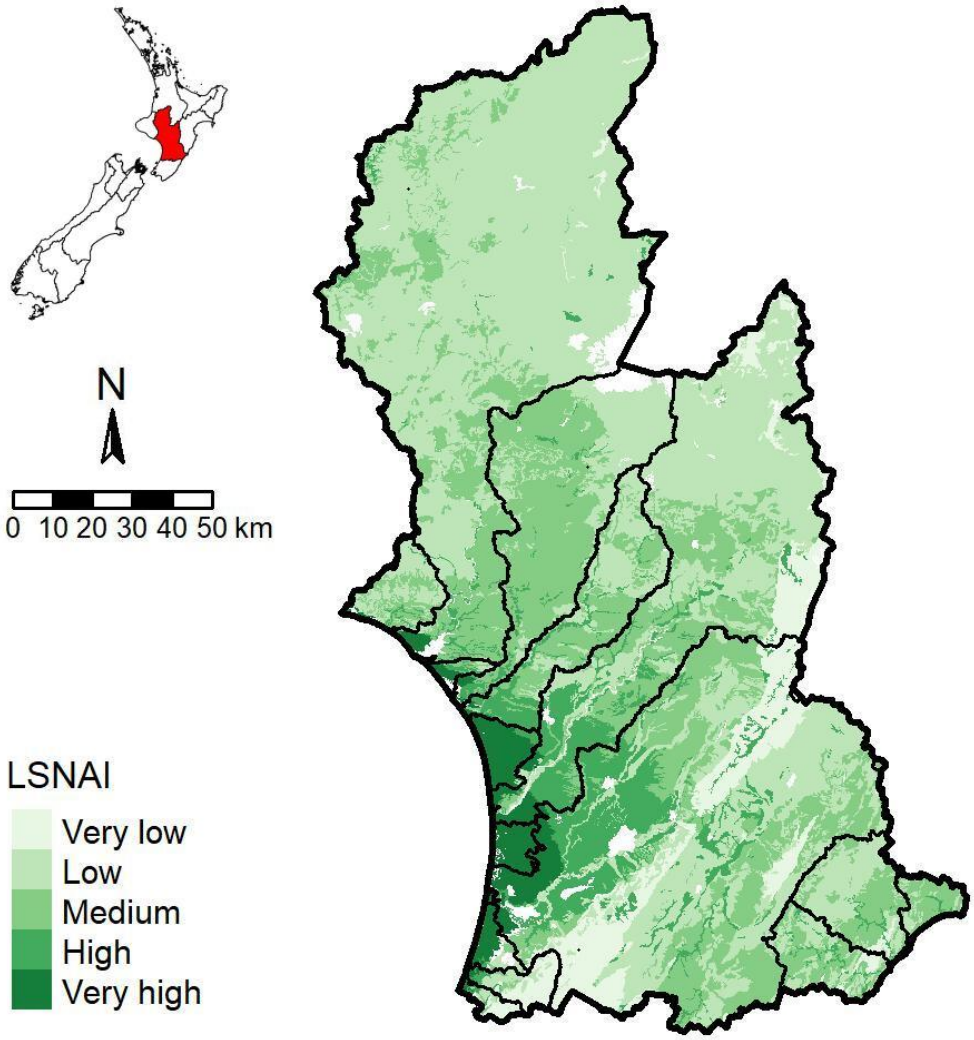

Figure 4.6: Mapping of the *LSNAI* classes based on the hierarchical cluster analysis of groundwater redox probability predictions by the XGBoost model and soil drainage and rock type classes for the Horizons region.

While a few other assessments of nitrogen attenuation have been undertaken in the Horizons region (Elwan et al., 2015; Singh and Horne, 2019; Snelder et al., 2020), only a qualitative comparison can be made between their estimation of nitrogen attenuation rates and the current study because of the different methodologies and the scales at which nitrogen attenuation has been refined, from landscape units (Singh and Horne, 2019) to sub-catchments (Elwan et al., 2015; Snelder et al., 2020). Elwan et al. (2015) quantified the soluble inorganic nitrogen (*SIN*) attenuation factors ranging from, 0.29 to 0.75, based a mass balance approach using the differences between estimates of average annual land use nitrogen export coefficients (kg ha^{-1} yr^{-1}) and calculated instream *SIN* yields (kg ha^{-1} yr^{-1}) across Tararua sub-catchments in the Manawatū catchment. Snelder et al. (2020)

also took a mass balance approach to calculating the total nitrogen (*TN*) attenuation coefficients (ranging from 0.1 to 0.9) for the Horizons region derived from the difference between estimates of land use based export nitrogen coefficients (kg ha^{-1} yr^{-1}) and calculated instream *TN* yields (kg ha^{-1} yr^{-1}) across different sub-catchments in the Horizons region. Singh et al. (2017b) developed a model for the Rangitīkei catchment to account for the influence of different hydrogeological settings on *SIN* attenuation capacity across its five sub-catchments. They defined land units based on a combination of rock and soil types and calibrated nitrate attenuation coefficients to produce a landscape nitrate attenuation index (*LNAI*) of different land units across the Tararua and Rangitīkei districts of the Horizons region (Singh and Horne, 2019). However, none of these methods/approaches (Elwan et al., 2015; Singh and Horne, 2019; Snelder et al., 2020) directly included information from groundwater redox conditions and landscape attributes together in their assessment of either sub-catchment scale nitrogen attenuation factor or landscape nitrogen attenuation index of different land units.

While all three models for the region (Figure 4.6; Singh and Horne, 2019; Snelder et al., 2020) suggest that the magnitude of subsurface nitrate attenuation is spatially variable, there are both similarities and differences in the spatial distribution of their assessments of subsurface nitrate attenuation potential across the study area. For example, in the upper Rangitīkei catchment, relatively higher potential of nitrogen attenuation have been calculated by Snelder et al (2020) and Singh and Horne (2019), yet a relatively low *LSNAI* was assessed in this study, likely due to prediction of high P(Oxidised) results in this part of the catchment (Figure 4.2). Wilson et al. (2020) also predicted oxidised groundwater conditions in the northern Rangitīkei catchment, in contrast to both Snelder et al.'s (2020) and Singh and Horne's (2019) prediction of relatively higher nitrogen attenuation potential for upper Rangitīkei catchment landscapes. However, a better agreement between the various models (Figure 4.6; Singh and Horne, 2019; Snelder et al., 2020) was observed across the eastern Manawatū catchment (also known as the Tararua catchment), where the nitrogen attenuation potential assessed in this study mostly varied between very low and medium *LSNAI* (Figure 4.6), corresponding very well with low to medium nitrogen attenuation coefficients quantified by Snelder et al. (2020) and between low and high attenuation in Singh and Horne (2019). Also, in the Whanganui catchment, both this study and that of Snelder et al. (2020) identified relatively low potential of nitrogen attenuation across the entire catchment.

The independent validation of XGBoost's redox predictions provides a useful assessment of the model's performance, however the validation studies used above, while assessing diverse soil and geological conditions, do not cover the full range of landscape types found in the Horizons region. An important source of uncertainty in this model is the somewhat narrow range of landscape characteristics that groundwater redox measurements have been drawn from. Groundwater redox data used here is particularly well represented for alluvium, loess over alluvium, volcanic deposits, windblown sands and gravel, but is underrepresented for other rock types such as greywacke, metamorphic rocks, sandstone and mudstone (Collins et al., 2025; Chapter 3). In addition, groundwater (subsurface) redox data is widely available in locations of flat relief but lacking in steeper areas such as hill country landscapes of the Horizons region. Few studies to date report on the variability of denitrification potential in hill country subsoils and seepage wetlands in the Horizons region (Chibuike et al., 2024, 2019; Sanwar, 2023; Sanwar et al., 2022). However, the XGBoost model trained and tested here could pose an uncertainty in the prediction and mapping of landscape subsurface nitrate attenuation potential in steeper hill country landscapes, which makes up more than 60 % of the Horizons region. Therefore, further research is required to better characterise and understand subsurface redox conditions in these steeper landscapes, particularly hill country landscape units. This will help reduce overall uncertainty in the further development and validation of the *LSNAI* to comprehensively model and map spatially variable subsurface nitrate attenuation potentiation of different landscape units across agricultural catchments.

4.5 Conclusion

Meeting the water quality standards prescribed by New Zealand's National Policy Statement for Freshwater Management requires modelling various land use scenarios and water quality measures to reduce nitrogen losses from farm- to catchment-scale. This study has developed a landscape subsurface nitrate-attenuation index to provide an estimate of subsurface nitrate attenuation potential of different landscape units for the Horizons region of New Zealand. The index integrates classification of groundwater redox status with key influencing landscape characteristics into the assessment and mapping of potential nitrate attenuation in the subsurface environment of different landscape units. Using a national groundwater redox data set, the machine-learning model

XGBoost was trained and tested to predict landscape unit subsurface redox status for the region's ~11,000 landscape units. The model predicted a probability of oxidised or reduced subsurface (groundwater) redox conditions. XGBoost was found to be a good predictor of landscape subsurface redox status, which was also demonstrated by ground-truthing the model's predictions against independently gathered data on shallow groundwater redox conditions and nitrate attenuation measurements at various field sites located in different landscapes in the region. By combining the prediction of landscape unit subsurface redox status, with the key influencing landscape variables of soil drainage and rock type characteristics, a hierarchical clustering analysis and unsupervised classification identified and mapped five landscape subsurface nitrate attenuation potential classes. These *LSNAI* attenuation classes, mapped from very low to very high nitrate attenuation potential, reflect the spatially variable nature of subsurface (groundwater) redox conditions in the Horizons region, potentially allowing for subsurface nitrate attenuation accounting to be realised at catchment-scale. The developed *LSNAI* broadly identifies the lowest subsurface nitrate attenuation potential in areas where well drained soils were underlain by gravels and greywacke rock types, with increasing potential of subsurface nitrate attenuation on the plains and at the western coast with reduced groundwater conditions. However, further research and testing are required to understand the effectiveness of applying the *LSNAI* for catchment-scale modelling of nitrogen losses to waterways, especially in steeper hilly landscapes where the subsurface (groundwater) redox data is currently limited. However, an accurate mapping and accounting of *LSNAI* is expected to improve simulation of various land use scenarios across agricultural catchments, based on potential for nitrate attenuation, and provide options for targeted and effective measures on reducing nitrogen losses at catchment-scale.

Acknowledgements

This study was conducted as part of a collaborative research programme between Massey University School of Agriculture and Environment (SAE) and Horizons Regional Council (HRC), New Zealand. HRC partly co-funded this study and provided in-kind support for groundwater data collected and analysed in this study. HRC co-funding and in-kind support is greatly appreciated. Other New Zealand regional and district councils also kindly provided groundwater quality data for this study. We also thank the anonymous reviewers whose contribution greatly improved the manuscript.

Chapter 5: Evaluation of Landscape Subsurface Nitrate-Attenuation Index using field observations

Brief introduction for thesis

This chapter addresses the lack of representative data in the national groundwater redox dataset (Chapter 3), which limits confidence in the *LSNAI* classifications (Chapter 4). To partially address this limitation, soil redox probes were deployed at three sites within a farm in the Horizons region to characterise subsurface redox conditions and evaluate *LSNAI* classifications against field observations. The selected sites span a range of *LSNAI* categories and soil drainage characteristics, providing a basis for targeted ground-truthing of the *LSNAI*.

5.1 Abstract

The Landscape Subsurface Nitrate-Attenuation Index (*LSNAI*) was developed to classify landscape units into five categories of subsurface nitrate attenuation potential (ranging from *Very low* to *Very high*). While the *LSNAI* has been evaluated in some landscape settings, further field-based testing is required to assess its performance across a broader range of conditions. This study deployed soil redox potential probes at multiple depths (30, 50, 70 and 90 cm) at three sites within a farm in the Horizons region to evaluate *LSNAI* classifications against observed subsurface redox conditions. The sites span *Low* (Ramiha silt loam), *Medium* (Shannon silt loam) and *High* (Tokomaru silt loam) *LSNAI* categories. The *Low LSNAI* soil (Ramiha) maintained oxidised conditions year-round (Eh > 300 mV), consistent with its well-drained soil morphology. The *Medium LSNAI* soil (Shannon) experienced intermittent reducing periods at 30 – 70 cm depths under wet conditions, aligning with imperfectly drained soil morphological characteristics, while the deeper horizons remained oxidised. The *High LSNAI* soil (Tokomaru), with its fragipan and perched water table, sustained longer periods of reducing conditions (Eh < 300 mV) at 30 – 70 cm depths, particularly during wet seasons. Overall, the observed soil redox conditions were broadly consistent with the assigned *LSNAI* categories, providing site-based evidence that supports the conceptual basis of the *LSNAI*. These findings represent targeted ground-truthing of the index and highlights the need for further evaluation across a wider range of landscape types.

5.2 Introduction

A Landscape Subsurface Nitrate-Attenuation Index (*LSNAI*) was previously developed to increase the spatial resolution of modelling and mapping of subsurface nitrate attenuation potential from sub-catchment scale to landscape-unit scale (Collins et al., 2025a). This was achieved by integrating key landscape characteristics known to influence subsurface denitrification – such as soil drainage, rock type and subsurface redox conditions – and classifying landscape units into five landscape subsurface nitrate attenuation categories ranging from *Very low* to *Very high*. This approach required the development of a machine learning predictive model for subsurface redox conditions for the entire Horizons region. An extreme gradient boosting (XGBoost) model was trained using a national groundwater data set (Collins et al., 2025b) and relevant landscape predictor variables such as rock type and soil carbon class (Newsome et al., 2008) to model the probability of oxidising or reducing subsurface redox conditions beneath each landscape unit across the region.

The XGBoost model performed well, achieving a sensitivity of 0.96 for oxidised conditions (the true positive rate) and a specificity of 0.80 for reduced conditions (the true negative rate) (Collins et al., 2025a; Section 4.4.1). In addition, the subsurface redox predictions were also ‘ground-truthed’ against shallow groundwater data collected from independent investigations into groundwater nitrate attenuation potential in the Horizons region (Collins et al., 2017; Collins, 2015; Gonzalez Moreno, 2019; Rivas et al., 2020, 2017, 2014; Smith et al., 2017). While the redox predictions aligned well with the groundwater observations (Collins et al., 2025a; Section 4.4.1.1), the groundwater data represented only a limited range of landscape types, mainly in flat areas (0-7° slope). This limitation arose because the field method used for sampling and testing – shallow groundwater piezometers – was only feasible in areas with water tables within a few metres of the ground surface and hydraulic conductivity is sufficient to allow groundwater extraction.

The analysis in Collins et al. (2025b) (Chapter 3) also showed that, although extensive, New Zealand’s groundwater redox data set is biased towards certain landscape types. *Flat* (0-7°) landscapes represent 22.4 % of New Zealand but contribute approximately 87.1 % of the redox data. In contrast, *easy hill* (16-25°) and *steep hill* (> 25°) landscapes represent 26.8 % and 38.7 % of New Zealand, but only 2.5 % and 0.3 % of the redox data set, respectively (Table 3.5). In New Zealand, hill country is defined as slopes > 15°, encompassing both *easy hill* and *steep hill* categories and accounts for approximately 70 % of the Horizons region.

The limited availability of subsurface redox data from steeper landscapes reduces confidence in the *LSNAI* predictions across the full range of landscape conditions represented in the region. To partially address this gap, targeted field-based ground-truthing of *LSNAI* categories was undertaken using direct measurements of soil redox potential. Recent advances in *in situ* soil redox measurement, such as the direct-push probe method developed by Vela et al. (2025), enable continuous redox monitoring of redox potential (*Eh*) with depth and have improved the understanding of subsurface redox zonation in unconsolidated sediments.

In this study, continuous soil redox probes (ORP-80-4-D, SWAP Instruments®) were deployed as a practical option to provide site-based observations of subsurface redox dynamics. These probes allow *Eh* to be monitored at fixed depths in the soil profile, providing direct and continuous measurements of redox conditions *in situ*. Three sites were selected to span *Low*, *Medium* and *High LSNAI* categories, enabling evaluation of how observed redox patterns align with *LSNAI* classifications across contrasting soil and landscape settings.

5.3 Methods and materials

5.3.1 Study site

The study took place at Massey University's hill country research farm, Tuapaka, located approximately 15 km east of Palmerston North (Figure 5.1). Tuapaka is a 476 ha farm featuring 111 ha of flats and 365 ha of hill country ranging from 100 to 360 metres above sea level (masl; Figure 5.1a; Massey University, 2025). Because of the topography, rainfall ranges from 900 mm per year on the flats to 1100 mm per year at the highest elevations of the farm. Local geology ranges from river terraces underlain by gravel on the flats, to marine sands and substantially older greywacke which outcrops at upper elevations (Figure 5.1b). Loess, a wind-blown deposit, covers much of these sediments and outcrops as a thick layer (Pollok and McLaughlin, 1986). Given the various topographic, climatic and geological features of the farm, a range of soil types (soil series) have developed. Nine soil series have been described on the farm, some with variants (Figure 5.1c; Pollok and McLaughlin, 1986). Soils range from well-drained on the hills to poorly drained on the flats.

The farm's landscape features are diverse enough to map three of the *LSNAI*'s nitrate attenuation potential categories: *Low*, *Medium* and *High* (Figure 5.1d). Different soil types are found across these *LSNAI* categories, but three contrasting soils will be studied in this chapter: the Ramiha silt loam, the Shannon silt loam and the Tokomaru silt loams (Figure 5.1).

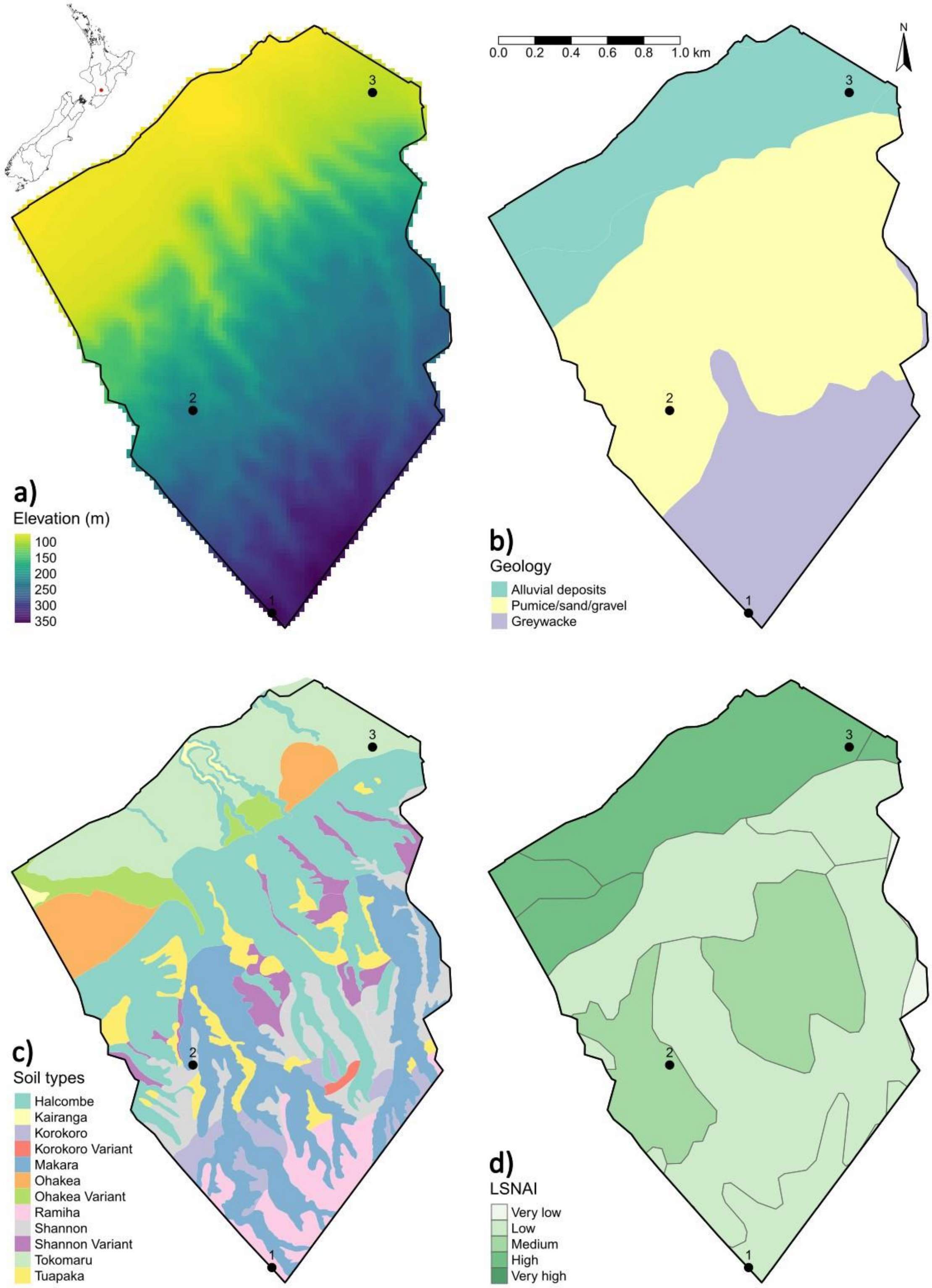

Figure 5.1: Tuapaka Farm with maps showing a) elevation; b) geology; c) soil types; and d) *LSNAI* categories. Study sites: 1 = Ramiha series, 2 = Shannon series and 3 = Tokomaru series.

5.3.1.1 Ramiha series

Soils from the Ramiha series are formed from loess over 1 m thick and feature the c. 25k year old volcanic ash, the Kawakawa tephra (Vandergoes et al., 2013). These soils have a medium (silt loam) texture throughout their profile and a strongly developed nutty structure that becomes blocky with depth. They are friable with moderately low bulk density, free draining and strongly leaching (Pollok and McLaughlin, 1986). A site was selected from the Ramiha series within the *Low LSNAI* category on the farm (Figure 5.1d), on 'undulating' slope conditions (4 – 7°), which is described as Ramiha silt loam and is a Brown soil in the New Zealand soil classification (Hewitt, 2010). This site had a P(Oxidised) of 0.95 and a P(Reduced) of 0.05 (Section 4.4.1).

5.3.1.2 Shannon series

Soils from the Shannon series formed from loess overlying marine sand deposits. They are characterised by an intermediate texture that becomes medium-fine with depth and a moderately developed nutty structure that becomes blocky with depth. The soils are friable near the surface but become firm and compact with depth, are moderately leached and have imperfect drainage (Pollok and McLaughlin, 1986). A site was selected from the Shannon series within the *Medium LSNAI* category on the farm (Figure 5.1d), on 'moderately steep' slope conditions (21 – 25°), which is described as Shannon silt loam and is a Pallic soil in the New Zealand soil classification (Hewitt, 2010). This site had a P(Oxidised) of 0.66 and a P(Reduced) of 0.34 (Section 4.4.1).

5.3.1.3 Tokomaru series

Soils from the Tokomaru series are also formed from loess and contain the Kawakawa tephra at about 2 m depth. They are pale coloured and medium textured with transitional horizons between topsoil and subsoil that contain mottles. The subsoils are highly mottled, medium to fine textured, moderately leached and imperfectly to poorly drained (Pollok and McLaughlin, 1986). A site was selected from the Tokomaru series within the *High LSNAI* category on the farm (Figure 5.1d), on 'flat to gently undulating' slope conditions (0 – 3°), which is described as Tokomaru silt loam and is also a Pallic soil in the New Zealand soil classification (Hewitt, 2010). This site had a P(Oxidised) of 0.08 and a P(Reduced) of 0.92 (Section 4.4.1).

5.3.2 Rainfall measurements

Rainfall measurements (daily total; mm) were taken from a climate station approximately 10 km south-west of the farm, known as Ngahere Park. The climate station was located at a similar elevation to the farm, at 106 masl. It is provided, and maintained, by Horizons Regional Council and uses the tipping bucket method to measure rainfall. In addition to local rainfall data, long-term climate information for the wider region was obtained from the National Climate Database, based on the Palmerston North Electronic Weather Station (EWS) climate station (25-year monthly averages, 2001-2025; Latitude -40.38195, Longitude 175.60915; 21 masl). This data set provides mean monthly rainfall and potential evapotranspiration (PET) values, including standard errors of the mean (SEM) (Figure 5.2).

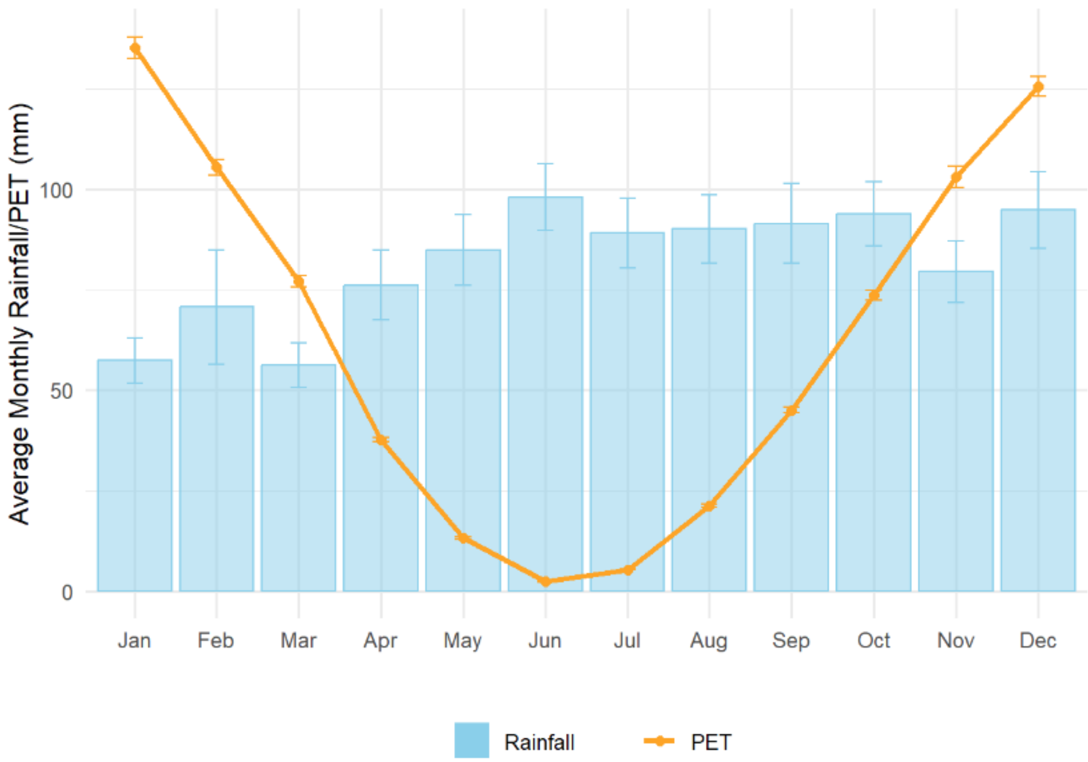

Figure 5.2: Mean monthly rainfall and PET at Palmerston North EWS (25-year averages, 2001-2025; NIWA National Climate Database).

Rainfall and PET demonstrate clear seasonal patterns. Rainfall generally peaks during the cooler months (May to October, 85-99 mm month^{-1}) and is lowest during late summer (January to March, 56-71 mm month^{-1}). Potential evapotranspiration, in contrast, is highest during the summer (January 135 mm month^{-1}, December 126 mm month^{-1}) and lowest in winter (June 2 mm month^{-1}, July 5 mm month^{-1}). During summer months, PET exceeds rainfall, indicating periods of potential water deficit, whereas in winter rainfall generally exceeds PET, reflecting seasonal water surplus and the risk of wet soil conditions in soils with impeded drainage. Rainfall SEM values are greatest in February indicating rainfall variability, while PET SEM remains relatively low throughout the year (Figure 5.2).

5.3.3 Soil profile description and physical properties

At each site, a soil pit approximately 1 m^3 in size was excavated to allow for a full soil profile description. Bulk density was then measured using a core method. At each sampling depth a flat shelf was cut into one side of the pit wall (e.g. at 5 cm depth). A metal corer (5 cm depth) was then driven vertically into the shelf using a hammer, spacer and a wooden block to minimise disturbance. Duplicate cores were taken at each depth. The corer and contained soil were carefully excavated, trimmed flush at both ends, and transported to the laboratory. Samples were oven-dried at 105 °C until constant weight (at least 16 hours) and weighed immediately upon removal to obtain the oven-dry soil mass. Bulk density was calculated from the oven-dry mass and the known volume of the corer, after correcting for the weight of the corer and container. Samples were collected at five depths per profile; the uppermost depth was always 5-10 cm, while subsequent depths varied according to site. Details of each soil profile, bulk density measurements and profile photographs are provided in Appendix D.

5.3.4 Soil redox potential (*Eh*) monitoring

Soil redox potential (*Eh*) was monitored at the three study sites (Ramiha, Shannon and Tokomaru soils) using SWAP Instruments®' ORP-80-4-D analogue soil redox probes. These probes measure the oxidation-reduction potential (ORP; mV) relative to an integrated silver/silver chloride (Ag/AgCl, 3 M KCl) reference electrode on the tip of the probe. To interpret the measurements against standard redox thresholds, the raw ORP readings were converted to *Eh* by adding +200 mV, the accepted correction factor for this reference electrode type (Fiedler et al., 2007). Each probe contains four platinum (99.99 % Pt) electrodes embedded in an epoxy glass fibre shaft. The electrodes are located at depths of 20, 40, 60 and 80 cm from the top of the probe. Each probe was installed vertically in pre-augered holes 10 cm below the soil surface (See Appendix E). As a result, soil redox measurements were made at depths of 30, 50, 70 and 90 cm below ground level. A temperature sensor is embedded 29 cm from the top of the probe (an installed depth of 39 cm) and is used for temperature compensation of soil redox measurements. Details of the installation of these probes are included in Appendix E. Data were recorded at 15-minute intervals using Campbell Scientific CR350 dataloggers throughout the 14-month logging period from July 2024 to August 2025.

A threshold of *Eh* 300 mV has been used as the point between oxidised and reduced soil conditions (Fiedler et al., 2007; Tanner et al., 1999; Zhang and Furman, 2021). This value is used to help identify when soil conditions would be suitable for subsurface denitrification to occur in the Ramiha, Shannon and Tokomaru soils.

5.4 Results and discussion

5.4.1 Soil physical and morphological features

The three study soils represent a continuum of soil drainage characteristics: well-drained (Ramiha silt loam); imperfectly drained (Shannon silt loam); and poorly drained (Tokomaru silt loam). As such, they feature different morphological properties, particularly in how redoximorphic features manifest. Redoximorphic features are formed by the processes of reduction, translocation and oxidation of Mn and/or Fe after soil saturation and desaturation (Vepraskas, 2015; Vepraskas et al., 2018). In the New Zealand soil classification, these features are referred to as a redox-mottled horizons, redox segregations, or reductimorphic horizons (Hewitt, 2010). These features are present to varying degrees in these three soils. Details of the soil profile descriptions can be found in Appendix D.

The Ramiha silt loam does not feature any low chroma colours and only medium mottles that may be related to earthworm activity in the ABw horizon (20 – 37 cm). The Shannon silt loam features light grey (low chroma) colours in the subsoil including the Bg1, Bg2 and 2Bg3 horizons (20 – 86 cm). Coarse distinct mottles are present in the Bg2 and 2Bg3 horizons. Redox mottles such as these are formed from the reduction and solubilisation of Fe and/or Mn, their translocation and concentration and subsequent oxidation and precipitation in the form of oxides (Hewitt, 2010). From 86 cm (2Bg4 horizon) it becomes a high chroma colour (10YR 6/8) with a few light grey (2.5Y 7/2 – 7/3) fine distinct mottles. The Tokomaru silt loam has further evidence of soil redox processes occurring throughout the profile. The topsoil horizons (Ap1 and Ap2) are low chroma colours with mottles related to root channels. In the subsoil (Bgt1, Bgt2 Bxg), low chroma grey colours are interspersed with high chroma brown colours and coarse prominent mottles occurring throughout. A fragipan is typical in this soil and has formed from 84 cm down (Bxg horizon). A fragipan is a non-cemented horizon that has a high bulk density, and high strength when dry (Hewitt, 2010).

These different soil morphological characteristics are also reflected in the different bulk densities of the soils. While soil bulk density increased with depth in all soils, the Ramiha silt loam had a smaller bulk density over the soil profile compared to the Shannon and Tokomaru soils. It ranged between 0.94 g/cm^3 near the top of the soil profile, to 1.38 g/cm^3 at the bottom. The bulk density in the Shannon and Tokomaru soils ranged from 1.28 to 1.67 g/cm^3 and 1.23 to 1.64 g/cm^3, respectively (Table D.2, Table D.4 and Table D.6). Differences reflect the influence of soil texture and structure on soil water retention and drainage, with the lower bulk density of the Ramiha silt loam consistent with greater porosity and aeration – conditions that limit the formation of redoximorphic features. In contrast, the high bulk density of the Tokomaru silt loam contributes to poor drainage and the prevalence of reducing conditions, as reflected in the extensive redox mottling and fragipan development.

5.4.2 Soil redox potential (*Eh*) monitoring

The monitoring period covers five seasons (Figure 5.3 and Figure 5.4), from winter 2024 (June, July, August), spring 2024 (September, October, November), summer 2024/25 (December, January, February), autumn 2025 (March, April, May) and winter 2025 (June, July, August). Monthly rainfall totals peaks in winter 2024 (August 2024) and steadily decline through to late summer 2025 (February 2025) before rising again to winter 2025. August 2024 recorded the highest monthly total with 207 mm while February 2024 recorded the smallest monthly total during the monitoring period, with 30 mm.

The soil redoximorphic features provide an indication of each soil's redox behaviour and potential for denitrification. The continuous measurement of soil *Eh,* by the soil redox probes (Figure 5.3 and Figure 5.4), provided further data by which to examine the temporal dynamics of subsurface redox conditions. In Figure 5.3 and Figure 5.4, the horizontal dashed red line marks the 300 mV *Eh* threshold: the measured *Eh* values above this indicate predominantly oxidised soil conditions, while the measured *Eh* values below suggest reducing soil conditions where subsurface denitrification is more likely.

In the Ramiha silt loam, soil *Eh* is relatively stable across all monitored soil depths (30, 50, 70, 90 cm) over the monitoring period (Figure 5.3). A slight decline in *Eh* from August 2024 to January 2025 is followed by recovery during February and March 2025, when rainfall is at its lowest. Soil *Eh* never falls below, or even approaches, the 300 mV *Eh* threshold, an indication of predominantly oxidised soil conditions in the Ramiha soil profile. This stability is consistent with the soil's low bulk density and well-drained soil profile morphology (Table D.1 and Table D.2).

In the Shannon silt loam, soil *Eh* was stable over the first two months of the monitoring period, in June and July 2024 before soil *Eh* decreased sharply in September 2024 (Figure 5.3). The sharp decrease in soil *Eh* was most pronounced for the 50 and 70 cm depths during this period (Figure 5.3). From September 2024, soil *Eh* at 30, 50 and 70 cm depths continues to rise on a monthly average basis until February 2025, while soil *Eh* at 90 cm steadily decreases over the same period (Figure 5.3). From February 2025 soil *Eh* is relatively stable on a monthly average basis except in July 2025 where soil *Eh* at 70 cm again falls sharply before recovering (Figure 5.3). On a monthly average basis, soil *Eh* stays above the 300 mV *Eh* threshold, however the daily time series shows more variable behaviour in soil *Eh* over the monitoring period, especially at the 30, 50 and 70 cm depths (Figure 5.4). Between approximately August and October 2024, soil *Eh* experiences several sharp falls and recoveries, at times falling below the 300 mV *Eh* threshold (Figure 5.4). While quantifying the rates of denitrification can be uncertain (Rivas et al., 2025), local testing of denitrification rates under different soil and rock types has shown that the reaction can occur quickly in favourable conditions (Collins et al., 2017; Gonzalez Moreno, 2019; Rivas et al., 2020). At 90 cm, soil *Eh* remained more stable and oxidised throughout the monitoring period reflecting the properties of the 2Bg4 horizon (86 – 105 cm), which appears more oxidised compared to the soil horizons above (Table D.3). Between August and November 2024, soil *Eh* at 30, 50 and 70 cm in the Tokomaru silt loam experiences prolonged periods of time below the 300 mV *Eh* threshold (Figure 5.3). From December 2024 soil *Eh* returns to oxidised conditions and remains stable from

January 2025 to May 2025. From approximately June 2025, soil *Eh* starts decreasing again for the 30, 50 and 70 cm depths, with the 30 and 50 cm depths rising in August 2025, coinciding with lower total rainfall in August 2025 (Figure 5.3). At 70 cm depth, coinciding with the Bgt2 horizon (66 – 84 cm depth; Table D.5), soil *Eh* is still reduced in August 2025, which potentially reflects the influence of the perched water table above the fragipan just below this sensor depth in the Bxg horizon (84 – 105+ cm; Table D.5). At 90 cm, soil *Eh* remained oxidised year-round with little variability, likely because the fragipan impedes downward soil water movement, creating the perched water table above but not around the deeper sensor location (90 cm).

Overall, the soil *Eh* monitoring aligns with the assessment of soil morphological observations: the well-drained Ramiha silt loam remained oxidised, the imperfectly drained Shannon silt loam showed intermittent soil reducing phases, and the poorly drained Tokomaru silt loam sustained prolonged soil reducing conditions (Table 5.1).

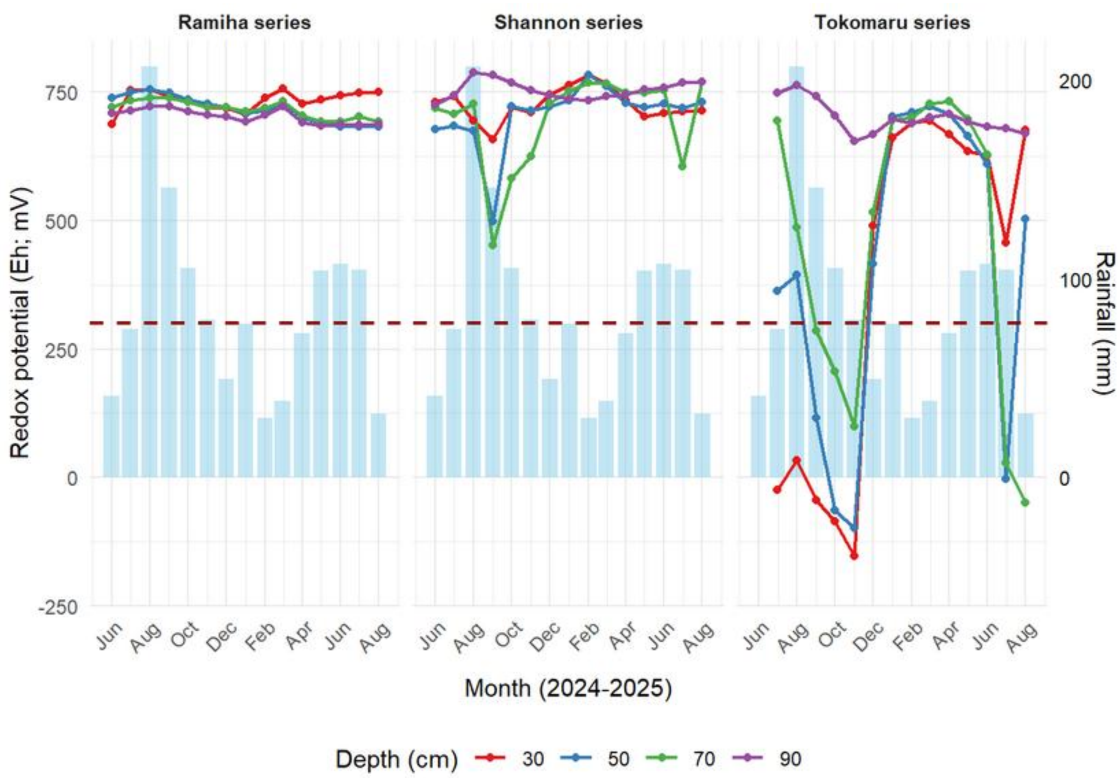

Figure 5.3: Monthly averages of soil *Eh* and rainfall for the Ramiha, Shannon and Tokomaru silt loam soils at Tuapaka Farm.

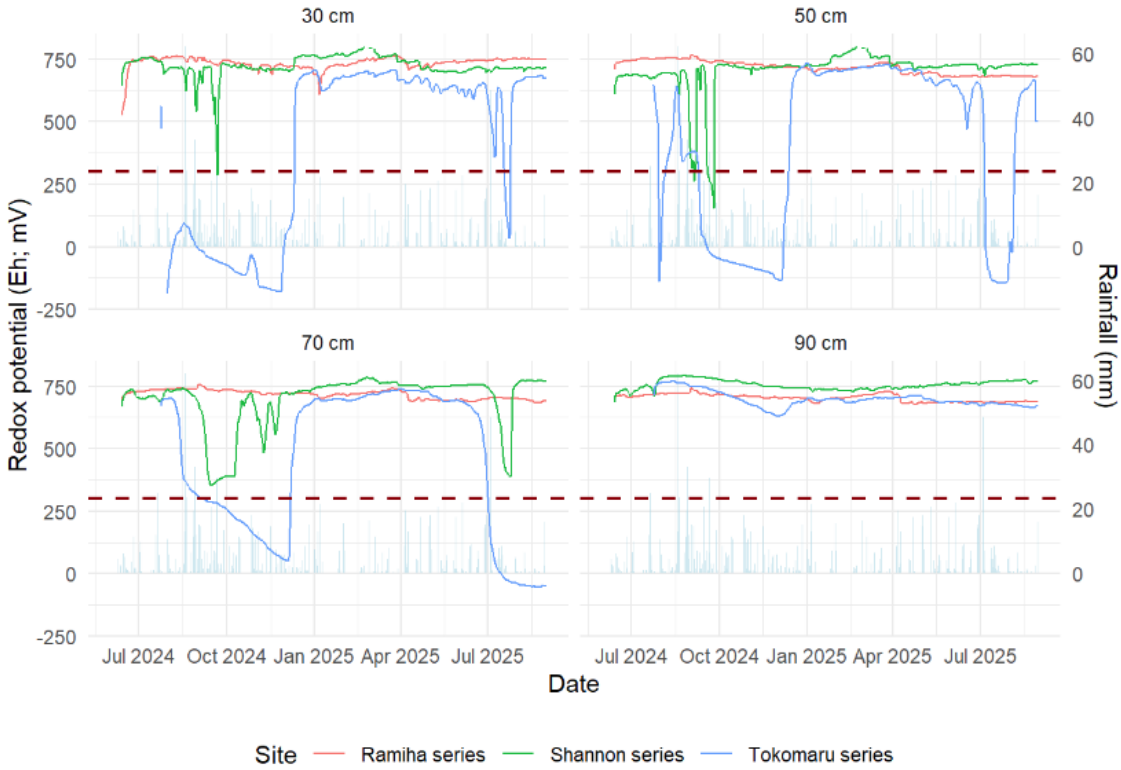

Figure 5.4: Daily timeseries of soil *Eh* and rainfall for the Ramiha, Shannon and Tokomaru silt loam soils at Tuapaka Farm.

Table 5.1: Summary of drainage status, *LSNAI*, probability of oxidised subsurface conditions, average spring soil redox potential (*Eh*) and soil morphological features for the Ramiha, Shannon and Tokomaru silt loam soils.

Soil type	Drainage status	*LSNAI*	P(Oxidised)	Average spring *Eh*		Morphological features
				Depth (cm)	*Eh* (mV)	
Ramiha	Well	Low	0.95	30	731	Lacks low chroma colours and shows only medium mottles, likely associated with earthworm activity in the ABw horizon (20-37 cm), indicating well-drained conditions.
				50	737	
				70	730	
				90	713	
Shannon	Imperfect	Medium	0.66	30	697	Exhibits light grey (low chroma) colours and coarse distinct mottles in the subsoil (20-86 cm) demonstrating active redoximorphic processes that diminish below 86 cm.
				50	646	
				70	553	
				90	769	
Tokomaru	Poor	High	0.08	30	-94	Extensive redoximorphic features throughout the profile, with low chroma colours and coarse mottles in the subsoil and a fragipan forming from approximately 84 cm.
				50	-16	
				70	197	
				90	701	

However, these field-based soil *Eh* data contrast with recent laboratory incubation assays of soils from Tuapaka where a high soil denitrification capacity for the Ramiha silt loam under controlled anoxic conditions was reported (Chibuike et al., 2019). In that study, the Ramiha silt loam had the highest dissolved organic carbon (DOC) concentrations and denitrification capacity of the different soils at Tuapaka, which is related to high contents of short-range-order minerals such as allophane. Reconciling this apparent discrepancy requires distinguishing between the potential for soil denitrification measured in the laboratory and the actual potential for soil denitrification to occur under local hydrological and redox (field) conditions. Laboratory incubation studies such as this involve saturating the soil samples for soil denitrification measurements, however due to the soil's well-drained structure, saturated conditions do not persist for long periods in this soil. In the present study, Ramiha silt loam's high DOC and carbon storage capacity may provide the biochemical potential for denitrification, but the persistently oxidised conditions observed via soil *Eh* monitoring indicate that this potential is rarely achieved under typical field conditions.

5.5 Conclusion

The *LSNAI* was developed to increase the spatial resolution of subsurface nitrate attenuation potential from sub-catchment scale to landscape-unit scale. A machine learning model was trained to predict the probability of subsurface oxidising or reducing conditions beneath each landscape unit in the Horizons region. However, steeper landscapes were under-represented in the model's training and validation data. Tuapaka Farm, containing *Low*, *Medium* and *High LSNAI* categories, provided an opportunity for targeted, field-based evaluation of *LSNAI* classification using soil morphological observations and *in situ* redox potential measurements at three sites (Ramiha, Shannon, and Tokomaru silt loams).

In the *Low LSNAI* category, the Ramiha silt loam, a well-drained soil with few soil redoximorphic features, maintained soil *Eh* values > 300 mV year-round, indicative of predominantly oxidised soil conditions. The *Medium LSNAI* category (Shannon silt loam) featured imperfect drainage with low chroma colours and mottling in the subsoil. The Soil *Eh* monitoring indicated intermittent reducing phases at 30, 50 and 70 cm depths during wet conditions, though these were usually not sustained for long periods of time. The *High LSNAI* category (Tokomaru silt loam) showed mottling throughout the soil profile and sustained reducing conditions (soil *Eh* < 300 mV) at 30-70 cm depths, particularly following wet periods. However, across all three soil sites, 90 cm depths remained oxidised – this condition was expected for the Ramiha soil, but unexpected for Shannon and Tokomaru soils. In the Tokomaru soil, a fragipan likely created a perched water table above it, while in the Shannon soil, coarser sandier textures at depth may have promoted more well-drained, oxidised soil conditions.

Overall, the soil morphological observations and soil *Eh* monitoring data were broadly consistent with the assigned *LSNAI* categories, providing site-based evidence supporting the conceptual basis of the *LSNAI*. These findings represent targeted ground-truthing of the index, rather than a comprehensive validation across all landscape types. Further field data collection across a wider range of soil and landscape conditions is required to more fully evaluate *LSNAI* performance across the region.

Acknowledgements

Dr Alan Palmer helped in the field with soil descriptions for the Ramiha, Shannon and Tokomaru silt loams. His assistance was much appreciated.

Chapter 6: Effective parameterisation of spatially variable landscape subsurface nitrate attenuation capacity to estimate river nitrate loads in agricultural catchments

Brief introduction for thesis

This chapter parameterises the *LSNAI* categories developed in Chapter 4, which classified landscape units in the Horizons region into five categories (ranging from *Very low* to *Very high*) based on their subsurface nitrate attenuation potential. To enable their use in catchment nitrogen modelling, the categories require parameterising to nitrogen attenuation factors (AF_N; values between 0 and 1). An export coefficient modelling approach is applied to calibrate the AF_N values.

This chapter has been prepared as a manuscript for publication and will be submitted to the *Journal of Contaminant Hydrology*.

6.1 Abstract

Intensive agricultural development has increased nutrient losses to freshwaters, affecting water quality and ecosystem health in agricultural landscapes. In New Zealand's Manawatū-Whanganui region, rivers require substantial reductions in nutrient loads to meet freshwater targets. The effectiveness of nitrogen reduction strategies depends on accounting for spatially variable nitrate attenuation in subsurface flow pathways. A key source of uncertainty in modelling river nitrogen loads has been the nitrate attenuation factor (AF_N), with estimates often ranging from 0.1 to 0.9. This study integrates a previously developed measure of landscape subsurface nitrate attenuation, known as the Landscape Subsurface Nitrate-Attenuation Index (*LSNAI*), into catchment-scale nutrient export coefficient modelling to identify AF_N values for different landscape units. Using observed river soluble inorganic nitrogen (*SIN*) loads, AF_N values were calibrated for different *LSNAI* categories across the entire region; this calibration was made for subsets based on the average annual river *SIN* load (< 500 t yr^{-1} and > 500 t yr^{-1}); and for individual catchments (Manawatū, Rangitīkei and Whanganui). Calibration of AF_N values for sub-catchments with loads < 500 *SIN* t yr^{-1} was less reliable (*RMSE* 215 *SIN* t yr^{-1}; *MAE* 140 *SIN* t yr^{-1}; *MAPE* 156 %; *MdAPE* 126 %) compared with sub-catchments with loads > 500 *SIN* t yr^{-1} (*RMSE* 698 *SIN* t yr^{-1}; *MAE* 503 *SIN* t yr^{-1}; *MAPE* 27 %; *MdAPE* 22 %) which showed more consistent and accurate *SIN* load predictions. Discrepancies between mass balance inferred AF_N values and *LSNAI* classifications in sub-catchments such as Rangitīkei at Pukeokahu suggest that some subsurface flow pathways can bypass river monitoring locations, potentially transferring soluble nitrogen to neighbouring downstream sub-catchments, highlighting the importance of local hydrogeological context. With further reductions in uncertainties related to subsurface pathways, this novel approach provides a robust framework for parameterising spatially variable AF_N rates across different landscape units in catchment-scale models. This will support more targeted nutrient management strategies and regulatory interventions to reduce nutrient losses and improve freshwater quality in agricultural landscapes.

6.2 Introduction

Runoff and leaching of nutrients (nitrogen and phosphorus) are increasingly associated with degradation of water quality in agricultural landscapes. Nitrate losses from agricultural land are a significant contributor to the degradation of freshwater environments, affecting ecological integrity, aquatic life, recreational use and drinking water supplies in many agricultural catchments (Bell et al., 2021; Keatley et al., 2011; Pacheco and Sanches Fernandes, 2016; Wilcock et al., 2011; Withers et al., 2014). Water-soluble nitrate leached from the soil profile can travel via subsurface pathways, where lateral water flow can discharge nitrate-contaminated water to surface water bodies (Dymond et al., 2013; Mcdowell et al., 2009; Welch et al., 2011; Zhu et al., 2019). Elevated nitrate concentrations in rivers and streams can trigger excessive biological growth, leading to oxygen depletion, harm to aquatic wildlife and reduced recreational amenity (Davies-Colley, 2013; Heisler et al., 2008).

The Manawatū-Whanganui (Horizons) region in New Zealand features diverse landscapes and intensive agricultural land uses, with some catchments experiencing significant water quality pressures (Fraser, 2023). While existing water quality mitigation strategies have achieved modest success in reducing nutrient (nitrogen) loading to streams (Spiekermann et al., 2018), further reductions are required to meet national and regional water quality targets (Fraser, 2021; Fraser & Snelder, 2020; Snelder, 2024). Rather than applying uniform water quality mitigation measures on farms across the region, a more effective approach is required which accounts for spatial variability in subsurface nitrate attenuation capacity. This more efficient approach would target interventions to areas where they are likely to achieve the greatest benefit (Legarth et al., 2022a, 2022b). To date, interventions have been targeted at agricultural areas with disproportionately high nutrient losses (Hashemi et al., 2018b; Packham et al., 2020). However, designing effective interventions depends not only on a robust understanding of nitrate losses from the root zone, but also on the effective accounting of the subsurface environment's capacity to attenuate nitrate – a process that varies spatially across landscapes (Blicher-Mathiesen et al., 2014; Collins et al., 2017; Rivas et al., 2020; Sarris et al., 2019; Singh and Horne, 2019).

Denitrification is the primary mechanism of subsurface nitrate attenuation and is strongly influenced by redox conditions in subsurface flow paths (Korom, 1992; Rivett et al., 2008). Reduced redox conditions, often driven by limited oxygen availability, facilitate denitrification in subsurface flow pathways. Numerous local (Clague et al., 2019; Collins et al., 2017; Rivas et al., 2017, 2020; Stenger et al., 2018) and international studies (Højberg et al., 2017; Jahangir et al., 2013a; Puckett and Cowdery, 2002; Stuart, 2018;

Welch et al., 2011) highlight the relationship between reduced groundwater conditions and denitrification potential in subsurface environments in agricultural catchments. Landscape characteristics such as soil drainage and rock type can also influence nitrate transport and denitrification dynamics in surface flow pathways (Clague et al., 2019; Collins et al., 2017; Rivas et al., 2017; Wu et al., 2018). Although actual subsurface denitrification rates have not been widely quantified (Rivas et al., 2025), subsurface nitrate attenuation has been observed across a wide range of hydrogeological settings (Böhlke et al., 2002; Jahangir et al., 2013a; Puckett and Cowdery, 2002; Rivas et al., 2020).

In New Zealand, national and regional studies have assessed and mapped subsurface redox conditions (Close et al., 2016; Collins et al., 2025b; Friedel et al., 2020; Sarris et al., 2024; Wilson et al., 2020, 2018). However, subsurface redox status and its associated denitrification potential have not been sufficiently parameterised to enable robust accounting of spatially variable subsurface nitrate attenuation within catchment-scale models. While some studies have achieved denitrification rate parameterisation to account for nitrate loads (Kim et al., 2021; Sarris et al., 2019), such approaches often require complex, data-intensive groundwater models that limit regional-scale application. This highlights the need for a simplified catchment-scale modelling approach, which avoids reliance on complex hydrogeological simulations, but accounts for spatially variable subsurface nitrate attenuation capacity, which in turn facilitates the estimation of river nutrient loads in agricultural catchments.

Singh et al. (2017a, 2017b) defined the nitrogen attenuation factor (AF_N), as representing the proportion of nitrogen removed during transport processes from the farm's root zone to receiving waters, in Tararua and Rangitīkei sub catchments in Manawatū-Whanganui (Horizons) region in New Zealand. To support this, a Landscape Subsurface Nitrate-Attenuation Index (*LSNAI*) has recently been developed for the whole of the Manawatū-Whanganui (Horizons) region (Collins et al., 2025a). The *LSNAI* incorporates predictions of subsurface redox conditions with key landscape factors – such as soil drainage and rock type – to model and map the spatially variable subsurface nitrate attenuation index of different land units. It classifies the landscape into five landscape subsurface nitrate attenuation categories, ranging from *Very low* to *Very high* (Collins et al., 2025a). However, to integrate the *LSNAI* into catchment-scale models, its categories must first be translated into, or expressed as, AF_N values. This integration is expected to enable the further development of a catchment-scale nutrient export coefficient modelling (ECM) framework (Cherry et al., 2008; Johnes, 1996; Johnes & Heathwaite, 1997), in which river nitrate loads are estimated by summing point and non-point sources of nitrate losses while accounting for spatially variable subsurface nitrate attenuation (AF_N) across different land units.

This study aims to quantify and effectively parameterise the *LSNAI* categories into spatially variable nitrate attenuation rates (AF_N) for their integration within the catchment-scale ECM framework to predict nitrate-N loads to the rivers across the Manawatū-Whanganui (Horizons) region in New Zealand. The study also aims to develop a simplified catchment-scale ECM to estimate catchment nitrate loads by integrating estimates of land use-derived root zone nitrate losses, *LSNAI*-derived AF_N values, point-source discharges and instream nitrogen uptake. Specifically, this study aims to (a) develop the catchment-scale ECM accounting for spatially variable subsurface nitrate attenuation capacity of different land units to estimate nitrate loads across the Horizons region, (b) establish a methodology to parameterise the *LSNAI* categories into spatially variable nitrate attenuation rates (AF_N), and (c) calibrate and validate the AF_N for each *LSNAI* class to predict average annual *SIN* loads across the study region.

6.3 Data and methods

6.3.1 Study area

The Manawatū-Whanganui region of New Zealand, also known as the Horizons region (Figure 6.1) covers 22,215 km^2 (2,221,500 ha) in the lower North Island of New Zealand. The region is characterised by several large river catchments that discharge into the Tasman Sea on the west coast (Figure 6.1a). Local geology ranges from Mesozoic-age basement greywacke exposed in the southern part of the region; an abundance of unconsolidated Plio-Pleistocene-age deposits throughout; and volcanic deposits in the north (Begg et al., 2005) (Figure 6.1b).

The Manawatū catchment is divided by two mountain ranges, known as the Ruahine and Tararua ranges, with the river flowing east to west through a narrow gorge, known as the Manawatū Gorge (Figure 6.1a, b). These two mountain ranges are formed by greywacke bedrock, as shown in Figure 6.1b, with the Ruahine Range in the north and Tararua Range in the south. The eastern half of the Manawatū catchment is also known as the Tararua catchment.

The region’s land use varies from native forest/conservation land and low intensity farming in steep and hill country areas, to intensive agriculture such as dairy farming and cropping on the river plains and coastal areas (Figure 6.1c). Soils in the region range from well-drained to poorly drained (Newsome et al., 2008), though drainage characteristics are highly dependent on a soil’s position in the landscape (Cowie et al., 1967; Cowie and Rijkse, 1977). Artificial drainage is a common feature in agricultural landscapes of the region, especially in lowland areas where poorly drained soils or shallow water tables exist. While the exact extent of artificial drainage has not been officially recorded, its likely extent has been modelled and mapped on the basis of land use intensity and other factors (Manderson, 2018).

Water quality concerns in the region are dominated by diffuse sources from agricultural activities (Roygard et al., 2012), with more than half of the water quality monitoring sites in the region categorised as ‘likely degrading’ or ‘very likely degrading’ for seven water quality variables (chlorophyll-*a*, visual clarity, dissolved reactive phosphorus (DRP), macroinvertebrate community index, NH_4-N, % cover of mat algae, and *SIN*) (Fraser, 2023). To achieve provisional water quality targets, reductions are required for total nitrogen (*TN*) from 46% (of the current load) in Whanganui and Whangaehu catchments, to 83% in Manawatū; and for total phosphorus from 48 % (of the current load) in Whangaehu to 84 % in Manawatū (Snelder, 2024).

The region’s diverse hydrogeological conditions have also been used to study local groundwater redox conditions and their potential for denitrification in surface flow pathways. Existence of spatially variable subsurface redox conditions had been established either through shallow groundwater monitoring (Gonzalez Moreno, 2019; Smith et al., 2017) using McMahon & Chapelle's (2008) classification, and/or through the single-well push-pull tests by observing the concentration of NO_3^--N against a conservative tracer (Collins et al., 2017; Collins, 2015; Gonzalez Moreno, 2019; Rivas et al., 2014, 2017, 2020). While a range of redox conditions were observed in shallow groundwaters in the region, subsurface denitrification was measured at only a few locations featuring reduced groundwater redox conditions. In addition, some hill country soils, including those areas with seepage wetlands, has been identified as potential hotspots for subsoil denitrification due to their elevated dissolved organic carbon levels (Chibuike et al., 2020, 2019).

Collins et al., (2025b) assessed groundwater redox conditions to be highly spatially variable and somewhat temporally stable across New Zealand landscapes, including the Manawatū-Whanganui region. Collins et al. (2025a) further assessed and mapped five *LSNAI* classes, ranging from *Very low* to *Very high*, to characterise areas of potential spatially variable subsurface nitrate attenuation in diverse land units across the study area (Table 4.6; Figure 6.1d). The *LSNAI* is a framework that assigned relative categories of subsurface nitrate attenuation to landscape units within the Horizons region. The *Very low* category was characterised exclusively by greywacke and well- or moderately-well drained soils and covers around 1,800 km^2 of the region (Table 4.6; Figure 4.5). The *Low* category was characterised by well-drained soils and a range of rock types, including mudstone and sandstone. It was also the largest single class covering approximately 12,000 km^2 of the region (Table 4.6; Figure 4.5). The *Medium LSNAI* category, covering around 6,000 km^2, was characterised by moderately-well or imperfectly drained soils with a larger proportion of mudstone and sandstone rock types compared with the *Low LSNAI* (Table 4.6; Figure 4.5). The *High* category was characterised by poorly drained or imperfectly drained soils, and predominantly alluvium or loess rock types and covers around 1,800 km^2 (Table 4.6; Figure 4.5). The *Very high* category was characterised exclusively by windblown sands on the western coast and includes a range of soil drainage classes. It was the smallest category, covering approximately 774 km^2 (Table 4.6; Figure 4.5). A high spatial variability in *LSNAI* classes potentially influences nitrate transport and attenuation in different land units across the region (Figure 6.1d).

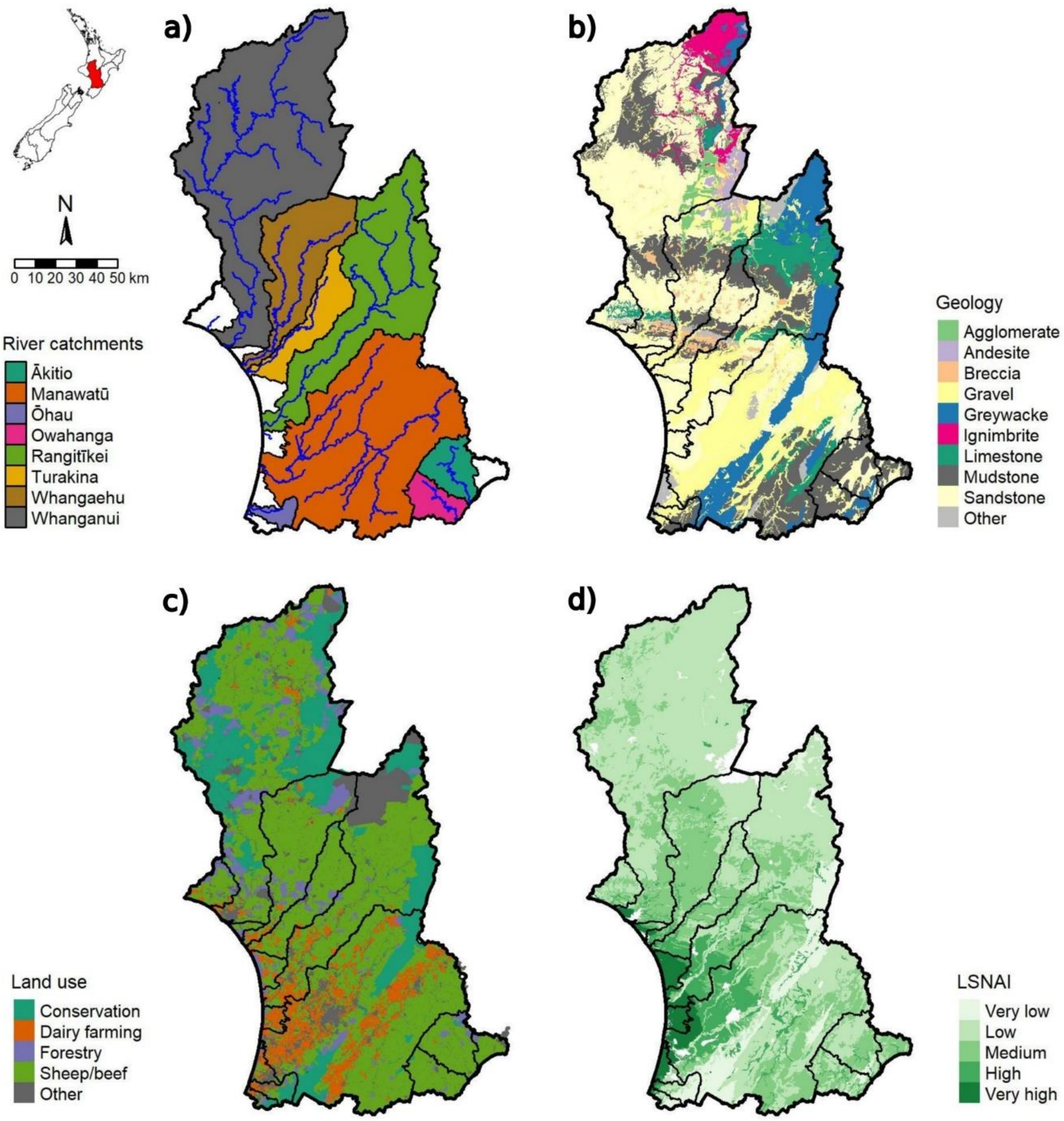

Figure 6.1: The Manawatū-Whanganui region, also known as the Horizons region, showing a) major river catchments, b) geological types (GNS Science, 2012), c) primary land uses (Herzig et al., 2020) and d) the *LSNAI* (Collins et al., 2025a).

6.3.2 Soluble inorganic nitrogen export coefficient model

The ECM framework aims to predict the loss of nutrients by calculating the sum of the individual losses exported from each nutrient source in a catchment (Johnes, 1996). Using this ECM approach, Singh et al. (2017a, 2017b) and Elwan (2018) developed hydrogeologic-based models to account for the influence of different soil types and underlying geology on the fate of *SIN* in the Rangitīkei and Tararua catchments. The average annual *SIN* loads were estimated with reasonable success when using spatially variable nitrate attenuation factors related to soil and rock types (such as texture, drainage rate and carbon content). Snelder et al. (2020) also developed catchment-scale water quality models for the Horizons region to estimate nitrogen loads and concentrations under various potential land management scenarios. The models used sub-catchment nitrogen export and attenuation coefficients and point source load estimates to estimate average annual *TN* loads in the region.

In this study, the ECM approach was further developed and applied by integrating key sources of nitrate losses and their potential attenuation in subsurface flow pathways via *LSNAI*-derived, calibrated AF_N values. It is important to note that the *LSNAI* was developed as part of an ECM framework for predicting instream nitrogen loads, rather than as a groundwater flow model or solute transport model. Mechanistic, process-based groundwater models typically require detailed characterisation of subsurface properties to simulate flow paths and travel times. In contrast, the *LSNAI* provides a simplified, spatially distributed representation of nitrate attenuation potential based on available landscape attributes, without explicitly representing subsurface flow processes or depth-dependent dynamics.

Average annual river *SIN* loads were calculated by summing the nitrogen contributions from individual landscape units, adding any point source (wastewater) discharges of *SIN* and subtracting instream nitrogen uptake. To establish a baseline, the unattenuated average annual river *SIN* load was first calculated as the aggregated root zone nitrate loss contributions from all relevant landscape units, assuming no subsurface nitrate attenuation. This includes point-source (wastewater) discharges and instream nitrogen uptake, as expressed in Equation 1:

$$Unattenuated\ SIN\ load\ \left(N\frac{t}{year}\right) = m\left(\sum(A \cdot N_{loss})\right) + D - N_{up} \qquad (Eq. 1)$$

Where:

m = conversion factor

A = area under each land use typology above the water quality monitoring station (in hectares)

N_{loss} = nitrogen loss rate related to a land use typology (in *SIN* kg ha^{-1} yr^{-1})
D = Wastewater discharge inputs (in *SIN* t yr^{-1})
N_{up} = Estimates of instream nitrogen uptake (in *SIN* t yr^{-1})

To account for spatially variable nitrate attenuation in subsurface environments, the attenuated average annual river *SIN* load was then calculated by adjusting root zone *SIN* losses with *LSNAI*-derived AF_N values and artificial drainage factors (*AD*). The AF_N adjustment reflects the proportion of nitrate losses reduced through subsurface nitrate attenuation, calculated as (1 – AF_N), where a higher AF_N indicates greater nitrate attenuation capacity. However, this capacity can be compromised by the presence of artificial drainage, which accelerates the removal of nitrate-enriched water from the soil profile. The influence of artificial drainage (where the likelihood of drainage is > 50 %; Manderson (2018)), was incorporated through an *AD* factor (1 for no drainage, 0.10 for drainage). The attenuated average annual river *SIN* load is therefore expressed in Equation 2:

$$SIN\ load\ \left(N\frac{t}{year}\right) = m\ \left(\sum\left(\ (A\ \cdot N_{loss})\cdot\left(1\ -\ (AF_N \cdot AD)\right)\right)\right) +\ D\ -\ N_{up} \qquad (Eq.\,2)$$

Where:
AF_N = Landscape subsurface nitrate attenuation factor, ranging from 0 to 1
AD = Artificial drainage factor, 1 for no drainage or 0.10 for drainage

6.3.3 Data inputs and sources

Parametrisation of catchment-scale unattenuated and spatially variable attenuated *SIN* load models (Equations 1 and 2) required the input of several data sets, including estimates of root zone N losses for each land use typology; point-source *SIN* contributions; instream *SIN* uptake; *LSNAI*-derived AF_N factor; artificial drainage extent; and the observed river *SIN* loads. The required data and inputs were collated from different data sources, described as follows.

6.3.3.1 Root zone soluble inorganic nitrogen losses

A land use typology-based inventory of contaminant losses was used to estimate root zone *SIN* losses for pastoral and non-pastoral farms across the region (Srinivasan et al., 2021). Environmental data such as climate (rainfall and winter soil temperature), landscape (slope) and soil attributes (such as drainage class) were combined with land use information in the Overseer Nutrient Budgets® tool to derive root zone *SIN* loss estimates (kg N ha^{-1} yr^{-1}; Monaghan et al., 2018; Srinivasan et al., 2021). As Overseer omits ammoniacal-N dynamics, and nitrite-N is present only in trace amounts due to its rapid conversion to nitrate-N, the estimates of root zone losses from Overseer relate primarily to nitrate-N (Ministry for the Environment and Ministry for Primary Industries, 2021). For dairy farms, estimated N losses were based on an analysis by Monaghan et al. (2018) who sought to benchmark nitrogen and phosphorus losses from New Zealand dairy farms while recognising landscape susceptibilities that may influence contaminant loss and transport in agricultural catchments. The root zone *SIN* losses (kg N ha^{-1} yr^{-1}) under sheep and beef land use typology were also estimated using Overseer (Srinivasan et al., 2021). For the remaining land uses described in the typology (deer; pastoral support land used for winter forage crop grazing; arable and mixed crops; vegetable growing; viticulture; forestry; and native bush), literature-based root zone *SIN* loss estimates (kg N ha^{-1} yr^{-1}) were used (Srinivasan et al., 2021).

To apply the typology to the Horizons region, land use, slope and moisture (rainfall) data were required. Land use data for the Horizons region (Figure 6.1 c; Herzig et al., 2020) were matched as best as possible to the typology land uses. This regional land use data does not separate ‘Beef’ and ‘Deer’ from the Sheep/beef category (which includes deer), but these are relatively minor farming categories for the region compared to Sheep/beef. Slope categories were derived from the NZLRI and reclassed into flat (0-7°); rolling (7-15°); easy hill (15-25°); and steep hill (>25°) classes. Four moisture (rainfall) categories were categorised as Irrigated, Wet (mean annual rainfall > 1700 mm), Moist (mean annual rainfall > 1100 mm) and Dry (mean annual rainfall < 1100 mm). Irrigated areas were mapped from 2020 data for the region (Dark, 2020) and rainfall data were obtained from average annual rainfall 1972-2016 (Ministry for the Environment, 2017).

6.3.3.2 Point source soluble inorganic nitrogen contributions

Point-source *SIN* discharges were quantified based on existing data of wastewater discharge monitoring across the study region. A number of wastewater treatment plants in the Horizons region discharge wastewater into the region's river network, from both municipal and industrial sources. There are a total of 29 wastewater discharges operating in the region that are consented to discharge > 20 m^3 d^{-1} (Cox et al., 2022; See Table F.1). *SIN* loads (t yr^{-1}) were calculated as the sum of the individual nitrate-N, nitrite-N and ammonium-N loads for each discharge. The mean concentration of each variable was calculated using continuous or discrete monitoring records for these discharges, and the average annual load for each variable was estimated by multiplying the mean concentration by the discharge volume (Fraser and Snelder, 2020).

6.3.3.3 Instream soluble inorganic nitrogen uptake

A source of *SIN* removal from freshwater environments is the growth of periphyton, a complex assemblage that primarily consists of benthic autotrophic algae, but may also include cyanobacteria, heterotrophic microbes and detritus (Haddadchi et al., 2020). When environmental conditions such as light availability, temperature and nutrient concentrations are favourable (Biggs and Close, 1989; Larned, 2010), periphyton can proliferate, at times reaching levels classified as 'nuisance periphyton' (Kilroy et al., 2020a; McArthur et al., 2010). Excessive periphyton growth assimilates soluble forms of nitrogen such as nitrate into the periphyton biomass as organic nitrogen, thereby removing nitrate from the water column. At certain flow thresholds, periphyton biomass is removed from the benthic substrate (Haddadchi et al., 2020; Kilroy et al., 2020b), resetting the accrual cycle and enabling renewed growth and *SIN* uptake during subsequent low-flow periods. There are no reliable estimates of the annual *SIN* uptake as a result of these instream processes in the Horizons region, however, Singh et al. (2017b) applied a simple model to estimate instream *SIN* uptake for the Rangitīkei catchment, outlined in Equation 3, as follows:

$$N_{up} = m\,(f_n \cdot AI \cdot P) \cdot (f_p \cdot W) \cdot N \qquad (Eq. 3)$$

Where:

N_{up} = Instream nitrogen uptake (in *SIN* t/year)

m = Conversion factor

f_n = Nitrogen content fraction of periphyton

AI = Autotrophic index (i.e. the ratio of periphyton biomass (ash-free dry mass) to chlorophyll-a)

P = Periphyton growth (mean chlorophyll-a mg/m^2)

f_p = Periphyton cover fraction

W = Wetted area (m^2)

N = Average number of periphyton growth accruals in a year

A number of input variables required in Equation 3 are provided by the River Environment Classification (REC), a database of catchment spatial attributes for New Zealand's river network (Snelder & Biggs, 2002). The REC divides the river network into more than more than 53,000 segments across the Horizons region, covering approximately 36,700 km of river length and assigns each segment a range of biophysical attributes, including hydrological and water quality data (Whitehead and Booker, 2020, 2019). Wetted area (W, m^2) is calculated as the product of segment length (m) and width (m) at mean annual low (summer) flow (Booker, 2010). Periphyton cover fraction (f_p, %) is provided as the modelled mean percentage cover of the riverbed (Kilroy et al., 2019), and periphyton growth (P; chlorophyll-a mg/m^2) as the modelled mean chlorophyll-a concentration for each segment (Kilroy et al., 2019).

However, the REC database does not provide estimates of either the nitrogen content fraction of periphyton (f_n, %) or the autotrophic index (AI) (Eq. 3). The nitrogen content fraction was assumed to be 0.05 (5 %) (Singh et al., 2017b). The AI is the ratio of ash free dry mass (AFDM; mg/m^2):chlorophyll-a (mg/m^2). Whereas chlorophyll-a represents the autotrophic component of a sample (i.e. algae), the AFDM represents the combined autotrophic and heterotrophic components (Biggs and Close, 1989). Lower values of AI (e.g. 50 to 100) indicate a community dominated by algae, while larger values (e.g. over 400) indicate a community dominated by heterotrophs and/or organic detritus (Biggs and Close, 1989). AFDM was collected early in Horizon's periphyton monitoring programme, however it was discontinued after an analysis of results showed AI did not increase, as expected, downstream of point source discharges (Kilroy, 2016). It was thought that AI may not be an appropriate indicator for the types of discharges being monitored in the region (Kilroy, 2016). Consequently, the AI value is not well characterised for the Horizons region, creating uncertainty when estimating instream nitrogen uptake from the river network.

To reduce this uncertainty in *AI* estimation, refinements were introduced to better represent spatial variability in periphyton accrual across the river network. Periphyton biomass was first adjusted for bed substrate composition using the river bed sediment cover data set of Haddadchi et al. (2018). Coarse, stable substrates such as cobble, boulder and bedrock provide suitable attachment surfaces for periphyton, whereas finer substrates such as sand and mud do not (Kilroy et al., 2019; Larned, 2010). Weighting factors were applied to the periphyton cover fraction (f_p) to scale potential periphyton biomass according to substrate suitability, with values ranging from 0.1 for mud, 0.75 for sand and 1.0 for stable substrates.

In addition, the *AI* was varied between river segments based on substrate composition, reflecting differences in community structure between thin algal biofilms on fine sediments (low *AI*) and filamentous periphyton mats on coarse substrates (high *AI*). Segment-specific *AI* values were calculated as weighted averages of substrate-specific values, ranging from 50 for mud, 150 for sand and 300 for stable substrates. This approach provides a more ecologically realistic representation of spatial variation in periphyton biomass composition across the river network.

Finally, an average of four periphyton accruals was assumed to occur each year (Eq. 3).

6.3.3.4 Spatially variable AF_N

The spatially variable AF_N (Eq. 2) is parametrised as per the *LSNAI* categories. The *LSNAI* had been mapped as five categories of subsurface nitrate attenuation, from *Very low* to *Very high,* at the landscape unit scale across the study region (Collins et al., 2025a). The landscape units are defined as a spatial area or unit of territory that shares similar physical and geographic characteristics (Campos-Campos et al., 2018). Each landscape unit contains attributes obtained from the New Zealand Land Resource Inventory (NZLRI; Newsome et al., 2008) that were used in the development of the *LSNAI* (Collins et al., 2025a). Extreme Gradient Boosting was used to predict landscape unit redox status by integrating a nationwide groundwater redox status data set (Collins et al., 2025b) with various landscape characteristics. Unsupervised classification was used to identify the five potential *LSNAI* classes among the Horizons region's landscape units (Collins et al., 2025a).

In this study, the *LSNAI* categorical classification is parameterised with initial estimates of spatially variable subsurface AF_N, according to their assessed subsurface nitrate attenuation potential. The *LSNAI* category of *Very low* was assigned an AF_N value of 0.1, and similarly *Low* [0.3], *Medium* [0.5], *High* [0.7], and *Very high* [0.9]. These initial estimates reflect observations of nitrate reduction in subsurface environments where oxidised subsurface environments tend to have a *Very low* or *Low* capacity for nitrate reduction, whereas reduced subsurface environments tend to have a *High* or *Very high* capacity for nitrate reduction (Clague et al., 2019; Collins et al., 2017; Rivas et al., 2017, 2020; Stenger et al., 2018). The assigned spatially variable AF_N, are then calibrated and validated by comparing the predicted with observed average annual river *SIN* loads (see section 6.3.4).

6.3.3.5 Artificial drainage extent

The spatially variable AF_N (Eq. 2) is adjusted for the artificial drainage extent of different land units. Artificial drainage has been employed in agricultural landscapes in New Zealand and around the world to increase the productivity of farmland, with both surface and subsurface artificial drainage used in poorly drained soils in New Zealand agricultural landscapes (Deuss et al., 2023; McLaren and Cameron, 1990). However, artificial drainage can compromise the effectiveness of any natural subsurface nitrate attenuation capacity by creating a shortcut from the subsurface environment to surface water (Barkle et al., 2021). While artificial drainage systems are not mapped directly in New Zealand, the soil conditions under which they are usually required means that their likelihood can be predicted in the landscape (Manderson, 2018). Using fuzzy set theory, Manderson (2018) estimated both the suitability of land for artificial drainage and the likelihood that land is artificially drained in New Zealand. Probabilities were interpreted as fuzzy confidence thresholds, with classifications ranging from *Not drained* (< 0.5), to *Drained with low confidence* (0.5 – 0.55), *moderate confidence* (0.55 – 0.6), and *high confidence* (> 0.6).

In this study, where the mapped *LSNAI* categories were intersected by the mapped artificial drainage extent (where the likelihood of drainage is > 50 %), the subsurface nitrate attenuation capacity was reduced by 90% to reflect the increased nitrate transfer pathway by drainage network. A factor of 0.10 was selected where drainage occurs to recognise that subsurface nitrate attenuation can occur quickly in some conditions (Rivas et al., 2025). Accordingly, the artificial drainage factor (*AD*) was approximated as 1 (i.e., no drainage, no change in AF_N value) or 0.10 (i.e. drainage and a 90% reduction AF_N value) (Eq. 2). This is considered a conservative approach to estimating the effect of artificial drainage on subsurface nitrate attenuation.

6.3.3.6 Observed river soluble inorganic nitrogen loads

Horizons Regional Council monitors continuous river water flows and discrete (monthly) water quality across the study region. Using existing water quality observations, Fraser (2021) calculated observed average annual river loads of *DRP*, *E. coli*, nitrate-N, nitrite-N ammonium-N, *TN*, total phosphorus and total suspended sediment. The observed average annual *SIN* load was calculated as the sum of the individual nitrate-N, nitrite-N and ammonium-N loads at 40 river water quality monitoring sites in the study region. Various methods were used to calculate the individual nitrate-N, nitrite-N and ammonium-N loads, including the flow stratification (Roygard et al., 2012), L7 and L5 methods (Cohn, 2005; Cohn et al., 1992, 1989). These rating curve methods (Cohn, 2005; Cohn et al., 1992, 1989; Roygard et al., 2012) exploit the relationship between nutrient concentrations and flow observations, which is usually necessary due to the low-frequency measurements of concentration (e.g. monthly), compared to the higher frequency of flow measurements (e.g. daily) (Snelder et al., 2017). The average annual river nitrate-N, nitrite-N and ammonium-N loads for the region were calculated for the ten-year period from 1 January 2010 to 31 December 2019, using flow and nutrient concentration pairs for each day of the sampling period, though data prior to this period were still used to define the concentration-flow rating curves (Fraser, 2021). Only sites that had at least nine out of 10 years, 80 % of quarters and at least 60 total observations were used in the analysis (Fraser, 2021). The model selection for each site (whether flow stratification, L7 or L5 was used) involved manual inspection of all possible rating curves and depended on the match between the model and functional and distributional characteristics of the data (Fraser, 2021; Snelder et al., 2017). The *SIN* load for each monitoring site is the sum of the individual nitrate-N, nitrite-N and ammonium-N loads. The quantified observed average annual river *SIN* loads can also be regarded as 'attenuated' loads because they incorporate all instream attenuation, subsurface attenuation and instream nitrogen uptake processes up to that point in the catchment. The observed average annual river *SIN* loads were used to calibrate and validate spatially variable *LSNAI*-derived AF_N (Eq. 2) to predict average annual river *SIN* loads in the study region.

6.3.4 Calibration and validation of *LSNAI*-derived AF_N rates

To derive effective subsurface AF_N rates for each *LSNAI* category, a general-purpose optimisation function (optim(); R Core Team, 2022) was used to minimise the root mean square error (*RMSE*) between the observed and predicted average annual river *SIN* loads at up to 40 river monitoring sites in the study region. The optimisation tool requires initial AF_N parameter values, which were assigned based on the *LSNAI* categories: *Very low* (0.1), *Low* (0.3), *Medium* (0.5), *High* (0.7), and *Very high* (0.9) (Section 6.3.3.4). The optimisation function employed the "L-BFGS-B" algorithm, which allows for box constraints (Byrd et al., 1995), i.e. the ability to set upper and lower bounds to the AF_N parameters. The objective function was specified to minimise the *RMSE* between the observed and predicted average annual river *SIN* loads. Specifically, the optimisation searched within the following intervals: *Very low* (0.05-0.15), *Low* (0.175-0.375), *Medium* (0.4-0.6), *High* (0.625-0.775), and *Very high* (0.85-0.95), with each *LSNAI* category constrained to a non-overlapping interval of between 0.1 and 0.2. A wider interval (0.2) was given to the *Low* and *Medium* categories, in recognition of the large amount of landscape units in these categories in the region compared to *Medium* (interval of 0.15) and *Very low* and V*ery high* (interval of 0.1). See Table 4.6 for further details about the area of each *LSNAI* category in the Horizons region. The final optimised AF_N rates were those that minimised this objective function across the entire monitoring network.

While *RMSE* served as the objective function during the model (Eq. 2) optimisation, additional metrics were also used to assess the model's performance, including mean absolute percentage error (*MAPE*); median absolute percentage error (*MdAPE*); mean absolute error (*MAE*); and *R*-squared (R^2) (Hyndman and Koehler, 2006; Willmott and Matsuura, 2005). Together, these metrics provide a more comprehensive evaluation of how well the parameterised AF_N categories in the ECM model (Eq. 2) predicted average annual river *SIN* loads relative to their observed values across the region.

There is assumed to be a slight mismatch between several of the inputs into the ECM model, as the root zone *SIN* losses represent mostly nitrate-N (Section 6.3.3.1), while the point-source *SIN* contributions (Section 6.3.3.2) and observed average annual river *SIN* loads (Section 6.3.3.6) comprise the sum of nitrate-N, nitrite-N and ammonium-N. However, in the predominantly oxidising conditions of instream environments, nitrite-N and ammonium-N rapidly convert to nitrate-N through nitrification (Wetzel, 2001). Therefore, this mismatch is considered to have a negligible effect on the comparison between predicted and observed average annual river *SIN* loads.

6.4 Results and discussion

6.4.1 Spatial variability of subsurface nitrate attenuation at sub-catchment scale

By comparing the observed and estimated unattenuated river *SIN* load (Eq. 1), the overall subsurface AF_N at the sub-catchment scale was estimated for each monitoring site (known as the 'mass balance' approach; Table 6.1). At most sites, the estimated unattenuated river *SIN* load exceeded the observed load by between 2.5 and 1189 %. At two sites, however (Ohura at Tokorima and Whanganui at Wades Landing, both in the Whanganui catchment), the opposite was observed, with the estimated unattenuated river *SIN* loads lower than the observed loads. This discrepancy may result from overestimation of the observed load, underestimation of the attenuated load, or a combination of both. Negative attenuation scores such as this highlights the substantial uncertainty involved in this analysis. Such uncertainty can arise from a number of sources, including errors in instream nitrogen load calculations (Elwan et al., 2018; Snelder et al., 2017); inaccuracies in land use data (Herzig et al., 2020); uncertainty regarding nitrogen leaching losses (Tavernet, 2023; Upton, 2018); and uncertainty related to periphyton proliferation and estimates of instream nitrogen uptake (Haddadchi et al., 2020; Kilroy et al., 2020b; Snelder et al., 2019). Together, these factors contribute to uncertainty in both observed and estimated unattenuated river *SIN* loads.

Across most sites, AF_N values ranged from 0.10 to 0.90, reflecting substantial spatial variability in subsurface nitrate attenuation processes (Table 6.1). Previous research has reported comparable values of AF_N within the region. For example, Elwan et al. (2018), also using *SIN*, applied a similar approach in the Tararua and Rangitīkei catchments, 15 sites of which overlap with this study. At two-thirds of the over-lapping sites, differences in estimated AF_N values were 0.1 or less, with 80 % within 0.2 (Table 6.1). Both studies identified Kumeti at Te Rehunga and Makuri at Tuscan Hills (Manawatū catchment) as sites with among the lowest AF_N value (< 0.3), and Rangitīkei at Pukeokahu as the site with the highest AF_N value (> 0.9) (Table 6.1). Snelder et al. (2020), while using *TN* in their analysis, also found the highest rates of AF_N at the Rangitīkei at Pukeokahu monitoring site, and low rates of AF_N across all Whanganui sites (Table 6.1).

Table 6.1: Observed and unattenuated average annual river *SIN* loads in the Horizons region. The subsurface AF_N represents the proportion of *SIN* load that is lost between the source (unattenuated *SIN* load) and the instream observation.

				AF_N		
Monitoring site	**Catchment**	**Observed *SIN* (t yr^{-1})**	**Unattenuated *SIN* (t yr^{-1})**	**This study**	**Elwan (2018)**	**Snelder et al. (2020)**
Ohura at Tokorima	Whanganui	906	629	-0.44		0.10
Whanganui at Wades Landing	Whanganui	3421	2980	-0.15		
Whanganui at Te Rewa	Whanganui	3864	3959	0.02		0.10
Makuri at Tuscan Hills	Manawatū	121	141	0.14	0.14	0.30
Kumeti at Te Rehunga	Manawatū	15	17	0.14	0.21	0.11
Whanganui at Pipiriki	Whanganui	2735	3704	0.26		0.10
Whanganui at Te Maire	Whanganui	1155	1597	0.28		0.10
Ongarue at Taringamotu	Whanganui	605	890	0.32		0.10
Tiraumea at Ngaturi	Manawatū	317	553	0.39	0.77	0.46
Whanganui at Cherry Grove	Whanganui	338	553	0.39		
Rangitīkei at McKelvies	Rangitīkei	1300	2436	0.47	0.69	0.49
Mangahao at Ballance	Manawatū	113	235	0.52	0.62	0.10
Turakina at ONeills Bridge	Turakina	264	580	0.54		0.40
Manawatū at Upper Gorge	Manawatū	1770	3897	0.55	0.50	0.35
Manawatū at Opiki Bridge	Manawatū	2226	5238	0.58		0.44
Manawatū at Teachers College	Manawatū	1892	4595	0.59		0.36
Mangatainoka at Brewery	Manawatū	346	872	0.60		0.20
Mangatoro at Mangahei Road	Manawatū	82	216	0.62	0.70	0.47
Rangitīkei at Onepuhi	Rangitīkei	640	1757	0.64	0.85	0.63
Ōhau at Gladstone Reserve	Ōhau	19	54	0.65		0.11
Whangaehu at Kauangaroa	Whangaehu	549	1648	0.67		0.50
Tokiahuru at Junction	Whangaehu	28	87	0.68		0.09
Mangatainoka at Larsons Road	Manawatū	19	59	0.68	0.61	0.10
Oroua at Awahuri Bridge	Manawatū	370	1164	0.68		0.68
Manawatū at Weber Road	Manawatū	259	824	0.69	0.74	0.45

Hautapu at US Rangitīkei River Conf	Rangitīkei	62	211	0.71		
Raparapawai at Jackson Road	Manawatū	28.8	100	0.71	0.71	0.59
Mangawhero at Pakihi Rd Bridge	Whangaehu	61	216	0.72		0.42
Oroua at Almadale Slackline	Manawatū	115	411	0.72		0.65
Manawatū at Hopelands	Manawatū	482	1764	0.73	0.66	0.37
Rangitīkei at Mangaweka	Rangitīkei	364	1358	0.70	0.87	0.68
Mangapapa at Troup Road	Manawatū	12	47	0.74	0.65	0.42
Tokomaru River at Horseshoe bend	Manawatū	8	35	0.77		
Hautapu at Papakai Road Bridge	Rangitīkei	31	140	0.78		
Pohangina at Mais Reach	Manawatū	81	398	0.80		0.64
Whakapapa at Footbridge	Whanganui	8	48	0.83		
Hautapu at Alabasters	Rangitīkei	24	140	0.83		0.70
Mangawhero at Raupiu Road	Whangaehu	104	744	0.83		0.53
Owahanga at Branscombe Bridge	Owahanga	39	410	0.90		0.60
Rangitīkei at Pukeokahu	Rangitīkei	36	464	0.92	0.94	0.75

The *SIN* attenuation factors in Table 6.1 highlight considerable spatial variability in subsurface nitrogen attenuation across the Horizons region. However, sub-catchment scale estimates represent aggregated differences at surface water monitoring sites, which often encompass large and heterogeneous areas. This aggregation can obscure finer-scale variability in subsurface nitrate attenuation processes. To address this, the *LSNAI* model (Eq. 2) was parameterised to estimate subsurface nitrogen attenuation at the landscape-unit scale, classifying from *Very low* to *Very high* nitrate attenuation (Collins et al., 2025a). This effective parametrisation provides a higher-resolution representation of subsurface nitrate attenuation variability within and across catchments.

A series of parametrisation tests were undertaken to assess whether calibration is more successful when applied across the entire region, or when stratified by load size or catchment.

6.4.2 Initial AF_N load estimates

As a baseline, *LSNAI*-derived AF_N values of *Very low* (0.1), *Low* (0.3), *Medium* (0.5), *High* (0.7) and *Very high* (0.9) were applied in Equation 1 to predict average annual river *SIN* loads for surface water quality monitoring sites. All monitoring sites were included except for Ohura at Tokorima and Whanganui at Wades Landing, which had shown negative AF_N values (Table 6.1). With these initial *LSNAI*-derived AF_N values, the catchment-scale nitrogen export model (Eq. 2) performance was moderate: *RMSE* 449 t yr^{-1}; *MAE* 267 t yr^{-1}; *MAPE* 126 %; *MdAPE* 90 %; and R^2 0.73, with average annual river *SIN* loads generally being over-predicted rather than under-predicted (Figure 6.2). The largest errors occurred at sites with smaller observed average annual river *SIN* loads (Table G.1). The most extreme case of over-prediction was Rangitīkei at Pukeokahu, with an error of 785 %. Other sites with large over-prediction errors included Owahanga at Branscombe Bridge with an error of 454 % (Table G.1); and Whakapapa at Footbridge with an error of 263 % (Table G.1). The most extreme under-prediction was Tiraumea at Ngaturi with an error of -60 % (Table G.1); followed by Makuri at Tuscan Hills with an error of -44 % (Table G.1); and Whanganui at Te Rewa with an error of -44 % (Table G.1).

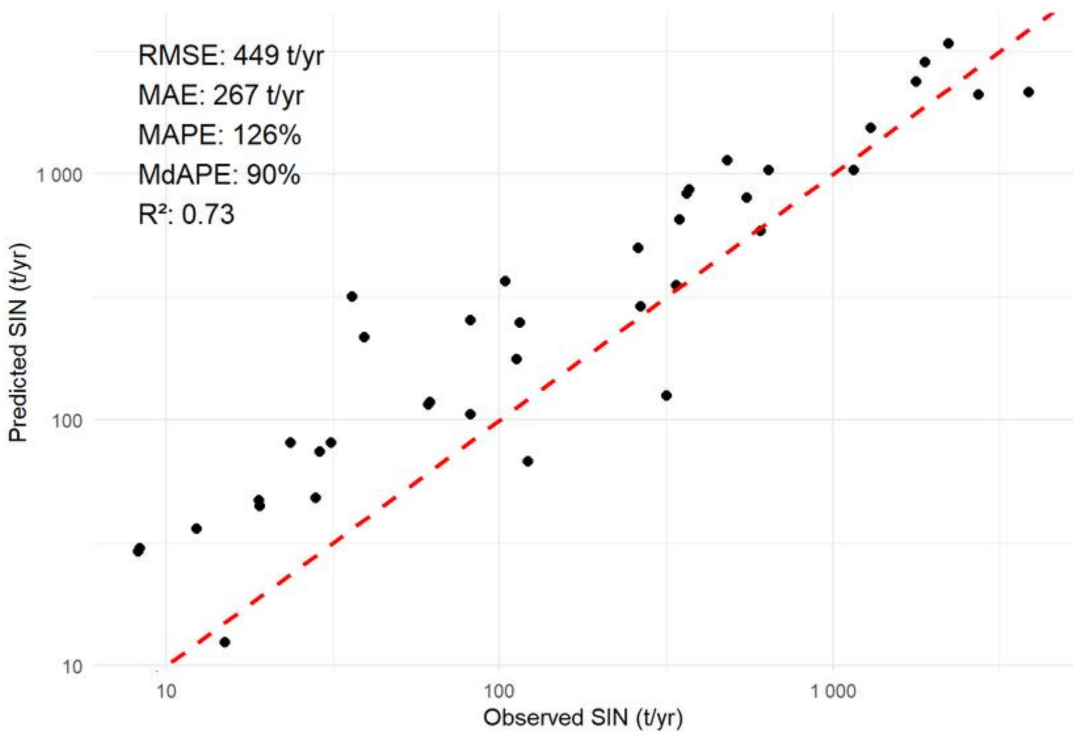

Figure 6.2: Observed and predicted average annual river *SIN* loads (t yr^{-1}) with initial AF_N values. Axes are $\log_{10}$-transformed. The red dashed line is the 1:1 line.

6.4.3 Regional calibration of AF_N for all sites

To find the best fit for the average annual river *SIN* loads, the initial values of *LSNAI*-derived AF_N values were calibrated using the optimisation method outlined in Section 6.3.4. As above, all river monitoring sites were included in this regional calibration, except the Ohura at Tokorima and Whanganui at Wades Landing, which had negative AF_N values (Table 6.1). The regional AF_N values were calibrated as *Very low* (0.150), *Low* (0.281), *Medium* (0.600), *High* (0.775) and *Very high* (0.950). However, this improved the model (Eq. 2) performance only slightly relative to the initial AF_N values, with *RMSE* reduced from 449 t yr^{-1} to 425 t yr^{-1}; *MAE* reduced from 267 t yr^{-1} to 244 t yr^{-1}; *MAPE* decreased from 126 % to 117 %; *MdAPE* reduced from 90 % to 76 %; and R^2 slightly increased from 0.73 to 0.76 (Figure 6.3). For those monitoring sites with the most extreme over- or under-predictions, errors were similar or worse than using the initial AF_N values (Section 6.4.2). The error at Rangitīkei at Pukeokahu increased from 785 % to 796 % (Table G.2); the error at Owahanga at Branscombe Bridge decreased from 485 % to 400 % (Table G.2); and the error at Whakapapa at Footbridge increased from 263 % to 277 % (Table G.2). Those sites with under-predicted average annual *SIN* loads included Tiraumea at Ngaturi where percentage error increased from -60 % to -74 % (Table G.2); the error at Makuri at Tuscan Hills increased from -44 % to -46 % (Table G.2); and the error at Whanganui at Te Rewa remained the same at -44 % (Table G.2).

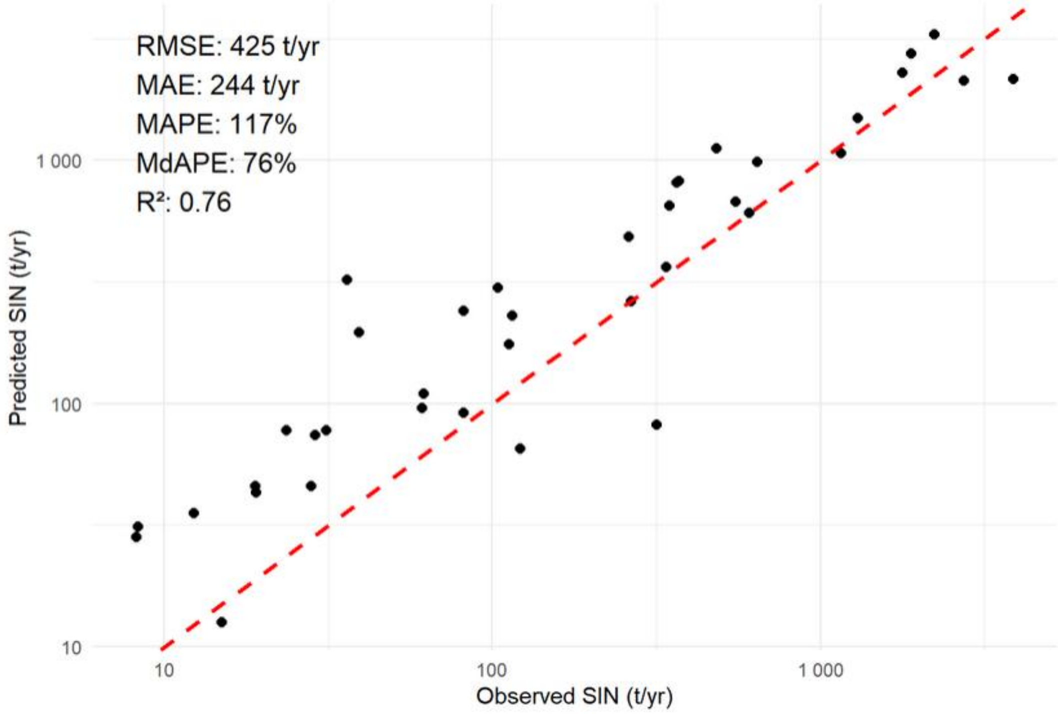

Figure 6.3: Observed and predicted average annual river *SIN* loads (t yr^{-1}) with calibrated AF_N values for all sites. Axes are $\log_{10}$-transformed. The red dashed line is the 1:1 line.

A clear pattern emerges when the observed average annual *SIN* loads are compared with the absolute percentage errors from the regional calibration. Sites with observed average annual *SIN* loads of < 500 t yr^{-1} generally had much larger percentage errors than those with observed average annual *SIN* of > 500 t yr^{-1} (Figure 6.4; Table G.2). The sites with the observed average annual *SIN* loads of > 500 t yr^{-1} had percentage errors ranging from -44 % to 55 %. This partly reflects the optimisation criteria (*RMSE*) used, which weighed improvements at large-load sites more heavily (Section 6.3.4). In addition, small catchments (observed average annual *SIN* load of < 500 t yr^{-1}) contain fewer and less diverse landscape units, reducing the potential for local estimation errors to balance out across the catchment. As a result, local discrepancies have a proportionally greater influence on total load estimates.

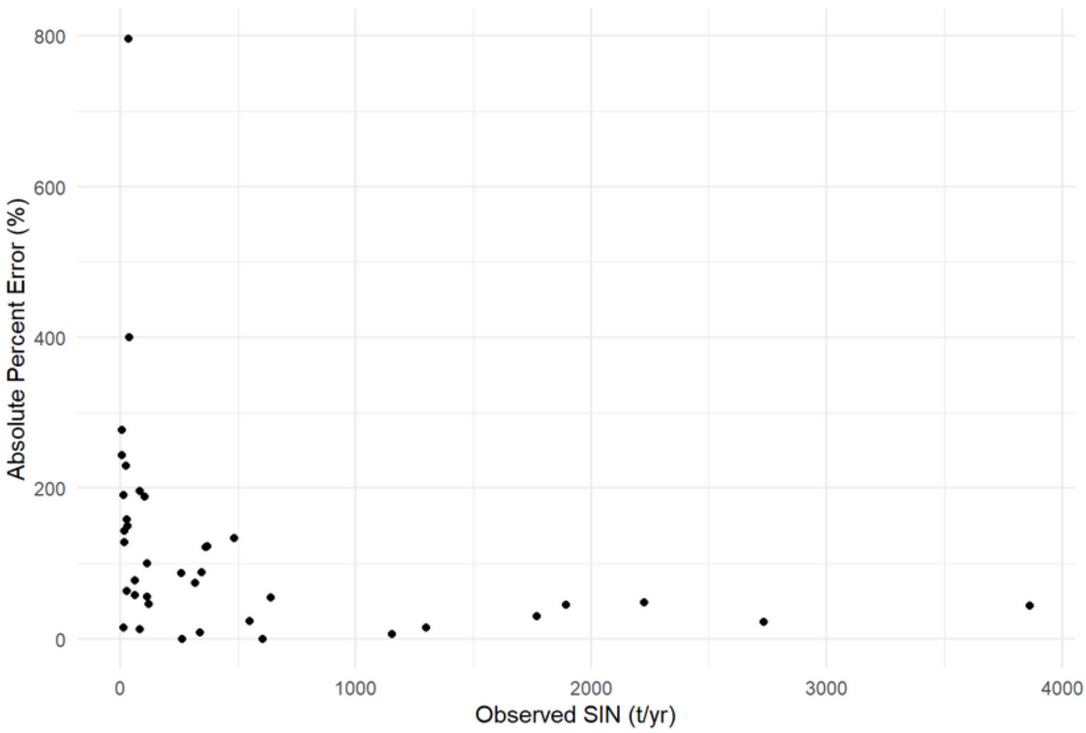

Figure 6.4: Observed average annual river *SIN* load (t yr^{-1}) and absolute percentage error (%) between the observed and average annual river *SIN* load (t yr^{-1}), as precited with the regionally calibrated AF_N values for all monitoring sites.

When the regionally calibrated AF_N values were applied to these two subsets of monitoring sites (observed average annual *SIN* loads of < 500 t yr^{-1} and observed average annual *SIN* loads of > 500 t yr^{-1}), further improvements can be seen in the model's performance metrics of the latter subset (Table 6.2). While *RMSE* and *MAE* are both larger, accounting for the larger range of monitoring site loads in this subset (from 549 average annual *SIN* t yr^{-1} at Whangaehu at Kauangaroa to 3864 average annual *SIN* t yr^{-1} at Whanganui at Te Rewa; Table G.2), both *MAPE* and *MdAPE* are reduced to 29 % and 27 %, respectively compared with 149 % and 123 % for the subset of the observed *SIN* loads < 500 t yr^{-1} (Table 6.2).

Table 6.2: Comparison of results for regionally calibrated AF_N values for all monitoring sites, monitoring sites with *SIN* loads < 500 t yr^{-1}, and monitoring sites with *SIN* loads > 500 t yr^{-1}.

Metric	Unit	Results with regionally calibrated AF_N values for all sites (Figure 6.3)	Results with regionally calibrated AF_N values applied to sites < 500 t yr^{-1}	Results with regionally calibrated AF_N values applied to sites > 500 t yr^{-1}
RMSE	*SIN* t yr^{-1}	425	209	752
MAE	*SIN* t yr^{-1}	244	134	553
MAPE	%	117	149	29

MdAPE	%	76	123	27
R^2		0.76	-1.22	0.44

6.4.4 Catchment-specific calibration of AF_N

The previous section (Section 6.4.3) calibrated the *LSNAI*-derived AF_N values by including all monitoring sites in the region. In this section, local calibrations were performed specifically for the region's major catchments (Manawatū, Rangitīkei and Whanganui). This was done to test whether a catchment-specific calibration approach can further improve *LSNAI*-derived AF_N values and river *SIN* load predictions.

6.4.4.1 AF_N calibration for the Manawatū catchment

Applying the regionally calibrated AF_N values to the Manawatū catchment, the model yielded an *RMSE* of 412 *SIN* t yr^{-1}; a *MAE* of 270 *SIN* t yr^{-1}; a *MAPE* of 100 %; a *MdAPE* of 88 %; and an R^2 of 0.64 for prediction of the average annual river *SIN* loads at 18 sites across the Manawatū catchments (Table 6.3). In the catchment-specific calibration using only Manawatū monitoring sites, the *LSNAI*-derived AF_N values were calibrated to *Very low* (0.150), *Low* (0.375), *Medium* (0.600), *High* (0.775) and *Very high* (0.900). Compared to the regionally calibrated AF_N values, the *Low* AF_N category value increased from 0.281 to 0.375, showing the Manawatū catchment required a higher rate of attenuation for the *Low LSNAI* category. The catchment-specific model performance showed improvement over both the regional calibration and the application of the regionally calibrated AF_N values in the Manawatū catchment: *RMSE* decreased to 305 *SIN* t yr^{-1}; *MAE* decreased to 208 *SIN* t yr^{-1}; *MAPE* decreased to 89 %; *MdAPE* decreased to 80 %; and R^2 improved to 0.81 (Table 6.3). More over-predictions occurred than under-predictions (Table G.3), with the largest over-prediction being Tokomaru at Horseshoe bend with a percentage error of 230 % (the observed *SIN* load of 8 t yr^{-1} versus a predicted *SIN* load of 27 t yr^{-1}). The largest under-prediction was Tiraumea at Ngaturi with a percentage error of -85 % (Table G.3; observed *SIN* load of 317 t yr^{-1} versus a predicted load of 47 t yr^{-1}).

Table 6.3: The model performance metrics comparing the observed and predicted *SIN* loads (t yr^{-1}) for the Manawatū catchment. Results are shown for the regionally calibrated AF_N values, the Manawatū catchment using regionally calibrated AF_N values, and the Manawatū catchment using locally calibrated AF_N values.

Metric	Unit	Results with regionally calibrated AF_N values (Figure 6.3)	Results with regionally calibrated AF_N values applied to Manawatū	Results with locally calibrated (Manawatū) AF_N values (Table G.3)
RMSE	*SIN* t yr^{-1}	425	412	305
MAE	*SIN* t yr^{-1}	244	270	208
MAPE	%	117	100	89
MdAPE	%	76	88	80
R^2		0.76	0.64	0.81

6.4.4.2 AF_N calibration for the Rangitīkei catchment

Applying the regionally calibrated AF_N values to the Rangitīkei yielded an *RMSE* of 253 *SIN* t yr^{-1}; a *MAE* of 203 *SIN* t yr^{-1}; a *MAPE* of 207 %; a *MdAPE* of 122 %; and an R^2 of 0.68 (Table 6.4). For local calibration using only Rangitīkei monitoring sites, AF_N values were calibrated to *Very low* (0.150), *Low* (0.375), *Medium* (0.600), *High* (0.775) and *Very high* (0.950). Compared to the regional AF_N values, the *Low* AF_N category value increased from 0.281 to 0.375, showing the Rangitīkei catchment required a higher rate of attenuation for the *Low LSNAI* category. The catchment-specific model performance showed improvement over both the regional calibration, and the application of the regionally calibrated AF_N values in the Manawatū catchment: *RMSE* decreased to 188 *SIN* t yr^{-1}; *MAE* decreased to 145 *SIN* t yr^{-1}; *MAPE* decreased to 169 %; *MdAPE* decreased to 95 %; and R^2 improved to 0.82 (Table 6.4). The monitoring site with the largest percentage error remained Rangitīkei at Pukeokahu, although this had improved, with an error of 682 % (Table G.4; the observed *SIN* load 36 t yr^{-1} versus a predicted *SIN* load of 281 t yr^{-1}).

Table 6.4: The model performance metrics comparing the observed and predicted *SIN* loads (t yr^{-1}) for the Rangitīkei catchment. Results are shown for the regionally calibrated AF_N values, the Rangitīkei catchment using regionally calibrated AF_N values, and the Rangitīkei catchment using locally calibrated AF_N values.

Metric	Unit	Results with regionally calibrated AF_N values (Figure 6.3)	Results with regionally calibrated AF_N values applied to Rangitīkei	Results with locally calibrated (Rangitīkei) AF_N values (Table G.4)
RMSE	*SIN* t yr^{-1}	425	253	188
MAE	*SIN* t yr^{-1}	244	203	145
MAPE	%	117	207	169
MdAPE	%	76	122	95
R^2		0.76	0.64	0.82

6.4.4.3 AF_N calibration for the Whanganui catchment

Applying the regionally calibrated AF_N values to the Whanganui catchment, the model yielded an *RMSE* of 741 *SIN* t yr^{-1}; a *MAE* of 408 *SIN* t yr-^{1}; a *MAPE* of 60 %; a *MdAPE* of 15 %; and an R^2 of 0.72 (Table 6.5). In the catchment-specific calibration using only Whanganui monitoring sites, AF_N values were calibrated to *Very low* (0.050), *Low* (0.175), *Medium* (0.400), *High* (0.625) and *Very high* (0.900). Compared to the regional AF_N values, all AF_N categories have been reduced, showing the Whanganui catchment required a lower rate of attenuation for all *LSNAI* categories. This is consistent with Snelder et al.'s (2020) view that the Whanganui has the lowest rate of nitrogen attenuation of any major catchment in the Horizons region. The catchment-specific model performance showed mostly improvement over both the regional calibration, and the application of the regionally calibrated AF_N values in the Whanganui catchment: *RMSE* decreased to 439 *SIN* t yr^{-1}; *MAE* decreased to 240 *SIN* t yr^{-1}; R^2 increased to 0.90; while similar but increased results were achieved for *MAPE* (73 %), *MdAPE* (23 %). The largest over-prediction error was Whakapapa at Footbridge at 358 % (Table G.5). The largest under-prediction error was Whanganui at Te Rewa at -27 % (Table G.5).

Table 6.5: The model performance metrics comparing the observed and predicted *SIN* loads (t yr^{-1}) for the Whanganui catchment. Results are shown for the regionally calibrated AF_N values, the Whanganui catchment using regionally calibrated AF_N values, and the Whanganui catchment using locally calibrated AF_N values.

Metric	Unit	Results with regionally calibrated AF_N values (Figure 6.3)	Results with regionally calibrated AF_N values applied to Whanganui	Results with locally calibrated (Whanganui) AF_N values (Table G.5)
RMSE	*SIN* t yr^{-1}	425	741	439
MAE	*SIN* t yr^{-1}	244	408	240
MAPE	%	117	60	73
MdAPE	%	76	15	23
R^2		0.76	0.72	0.90

6.4.5 Comparison of sub-catchment mass balance and *LSNAI* approaches to quantify AF_N at catchment-scale

Two approaches to estimating AF_N have been outlined in this chapter, the mass balance approach where AF_N is inferred from the observed average annual river *SIN* loads versus the estimated unattenuated average annual *SIN* loads (Section 6.4.1); and the *LSNAI* mapping approach where the *LSNAI*-derived AF_N categories are calibrated to observed average annual *SIN* loads (Section 6.4.3 and Section 6.4.4). However, these approaches are not directly comparable because of the scale at which they refine AF_N: at the sub-catchment scale for the mass balance approach; and at the landscape unit scale for the *LSNAI* approach. To compare these approaches, the *LSNAI* categories within each monitoring site were summarised (Appendix H) to compare with the mass balance-derived AF_N values (Table 6.1). The monitoring sites with the largest positive and negative regional calibration errors (Section 6.4.3, Figure 6.3, Table G.2) were compared with their respective monitoring sites from the *LSNAI* summaries (Appendix H).

Rangitīkei at Pukeokahu had the largest calibration error with an over-estimation of 796 % (Table G.2) in the average annual river *SIN* load, predicted by the *LSNAI*-derived AF_N. However, Rangitīkei at Pukeokahu also had the highest AF_N value quantified by the mass balance calculations in this analysis and that of Elwan (2018) and Snelder et al. (2020), identifying an AF_N value of 0.92, 0.94 and 0.75, respectively (Table 6.1). However, the *LSNAI* categorised this catchment predominantly as *Low* (79.9 %) and *Very low* (17.4 %) subsurface nitrate attenuation potential land units (Table H.28). Most soils are well drained (97 %; Table H.28), which are typically associated with oxidising subsurface conditions (Clague et al., 2019; Rivas et al., 2020; Table 3.7), while the geology is mainly volcanic ash, greywacke and sandstone (Table H.28). In Chapter 3, groundwater redox data suggest that these rock types tend to be oxidised: volcanic ash over greywacke (73.9 % oxidised; Table 3.4) and volcanic ash over sandstone (84.8 % oxidised; Table 3.4) together make up more than half the catchment (Table H.28). Greywacke is generally mixed (70.9 %; Table 3.4), while sandstone is split between oxidised and reduced conditions (40.6 % and 47.4 %, respectively; Table 3.4). Although these rock types are under-represented in the groundwater redox data set (Table 3.4), the available data suggest that the catchment is more likely to be oxidising and therefore not strongly conducive to significant nitrate attenuation in the subsurface environment.

Owahanga at Branscombe Bridge also had a calibration error with an over-estimation of 400 % (Table G.2) in the average annual river *SIN* load, predicted by the *LSNAI*-derived AF_N. Like Rangitīkei at Pukeokahu, this site also showed a very high sub-catchment scale AF_N inferred from the mass balance estimates (0.90; Table 6.1). However, the *LSNAI* classified this catchment as mainly *Medium* (45.6 %) and *Low* (40.4 %) subsurface nitrate attenuation potential land units, underlain by mudstone (47 %), argillite (21.9 %) and sandstone (15.9 %) rock types (Table H.23). Although no groundwater redox data were available for argillite (Table 3.4), the other rock types (mudstone and sandstone) suggest reducing subsurface conditions occur in the catchment (Table 3.4), though the quantified sub-catchment AF_N value of 0.90 is still reasonably high for the *Medium* and *Low LSNAI* categories.

Whakapapa at Footbridge had a calibration error with an over-estimation of 277 % (Table G.2) in the average annual river *SIN* load, predicted by the *LSNAI*-derived AF_N. However, Whakapapa at Footbridge also had a very high sub-catchment AF_N value inferred from the mass balance estimates (0.83; Table 6.1). The *LSNAI* classified this catchment as *Low* (100 %) subsurface nitrate attenuation potential land units, underlain almost exclusively by volcanic deposits and well drained soils (Table H.34).

The discrepancy between the sub-catchment mass balance AF_N value (Table 6.1), and the *LSNAI* assessment at these sites (Appendix H) may be due to the fact that not all the *SIN* lost through the soil profile (i.e. leached with groundwater recharge) flows to the river monitoring site at the sub-catchment. Subsurface transport pathways may be potentially responsible for diverting leached *SIN* (that is lost through the soil profile) via regional groundwater flows away from the sub-catchment outlet at the monitoring site. This phenomenon is known as inter-catchment groundwater flow (IGF), defined as groundwater flows across surface topographic divides (Bouaziz et al., 2018; Chen et al., 2024; Oda et al., 2024). Geological features such as faults, dipping beds or highly permeable conduits can divert groundwater flows to adjacent catchments (Bouaziz et al., 2018), effectively bypassing sub-catchment monitoring stations. While IGF is often overlooked in hydrological studies, it can account for up to 90 % of flows leaving a catchment as groundwater export (Schaller and Fan, 2009).

For Rangitīkei at Pukeokahu and Whakapapa at Footbridge at least, the prevalence of volcanically derived deposits and well-drained soils may not only promote oxidised conditions but also enhance groundwater losses through well-drained, porous soil and rock, potentially allowing nitrogen to bypass the monitoring site and be transported into neighbouring catchments. Well-drained soils account for 97 % and 100 % in these catchments, respectively. Rangitīkei at Pukeokahu and Whakapapa at Footbridge are located in the headwaters of their catchments, with no further monitoring sites upstream of these monitoring sites. Similarly, at Owahanga at Branscombe Bridge, the catchment is small and coastal (Figure 6.1a), and despite some indications of subsurface reducing conditions, its observed river *SIN* load may not fully capture losses that are instead transported via groundwater flows to the sea or to adjacent catchments. These circumstances could potentially create difficulties in calibrating *LSNAI*-derived AF_N values to the observed river *SIN* loads at some sites.

In contrast, the monitoring sites Tiraumea at Ngaturi, Makuri at Tuscan Hills and Whanganui at Te Rewa had the largest negative calibration errors with an under-estimation of -74 %, -46 % and -44 %, respectively (Table G.2), in the average annual river *SIN* load, predicted by the *LSNAI*-derived AF_N. However, not only are these errors smaller than those of the monitoring sites with positive calibration errors, their *LSNAI* classifications are more consistent with their inferred mass balance-derived AF_N values. Tiraumea at Ngaturi had a mass balance AF_N value of 0.39 (Table 6.1), consistent with how the *LSNAI* classified this catchment, with 57.9 % *Medium* and 34.9 % *Low* AF_N categories (Table H.30). Much of the catchment consists of mudstone (43 %) and sandstone (29.2 %) which lean towards being reduced in the groundwater redox data set (Table 3.4). Makuri at Tuscan Hills had a mass balance AF_N value of 0.14 (Table 6.1), also consistent with how the *LSNAI* classified this catchment, with 63.1 % *Low* and 27.8 % *Medium* AF_N categories (Table H.5). Here though, limestone makes up the largest rock type in the catchment (44.4 %) followed by mudstone (22.3 %) and sandstone (19.5 %). Finally, Whanganui at Te Rewa had a mass-balance AF_N value of 0.02 (Table 6.1) and is also consistent with how the *LSNAI* classified this catchment, with 84.8 % of the catchment classified as *Low* (Table H.39).

A potential reason for the under-estimation at these monitoring sites is due to the large instream *SIN* uptake component as a proportion of the total root zone *SIN* losses (Table I.1). While the mean instream *SIN* uptake as a proportion of root zone *SIN* losses is 16.1 % for all monitoring sites, for Makuri at Tuscan Hills and Tiraumea at Ngaturi it is 34.8 % and 52.1 %, respectively. Similarly, for Whanganui at Te Rewa, 26.6 % of the root zone losses are estimated to be removed through instream uptake before reaching the monitoring site. These estimates are uncertain and relatively large compared to the remaining monitoring sites in the data set, which may partially explain why the average annual river *SIN* load has been under-predicted at these sites.

Comparing the sub-catchment mass balance and *LSNAI* approaches offers important insights into how effectively each approach estimates AF_N. Although these approaches refine AF_N at different scales, the summarised *LSNAI* categories (Appendix H) provide a basis for comparing the mass balance-derived AF_N estimates (Table 6.1). Most importantly, the mass balance approach may over-estimate AF_N because it does not consider potential subsurface flows that bypass the catchment monitoring site. For example, the Rangitīkei at Pukeokahu monitoring site has a very high mass balance AF_N value but given the porous hydrogeology and oxidising nature of the rock types, it suggests there is subsurface flow pathways transferring leached *SIN* to neighbouring catchments, rather than true subsurface nitrate attenuation occurring. The *LSNAI* approach does not take into account these potential subsurface flows either, but in this case, it is potentially more realistic in mapping the extent of subsurface nitrate attenuation potential of different land units occurring in the catchment because it takes account of subsurface redox conditions, rock types and soil drainage characteristics (Section 4.4.2).

The sub-catchment mass balance calculation offers advantages in its simplicity and a direct estimate of AF_N within a sub-catchment (Table 6.1). However, their scale is constrained by the availability and location of river water quality monitoring sites, which are mostly available at a spatially lower resolution across a catchment. This approach does not capture the natural variability of subsurface nitrate attenuation dynamics of different land units within a sub-catchment. The sub-catchment scale mass balance estimates also assume that all the rootzone *SIN* leached with groundwater recharge will reach the river monitoring site. As a result, sub-catchment scale nitrogen mass balance estimates can be misleading in some sub-catchments, where subsurface groundwater flow and nitrogen losses are not fully captured and measured at the river monitoring sites, such as where IGF occurs. For example, subsurface groundwater flow pathways may divert a portion of leached *SIN* to neighbouring downstream sub-catchments or directly to the coast, which is likely the case in the Rangitīkei at Pukeokahu and Whakapapa at Footbridge sub-catchments.

In contrast, the *LSNAI* identified AF_N categories at landscape unit scale, providing higher spatial resolution and a process-based assessment of subsurface nitrate attenuation potential, reducing the influence of subsurface flow bypasses. However, the challenge remains in effectively parameterising and calibrating *LSNAI*-derived AF_N values in such sub-catchments, because it is unknown what proportion of the observed river *SIN* loads at the river monitoring site represents inputs from the sub-catchment root zone versus contributions or losses mediated by groundwater flows at catchment-scale. This could be potentially assessed by constructing sub-catchment water balances or detailed groundwater flow models to further refine mapping and calibrations of *LSNAI*-derived AF_N of different land units at catchment-scale.

6.5 Conclusion

This study applied and tested a catchment nutrient ECM framework, integrating land use derived *SIN* losses; point source discharges; estimates of instream uptake; and artificial drainage estimates, to parameterise the *LSNAI*'s categorical variables to model average annual river *SIN* loads. The observed average annual river *SIN* loads at river water quality monitoring sites were used to calibrate the AF_N value for each *LSNAI* category (from *Very low* to *Very high*) on a regional basis (Section 6.4.3) and on a catchment basis (Section 6.4.4). Results demonstrated that calibration errors were highest for monitoring sites with river *SIN* loads < 500 t yr^{-1} (*RMSE* 209 *SIN* t yr^{-1}; *MAE* 134 *SIN* t yr^{-1}; *MAPE* 149 %; *MdAPE* 123 %) compared with monitoring sites with river *SIN* loads > 500 t yr^{-1} (*RMSE* 752 *SIN* t yr^{-1}; *MAE* 553 *SIN* t yr^{-1}; *MAPE* 29 %; *MdAPE* 27 %). The average annual river *SIN* load predictions were slightly improved when separate catchment-specific calibrations were performed for the Manawatū (*RMSE* 305 *SIN* t yr^{-1}; *MAE* 208 *SIN* t yr^{-1}; *MAPE* 89 %; *MdAPE* 80 %), Rangitīkei (*RMSE* 188 *SIN* t yr^{-1}; *MAE* 145 *SIN* t yr^{-1}; *MAPE* 169 %; *MdAPE* 95 %) and Whanganui (*RMSE* 439 *SIN* t yr^{-1}; *MAE* 240 *SIN* t yr^{-1}; *MAPE* 73 %; *MdAPE* 23 %) catchments, rather than applying the regional calibration of *LSNAI*-derived AF_N values to these catchments.

However, potential uncertainties in the ECM inputs (such as the estimates of land use derived *SIN* root zone losses, instream nitrogen attenuation, observed river *SIN* loads and the effect of artificial drainage) can contribute to the calibration errors. Furthermore, a comparison between the sub-catchment mass balance and *LSNAI* approaches to the quantification of AF_N values revealed a further source of uncertainty for both approaches. Subsurface flows of the root zone leached *SIN* within a sub-catchment are assumed to flow to the relevant river monitoring site, however, it could potentially be bypassed and transported into downstream neighbouring sub-catchments. This detail emerged when comparing the AF_N values derived from the mass balance approach with summaries of *LSNAI*, soil drainage and rock type categories for each monitoring site. The mass balance approach can over-estimate AF_N by assuming all root zone losses will flow to the monitoring site, but the *LSNAI* partially avoids this as it is based on subsurface redox conditions, soil drainage and rock type characteristics. However, the *LSNAI* is still vulnerable to calibration errors because it is unknown what proportion of the observed river *SIN* load represents inputs from the sub-catchment root zone versus contributions mediated by groundwater flows.

Chapter 7: Synthesis and conclusions

The aim of this thesis was to refine the estimates of subsurface nitrate attenuation potential in New Zealand agricultural landscapes. During the development of the One Plan, the Horizons Regional Council's resource management plan, the nitrogen attenuation coefficient (*R*) was assumed to be 0.5 throughout the Manawatū and other priority catchments (Clothier et al., 2007) (Figure 7.1). Subsurface nitrate attenuation was known to be spatially variable, but methods and data were lacking to refine this estimate to scales more reflective of natural variability. Starting in 2017, estimates were refined to sub-catchment scale and expressed as the nitrogen attenuation factor (AF_N) to map greater spatial variability in nitrogen attenuation dynamics across the region (Elwan et al., 2018; Singh et al., 2017a, 2017b) (Figure 7.1). At sub-catchment scale, the spatial variability of AF_N is demonstrated, but still obscures natural subsurface nitrate attenuation dynamics of diverse land units across these sub-catchments. In this thesis, the Landscape Subsurface Nitrate-Attenuation Index (*LSNAI*), has been developed as a novel approach to reflect the natural spatial variability of subsurface nitrate attenuation potential across land units; and to represent this variability at a scale relevant for land use decisions, mitigation strategies and regulatory application (Figure 7.1). Landscape units provide the spatial framework for upscaling proxies of subsurface denitrification potential, such as soil-hydrobiogeological properties and subsurface redox conditions, in order to model and map five *LSNAI* categories of land units across New Zealand's agricultural landscapes.

This chapter synthesises the findings of Chapters 3-6, from collating and assessing a national-scale data set of groundwater redox conditions in New Zealand (Chapter 3); developing the *LSNAI* mapping tool for the Horizons region based on landscape variables and groundwater redox predictions (Chapter 4); validating the *LSNAI* categories in hill country landscapes (Chapter 5); and parameterising the *LSNAI* categories to provide calibrated estimates of subsurface AF_N at landscape unit scale (Chapter 6).

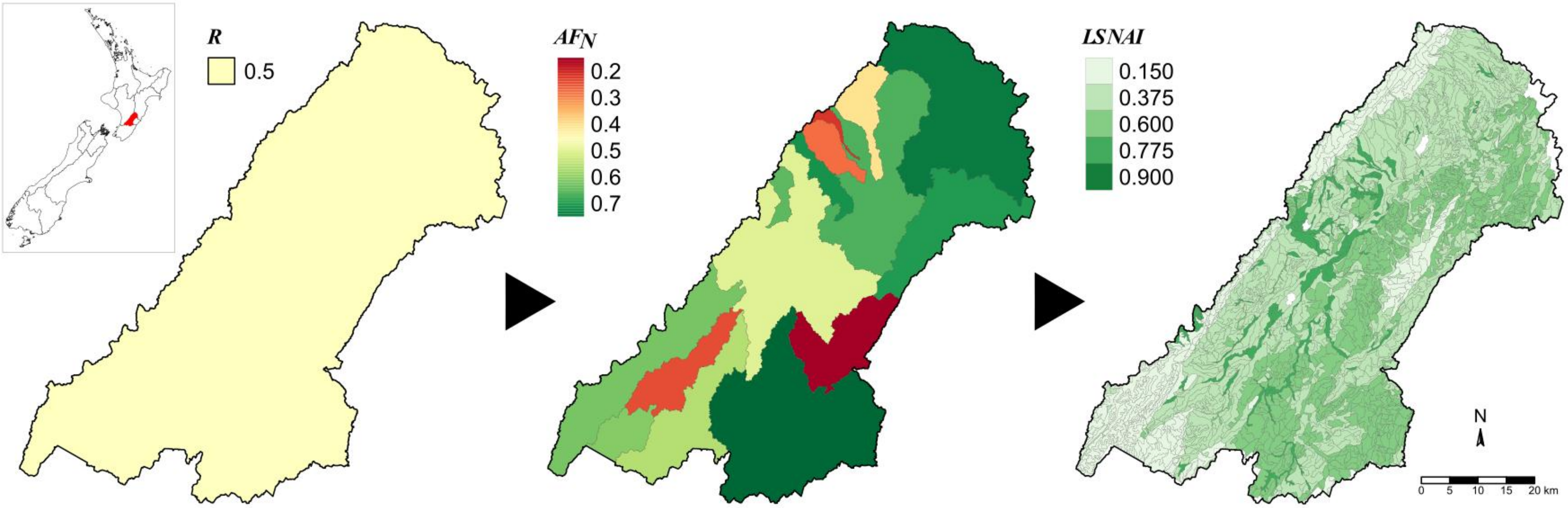

Figure 7.1: Example of the refinement of subsurface nitrogen attenuation dynamics in the Tararua catchment of the Horizons region, New Zealand. From the nitrogen transmission coefficient (*R*; Clothier et al., 2007), to the sub-catchment mass balance based nitrogen attenuation factor (AF_N; Elwan et al., 2018), and the Landscape Subsurface Nitrate-Attenuation Index (*LSNAI*; Collins et al., 2025a).

This thesis demonstrates that subsurface nitrate attenuation is more effectively represented at landscape unit-scale than as a uniform or sub-catchment-aggregated process. The *LSNAI* captures heterogeneity in soil, lithological and subsurface redox conditions that drive denitrification potential across landscapes.

A key finding of this research is that subsurface redox conditions, a primary driver of subsurface nitrate attenuation, are both spatially variable and unevenly represented in available data sets. The national groundwater redox data set compiled in Chapter 3 revealed a bias toward lowland and alluvial environments, with steeper, complex landscapes under-represented. Despite this limitation, predictive modelling of subsurface redox conditions using landscape attributes as predictor variables proved effective. The XGBoost model developed in Chapter 4 demonstrated that key variables such as soil drainage and rock type are strong predictors of landscape unit subsurface redox status (oxidised or reduced subsurface conditions). These predictions enabled the development of the *LSNAI* by integrating landscape unit subsurface redox probabilities with soil and rock type characteristics to classify landscape units into five categories of nitrate attenuation potential (from *Very low* to *Very high*). This represents a shift from coarse, sub-catchment-scale estimates toward a finer scale resolution framework that better reflects natural spatial variability.

Field-based observations of soil redox potential provided a means to evaluate *LSNAI* classifications and partially address the limitations identified in Chapter 3. Differences in soil redox potential dynamics observed across contrasting soil types aligned with the assigned *LSNAI* categories, providing site-based evidence supporting the conceptual basis of the *LSNAI*. However, these observations also highlighted temporal variability in subsurface redox conditions (also identified in Chapter 3) and reinforced that the *LSNAI* represents a simplified, steady-state estimate of nitrate attenuation potential, rather than a dynamic, process-based representation of subsurface processes.

In Chapter 6, application of the *LSNAI* within an export coefficient modelling framework demonstrated its practical use for estimating instream river nitrogen loads. Parameterisation of *LSNAI* categories into AF_N values allowed landscape unit-scale spatial variability in subsurface nitrate attenuation to be incorporated into catchment-scale modelling. While this improved representation of subsurface nitrate attenuation relative to uniform or sub-catchment approaches, calibration results indicated that additional factors, such as catchment-specific hydrogeology and inter-catchment groundwater flows, can influence nitrogen transport and are not fully captured within the current *LSNAI* framework.

Together, these findings demonstrate that incorporating estimates of subsurface nitrate attenuation at landscape unit-scale provides a more realistic and management-relevant basis for estimating nitrogen losses and informing appropriate land use and mitigation strategies.

7.1 Limitations and generalisability

The *LSNAI* framework was developed from data sets available nationwide, including groundwater redox data, and data on soil properties, rock type and other landscape characteristics. It is therefore transferable to other regions and would support broad applicability across New Zealand agricultural landscapes. However, several limitations restrict its generalisability. First, predictions of subsurface redox conditions depend on the availability and representativeness of groundwater data, which are biased toward lowland and alluvial environments. Although field-based evaluation of the *LSNAI* categories is useful and provide some confidence in the *LSNAI*'s applicability, it can only partially address this limitation. Second, the *LSNAI* does not specifically represent subsurface flow pathways, residence times or depth-dependent processes. It should therefore only be interpreted as a simplified representation of subsurface nitrate attenuation potential, rather than a process-based mechanistic model of nitrate transport. Third, calibration results suggest that catchment-specific factors, such as hydrogeology and inter-catchment groundwater flows, may influence nitrogen attenuation beyond what can be captured in the current framework.

7.2 Recommendations

Research into the spatial variability of subsurface nitrate attenuation potential is ongoing and the *LSNAI* developed in this thesis provides a novel approach to this field. Like many advances, it has been developed using imperfect data and several sources of uncertainty currently limit its accuracy when predicting river *SIN* loads at sub-catchment scale.

Addressing these uncertainties will strengthen the *LSNAI*'s value as a tool for land and water management in New Zealand's agricultural catchments. Potential avenues for future research include:

- **Expand validation of subsurface redox conditions in hill country landscapes.** Groundwater redox data are abundant for flat landscapes but scarce for hill country, which represents ~ 70 % of the Horizons region. This is a major source of uncertainty because the *LSNAI* is based on modelled subsurface redox status at landscape unit scale. While soil redox probe measurements made in this study supported the *LSNAI* categories, broader data sets are required to confirm its applicability across diverse hill country environments. Developing a method to validate subsurface redox conditions at scale, in a way that is repeatable and cost-effective, would substantially reduce potential uncertainty in the *LSNAI*'s classification of hill country land units.
- **Further validate *LSNAI* categories in a wider range of soil and rock type combinations.** Additional validation could be achieved through integrated measurements of subsurface nitrate attenuation using combinations of groundwater redox monitoring, push-pull tests and soil redox potential (*Eh*) measurements across a wider range of rock types and soil drainage classes.
- **Refine estimates of instream *SIN* uptake and attenuation.** Periphyton uptake plays a crucial role in regulating river *SIN* loads, yet robust estimates of annual uptake (t yr^{-1}) have not been quantified for the Horizons region. Current regional estimates of instream *SIN* uptake as a proportion of root zone losses range widely, from 0.7 % to 52.1 %. Improving these estimates at stream-reach or sub-catchment scale would reduce uncertainty in average annual river *SIN* load modelling and improve calibration of AF_N values.
- **Quantify the effects of artificial drainage on subsurface nitrate attenuation**. Artificial drainage can significantly reduce the time available for denitrification to occur by creating a shortcut between the root zone and surface water. This study adopted a conservative assumption that artificial drainage reduces subsurface nitrate attenuation potential by 90 %. More precise quantification of this effect would reduce uncertainty in *SIN* load modelling and improve AF_N calibration.
- **Construct and analyse sub-catchment water balances.** Current *LSNAI*-derived and mass balance-based AF_N calibrations assume that subsurface *SIN* flows

remain within a sub-catchment and are fully accounted for at its monitoring site. However, as outlined in Section 6.4.5, subsurface transfers across catchment boundaries, known as IGF, may occur, leading to under- or over-estimation of subsurface nitrate attenuation rates. Constructing site-specific water balances for river monitoring sites would help identify and quantify unaccounted *SIN* losses, thereby improving the reliability of *LSNAI*-based predictions.

7.3 Concluding remarks

This thesis demonstrates that subsurface nitrate attenuation can be more accurately and usefully represented at landscape unit-scale by integrating landscape-scale influences on subsurface processes. Previous approaches in the Horizons region had applied either uniform assumptions, or sub-catchment scale mass balance methods to estimating subsurface nitrate attenuation. While both approaches represent practical solutions to a complex challenge, neither adequately captures the natural variability of subsurface nitrate attenuation potential across diverse land units within agricultural catchments.

To address this limitation, this thesis developed the Landscape Subsurface Nitrate-Attenuation Index (*LSNAI*), a new spatial framework that integrates modelled subsurface redox conditions with key landscape attributes at landscape unit scale. This represents a significant advance over previous approaches, enabling the mapping and modelling of subsurface nitrate attenuation at a resolution that reflects natural spatial variability. By incorporating this variability into modelling frameworks, the *LSNAI* provides a more realistic basis for estimating nitrogen losses. From a management perspective, the *LSNAI* enables a more targeted approach to reducing nitrogen losses, for example by identifying areas of low attenuation capacity where interventions are likely to be most effective. This supports the alignment of land use decisions with the natural capacity of the landscape to attenuate nitrogen, improving both environmental outcomes and the efficiency of mitigation strategies.

Nevertheless, uncertainties remain in the calibration and validation of *LSNAI*-derived subsurface nitrate attenuation factors, particularly within under-represented landscapes. Additional uncertainties also relate to quantifying instream *SIN* uptake and accounting for subsurface *SIN* transfers between sub-catchments. Addressing these through further field validation and model refinement will enhance the *LSNAI*'s predictive accuracy and broaden its applicability.

Overall, the *LSNAI* provides a practical, scalable and scientifically grounded framework that integrates landscape characteristics with subsurface processes. It offers a practical pathway toward more effective and sustainable management of agricultural nitrogen impacts on water quality, both within the Horizons region and in other New Zealand agricultural catchments.

References

Abrahamsen, P., Hansen, S., 2000. Daisy: an open soil-crop-atmosphere system model. Environ. Model. Softw. 15, 313–330. https://doi.org/10.1016/s1364-8152(00)00003-7

Addy, K., Kellogg, D.Q., Gold, A.J., Groffman, P.M., Ferendo, G., Sawyer, C., 2002. In Situ Push–Pull Method to Determine Ground Water Denitrification in Riparian Zones. J. Environ. Qual. 31, 1017–1024. https://doi.org/10.2134/jeq2002.1017

Alexander, P., Rounsevell, M.D.A., Dislich, C., Dodson, J.R., Engström, K., Moran, D., 2015. Drivers for global agricultural land use change: The nexus of diet, population, yield and bioenergy. Glob. Environ. Change 35, 138–147. https://doi.org/10.1016/j.gloenvcha.2015.08.011

Alexander, R.B., Elliott, A.H., Shankar, U., McBride, G.B., 2002. Estimating the sources and transport of nutrients in the Waikato River Basin, New Zealand. Water Resour. Res. 38. https://doi.org/10.1029/2001WR000878

Anas, M., Liao, F., Verma, K.K., Sarwar, M.A., Mahmood, A., Chen, Z.-L., Li, Q., Zeng, X.-P., Liu, Y., Li, Y.-R., 2020. Fate of nitrogen in agriculture and environment: agronomic, eco-physiological and molecular approaches to improve nitrogen use efficiency. Biol. Res. 53, 47. https://doi.org/10.1186/s40659-020-00312-4

Anderson, T.R., Goodale, C.L., Groffman, P.M., Walter, M.T., 2014a. Assessing denitrification from seasonally saturated soils in an agricultural landscape: A farm-scale mass-balance approach. Agric. Ecosyst. Environ. 189, 60–69. https://doi.org/10.1016/j.agee.2014.03.026

Anderson, T.R., Groffman, P.M., Kaushal, S.S., Walter, M.T., 2014b. Shallow Groundwater Denitrification in Riparian Zones of a Headwater Agricultural Landscape. J. Environ. Qual. 43, 732–744. https://doi.org/10.2134/jeq2013.07.0303

Arauzo, M., Valladolid, M., 2013. Drainage and N-leaching in alluvial soils under agricultural land uses: Implications for the implementation of the EU Nitrates Directive. Agric. Ecosyst. Environ. 179, 94–107. https://doi.org/10.1016/j.agee.2013.07.013

Avendaño Veas, F., 2023. Quantifying and reducing nitrogen leaching under intensive vegetable production in Horowhenua (Doctor of Philosophy). Massey University, Palmerston North, New Zealand. https://mro.massey.ac.nz

Ballantine, D.J., Davies-Colley, R.J., 2014. Water quality trends in New Zealand rivers: 1989–2009. Environ. Monit. Assess. 186, 1939–1950. https://doi.org/10.1007/s10661-013-3508-5

Barbieri, M., Carrera, J., Sanchez-Vila, X., Ayora, C., Cama, J., Köck-Schulmeyer, M., López De Alda, M., Barceló, D., Tobella Brunet, J., Hernández García, M., 2011. Microcosm experiments to control anaerobic redox conditions when studying the fate of organic micropollutants in aquifer material. J. Contam. Hydrol. 126, 330–345. https://doi.org/10.1016/j.jconhyd.2011.09.003

Barkle, G., Stenger, R., Moorhead, B., Clague, J., 2021. The importance of the hydrological pathways in exporting nitrogen from grazed artificially drained land. J. Hydrol. 597, 126218. https://doi.org/10.1016/j.jhydrol.2021.126218

Barringer, J., Wilde, H., Willoughby, J., Burgham, S., Hewitt, A., Gibb, R., Newsome, P.J.F., Rijkse, W.C., 1998. Restructuring the New Zealand Land Resource Inventory to meet the changing needs for spatial information in environmental research and management, in: 10th Colloquium of the Spatial Information Research Centre. University of Otago, New Zealand, pp. 25–33.

Becker, R., Schüth, C., Merz, R., Khaliq, T., Usman, M., Beek, T.A.D., Kumar, R., Schulz, S., 2023. Increased heat stress reduces future yields of three major crops in Pakistan's Punjab region despite intensification of irrigation. Agric. Water Manag. 281, 108243. https://doi.org/10.1016/j.agwat.2023.108243

Bedi, S., Samal, A., Ray, C., Snow, D., 2020. Comparative evaluation of machine learning models for groundwater quality assessment. Environ. Monit. Assess. 192, 776. https://doi.org/10.1007/s10661-020-08695-3

Begg, J.G., Palmer, A., Gyopari, M., 2005. Geological synopsis of the Manawatu-Horowhenua area for a review of the region's hydrogeology (No. 2005/EXT/687). Horizons Regional Council, Palmerston North, New Zealand. https://archivescentral.org.nz/records

Bekesi, G., 1999. Nitrate-Nitrogen in Horowhenua Groundwater (No. 99/INT/154). Horizons Regional Council, Palmerston North, New Zealand. https://archivescentral.org.nz/records

Bell, V.A., Naden, P.S., Tipping, E., Davies, H.N., Carnell, E., Davies, J.A.C., Dore, A.J., Dragosits, U., Lapworth, D.J., Muhammed, S.E., Quinton, J.N., Stuart, M., Tomlinson, S., Wang, L., Whitmore, A.P., Wu, L., 2021. Long term simulations of macronutrients (C, N and P) in UK freshwaters. Sci. Total Environ. 776, 145813. https://doi.org/10.1016/j.scitotenv.2021.145813

Beven, K., 2012. Rainfall-Runoff Modelling: The Primer, 1st ed. Wiley. https://doi.org/10.1002/9781119951001

Bibi, S., Saifullah, Naeem, A., Dahlawi, S., 2016. Environmental Impacts of Nitrogen Use in Agriculture, Nitrate Leaching and Mitigation Strategies, in: Hakeem, K.R., Akhtar, J., Sabir, M. (Eds.), Soil Science: Agricultural and Environmental Prospectives. Springer International Publishing, Cham, pp. 131–157. https://doi.org/10.1007/978-3-319-34451-5_6

Bieger, K., Arnold, J.G., Rathjens, H., White, M.J., Bosch, D.D., Allen, P.M., Volk, M., Srinivasan, R., 2017. Introduction to SWAT+, A Completely Restructured Version of the Soil and Water Assessment Tool. J. Am. Water Resour. Assoc. 53, 115–130. https://doi.org/10.1111/1752-1688.12482

Biggs, B.J.F., Close, M.E., 1989. Periphyton biomass dynamics in gravel bed rivers: the relative effects of flows and nutrients. Freshw. Biol. 22, 209–231. https://doi.org/10.1111/j.1365-2427.1989.tb01096.x

Billy, C., Birgand, F., Ansart, P., Peschard, J., Sebilo, M., Tournebize, J., 2013. Factors controlling nitrate concentrations in surface waters of an artificially drained agricultural watershed. Landsc. Ecol. 28, 665–684. https://doi.org/10.1007/s10980-013-9872-2

Blicher-Mathiesen, G., Andersen, H.E., Carstensen, J., Børgesen, C.D., Hasler, B., Windolf, J., 2014. Reprint of "Mapping of nitrogen risk areas." Agric. Ecosyst. Environ. 198, 83–93. https://doi.org/10.1016/j.agee.2014.06.031

Böhlke, J.K., Wanty, R., Tuttle, M., Delin, G., Landon, M., 2002. Denitrification in the recharge area and discharge area of a transient agricultural nitrate plume in a glacial outwash sand aquifer, Minnesota. Water Resour. Res. 38, 10-1-10–26. https://doi.org/10.1029/2001wr000663

Boisson, A., De Anna, P., Bour, O., Le Borgne, T., Labasque, T., Aquilina, L., 2013. Reaction chain modeling of denitrification reactions during a push–pull test. J. Contam. Hydrol. 148, 1–11. https://doi.org/10.1016/j.jconhyd.2013.02.006

Booker, D.J., 2010. Predicting wetted width in any river at any discharge. Earth Surf. Process. Landf. 35, 828–841. https://doi.org/10.1002/esp.1981

Børgesen, C.D., Pullens, J.W., Zhao, J., Blicher-Mathiesen, G., Sørensen, P., Olesen, J.E., 2022. NLES5 – An empirical model for estimating nitrate leaching from the root zone of agricultural land. Eur. J. Agron. 134, 126465. https://doi.org/10.1016/j.eja.2022.126465

Bouaziz, L., Weerts, A., Schellekens, J., Sprokkereef, E., Stam, J., Savenije, H., Hrachowitz, M., 2018. Redressing the balance: quantifying net intercatchment groundwater flows. Hydrol. Earth Syst. Sci. 22, 6415–6434. https://doi.org/10.5194/hess-22-6415-2018

Brathwaite, R.L., Gazley, M.F., Christie, A.B., 2017. Provenance of titanomagnetite in ironsands on the west coast of the North Island, New Zealand. J. Geochem. Explor. 178, 23–34. https://doi.org/10.1016/j.gexplo.2017.03.013

Breiman, L., 2001. Random Forests. Mach. Learn. 45, 5–32. https://doi.org/10.1023/A:1010933404324

Buckthought, L.E., Clough, T.J., Cameron, K.C., Di, H.J., Shepherd, M.A., 2015. Urine patch and fertiliser N interaction: Effects of fertiliser rate and season of urine application on nitrate leaching and pasture N uptake. Agric. Ecosyst. Environ. 203, 19–28. https://doi.org/10.1016/j.agee.2015.01.019

Burbery, L., 2018. Nitrate reactivity in groundwater: A brief review of the science, practical methods of assessment, and collation of results from New Zealand field investigations. J. Hydrol. N. Z. 57, 41–70. https://www.hydrologynz.org.nz/journal-of-hydrology

Byrd, R.H., Lu, P., Nocedal, J., Zhu, C., 1995. A Limited Memory Algorithm for Bound Constrained Optimization. SIAM J. Sci. Comput. 16, 1190–1208. https://doi.org/10.1137/0916069

Cameron, K.C., Di, H.J., Moir, J.L., 2013. Nitrogen losses from the soil/plant system: a review. Ann. Appl. Biol. 162, 145–173. https://doi.org/10.1111/aab.12014

Campos-Campos, O., Cruz-Cárdenas, G., Aquino, R.J.C., Moncayo-Estrada, R., Machuca, M.A.V., Meléndez, L.A.Á., 2018. Historical delineation of landscape units using physical geographic characteristics and land use/cover Change. Open Geosci. 10, 45–57. https://doi.org/10.1515/geo-2018-0004

Cao, S., Yin, P., Liu, C., Hu, X., Liu, Y., Zhao, Y., Guan, X., Li, Y., 2025. Deciphering denitrification drivers in a high-nitrogen estuary: Insights from stable isotope analysis and microbial molecular techniques. Sci. Total Environ. 969, 178987. https://doi.org/10.1016/j.scitotenv.2025.178987

Carter, R.M., Naish, T.R., 1998. A review of Wanganui Basin, New Zealand: global reference section for shallow marine, Plio–Pleistocene (2.5–0 Ma) cyclostratigraphy. Sediment. Geol. 122, 37–52. https://doi.org/10.1016/S0037-0738(98)00097-9

Chan, P.L.R., Arhonditsis, G.B., Thompson, K.A., Eimers, M.C., 2024. A regional examination of the footprint of agriculture and urban cover on stream water quality. Sci. Total Environ. 945, 174157. https://doi.org/10.1016/j.scitotenv.2024.174157

Chen, H.-Y., Yeh, H.-F., Ke, C.-C., Yang, Y.-S., Huang, C.-C., 2024. Deciphering inter-catchment groundwater flow: A water balance perspective in the Choshui River Basin, Taiwan. J. Hydrol. Reg. Stud. 53, 101742. https://doi.org/10.1016/j.ejrh.2024.101742

Chen, T., Guestrin, C., 2016. XGBoost: A Scalable Tree Boosting System, in: Proceedings of the 22nd ACM SIGKDD International Conference on Knowledge Discovery and Data Mining. ACM, San Francisco California USA, pp. 785–794. https://doi.org/10.1145/2939672.2939785

Cherry, K.A., Shepherd, M., Withers, P.J.A., Mooney, S.J., 2008. Assessing the effectiveness of actions to mitigate nutrient loss from agriculture: A review of methods. Sci. Total Environ. 406, 1–23. https://doi.org/10.1016/j.scitotenv.2008.07.015

Chibuike, G., Burkitt, L., Bretherton, M., Camps-Arbestain, M., Singh, R., Bishop, P., Hedley, C., Roudier, P., 2019. Dissolved organic carbon concentration and denitrification capacity of a hill country sub-catchment as affected by soil type and slope. N. Z. J. Agric. Res. 62, 354–368. https://doi.org/10.1080/00288233.2018.1508041

Chibuike, G., Burkitt, L., Camps-Arbestain, M., Singh, R., Bretherton, M., Bishop, P., Shen, Q., 2020. Denitrification Capacity of Hill Country Wet and Dry Area Soils as Influenced by Dissolved Organic Carbon Concentration and Chemistry. Wetlands 40, 681–691. https://doi.org/10.1007/s13157-019-01223-1

Chibuike, G., Singh, R., Burkitt, L., 2024. The effects of pastoral hill country natural landscape features and land management practices on nitrate losses and its potential attenuation for improved water quality. J. Sustain. Agric. Environ. 3, e12096. https://doi.org/10.1002/sae2.12096

Cichota, R., Snow, V.O., 2009. Estimating nutrient loss to waterways—an overview of models of relevance to New Zealand pastoral farms. N. Z. J. Agric. Res. 52, 239–260. https://doi.org/10.1080/00288230909510509

Clague, J.C., Stenger, R., Clough, T.J., 2015. Evaluation of the stable isotope signatures of nitrate to detect denitrification in a shallow groundwater system in New Zealand. Agric. Ecosyst. Environ. 202, 188–197. https://doi.org/10.1016/j.agee.2015.01.011

Clague, J. C., Stenger, R., Clough, T.J., 2015. Denitrification in the shallow groundwater system of a lowland catchment: A laboratory study. Catena 131, 109–118. https://doi.org/10.1016/j.catena.2015.03.012

Clague, J.C., Stenger, R., Morgenstern, U., 2019. The influence of unsaturated zone drainage status on denitrification and the redox succession in shallow groundwater. Sci. Total Environ. 660, 1232–1244. https://doi.org/10.1016/j.scitotenv.2018.12.383

Clayden, B., Webb, T.H., 1994. Criteria for defining the soil form: the fourth category of the New Zealand Soil Classification. Landcare Research New Zealand, Lincoln, New Zealand. https://doi.org/10.7931/DL1-LRSS-3-1994

Close, M.E., Abraham, P., Humphries, B., Lilburne, L., Cuthill, T., Wilson, S., 2016. Predicting groundwater redox status on a regional scale using linear discriminant analysis. J. Contam. Hydrol. 191, 19–32. https://doi.org/10.1016/j.jconhyd.2016.04.006

Clothier, B., Green, S., 2017. The leaching and runoff of nutrients from vinyards, in: Currie, L.D., Hedley, M.J. (Eds.), Science and Policy: Nutrient Management Challenges for the Next Generation, Occasional Report No. 30. Fertilizer and Lime Research Centre, Massey University, Palmerston North, New Zealand, p. 7.

Clothier, B., Mackay, A., Carran, A., Gray, R., Parfitt, R., Francis, G., Manning, M., Duerer, M., Green, S., 2007. Farm Strategies for Contaminant Management (No. 2007/EXT/870). Horizons Regional Council, Palmerston North, New Zealand. http://flrc.massey.ac.nz/publications.html

Cohn, T.A., 2005. Estimating contaminant loads in rivers: An application of adjusted maximum likelihood to type 1 censored data. Water Resour. Res. 41, 2004WR003833. https://doi.org/10.1029/2004WR003833

Cohn, T.A., Caulder, D.L., Gilroy, E.J., Zynjuk, L.D., Summers, R.M., 1992. The validity of a simple statistical model for estimating fluvial constituent loads: An Empirical study involving nutrient loads entering Chesapeake Bay. Water Resour. Res. 28, 2353–2363. https://doi.org/10.1029/92WR01008

Cohn, T.A., Delong, L.L., Gilroy, E.J., Hirsch, R.M., Wells, D.K., 1989. Estimating constituent loads. Water Resour. Res. 25, 937–942. https://doi.org/10.1029/WR025i005p00937

Collins, S., Singh, R., Rivas, A., Palmer, A., Horne, D., Manderson, A., Roygard, J., Matthews, A., 2017. Transport and potential attenuation of nitrogen in shallow groundwaters in the lower Rangitikei catchment, New Zealand. J. Contam. Hydrol. 206, 55–66. https://doi.org/10.1016/j.jconhyd.2017.10.002

Collins, S.B., 2015. Investigating the Transport and Fate of Nitrogen from Farms to River in the Lower Rangitikei Catchment (Master of Science). Massey University, Palmerston North, New Zealand. https://mro.massey.ac.nz

Collins, S.B., Singh, R., Mead, S.R., Horne, D.J., 2025a. Modelling and mapping of subsurface nitrate-attenuation index in agricultural landscapes. J. Environ. Manage. 384, 125628. https://doi.org/10.1016/j.jenvman.2025.125628

Collins, S.B., Singh, R., Mead, S.R., Horne, D.J., Roygard, J.K.F., 2025b. Assessment of spatial variability and temporal stability of groundwater redox conditions in New Zealand. Environ. Monit. Assess. 197, 58. https://doi.org/10.1007/s10661-024-13427-y

Costa, J.L., Massone, H., Martínez, D., Suero, E.E., Vidal, C.M., Bedmar, F., 2002. Nitrate contamination of a rural aquifer and accumulation in the unsaturated zone. Agric. Water Manag. 57, 33–47. https://doi.org/10.1016/S0378-3774(02)00036-7

Cowie, J.D., Fitzgerald, P., Owers, W., 1967. Soils of the Manawatu-Rangitikei Sand Country. NZ Soil Bureau Bulletin 29. https://doi.org/10.7931/dl1-sbb-029

Cowie, J.D., Rijkse, W.C., 1977. Soils of the Manawatu County, North Island, New Zealand. Department of Scientific and Industrial Research, Wellington, New Zealand. https://doi.org/10.7931/DL1-SSR-30-1

Cox, T., Kerr, T., Snelder, T., Fraser, C., 2022. Manawatu-Whanganui region catchment nutrient models: model updates (No. 2022/EXT/1770). Horizons Regional Council, Palmerston North, New Zealand. https://archivescentral.org.nz/records

Cox, T., Snelder, T., Kerr, T., Fraser, C., 2023. Manawatu-Whanganui region catchment nutrient models: model scenarios (No. 2024/EXT/1841). Horizons Regional Council, Palmerston North, New Zealand. https://archivescentral.org.nz/records

Daniel, T.J., Richendrfer, J., Falta, R., Murdoch, L., Lin, H., Darnault, C.J.G., 2023. Numerical modeling of groundwater flow and nitrate transport in karst and wastewater irrigated agricultural and forest landscapes, PA, USA. Agrosystems Geosci. Environ. 6, e20427. https://doi.org/10.1002/agg2.20427

Dark, A., 2020. National irrigated land spatial dataset: 2020 Update (Client report for the Ministry for the Environment No. RD21004-1). Aqualinc Research Limited, Christchurch, New Zealand. https://data.mfe.govt.nz/

Daughney, C.J., Reeves, R.R., 2005. Definition of hydrochemical facies in the New Zealand National Groundwater Monitoring Programme. J. Hydrol. N. Z. 44, 105–130. https://environment.govt.nz/publications/

David, M.B., Flint, C.G., Gentry, L.E., Dolan, M.K., Czapar, G.F., Cooke, R.A., Lavaire, T., 2015. Navigating the socio-bio-geo-chemistry and engineering of nitrogen management in two Illinois tile-drained watersheds. J. Environ. Qual. 44, 368–381. https://doi.org/10.2134/jeq2014.01.0036

Davies-Colley, R.J., 2013. River water quality in New Zealand: An introduction and overview, in: Ecosystem Services in New Zealand. Manaaki Whenua Press, Lincoln, N.Z.

Deakin, J., Flynn, R., Archbold, M., Daly, D., O'Brien, R., Orr, A., Misstear, B., 2016. Understanding pathways transferring nutrients to streams: Review of a major Irish study and its implications for determining water quality management strategies. Biol. Environ. 116B. https://doi.org/10.3318/BIOE.2016.19

DeSimone, L.A., Pope, J.P., Ransom, K.M., 2020. Machine-learning models to map pH and redox conditions in groundwater in a layered aquifer system, Northern Atlantic Coastal Plain, eastern USA. J. Hydrol. Reg. Stud. 30, 100697. https://doi.org/10.1016/j.ejrh.2020.100697

DeSimone, L.A., Ransom, K.M., 2021. Manganese in the Northern Atlantic Coastal Plain aquifer system, eastern USA—Modeling regional occurrence with pH, redox, and machine learning. J. Hydrol. Reg. Stud. 37, 100925. https://doi.org/10.1016/j.ejrh.2021.100925

Destouni, G., Lindgren, G.A., Gren, I.-M., 2006. Effects of Inland Nitrogen Transport and Attenuation Modeling on Coastal Nitrogen Load Abatement. Environ. Sci. Technol. 40, 6208–6214. https://doi.org/10.1021/es060025j

Deuss, K.E., Almond, P.C., Carrick, S., Kees, L.J., 2023. Identification, mapping, and characterisation of a mature artificial mole channel network using ground-penetrating radar. Agric. Water Manag. 288, 108477. https://doi.org/10.1016/j.agwat.2023.108477

D'Haene, K., De Waele, J., De Neve, S., Hofman, G., 2022. Spatial distribution of the relationship between nitrate residues in soil and surface water quality revealed through attenuation factors. Agric. Ecosyst. Environ. 330, 107889. https://doi.org/10.1016/j.agee.2022.107889

Di, H.J., Cameron, K.C., 2002. Nitrate leaching in temperate agroecosystems: Sources, factors and mitigating strategies. Nutr. Cycl. Agroecosystems 64, 237–256. https://doi.org/10.1023/A:1021471531188

Dinnes, D.L., Karlen, D.L., Jaynes, D.B., Kaspar, T.C., Hatfield, J.L., Colvin, T.S., Cambardella, C.A., 2002. Nitrogen Management Strategies to Reduce Nitrate Leaching in Tile-Drained Midwestern Soils. Agron. J. 94, 153–171. https://doi.org/10.2134/agronj2002.1530

Dodla, S., Wang, J., Delaune, R., Cook, R., 2008. Denitrification potential and its relation to organic carbon quality in three coastal wetland soils. Sci. Total Environ. 407, 471–480. https://doi.org/10.1016/j.scitotenv.2008.08.022

Dorado-Guerra, D.Y., Corzo-Pérez, G., Paredes-Arquiola, J., Pérez-Martín, M.Á., 2022. Machine learning models to predict nitrate concentration in a river basin. Environ. Res. Commun. 4, 125012. https://doi.org/10.1088/2515-7620/acabb7

Dymond, J.R., Ausseil, A.G.E., Parfitt, R.L., Herzig, A., McDowell, R.W., 2013. Nitrate and phosphorus leaching in New Zealand: A national perspective. N. Z. J. Agric. Res. 56, 49–59. https://doi.org/10.1080/00288233.2012.747185

Elliott, A.H., Alexander, R.B., Schwarz, G.E., Shankar, U., Sukias, J.P.S., McBride, G.B., 2005. Estimation of nutrient sources and transport for New Zealand using the hybrid mechanistic-statistical model SPARROW. J. Hydrol. N. Z. 44, 1–27. https://www.hydrologynz.org.nz/journal-of-hydrology

Elwan, A., 2018. Accounting of nitrogen attenuation in agricultural catchments (Doctor of Philosophy). Massey University, Palmerston North, New Zealand. https://mro.massey.ac.nz

Elwan, A., Singh, R., Horne, D., Roygard, J., Clothier, B., 2015. Nitrogen attenuation factor: can it tell a story about nutrients in different subsurface environments?, in: Currie, L.D., Burkitt, L.L. (Eds.), Moving Farm Systems to Improved Nutrient Attenuation, Occasional Report No. 28. Fertilizer and Lime Research Centre, Massey University, Palmerston North, New Zealand, p. 12. http://flrc.massey.ac.nz/publications.html

Elwan, A., Singh, R., Patterson, M., Roygard, J., Horne, D., Clothier, B., Jones, G., 2018. Influence of sampling frequency and load calculation methods on quantification of annual river nutrient and suspended solids loads. Environ. Monit. Assess. 190. https://doi.org/10.1007/s10661-017-6444-y

Eschenbach, W., Well, R., Walther, W., 2015. Predicting the denitrification capacity of sandy aquifers from in situ measurements using push–pull^{15} N tracer tests. Biogeosciences 12, 2327–2346. https://doi.org/10.5194/bg-12-2327-2015

Everitt, B.S., Landau, S., Leese, M., Stahl, D., 2011. Cluster Analysis, 1st ed, Wiley Series in Probability and Statistics. Wiley. https://doi.org/10.1002/9780470977811

Fawcett, T., 2006. An introduction to ROC analysis. Pattern Recognit. Lett. 27, 861–874. https://doi.org/10.1016/j.patrec.2005.10.010

Fenton, O., Richards, K.G., Kirwan, L., Khalil, M.I., Healy, M.G., 2009. Factors affecting nitrate distribution in shallow groundwater under a beef farm in South Eastern Ireland. J. Environ. Manage. 90, 3135–3146. https://doi.org/10.1016/j.jenvman.2009.05.024

Fenton, O., Schulte, R.P.O., Jordan, P., Lalor, S.T.J., Richards, K.G., 2011. Time lag: A methodology for the estimation of vertical and horizontal travel and flushing timescales to nitrate threshold concentrations in Irish aquifers. Environ. Sci. Policy 14, 419–431. https://doi.org/10.1016/j.envsci.2011.03.006

Fernandes, S.O., Bharathi, P.A.L., Bonin, P.C., Michotey, V.D., 2010. Denitrification: An Important Pathway for Nitrous Oxide Production in Tropical Mangrove Sediments (Goa, India). J. Environ. Qual. 39, 1507–1516. https://doi.org/10.2134/jeq2009.0477

Fiedler, S., Vepraskas, M.J., Richardson, J.L., 2007. Soil Redox Potential: Importance, Field Measurements, and Observations, in: Advances in Agronomy. Elsevier, pp. 1–54. https://doi.org/10.1016/S0065-2113(06)94001-2

Finkelstein, M.M., Verma, D.K., 2001. Exposure Estimation in the Presence of Nondetectable Values: Another Look. AIHAJ - Am. Ind. Hyg. Assoc. 62, 195–198. https://doi.org/10.1080/15298660108984622

Fowler, D., Coyle, M., Skiba, U., Sutton, M.A., Cape, J.N., Reis, S., Sheppard, L.J., Jenkins, A., Grizzetti, B., Galloway, J.N., Vitousek, P., Leach, A., Bouwman, A.F., Butterbach-Bahl, K., Dentener, F., Stevenson, D., Amann, M., Voss, M., 2013. The global nitrogen cycle in the twenty-first century. Philos. Trans. R. Soc. B Biol. Sci. 368, 20130164. https://doi.org/10.1098/rstb.2013.0164

Fraser, C., 2023. State and trends for water quality in rivers, lakes, coastal and estuary sites in the Manawatū-Whanganui Region (No. 2023/EXT/1824). Horizons Regional Council, Palmerston North, New Zealand. https://archivescentral.org.nz/records

Fraser, C., 2021. Load calculations for rivers of the Manawatū-Whanganui region to 31 December 2019 (No. 2021/EXT/1748). Horizons Regional Council, Palmerston North, New Zealand. https://archivescentral.org.nz/records

Fraser, C., Snelder, T., 2020. Load calculations and spatial modelling of state, trends and contaminant yields (No. 2019/EXT/1672). Horizons Regional Council, Palmerston North, New Zealand. https://archivescentral.org.nz/records

Friedel, M.J., Wilson, S.R., Close, M.E., Buscema, M., Abraham, P., Banasiak, L., 2020. Comparison of four learning-based methods for predicting groundwater redox status. J. Hydrol. 580, 124200. https://doi.org/10.1016/j.jhydrol.2019.124200

Fróna, D., Szenderák, J., Harangi-Rákos, M., 2019. The Challenge of Feeding the World. Sustainability 11, 5816. https://doi.org/10.3390/su11205816

Ghane, E., Fausey, N.R., Brown, L.C., 2015. Modeling nitrate removal in a denitrification bed. Water Res. 71, 294–305. https://doi.org/10.1016/j.watres.2014.10.039

GNS Science, 2012. Geological Map of New Zealand [Digital data]. https://doi.org/10.21420/QF82-7D42

Godfray, H.C.J., Garnett, T., 2014. Food security and sustainable intensification. Philos. Trans. R. Soc. B Biol. Sci. 369, 20120273. https://doi.org/10.1098/rstb.2012.0273

Gonzalez Moreno, M.A., 2019. Assessment of biogeochemical transformation of nitrate in shallow groundwater in the agricultural landscape (Master of Science). Massey University, Palmerston North, New Zealand. https://mro.massey.ac.nz

Graf, D.R.H., Zhao, M., Jones, C.M., Hallin, S., 2016. Soil type overrides plant effect on genetic and enzymatic N2O production potential in arable soils. Soil Biol. Biochem. 100, 125–128. https://doi.org/10.1016/j.soilbio.2016.06.006

Groffman, P.M., Altabet, M.A., Böhlke, J.K., Butterbach-Bahl, K., David, M.B., Firestone, M.K., Giblin, A.E., Kana, T.M., Nielsen, L.P., Voytek, M.A., 2006. Methods for measuring denitrification: Diverse approaches to a difficult problem. Ecol. Appl. 16, 2091–2122. https://doi.org/10.1890/1051-0761(2006)016%255B2091:MFMDDA%255D2.0.CO;2

Guo, Y., Wang, X., Melching, C., Nan, Z., 2022. Identification method and application of critical load contribution areas based on river retention effect. J. Environ. Manage. 305, 114314. https://doi.org/10.1016/j.jenvman.2021.114314

Haddadchi, A., Booker, D.J., Measures, R.J., 2018. Predicting river bed substrate cover proportions across New Zealand. CATENA 163, 130–146. https://doi.org/10.1016/j.catena.2017.12.014

Haddadchi, A., Kuczynski, A., Hoyle, J.T., Kilroy, C., Booker, D.J., Hicks, M., 2020. Periphyton removal flows determined by sediment entrainment thresholds. Ecol. Model. 434, 109263. https://doi.org/10.1016/j.ecolmodel.2020.109263

Hansen, A.L., Christensen, B.S.B., Ernstsen, V., He, X., Refsgaard, J.C., 2014. A concept for estimating depth of the redox interface for catchment-scale nitrate modelling in a till area in Denmark. Hydrogeol. J. 22, 1639–1655. https://doi.org/10.1007/s10040-014-1152-y

Hansen, A.L., Refsgaard, J.C., Olesen, J.E., Børgesen, C.D., 2017. Potential benefits of a spatially targeted regulation based on detailed N-reduction maps to decrease N-load from agriculture in a small groundwater dominated catchment. Sci. Total Environ. 595, 325–336. https://doi.org/10.1016/j.scitotenv.2017.03.114

Hansen, B., Aamand, J., Blicher-Mathiesen, G., Christiansen, A.V., Claes, N., Dalgaard, T., Frederiksen, R.R., Jacobsen, B.H., Jakobsen, R., Kallesøe, A., Kim, H., Koch, J., Møller, I., Madsen, R.B., Schaper, S., Sandersen, P.B.E., Voutchkova, D.D., Wiborg, I., 2024. Assessing groundwater denitrification spatially is the key to targeted agricultural nitrogen regulation. Sci. Rep. 14. https://doi.org/10.1038/s41598-024-55984-9

Hashemi, F., Olesen, J.E., Børgesen, C.D., Tornbjerg, H., Thodsen, H., Dalgaard, T., 2018a. Potential benefits of farm scale measures versus landscape measures for reducing nitrate loads in a Danish catchment. Sci. Total Environ. 637–638, 318–335. https://doi.org/10.1016/j.scitotenv.2018.04.390

Hashemi, F., Olesen, J.E., Hansen, A.L., Børgesen, C.D., Dalgaard, T., 2018b. Spatially differentiated strategies for reducing nitrate loads from agriculture in two Danish catchments. J. Environ. Manage. 208, 77–91. https://doi.org/10.1016/j.jenvman.2017.12.001

Hasler, B., Hansen, L.B., Andersen, H.E., Termansen, M., 2019. Cost-effective abatement of non-point source nitrogen emissions – The effects of uncertainty in retention. J. Environ. Manage. 246, 909–919. https://doi.org/10.1016/j.jenvman.2019.05.140

Heisler, J., Glibert, P.M., Burkholder, J.M., Anderson, D.M., Cochlan, W., Dennison, W.C., Dortch, Q., Gobler, C.J., Heil, C.A., Humphries, E., Lewitus, A., Magnien, R., Marshall, H.G., Sellner, K., Stockwell, D.A., Stoecker, D.K., Suddleson, M., 2008. Eutrophication and harmful algal blooms: A scientific consensus. Harmful Algae 8, 3–13. https://doi.org/10.1016/j.hal.2008.08.006

Herridge, D.F., Peoples, M.B., Boddey, R.M., 2008. Global inputs of biological nitrogen fixation in agricultural systems. Plant Soil 311, 1–18. https://doi.org/10.1007/s11104-008-9668-3

Herzig, A., Manderson, A., Jolly, B., Barnes, M., Baish, L., 2020. Opportunities and constraints on intensive land-use expansion in the Horizons Region (No. 2020/EXT/1796). Horizons Regional Council, Palmerston North, New Zealand. https://archivescentral.org.nz/records

Hewitt, A.E., 2010. New Zealand Soil Classification, 3rd ed. Manaaki Whenua Press, Lincoln, Canterbury, New Zealand.

Hill, A.R., 1990. Ground water flow paths in relation to nitrogen chemistry in the near-stream zone. Hydrobiologia 206, 39–52. https://doi.org/10.1007/BF00018968

Hofmann, H., Newborn, D., Cartwright, I., Cendón, D.I., Raiber, M., 2020. Groundwater mean residence times of a subtropical barrier sand island. Hydrol. Earth Syst. Sci. 24, 1293–1318. https://doi.org/10.5194/hess-24-1293-2020

Højberg, A.L., 2018. On the track of targeted regulation of nitrate-experiences from Denmark, in: Currie, L.D., Christensen, C.L. (Eds.), Farm Environmental Planning – Science, Policy and Practice, Occasional Report No. 31. Fertilizer and Lime Research Centre, Massey University, Palmerston North, New Zealand, p. 9. http://flrc.massey.ac.nz/publications.html

Højberg, A.L., Hansen, A.L., Wachniew, P., Żurek, A.J., Virtanen, S., Arustiene, J., Strömqvist, J., Rankinen, K., Refsgaard, J.C., 2017. Review and assessment of nitrate reduction in groundwater in the Baltic Sea Basin. J. Hydrol. Reg. Stud. 12, 50–68. https://doi.org/10.1016/j.ejrh.2017.04.001

Holzworth, D., Huth, N.I., Fainges, J., Brown, H., Zurcher, E., Cichota, R., Verrall, S., Herrmann, N.I., Zheng, B., Snow, V., 2018. APSIM Next Generation: Overcoming challenges in modernising a farming systems model. Environ. Model. Softw. 103, 43–51. https://doi.org/10.1016/j.envsoft.2018.02.002

Horizons Regional Council, 2014. One Plan. The Consolidated Regional Policy Statement, Regional Plan and Regional Coastal Plan for the Manawatu-Whanganui Region (No. 2014/EXT/1338). Horizons Regional Council, Palmerston North, New Zealand. https://archivescentral.org.nz/records

Hu, Y., Fitzpatrick, L., Fry, L.M., Mason, L., Read, L.K., Goering, D.C., 2021. Edge-of-field runoff prediction by a hybrid modeling approach using causal inference. Environ. Res. Commun. 3, 075003. https://doi.org/10.1088/2515-7620/ac0d0a

Huang, P., Zhang, J., Zhu, A., Li, X., Ma, D., Xin, X., Zhang, C., Wu, S., Garland, G., Pereira, E.I.P., 2018. Nitrate accumulation and leaching potential reduced by coupled water and nitrogen management in the Huang-Huai-Hai Plain. Sci. Total Environ. 610–611, 1020–1028. https://doi.org/10.1016/j.scitotenv.2017.08.127

Hübner, U., Wurzbacher, C., Helbling, D.E., Drewes, J.E., 2022. Engineering of managed aquifer recharge systems to optimize biotransformation of trace organic chemicals. Curr. Opin. Environ. Sci. Health 27, 100343. https://doi.org/10.1016/j.coesh.2022.100343

Hyndman, R.J., Koehler, A.B., 2006. Another look at measures of forecast accuracy. Int. J. Forecast. 22, 679–688. https://doi.org/10.1016/j.ijforecast.2006.03.001

Istok, J.D., 2013. Push-Pull Tests for Site Characterization, Lecture Notes in Earth System Sciences. Springer Berlin Heidelberg, Berlin, Heidelberg. https://doi.org/10.1007/978-3-642-13920-8

Istok, J.D., Humphrey, M.D., Schroth, M.H., Hyman, M.R., O'Reilly, K.T., 1997. Single-Well, "Push-Pull" Test for In Situ Determination of Microbial Activities. Groundwater 35, 619–631. https://doi.org/10.1111/j.1745-6584.1997.tb00127.x

Jacobsen, B.H., Hansen, A.L., 2016. Economic gains from targeted measures related to non-point pollution in agriculture based on detailed nitrate reduction maps. Sci. Total Environ. 556, 264–275. https://doi.org/10.1016/j.scitotenv.2016.01.103

Jahangir, M.M.R., Johnston, P., Addy, K., Khalil, M.I., Groffman, P.M., Richards, K.G., 2013a. Quantification of in situ denitrification rates in groundwater below an arable and a grassland system. Water. Air. Soil Pollut. 224. https://doi.org/10.1007/s11270-013-1693-z

Jahangir, M.M.R., Johnston, P., Barrett, M., Khalil, M.I., Groffman, P.M., Boeckx, P., Fenton, O., Murphy, J., Richards, K.G., 2013b. Denitrification and indirect N2O emissions in groundwater: Hydrologic and biogeochemical influences. J. Contam. Hydrol. 152, 70–81. https://doi.org/10.1016/j.jconhyd.2013.06.007

Jahangir, M.M.R., Johnston, P., Khalil, M.I., Richards, K.G., 2012. Linking hydrogeochemistry to nitrate abundance in groundwater in agricultural settings in Ireland. J. Hydrol. 448–449, 212–222. https://doi.org/10.1016/j.jhydrol.2012.04.054

Jaynes, D.B., Isenhart, T.M., 2019. Performance of Saturated Riparian Buffers in Iowa, USA. J. Environ. Qual. 48, 289–296. https://doi.org/10.2134/jeq2018.03.0115

Jenkins, B.R., 2019. Management of cumulative impacts: Lessons from Canterbury, New Zealand. Int. J. Environ. Impacts Manag. Mitig. Recovery 2, 259–271. https://doi.org/10.2495/EI-V2-N3-259-271

Jiménez-de-Santiago, D.E., Lidón, A., Bosch-Serra, À.D., 2019. Soil Water Dynamics in a Rainfed Mediterranean Agricultural System. Water 11, 799. https://doi.org/10.3390/w11040799

Johnes, P.J., 1996. Evaluation and management of the impact of land use change on the nitrogen and phosphorus load delivered to surface waters: the export coefficient modelling approach. J. Hydrol. 183, 323–349. https://doi.org/10.1016/0022-1694(95)02951-6

Johnes, P.J., Heathwaite, A.L., 1997. Modelling the impact of land use change on water quality in agricultural catchments. Hydrol. Process. 11, 269–286. https://doi.org/10.1002/(SICI)1099-1085(19970315)11:3%253C269::AID-HYP442%253E3.0.CO;2-K

Ju, X.T., Kou, C.L., Zhang, F.S., Christie, P., 2006. Nitrogen balance and groundwater nitrate contamination: Comparison among three intensive cropping systems on the North China Plain. Environ. Pollut. 143, 117–125. https://doi.org/10.1016/j.envpol.2005.11.005

Ju, X.-T., Xing, G.-X., Chen, X.-P., Zhang, S.-L., Zhang, L.-J., Liu, X.-J., Cui, Z.-L., Yin, B., Christie, P., Zhu, Z.-L., Zhang, F.-S., 2009. Reducing environmental risk by improving N management in intensive Chinese agricultural systems. Proc. Natl. Acad. Sci. 106, 3041–3046. https://doi.org/10.1073/pnas.0813417106

Kanungo, T., Mount, D.M., Netanyahu, N.S., Piatko, C.D., Silverman, R., Wu, A.Y., 2002. An efficient k-means clustering algorithm: analysis and implementation. IEEE Trans. Pattern Anal. Mach. Intell. 24, 881–892. https://doi.org/10.1109/TPAMI.2002.1017616

Kaown, D., Koh, E.-H., Mayer, B., Kim, H., Park, D.K., Park, B.-H., Lee, K.-K., 2018. Application of multiple-isotope and groundwater-age data to identify factors affecting the extent of denitrification in a shallow aquifer near a river in South Korea. Hydrogeol. J. 26, 2009–2020. https://doi.org/10.1007/s10040-017-1716-8

Keatley, B.E., Bennett, E.M., MacDonald, G.K., Taranu, Z.E., Gregory-Eaves, I., 2011. Land-Use Legacies Are Important Determinants of Lake Eutrophication in the Anthropocene. PLoS ONE 6, e15913. https://doi.org/10.1371/journal.pone.0015913

Keller, A.A., Chen, X., Fox, J., Fulda, M., Dorsey, R., Seapy, B., Glenday, J., Bray, E., 2014. Attenuation Coefficients for Water Quality Trading. Environ. Sci. Technol. 48, 6788–6794. https://doi.org/10.1021/es500202x

Kemp, P.D., Lopez, I.F., 2016. Hill country pastures in the southern North Island of New Zealand: an overview. NZGA Res. Pract. Ser. 16, 289–297. https://doi.org/10.33584/rps.16.2016.3241

Kendall, C., 1998. Tracing Nitrogen Sources and Cycling in Catchments, in: Kendall, C., McDonnel, J.J. (Eds.), Isotope Tracers in Catchment Hydrology. Elsevier, pp. 519–576. https://doi.org/10.1016/b978-0-444-81546-0.50023-9

Kendall, C., Elliott, E.M., Wankel, S.D., 2008. Tracing Anthropogenic Inputs of Nitrogen to Ecosystems, in: Stable Isotopes in Ecology and Environmental Science: Second Edition. John Wiley & Sons, Ltd, pp. 375–449. https://doi.org/10.1002/9780470691854.ch12

Ki, M.G., Koh, D.C., Yoon, H., Kim, H., 2015. Temporal variability of nitrate concentration in groundwater affected by intensive agricultural activities in a rural area of Hongseong, South Korea. Environ. Earth Sci. 74, 6147–6161. https://doi.org/10.1007/s12665-015-4637-7

Kilroy, C., 2016. Periphyton in the Manawatu-Whanganui region (No. 2016/EXT/1494). Horizons Regional Council, Palmerston North, New Zealand. https://archivescentral.org.nz/records

Kilroy, C., Brown, L., Carlin, L., Lambert, P., Sinton, A., Wech, J.A., Howard-Williams, C., 2020a. Nitrogen stimulation of periphyton biomass in rivers: Differential effects of ammonium-N and nitrate-N. Freshw. Sci. 39, 485–496. https://doi.org/10.1086/710081

Kilroy, C., Stephens, T., Greenwood, M., Wech, J., Brown, L., Matthews, A., Patterson, Maree, Patterson, Mike, 2020b. Improved predictability of peak periphyton in rivers using site-specific accrual periods and long-term water quality datasets. Sci. Total Environ. 736, 139362. https://doi.org/10.1016/j.scitotenv.2020.139362

Kilroy, C., Whitehead, A., Howard, S., Greenwood, M., 2019. Modelling periphyton in New Zealand rivers. Part 1: An analysis of current data and development of national predictions (Client report for the Ministry for the Environment No. 2019002CH). National Institute of Water & Atmospheric Research Ltd, Christchurch, New Zealand.

Kim, H., Høyer, A.S., Jakobsen, R., Thorling, L., Aamand, J., Maurya, P.K., Christiansen, A.V., Hansen, B., 2019. 3D characterization of the subsurface redox architecture in complex geological settings. Sci. Total Environ. 693. https://doi.org/10.1016/j.scitotenv.2019.133583

Kim, H., Jakobsen, R., Aamand, J., Claes, N., Erlandsen, M., Hansen, B., 2021. Upscaling of Denitrification Rates from Point to Catchment Scales for Modeling of Nitrate Transport and Retention. Environ. Sci. Technol. 55, 15821–15830. https://doi.org/10.1021/acs.est.1c04593

Kim, H., Møller, I., Thorling, L., Hansen, B., 2025. Sediment color as a predictor of the subsurface redox conditions at large scale. Appl. Geochem. 190, 106493. https://doi.org/10.1016/j.apgeochem.2025.106493

Kim, Y., Kim, J.H., Son, B.H., Oa, S.W., 2005. A single well push–pull test method for in situ determination of denitrification rates in a nitrate-contaminated groundwater aquifer. Water Sci. Technol. 52, 77–86. https://doi.org/10.2166/wst.2005.0230

King, P.R., 2000. Tectonic reconstructions of New Zealand: 40 Ma to the Present. N. Z. J. Geol. Geophys. 43, 611–638. https://doi.org/10.1080/00288306.2000.9514913

Klaus, V.H., Friedritz, L., Hamer, U., Kleinebecker, T., 2020. Drought boosts risk of nitrate leaching from grassland fertilisation. Sci. Total Environ. 726, 137877. https://doi.org/10.1016/j.scitotenv.2020.137877

Knoll, L., Breuer, L., Bach, M., 2020. Nation-wide estimation of groundwater redox conditions and nitrate concentrations through machine learning. Environ. Res. Lett. 15, 064004. https://doi.org/10.1088/1748-9326/ab7d5c

Koch, J., Kim, H., Tirado-Conde, J., Hansen, B., Møller, I., Thorling, L., Troldborg, L., Voutchkova, D., Højberg, A.L., 2024. Modeling groundwater redox conditions at national scale through integration of sediment color and water chemistry in a machine learning framework. Sci. Total Environ. 947, 174533. https://doi.org/10.1016/j.scitotenv.2024.174533

Koch, J., Stisen, S., Refsgaard, J.C., Ernstsen, V., Jakobsen, P.R., Højberg, A.L., 2019. Modeling Depth of the Redox Interface at High Resolution at National Scale Using Random Forest and Residual Gaussian Simulation. Water Resour. Res. 55, 1451–1469. https://doi.org/10.1029/2018WR023939

Kolbe, T., De Dreuzy, J.-R., Abbott, B.W., Aquilina, L., Babey, T., Green, C.T., Fleckenstein, J.H., Labasque, T., Laverman, A.M., Marçais, J., Peiffer, S., Thomas, Z., Pinay, G., 2019. Stratification of reactivity determines nitrate removal in groundwater. Proc. Natl. Acad. Sci. 116, 2494–2499. https://doi.org/10.1073/pnas.1816892116

Korom, S.F., 1992. Natural denitrification in the saturated zone: A review. Water Resour. Res. 28, 1657–1668. https://doi.org/10.1029/92WR00252

Kouanda, A., Hua, G., 2021. Determination of nitrate removal kinetics model parameters in woodchip bioreactors. Water Res. 195, 116974. https://doi.org/10.1016/j.watres.2021.116974

Kralik, M., 2015. How to Estimate Mean Residence Times of Groundwater. Procedia Earth Planet. Sci. 13, 301–306. https://doi.org/10.1016/j.proeps.2015.07.070

Kruisdijk, E., Eisfeld, C., Stuyfzand, P.J., Van Breukelen, B.M., 2022. Denitrification kinetics during aquifer storage and recovery of drainage water from agricultural land. Sci. Total Environ. 849, 157791. https://doi.org/10.1016/j.scitotenv.2022.157791

Kuhn, M., Silge, J., 2022. Tidy Modeling with R: a framework for modeling in the Tidyverse, First edition. ed. O'Reilly, Sebastopol, CA, USA.

Kuhn, M., Vaughan, D., n.d. Boosted trees [WWW Document]. URL https://parsnip.tidymodels.org/reference/boost_tree.html (accessed 8.8.24).

Kuhn, M., Wickham, H., 2020. Tidymodels: a collection of packages for modeling and machine learning using tidyverse principles. https://www.tidymodels.org

Kuo, C.-H., Li, P.-Y., Lin, J.-Y., Chen, Y.-L., 2022. Integrating Stable Isotopes with Mean Residence Time Estimation to Characterize Groundwater Circulation in a Metamorphic Geothermal Field in Yilan, Taiwan. Water 14, 97. https://doi.org/10.3390/w14010097

Larned, S.T., 2010. A prospectus for periphyton: recent and future ecological research. J. North Am. Benthol. Soc. 29, 182–206. https://doi.org/10.1899/08-063.1

Legarth, E., Singh, R., Horne, D.J., 2022a. Modelling nitrate loads to rivers - Integration of farm-scale and catchment-scale models including spatially variable nitrate attenuation capacity, in: Adaptive Strategies for Future Farming, Occasional Report No. 34. Farmed Landscapes Research Centre, Massey University, Palmerston North, New Zealand, p. 17. http://flrc.massey.ac.nz/publications.html

Legarth, E., Singh, R., Horne, D.J., 2022b. Modelling nitrate loads to rivers - Evaluation of in-field and catchment-scale mitigation measures, in: Adaptive Strategies for Future Farming, Occasional Report No. 34. Farmed Landscapes Research Centre, Massey University, Palmerston North, New Zealand, p. 10. http://flrc.massey.ac.nz/publications.html

Lenhart, S., Ortmeyer, F., Banning, A., 2021. Denitrification in the vadose zone: Modelling with percolating water prognosis and denitrification potential. J. Contam. Hydrol. 242, 103843. https://doi.org/10.1016/j.jconhyd.2021.103843

Lycus, P., Soriano-Laguna, M.J., Kjos, M., Richardson, D.J., Gates, A.J., Milligan, D.A., Frostegård, Å., Bergaust, L., Bakken, L.R., 2018. A bet-hedging strategy for denitrifying bacteria curtails their release of N_2O. Proc. Natl. Acad. Sci. 115, 11820–11825. https://doi.org/10.1073/pnas.1805000115

Lynn, I.H., Manderson, A.K., Page, M.J., Harmsworth, G.R., Eyles, G.O., Douglas, G.B., Mackay, A.D., Newsome, P.J.F., 2009. Land Use Capability Survey Handbook - a New Zealand handbook for the classification of land, 3rd ed. AgResearch, Landcare Research, GNS Science, Hamilton, Lincoln, Lower Hutt. https://doi.org/10.7931/DL1MG6

MacLeod, C.J., Moller, H., 2006. Intensification and diversification of New Zealand agriculture since 1960: An evaluation of current indicators of land use change. Agric. Ecosyst. Environ. 115, 201–218. https://doi.org/10.1016/j.agee.2006.01.003

Madsen, R.B., Kim, H., Kallesøe, A.J., Sandersen, P.B.E., Norvin Vilhelmsen, T., Hansen, T.M., Vest Christiansen, A., Møller, I., Hansen, B., 2021. 3D multiple-point geostatistical simulation of joint subsurface redox and geological architectures. Hydrol Earth Syst Sci 25, 2759–2787. https://doi.org/10.5194/hess-25-2759-2021

Magesan, G.N., Dalgety, J., Lee, R., Luo, J., Van Oostrom, A.J., 1999. Preferential Flow and Water Quality in Two New Zealand Soils Previously Irrigated with Wastewater. J. Environ. Qual. 28, 1528–1532. https://doi.org/10.2134/jeq1999.00472425002800050018x

Manderson, A., 2018. Mapping the extent of artificial drainage in New Zealand (Client Report for Lincoln Agritech No. Contract Report: LC3325). Manaaki Whenua, Palmerston North, New Zealand. https://www.landcareresearch.co.nz/publications/

Martindale, H., Van Der Raaij, R., Daughney, C.J., Morgenstern, U., Singh, R., Jha, N., Hadfield, J., 2019. Assessment of excess N2 for quantifying actual denitrification in New Zealand groundwater systems. J. Hydrol. N. Z. 58, 1–17.

Massey University, 2025. Tuapaka Farm - Massey University [WWW Document]. Tuapaka Farm. URL https://www.massey.ac.nz/about/massey-subsidiaries-and-commercial-ventures/massey-farms/tuapaka-farm/ (accessed 7.31.25).

McAleer, E.B., Coxon, C.E., Richards, K.G., Jahangir, M.M.R., Grant, J., Mellander, P.E., 2017. Groundwater nitrate reduction versus dissolved gas production: A tale of two catchments. Sci. Total Environ. 586, 372–389. https://doi.org/10.1016/j.scitotenv.2016.11.083

McArthur, K.J., Roygard, J., Clark, M., 2010. Understanding variations in the limiting nitrogen and phosphorus status of rivers in the Manawatu-Wanganui Region, New Zealand. J. Hydrol. N. Z. 49, 15–33. https://www.hydrologynz.org.nz/journal-of-hydrology

McDowell, R.W., Cox, N., Snelder, T.H., 2017. Assessing the Yield and Load of Contaminants with Stream Order: Would Policy Requiring Livestock to Be Fenced Out of High-Order Streams Decrease Catchment Contaminant Loads? J. Environ. Qual. 46, 1038–1047. https://doi.org/10.2134/jeq2017.05.0212

Mcdowell, R.W., Larned, S.T., Houlbrooke, D.J., 2009. Nitrogen and phosphorus in New Zealand streams and rivers: Control and impact of eutrophication and the influence of land management. N. Z. J. Mar. Freshw. Res. 43, 985–995. https://doi.org/10.1080/00288330909510055

McDowell, R.W., Simpson, Z.P., Ausseil, A.G., Etheridge, Z., Law, R., 2021. The implications of lag times between nitrate leaching losses and riverine loads for water quality policy. Sci. Rep. 11, 16450. https://doi.org/10.1038/s41598-021-95302-1

McLaren, R.G., Cameron, K.C., 1990. Soil science: an introduction to the properties and management of New Zealand soils. Oxford University Press, Auckland, N.Z.

McLarin, W., Bekesi, G., Brown, L., McConchie, J., 1999. Nitrate contamination of the unconfined aquifer, Manakau, Horowhenua, New Zealand. J. Hydrol. N. Z. 38, 211–235. https://www.hydrologynz.org.nz/journal-of-hydrology

McMahon, P.B., Chapelle, F.H., 2008. Redox processes and water quality of selected principal aquifer systems. Ground Water 46, 259–271. https://doi.org/10.1111/j.1745-6584.2007.00385.x

McPhillips, L.E., Groffman, P.M., Goodale, C.L., Walter, M.T., 2015. Hydrologic and Biogeochemical Drivers of Riparian Denitrification in an Agricultural Watershed. Water. Air. Soil Pollut. 226, 169. https://doi.org/10.1007/s11270-015-2434-2

Me, W., Abell, J.M., Hamilton, D.P., 2015. Effects of hydrologic conditions on SWAT model performance and parameter sensitivity for a small, mixed land use catchment in New Zealand. Hydrol. Earth Syst. Sci. 19, 4127–4147. https://doi.org/10.5194/hess-19-4127-2015

Mellander, P.E., Melland, A.R., Murphy, P.N.C., Wall, D.P., Shortle, G., Jordan, P., 2014. Coupling of surface water and groundwater nitrate-N dynamics in two permeable agricultural catchments. J. Agric. Sci. 152, S107–S124. https://doi.org/10.1017/S0021859614000021

Milne, J., 2019. National Environmental Monitoring Standards for Discrete Water Quality Part 1 of 4: Sampling, Measuring, Processing and Archiving of Discrete Groundwater Quality Data, National Environmental Monitoring Standards. New Zealand Ministry for the Environment. https://www.nems.org.nz/

Ministry for the Environment, 2024. National Policy Statement for Freshwater Management 2020. Ministry for the Environment, Wellington, New Zealand. https://environment.govt.nz/publications/

Ministry for the Environment, 2017. Average annual rainfall 1972-2016. https://data.mfe.govt.nz

Ministry for the Environment, Ministry for Primary Industries, 2021. Government response to the findings of the Overseer peer review report (No. ME 1582).

Ministry for the Environment, Wellington, New Zealand. https://environment.govt.nz/publications/

Molénat, J., Gascuel-Odoux, C., 2002. Modelling flow and nitrate transport in groundwater for the prediction of water travel times and of consequences of land use evolution on water quality. Hydrol. Process. 16, 479–492. https://doi.org/10.1002/hyp.328

Monaghan, R., Mercer, G., Smith, C., Gray, C., De Klein, C., Mapp, N., Meenken, E., Eikass, H., Burger, D., 2018. Benchmarking and mitigating contaminant losses to water, and GHG emissions to air, for key dairy farm typologies (Client Report for DairyNZ No. RE450/2017/081). AgResearch Ltd. https://www.dairynz.co.nz

Monaghan, R.M., Wilcock, R.J., Smith, L.C., Tikkisetty, B., Thorrold, B.S., Costall, D., 2007. Linkages between land management activities and water quality in an intensively farmed catchment in southern New Zealand. Agric. Ecosyst. Environ. 118, 211–222. https://doi.org/10.1016/j.agee.2006.05.016

Montcoudiol, N., Molson, J., Lemieux, J.-M., 2018. Numerical modelling in support of a conceptual model for groundwater flow and geochemical evolution in the southern Outaouais Region, Quebec, Canada. Can. Water Resour. J. Rev. Can. Ressour. Hydr. 43, 240–261. https://doi.org/10.1080/07011784.2017.1323560

Morgenstern, U., Daughney, C.J., Leonard, G., Gordon, D., Donath, F.M., Reeves, R., 2015. Using groundwater age and hydrochemistry to understand sources and dynamics of nutrient contamination through the catchment into Lake Rotorua, New Zealand. Hydrol. Earth Syst. Sci. 19, 803–822. https://doi.org/10.5194/hess-19-803-2015

Morgenstern, U., Davidson, P., Townsend, D.B., White, P.A., van der Raaij, R.W., Stewart, M.K., Moreau, M., Daughney, C.J., 2019. From rain through river catchment to aquifer: the flow of water through the Wairau hydrologic system (GNS Science Report No. 2019/63). Institute of Geological and Nuclear Sciences, Lower Hutt, New Zealand.

Morgenstern, U., Martindale, H., Stewart, M., Trompetter, V., van der Raaij, R., Toews, M., Townsend, D., 2017. Groundwater Dynamics Source & Hydrochemical Processes as Inferred from Horizons Regional Age Tracer Data (No. 2017/EXT/1525). Horizons Regional Council, Palmerston North, New Zealand. https://archivescentral.org.nz/records

Mortimer, N., 2004. New Zealand's Geological Foundations. Gondwana Res. 7, 261–272. https://doi.org/10.1016/S1342-937X(05)70324-5

Musacchio, A., Mas-Pla, J., Soana, E., Re, V., Sacchi, E., 2021. Governance and groundwater modelling: Hints to boost the implementation of the EU Nitrate Directive. The Lombardy Plain case, N Italy. Sci. Total Environ. 782, 146800. https://doi.org/10.1016/j.scitotenv.2021.146800

Newsome, P.J.F., Wilde, R.H., Willoughby, E.J., 2008. Land resource information system spatial data layers. Data dictionary. Landcare Research NZ Ltd. https://lris.scinfo.org.nz/document/9162-lris-data-dictionary-v3/

Niazkar, M., Menapace, A., Brentan, B., Piraei, R., Jimenez, D., Dhawan, P., Righetti, M., 2024. Applications of XGBoost in water resources engineering: A systematic literature review (Dec 2018–May 2023). Environ. Model. Softw. 174, 105971. https://doi.org/10.1016/j.envsoft.2024.105971

Nikolenko, O., Jurado, A., Borges, A.V., Knöller, K., Brouyère, S., 2018. Isotopic composition of nitrogen species in groundwater under agricultural areas: A review. Sci. Total Environ. 621, 1415–1432. https://doi.org/10.1016/j.scitotenv.2017.10.086

Oda, T., Iwasaki, K., Egusa, T., Kubota, T., Iwagami, S., Iida, S., Momiyama, H., Shimizu, T., 2024. Scale-Dependent Inter-Catchment Groundwater Flow in Forested Catchments: Analysis of Multi-Catchment Water Balance Observations in Japan. Water Resour. Res. 60, e2024WR037161. https://doi.org/10.1029/2024WR037161

Orr, A., Nitsche, J., Archbold, M., Deakin, J., Ofterdinger, U., Flynn, R., 2016. The influence of bedrock hydrogeology on catchment-scale nitrate fate and transport in fractured aquifers. Sci. Total Environ. 569–570, 1040–1052. https://doi.org/10.1016/j.scitotenv.2016.06.148

Pacheco, F.A.L., Sanches Fernandes, L.F., 2016. Environmental land use conflicts in catchments: A major cause of amplified nitrate in river water. Sci. Total Environ. 548–549, 173–188. https://doi.org/10.1016/j.scitotenv.2015.12.155

Packham, I., Mockler, E., Archbold, M., Mannix, A., Daly, D., Deakin, J., Bruen, M., 2020. Catchment Characterisation Tool: Prioritising Critical Source Areas for managing diffuse nitrate pollution. Environ. Model. Assess. 25, 23–39. https://doi.org/10.1007/s10666-019-09683-9

Palta, M.M., Ehrenfeld, J.G., Groffman, P.M., 2013. Denitrification and Potential Nitrous Oxide and Carbon Dioxide Production in Brownfield Wetland Soils. J. Environ. Qual. 42, 1507–1517. https://doi.org/10.2134/jeq2012.0392

Paradis, D., Ballard, J.-M., Lefebvre, R., Savard, M.M., 2018. Multi-scale nitrate transport in a sandstone aquifer system under intensive agriculture. Hydrogeol. J. 26, 511–531. https://doi.org/10.1007/s10040-017-1668-z

Peña-Haro, S., García-Prats, A., Pulido-Velazquez, M., 2014. Influence of soil and climate heterogeneity on the performance of economic instruments for reducing nitrate leaching from agriculture. Sci. Total Environ. 499, 510–519. https://doi.org/10.1016/j.scitotenv.2014.07.029

Pinay, G., Peiffer, S., De Dreuzy, J.R., Krause, S., Hannah, D.M., Fleckenstein, J.H., Sebilo, M., Bishop, K., Hubert-Moy, L., 2015. Upscaling Nitrogen Removal Capacity from Local Hotspots to Low Stream Orders' Drainage Basins. Ecosystems 18, 1101–1120. https://doi.org/10.1007/s10021-015-9878-5

Pollok, J.A., McLaughlin, B., 1986. A user-friendly guide to the soils of Tuapaka Farm, Tuapaka Farm Series. Massey University, Palmerston North, New Zealand.

Puckett, L.J., Cowdery, T.K., 2002. Transport and fate of nitrate in a glacial outwash aquifer in relation to ground water age, land use practices, and redox processes. J. Environ. Qual. 31, 782–796. https://doi.org/10.2134/jeq2002.0782

R Core Team, 2022. R: A Language and Environment for Statistical Computing. https://www.r-project.org/

Ransom, K.M., Nolan, B.T., Stackelberg, P.E., Belitz, K., Fram, M.S., 2022. Machine learning predictions of nitrate in groundwater used for drinking supply in the conterminous United States. Sci. Total Environ. 807, 151065. https://doi.org/10.1016/j.scitotenv.2021.151065

Refsgaard, J.C., Auken, E., Bamberg, C.A., Christensen, B.S.B., Clausen, T., Dalgaard, E., Effersø, F., Ernstsen, V., Gertz, F., Hansen, A.L., He, X., Jacobsen, B.H., Jensen, K.H., Jørgensen, F., Jørgensen, L.F., Koch, J., Nilsson, B., Petersen, C., De Schepper, G., Schamper, C., Sørensen, K.I., Therrien, R., Thirup, C., Viezzoli, A., 2014. Nitrate reduction in geologically heterogeneous catchments - A framework for assessing the scale of predictive capability of hydrological models. Sci. Total Environ. 468–469, 1278–1288. https://doi.org/10.1016/j.scitotenv.2013.07.042

Rissmann, C., Pearson, L.K., Lindsay, J., Beyer, M., Marapara, T., Badenhop, A., Martin, A., 2018. Integrated Landscape Mapping of Water Quality for Farm Planning - Applying a High Resolution Physiographic Approach To the Waituna Catchment, Southland, in: Farm Environmental Planning – Science, Policy and Practice, Occasional Report No. 31. Fertilizer and Lime Research Centre, Massey University, Palmerston North, New Zealand, pp. 1–19. http://flrc.massey.ac.nz/publications.html

Rivas, A., 2018. Characterisation of denitrification in the subsurface environment of the Manawatū catchment, New Zealand (Doctor of Philosophy). Massey University, Palmerston North, New Zealand. https://mro.massey.ac.nz

Rivas, A., Singh, R., Bishop, P., Horne, D., Roygard, J., Hedley, M., 2014. Measuring denitrification in the subsurface environment of the Manawatu River catchment, in: Currie, L.D., Christensen, C.L. (Eds.), Nutrient Management for the Farm, Catchment and Community, Occasional Report No. 27. Fertilizer and Lime Research Centre, Massey University, Palmerston North, New Zealand, p. 13. http://flrc.massey.ac.nz/publications.html

Rivas, A., Singh, R., Horne, D., Roygard, J., Matthews, A., Hedley, M., 2025. Quantification of denitrification rate in shallow groundwater using the single-well, push-pull test technique. J. Contam. Hydrol. 269, 104500. https://doi.org/10.1016/j.jconhyd.2025.104500

Rivas, A., Singh, R., Horne, D., Roygard, J., Matthews, A., Hedley, M.J., 2017. Denitrification potential in the subsurface environment in the Manawatu River catchment, New Zealand: Indications from oxidation-reduction conditions, hydrogeological factors, and implications for nutrient management. J. Environ. Manage. 197, 476–489. https://doi.org/10.1016/j.jenvman.2017.04.015

Rivas, A., Singh, R., Horne, D.J., Roygard, J., Matthews, A., Hedley, M.J., 2020. Contrasting subsurface denitrification characteristics under temperate pasture lands and its implications for nutrient management in agricultural catchments. J. Environ. Manage. 272, 111067. https://doi.org/10.1016/j.jenvman.2020.111067

Rivett, M.O., Buss, S.R., Morgan, P., Smith, J.W.N., Bemment, C.D., 2008. Nitrate attenuation in groundwater: A review of biogeochemical controlling processes. Water Res. 42, 4215–4232. https://doi.org/10.1016/j.watres.2008.07.020

Rivett, M.O., Smith, J.W.N., Buss, S.R., Morgan, P., 2007. Nitrate occurrence and attenuation in the major aquifers of England and Wales. Q. J. Eng. Geol. Hydrogeol. 40, 335–352. https://doi.org/10.1144/1470-9236/07-032

Robertson, C., Schipper, L., Pinxterhuis, I., Edwards, J.P., Doole, G., Romera, Á., 2025. New Zealand dairy farm system solutions that balance reductions in nitrogen leaching with profitability – a case study. N. Z. J. Agric. Res. 68, 424–444. https://doi.org/10.1080/00288233.2023.2269136

Robertson, G.P., 1997. Nitrogen Use Efficiency in Row-Crop Agriculture: Crop Nitrogen Use and Soil Nitrogen Loss, in: Ecology in Agriculture. Elsevier, pp. 347–365. https://doi.org/10.1016/b978-012378260-1/50011-7

Robertson, G.P., Groffman, P.M., 2015. Nitrogen Transformations, in: Soil Microbiology, Ecology and Biochemistry. Elsevier, pp. 421–446. https://doi.org/10.1016/B978-0-12-415955-6.00014-1

Rosecrans, C.Z., Nolan, B.T., Gronberg, J.A.M., 2017. Prediction and visualization of redox conditions in the groundwater of Central Valley, California. J. Hydrol. 546, 341–356. https://doi.org/10.1016/j.jhydrol.2017.01.014

Rosen, M.R., White, P.A. (Eds.), 2001. Groundwaters of New Zealand. New Zealand Hydrological Society, Wellington, N.Z.

Rosenstock, T.S., Liptzin, D., Dzurella, K., Fryjoff-Hung, A., Hollander, A., Jensen, V., King, A., Kourakos, G., McNally, A., Stuart Pettygrove, G., Quinn, J., Viers, J.H., Tomich, T.P., Harter, T., 2014. Agriculture's contribution to nitrate contamination of Californian groundwater (1945-2005). J. Environ. Qual. 43, 895–907. https://doi.org/10.2134/jeq2013.10.0411

Roygard, J.K.F., McArthur, K.J., Clark, M.E., 2012. Diffuse contributions dominate over point sources of soluble nutrients in two sub-catchments of the Manawatu River, New Zealand. N. Z. J. Mar. Freshw. Res. 46, 219–241. https://doi.org/10.1080/00288330.2011.632425

Rutherford, J.C., Palliser, C.C., MacCormick, A., 2019. Eutrophication In Lake Rotorua. 2. Using ROTAN and OVERSEER to model historic, present and future nitrogen loads. N. Z. J. Mar. Freshw. Res. 53, 128–161. https://doi.org/10.1080/00288330.2018.1505643

Sacchi, E., Acutis, M., Bartoli, M., Brenna, S., Delconte, C.A., Laini, A., Pennisi, M., 2013. Origin and fate of nitrates in groundwater from the central Po plain: Insights from isotopic investigations. Appl. Geochem. 34, 164–180. https://doi.org/10.1016/j.apgeochem.2013.03.008

Saggar, S., Jha, N., Deslippe, J., Bolan, N.S., Luo, J., Giltrap, D.L., Kim, D.-G., Zaman, M., Tillman, R.W., 2013. Denitrification and N2O:N2 production in temperate grasslands: Processes, measurements, modelling and mitigating negative impacts. Sci. Total Environ. 465, 173–195. https://doi.org/10.1016/j.scitotenv.2012.11.050

Sanwar, S., 2023. Characterisation and potential optimisation of seepage wetlands for nitrate mitigation in New Zealand hill country (Doctor of Philosophy). Massey University, Palmerston North, New Zealand. https://mro.massey.ac.nz

Sanwar, S., Burkitt, L., Singh, R., Bretherton, M., Kereszturi, G., 2022. Hill country wetland hydrological characterisation for nitrate attenuation, in: Christensen, C.L., Singh, R., Horne, D.J. (Eds.), Adaptive Strategies for Future Farming, Occasional Report No. 34. Farmed Landscapes Research Centre, Massey University, Palmerston North, New Zealand, p. 11. http://flrc.massey.ac.nz/publications.html

Sarris, T.S., Scott, D.M., Close, M.E., Humphries, B., Moore, C., Burbery, L.F., Rajanayaka, C., Barkle, G., Hadfield, J., 2019. The effects of denitrification parameterization and potential benefits of spatially targeted regulation for the reduction of N-discharges from agriculture. J. Environ. Manage. 247, 299–312. https://doi.org/10.1016/j.jenvman.2019.06.074

Sarris, T.S., Wilson, S.R., Close, M.E., Abraham, P., Kenny, A., 2024. Reducing Uncertainty of Groundwater Redox Condition Predictions at National Scale, for Decision Making and Policy. Environ. Manage. https://doi.org/10.1007/s00267-024-02098-7

Savage, C., Leavitt, P.R., Elmgren, R., 2010. Effects of land use, urbanization, and climate variability on coastal eutrophication in the Baltic Sea. Limnol. Oceanogr. 55, 1033–1046. https://doi.org/10.4319/lo.2010.55.3.1033

Scarsbrook, M.R., Melland, A.R., 2015. Dairying and water-quality issues in Australia and New Zealand. Anim. Prod. Sci. 55, 856–868. https://doi.org/10.1071/AN14878

Schäfer, G., Lincker, M., Sessini, A., Carletti, A., 2024. Numerical Groundwater Model to Assess the Fate of Nitrates in the Coastal Aquifer of Arborea (Sardinia, Italy). Water 16, 2729. https://doi.org/10.3390/w16192729

Schaller, M.F., Fan, Y., 2009. River basins as groundwater exporters and importers: Implications for water cycle and climate modeling. J. Geophys. Res. Atmospheres 114, 2008JD010636. https://doi.org/10.1029/2008JD010636

Schürmann, A., Schroth, M.H., Saurer, M., Bernasconi, S.M., Zeyer, J., 2003. Nitrate-consuming processes in a petroleum-contaminated aquifer quantified using push–pull tests combined with 15N isotope and acetylene-inhibition methods. J. Contam. Hydrol. 66, 59–77. https://doi.org/10.1016/S0169-7722(03)00007-X

Scott, M., 2015. The current state of groundwater quality in the upper Waitaki (No. R15/42). Environment Canterbury Regional Council, Christchurch. https://www.ecan.govt.nz/data/document-library

Seibert, S., Atteia, O., Ursula Salmon, S., Siade, A., Douglas, G., Prommer, H., 2016. Identification and quantification of redox and pH buffering processes in a heterogeneous, low carbonate aquifer during managed aquifer recharge. Water Resour. Res. 52, 4003–4025. https://doi.org/10.1002/2015WR017802

Seitzinger, S., Harrison, J.A., Böhlke, J.K., Bouwman, A.F., Lowrance, R., Peterson, B., Tobias, C., Van Drecht, G., 2006. Denitrification across landscapes and waterscapes: A synthesis. Ecol. Appl. 16, 2064–2090. https://doi.org/10.1890/1051-0761(2006)016%255B2064:DALAWA%255D2.0.CO;2

Seitzinger, S.P., Nielsen, L.P., Caffrey, J., Christensen, P.B., 1993. Denitrification measurements in aquatic sediments: A comparison of three methods. Biogeochemistry 23, 147–167. https://doi.org/10.1007/BF00023750

Selbie, D.R., Buckthought, L.E., Shepherd, M.A., 2015. The Challenge of the Urine Patch for Managing Nitrogen in Grazed Pasture Systems. Adv. Agron. 129, 229–292. https://doi.org/10.1016/bs.agron.2014.09.004

Severe, E., Errigo, I.M., Proteau, M., Sayedi, S.S., Kolbe, T., Marçais, J., Thomas, Z., Petton, C., Rouault, F., Vautier, C., De Dreuzy, J.-R., Moatar, F., Aquilina, L., Wood, R.L., LaBasque, T., Lécuyer, C., Pinay, G., Abbott, B.W., 2023. Deep denitrification: Stream and groundwater biogeochemistry reveal contrasted but connected worlds above and below. Sci. Total Environ. 880, 163178. https://doi.org/10.1016/j.scitotenv.2023.163178

Shah, D.B., Coulman, G.A., 1978. Kinetics of nitrification and denitrification reactions. Biotechnol. Bioeng. 20, 43–72. https://doi.org/10.1002/bit.260200105

Shaheen, S.M., Wang, J., Baumann, K., Wang, S.-L., Leinweber, P., Rinklebe, J., 2021. Redox-induced mobilization of phosphorus in groundwater affected arable soil profiles. Chemosphere 275, 129928. https://doi.org/10.1016/j.chemosphere.2021.129928

Shepherd, M., Wheeler, D., 2010. Overseer ® Nutrient Budgets – the Next Generation, in: Farming's Future: Minimising Footprints and Maximising Margins, Occasional Report No. 23. Fertilizer and Lime Research Centre, Massey University, Palmerston North, New Zealand, p. 9. https://flrc.massey.ac.nz/publications.html

Singh, R., Elwan, A., Horne, D., Manderson, A., Patterson, M., 2017a. Predicting land-based nitrogen loads and attenuation in the Rangitikei River catchment - the model development, in: Currie, L.D., Hedley, M.J. (Eds.), Science and Policy: Nutrient Management Challenges for the Next Generation, Occasional Report No. 30. Fertilizer and Lime Research Centre, Massey University, Palmerston North, New Zealand, p. 13. https://flrc.massey.ac.nz/publications.html

Singh, R., Elwan, A., Horne, D., Matthews, A., 2017b. Nitrogen accounting in the Rangitikei catchment (No. 2017/EXT/1529). Horizons Regional Council, Palmerston North, New Zealand. https://archivescentral.org.nz/records

Singh, R., Horne, D.J., 2019. Water-quality issues facing dairy farming: potential natural and built attenuation of nitrate losses in sensitive agricultural catchments. Anim. Prod. Sci. 60, 67. https://doi.org/10.1071/AN19142

Singh, S.K., Zeddies, M., Shankar, U., Griffiths, G.A., 2019. Potential groundwater recharge zones within New Zealand. Geosci. Front. 10, 1065–1072. https://doi.org/10.1016/j.gsf.2018.05.018

Singleton, M.J., Esser, B.K., Moran, J.E., Hudson, G.B., McNab, W.W., Harter, T., 2007. Saturated Zone Denitrification: Potential for Natural Attenuation of Nitrate Contamination in Shallow Groundwater Under Dairy Operations. Environ. Sci. Technol. 41, 759–765. https://doi.org/10.1021/es061253g

Smith, G., Singh, R., Matthews, A., 2017. Assessing Farm-Scale Nutrient Flow Pathways and Nitrate Attenuation in Rangitikei Sand Country, in: Currie, L.D., Hedley, M.J. (Eds.), Science and Policy: Nutrient Management Challenges for the Next Generation, Occasional Report No. 30. Fertilizer and Lime Research Centre, Massey University, Palmerston North, New Zealand, p. 12. http://flrc.massey.ac.nz/publications.html

Snelder, T., 2024. Assessment of nutrient load reductions to achieve freshwater objectives in the rivers of the Manawatū-Whanganui Region (No. 2024/EXT/1845). Horizons Regional Council, Palmerston North, New Zealand. https://archivescentral.org.nz/records

Snelder, T., Cox, T., Fraser, C., Elliott, S., Kerr, T., 2023. Quantifying Catchment Nutrient Modelling Parameters: An analysis using the available New Zealand data (Client Report No. 2023– 03). Land Water People Ltd, Lyttleton, New Zealand. https://landuseopportunities.nz/

Snelder, T., Cox, T., Kerr, T., Fraser, C., Collins, S., 2020. Manawatū-Whanganui Region Catchment Nitrogen Models Supporting Regional Plan Change 2 (No. 2020/EXT/1697). Horizons Regional Council, Palmerston North, New Zealand. https://archivescentral.org.nz/records

Snelder, T.H., Biggs, B.J.F., 2002. Multi-scale river environment classification for water resources management. JAWRA J. Am. Water Resour. Assoc. 38, 1225–1239. https://doi.org/10.1111/j.1752-1688.2002.tb04344.x

Snelder, T.H., Larned, S.T., McDowell, R.W., 2018. Anthropogenic increases of catchment nitrogen and phosphorus loads in New Zealand. N. Z. J. Mar. Freshw. Res. 52, 336–361. https://doi.org/10.1080/00288330.2017.1393758

Snelder, T.H., McDowell, R.W., Fraser, C.E., 2017. Estimation of Catchment Nutrient Loads in New Zealand Using Monthly Water Quality Monitoring Data. J. Am. Water Resour. Assoc. 53, 158–178. https://doi.org/10.1111/1752-1688.12492

Snelder, T.H., Moore, C., Kilroy, C., 2019. Nutrient Concentration Targets to Achieve Periphyton Biomass Objectives Incorporating Uncertainties. JAWRA J. Am. Water Resour. Assoc. 55, 1443–1463. https://doi.org/10.1111/1752-1688.12794

Spiekermann, R., Dymond, J., Manderson, A., Basher, L., 2018. SedNetNZ, SLUI and contaminant generation Part 2 Nitrogen, phosphorus and E. coli (No. 2018/EXT/1615). Horizons Regional Council, Palmerston North, New Zealand.

Srinivasan, M.S., Muirhead, R.W., Singh, S.K., Monaghan, R.M., Stenger, R., Close, M.E., Manderson, A., Drewry, J.J., Smith, L.C., Selbie, D., Hodson, R., 2021. Development of a national-scale framework to characterise transfers of N, P and *Escherichia coli* from land to water. N. Z. J. Agric. Res. 64, 286–313. https://doi.org/10.1080/00288233.2020.1713822

Steiness, M., Jessen, S., Van’T Veen, S.G.M., Kofod, T., Højberg, A.L., Engesgaard, P., 2021. Nitrogen-Loads to Streams: Importance of Bypass Flow and Nitrate

Removal Processes. J. Geophys. Res. Biogeosciences 126, e2020JG006111. https://doi.org/10.1029/2020JG006111

Stenger, R., Clague, J.C., Morgenstern, U., Clough, T.J., 2018. Vertical stratification of redox conditions, denitrification and recharge in shallow groundwater on a volcanic hillslope containing relict organic matter. Sci. Total Environ. 639, 1205–1219. https://doi.org/10.1016/j.scitotenv.2018.05.122

Stewart, M.K., Stevens, G., Thomas, J.T., van der Raaij, R., Trompetter, V., 2011. Nitrate sources and residence times of groundwater in the Waimea Plains, Nelson. J. Hydrol. N. Z. 50, 313–338.

Stuart, M.E., 2018. Review of denitrification potential in groundwater of England (British Geological Survey Open Report No. OR/18/011). British Geological Survey. http://nora.nerc.ac.uk/id/eprint/522242/

Tanner, C.C., D'Eugenio, J., McBride, G.B., Sukias, J.P.S., Thompson, K., 1999. Effect of water level fluctuation on nitrogen removal from constructed wetland mesocosms. Ecol. Eng. 12, 67–92. https://doi.org/10.1016/S0925-8574(98)00055-X

Tavernet, J.P., 2023. Sensitivity and uncertainty analyses for N-loss estimates by the Overseer model, in: Diverse Solutions for Efficient Land, Water and Nutrient Use, Occasional Report No. 35. Farmed Landscapes Research Centre, Massey University, Palmerston North, New Zealand, p. 8. http://flrc.massey.ac.nz/publications.html

Tesoriero, A.J., Liebscher, H., Cox, S.E., 2000. Mechanism and rate of denitrification in an agricultural watershed: Electron and mass balance along groundwater flow paths. Water Resour. Res. 36, 1545–1559. https://doi.org/10.1029/2000WR900035

Tesoriero, A.J., Spruill, T.B., Mew, H.E., Farrell, K.M., Harden, S.L., 2005. Nitrogen transport and transformations in a coastal plain watershed: Influence of geomorphology on flow paths and residence times. Water Resour. Res. 41, 2003WR002953. https://doi.org/10.1029/2003WR002953

Tesoriero, A.J., Terziotti, S., Abrams, D.B., 2015. Predicting Redox Conditions in Groundwater at a Regional Scale. Environ. Sci. Technol. 49, 9657–9664. https://doi.org/10.1021/acs.est.5b01869

Tesoriero, A.J., Wherry, S.A., Dupuy, D.I., Johnson, T.D., 2024. Predicting Redox Conditions in Groundwater at a National Scale Using Random Forest

Classification. Environ. Sci. Technol. 58, 5079–5092. https://doi.org/10.1021/acs.est.3c07576

Thomas, N., 2017. Santoft groundwater model report (No. 2017/EXT/1556). Horizons Regional Council, Palmerston North, New Zealand. https://archivescentral.org.nz/records

Tiemeyer, B., Kahle, P., Lennartz, B., 2006. Nutrient losses from artificially drained catchments in North-Eastern Germany at different scales. Agric. Water Manag. 85, 47–57. https://doi.org/10.1016/j.agwat.2006.03.016

Tilman, D., Balzer, C., Hill, J., Befort, B.L., 2011. Global food demand and the sustainable intensification of agriculture. Proc. Natl. Acad. Sci. 108, 20260–20264. https://doi.org/10.1073/pnas.1116437108

Tscharntke, T., Clough, Y., Wanger, T.C., Jackson, L., Motzke, I., Perfecto, I., Vandermeer, J., Whitbread, A., 2012. Global food security, biodiversity conservation and the future of agricultural intensification. Biol. Conserv. 151, 53–59. https://doi.org/10.1016/j.biocon.2012.01.068

Upton, S., 2024. A review of freshwater models used to support the regulation and management of water in New Zealand. Parliamentary Commissioner for the Environment, Wellington, New Zealand. https://pce.parliament.nz/

Upton, S., 2018. Overseer and regulatory oversight: Models, uncertainty and cleaning up our waterways. Parliamentary Commissioner for the Environment, Wellington, New Zealand. https://pce.parliament.nz/

Vandergoes, M.J., Hogg, A.G., Lowe, D.J., Newnham, R.M., Denton, G.H., Southon, J., Barrell, D.J.A., Wilson, C.J.N., McGlone, M.S., Allan, A.S.R., Almond, P.C., Petchey, F., Dabell, K., Dieffenbacher-Krall, A.C., Blaauw, M., 2013. A revised age for the Kawakawa/Oruanui tephra, a key marker for the Last Glacial Maximum in New Zealand. Quat. Sci. Rev. 74, 195–201. https://doi.org/10.1016/j.quascirev.2012.11.006

Vela, I.Y., Jensen, P.E., Nebel, L., Kelstrup, P.H., 2025. Method and System for Soil and Groundwater In Situ Redox Potential (Eh) Logging. ACS EST Water 5, 1075–1085. https://doi.org/10.1021/acsestwater.4c00200

Vepraskas, M.J., 2015. Redoximorphic Features for Identifying Aquic Conditions (No. Technical Bulletin 301). North Carolina State Univesity, Raleigh, North Carolina.

Vepraskas, M.J., Lindbo, D.L., Stolt, M.H., 2018. Redoximorphic Features, in: Interpretation of Micromorphological Features of Soils and Regoliths. Elsevier, pp. 425–445. https://doi.org/10.1016/B978-0-444-63522-8.00015-2

Vidon, P., Allan, C., Burns, D., Duval, T.P., Gurwick, N., Inamdar, S., Lowrance, R., Okay, J., Scott, D., Sebestyen, S., 2010. Hot spots and hot moments in riparian zones: Potential for improved water quality management. J. Am. Water Resour. Assoc. 46, 278–298. https://doi.org/10.1111/j.1752-1688.2010.00420.x

Vidon, P., Hill, A.R., 2004. Denitrification and patterns of electron donors and acceptors in eight riparian zones with contrasting hydrogeology. Biogeochemistry 71, 259–283. https://doi.org/10.1007/s10533-004-9684-1

Viera, A.J., Garrett, J.M., 2005. Understanding interobserver agreement: the kappa statistic. Fam. Med. 37, 360–363. https://pubmed.ncbi.nlm.nih.gov/15883903/

Vogeler, I., Vibart, R., Mackay, A., Dennis, S., Burggraaf, V., Beautrais, J., 2014. Modelling pastoral farm systems — Scaling from farm to region. Sci. Total Environ. 482–483, 305–317. https://doi.org/10.1016/j.scitotenv.2014.02.134

Wang, F., Sun, Z., Zheng, S., Yu, J., Liang, X., 2018. An Integrated Approach to Identify Critical Source Areas of Agricultural Nonpoint-Source Pollution at the Watershed Scale. J. Environ. Qual. 47, 922–929. https://doi.org/10.2134/jeq2017.12.0469

Wang, L., Stuart, M.E., Lewis, M.A., Ward, R.S., Skirvin, D., Naden, P.S., Collins, A.L., Ascott, M.J., 2016. The changing trend in nitrate concentrations in major aquifers due to historical nitrate loading from agricultural land across England and Wales from 1925 to 2150. Sci. Total Environ. 542, 694–705. https://doi.org/10.1016/j.scitotenv.2015.10.127

Watkins, N., Selbie, D., 2015. Technical Description of OVERSEER for Regional Councils: Report prepared for Bay of Planty Regional Council (No. RE500/2015/084). AgResearch Ltd. https://overseer.org.nz

Welch, H.L., Green, C.T., Coupe, R.H., 2011. The fate and transport of nitrate in shallow groundwater in northwestern Mississippi, USA. Hydrogeol. J. 19, 1239–1252. https://doi.org/10.1007/s10040-011-0748-8

Wells, N.S., Baisden, W.T., Horton, T., Clough, T.J., 2016. Spatial and temporal variations in nitrogen export from a New Zealand pastoral catchment revealed by stream water nitrate isotopic composition. Water Resour. Res. 52, 2840–2854. https://doi.org/10.1002/2015WR017642

Wetzel, R.G., 2001. Limnology: lake and river ecosystems, 3rd ed. Academic Press, San Diego, CA, USA.

Wheeler, D.M., 2022. Technical Manual for the description of the OVERSEER® Nutrient Budgets engine - Block nutrient budgets. AgResearch Ltd. https://support.overseer.org.nz

White, P.A., 2001. Groundwater Resources in New Zealand, in: White, P.A., Rosen, M.R. (Eds.), Groundwaters of New Zealand. New Zealand Hydrological Society Inc., Wellington, New Zealand, pp. 45–75.

White, P.A., Moreau, M., Mourot, F., Rawlinson, Z., 2019. New Zealand Groundwater Atlas: Hydrogeological-Unit Map of New Zealand (Consultancy Report No. 2019/144). Institute of Geological and Nuclear Sciences, Lower Hutt, New Zealand. https://www.gns.cri.nz/data-and-resources/new-zealand-hydrogeological-unit-map/

Whitehead, A.L., Booker, D.J., 2020. NZ River Maps: An interactive online tool for mapping predicted freshwater variables across New Zealand [WWW Document]. NZ River Maps. URL https://shiny.niwa.co.nz/nzrivermaps/ (accessed 3.4.25).

Whitehead, A.L., Booker, D.J., 2019. Communicating biophysical conditions across New Zealand's rivers using an interactive webtool. N. Z. J. Mar. Freshw. Res. 53, 278–287. https://doi.org/10.1080/00288330.2018.1532914

Wilcock, R.J., Nash, D., Schmidt, J., Larned, S.T., Rivers, M.R., Feehan, P., 2011. Inputs of nutrients and fecal bacteria to freshwaters from irrigated agriculture: Case studies in Australia and New Zealand. Environ. Manage. 48, 198–211. https://doi.org/10.1007/s00267-011-9644-1

Willmott, C., Matsuura, K., 2005. Advantages of the mean absolute error (MAE) over the root mean square error (RMSE) in assessing average model performance. Clim. Res. 30, 79–82. https://doi.org/10.3354/cr030079

Wilson, S.R., Close, M.E., Abraham, P., 2018. Applying linear discriminant analysis to predict groundwater redox conditions conducive to denitrification. J. Hydrol. 556, 611–624. https://doi.org/10.1016/j.jhydrol.2017.11.045

Wilson, S.R., Close, M.E., Abraham, P., Sarris, T.S., Banasiak, L., Stenger, R., Hadfield, J., 2020. Achieving unbiased predictions of national-scale groundwater redox conditions via data oversampling and statistical learning. Sci. Total Environ. 705, 135877. https://doi.org/10.1016/j.scitotenv.2019.135877

Withers, P.J.A., Neal, C., Jarvie, H.P., Doody, D.G., 2014. Agriculture and eutrophication: Where do we go from here? Sustain. Switz. 6, 5853–5875. https://doi.org/10.3390/su6095853

Wriedt, G., Rode, M., 2006. Modelling nitrate transport and turnover in a lowland catchment system. J. Hydrol. 328, 157–176. https://doi.org/10.1016/j.jhydrol.2005.12.017

Wright, J., 2015. Water quality in New Zealand: Land use and nutrient pollution. Parliamentary Commissioner for the Environment, Wellington, New Zealand. https://pce.parliament.nz/

Wu, Y., Xu, L., Wang, S., Wang, Z., Shang, J., Li, X., Zheng, C., 2018. Nitrate attenuation in low-permeability sediments based on isotopic and microbial analyses. Sci. Total Environ. 618, 15–25. https://doi.org/10.1016/j.scitotenv.2017.11.039

Xie, F., Cai, G., Li, G., Li, H., Chen, X., Liu, Y., Zhang, W., Zhang, J., Zhao, X., Tang, Z., 2024. Basin-wide tracking of nitrate cycling in Yangtze River through dual isotope and machine learning. Sci. Total Environ. 912, 169656. https://doi.org/10.1016/j.scitotenv.2023.169656

Xu, F., Li, P., 2024. Biogeochemical mechanisms of iron (Fe) and manganese (Mn) in groundwater and soil profiles in the Zhongning section of the Weining Plain (northwest China). Sci. Total Environ. 939, 173506. https://doi.org/10.1016/j.scitotenv.2024.173506

Yang, M., Lee, J., Jang, S., Annable, M.D., Jawitz, J.W., 2023. Nitrate attenuation potential in karst conduits and aquifer matrix. J. Hydrol. 624, 129896. https://doi.org/10.1016/j.jhydrol.2023.129896

Yoshinari, T., Hynes, R., Knowles, R., 1977. Acetylene inhibition of nitrous oxide reduction and measurement of denitrification and nitrogen fixation in soil. Soil Biol. Biochem. 9, 177–183. https://doi.org/10.1016/0038-0717(77)90072-4

Yuan, M., Li, P., Lu, Z., Chen, Z., 2024. Decreased soil N2O and N2 emissions during the succession of subtropical forests. Plant Soil. https://doi.org/10.1007/s11104-024-06868-4

Yulianti, M., Özkundakci, D., Ridwansyah, I., 2025. Simulating water balance and nutrient losses in a pastoral catchment using the SWAT+ model: added value of isotope data. Hydrol. Sci. J. 70, 127–143. https://doi.org/10.1080/02626667.2024.2423047

Zarour, H., 2008. Groundwater Resources in the Manawatu-Wanganui Region (No. 2008/EXT/948). Horizons Regional Council, Palmerston North, New Zealand. https://archivescentral.org.nz/records

Zhang, X., Davidson, E.A., Mauzerall, D.L., Searchinger, T.D., Dumas, P., Shen, Y., 2015. Managing nitrogen for sustainable development. Nature 528, 51–59. https://doi.org/10.1038/nature15743

Zhang, Z., Furman, A., 2021. Soil redox dynamics under dynamic hydrologic regimes - A review. Sci. Total Environ. 763, 143026. https://doi.org/10.1016/j.scitotenv.2020.143026

Zhou, J. -B., Chen, Z. -J., Liu, X. -J., Zhai, B. -N., Powlson, D.S., 2010. Nitrate accumulation in soil profiles under seasonally open ‘sunlight greenhouses’ in northwest China and potential for leaching loss during summer fallow. Soil Use Manag. 26, 332–339. https://doi.org/10.1111/j.1475-2743.2010.00284.x

Zhu, A., Chen, J., Gao, L., Shimizu, Y., Liang, D., Yi, M., Cao, L., 2019. Combined microbial and isotopic signature approach to identify nitrate sources and transformation processes in groundwater. Chemosphere 228, 721–734. https://doi.org/10.1016/j.chemosphere.2019.04.163

Zhu, X., Miao, P., Zhu, H., Li, W., Liang, X., Wang, L., Chen, Z., Zhou, J., 2024. Extreme precipitation accelerates nitrate leaching in the intensive agricultural region with thick unsaturated zones. Sci. Total Environ. 918, 170789. https://doi.org/10.1016/j.scitotenv.2024.170789

Zimmerman, E.K., Tyndall, J.C., Schulte, L.A., 2019. Using Spatially Targeted Conservation to Evaluate Nitrogen Reduction and Economic Opportunities for Best Management Practice Placement in Agricultural Landscapes. Environ. Manage. https://doi.org/10.1007/s00267-019-01190-7

Appendix A

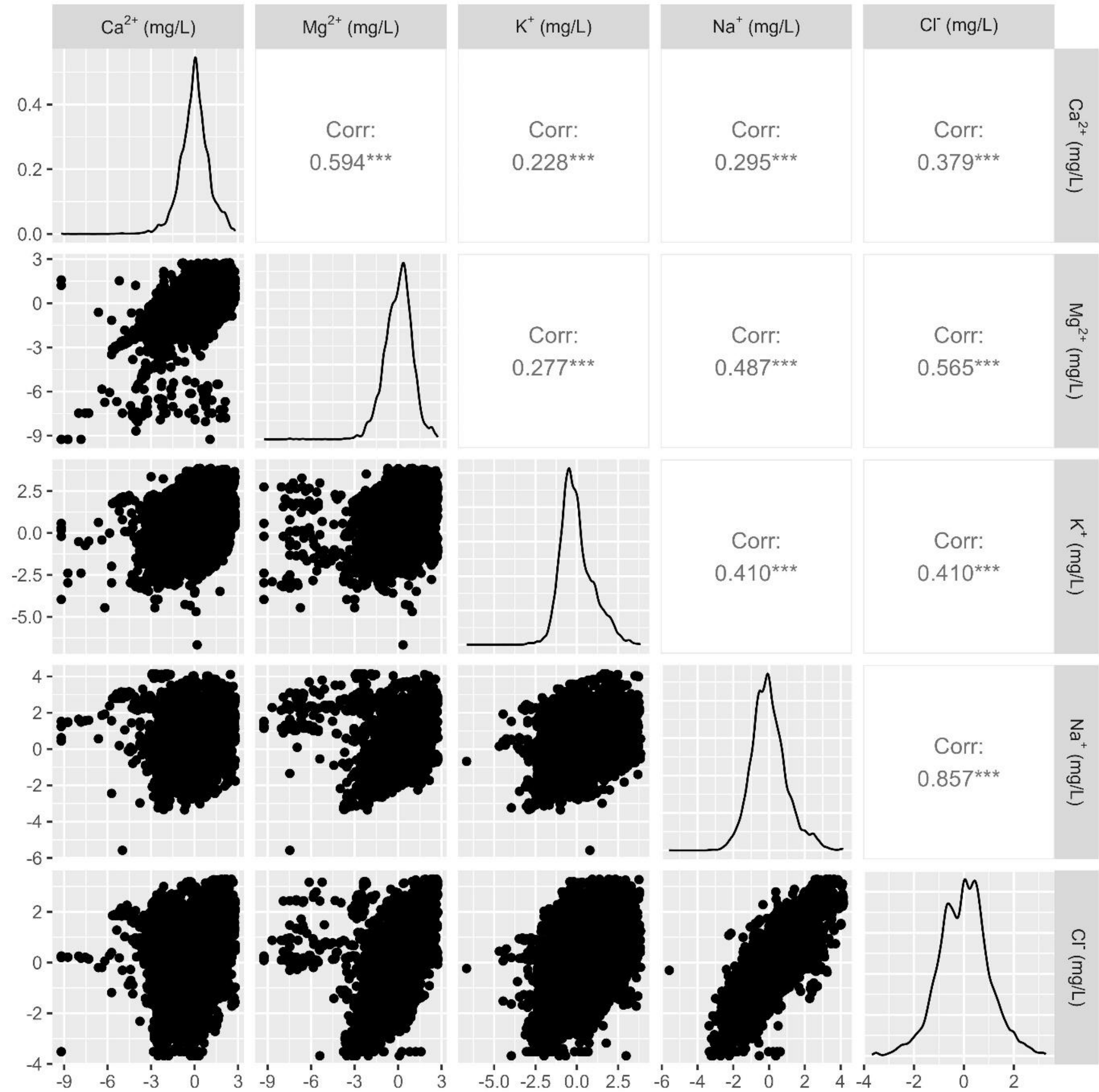

Figure A.1: Correlation plots of predictor variables. Reproduced with permission from Springer Nature.

Appendix B

Table B.1: Distribution of groundwater redox conditions among soil chemical and physical attributes in New Zealand. Reproduced with permission from Springer Nature.

	NZ distribution (%)	Redox data (%)	Oxidised (%)	Mixed (%)	Reduced (%)
Phosphate retention class					
Very high	3.8	3.8	74.8	14.5	10.7
High	9.8	4.7	59.3	14.7	26.0
Medium	43.6	21.4	68.6	13.8	17.5
Low	29.5	55.5	69.2	11.7	19.1
Very low	7.7	8.7	59.2	15.9	24.9
Not specified	5.6	6.0	54.1	15.1	30.8
Total	100.0	100.1	•	•	•
Cation exchange capacity (CEC) class					
Very high	1.1	3.0	33.3	18.6	48.1
High	12.0	3.2	63.2	17.0	19.8
Medium	53.8	45.7	66.6	13.5	19.8
Low	25.7	40.3	73.7	11.0	15.3
Very low	1.7	1.9	37.5	19.0	43.6
Not specified	5.6	6.0	54.1	15.1	30.8
Total	99.9	100.1	•	•	•
Plant rooting depth					
Very deep	12.1	17.3	70.9	14.0	15.1
Deep	11.0	12.9	56.3	16.5	27.2
Moderately deep	29.3	16.8	62.8	16.0	21.2
Slightly deep	20.8	19.1	74.4	10.7	14.9
Shallow	17.7	25.4	71.6	9.5	18.9
Very shallow	3.4	2.5	54.3	15.2	30.4
Not specified	5.6	6.0	54.1	15.1	30.8
Total	99.9	100.0	•	•	•
Profile available water					
Very high	2.7	3.6	73.7	15.8	10.5
High	13.3	15.2	57.5	18.1	24.4
Moderately high	29.8	39.7	69.6	11.7	18.7
Moderate	32.5	20.4	68.3	11.5	20.1
Low	14.7	13.7	71.2	11.1	17.7
Very low	3.0	1.3	78.4	16.0	5.7
Not specified	4.0	6.0	54.1	15.1	30.8
Total	100.0	99.9	•	•	•
Macroporosity class					
Very high	8.5	13.7	67.0	12.0	21.1
High	19.0	27.6	81.9	9.0	9.1

Moderate	45.2	30.2	71.5	12.4	16.2
Low	14.0	16.0	45.4	18.4	36.2
Very low	7.7	6.6	49.3	19.3	31.4
Not specified	5.6	6.0	54.1	15.1	30.8
Total	100.0	100.1	•	•	•

Appendix C

Table C.1: List of variables that were used trained to predict subsurface redox conditions in the XGBoost model.

Variable name	**Description**	**Categories**	**Units**
Rock type	A combination of 'Top rock' and 'Base rock' in the NZLRI. Top rock is the first named entire rock type, irrespective of underlying stratigraphy and base rock identifies the principal basement lithology.	Greywacke	
		Metamorphic rocks	
		Alluvium	
		Sandstone	
		Mudstone	
		Volcanic deposits	
		Igneous rocks	
		Volcanic ash over Volcanic deposits	
		Volcanic ash	
		Argillite	
		Volcanic ash over Greywacke	
		Loess over Alluvium	
		Volcanic ash over Sandstone	
		Unconsolidated sediments	
		Conglomerate	
		Loess over Sandstone	
		Windblown sands	
		Alluvium over Greywacke	
		Volcanic ash over Mudstone	
		Loess over Greywacke	
		Limestone	
		Gravels	
		Volcanic ash over Unconsolidated sediments	
		Loess	
		Loess over Gravels	
		Other	
Gravel class	Gravel class refers to the weighted average stone content in the soil profile (0-0.9m), expressed as a percentage.	Non-gravelly	<5 %
		Slightly gravelly	5-15 %
		Moderately gravelly	15-35 %
		Very gravelly	35-70 %
		Extremely gravelly	>70 %
Slope class	Slope class refers to a physiographic area of relatively homogeneous average relief.	Flat	0-7°
		Rolling	8-15°
		Easy hill	16-25°

		Steep hill	>25°
Flood class	Flood class refers to a measure of flood risk expressed as a flood return interval in years.	Nil	Nil
		Slight	<1 in 60
		Moderate	1 in 20 – 1 in 60
		Moderately severe	1 in 10 – 1 in 20
		Severe	1 in 5 – 1 in 10
		Very severe	>1 in 5
Carbon class	Total carbon (organic matter content) is estimated as weighted averages for the upper part of the soil profile (0-0.2 m)	Very high	20-60 %
		High	10-19.9 %
		Medium	4-9.9 %
		Low	2-3.9 %
		Very low	0-1.9 %
pH class	pH classes are given for the minimum pH content in the 0.2-0.6 m soil depth.	High	>7.5 pH
		Moderately high	6.5-7.5 pH
		Near neutral	5.8-6.4 pH
		Moderately low	5.5-5.7 pH
		Low	4.9-5.4 pH
		Very low	<4.9 pH
Soil drainage class	Soil drainage classes are assessed using a criteria of soil depth and duration of water tables inferred from soil colours and mottles.	Very poor	See below for classification details.
		Poor	
		Imperfect	
		Moderately well	
		Well	
Permeability class	Permeability class refers to the rate at which water moves through saturated soil.	Slow	<4 mm/h
		Moderate	4-72 mm/h
		Rapid	72-288 mm/h
Phosphate retention class	Phosphate retention is estimated as weighted averages for the upper part of the soil profile (0-0.2 m), expressed as a percentage.	Very high	85-100 %
		High	60-84 %
		Medium	30-59 %
		Low	10-29 %
		Very low	0-9 %
Cation exchange capacity (CEC) class	CEC is estimated as weighted averages for the soil profile from 0-0.6 m.	Very high	>40 meq./100 g
		High	25-39.9 meq./100 g
		Medium	12-24.9 meq./100 g
		Low	6-11.9 meq./100 g
		Very low	0-5.9 meq./100 g
Potential rooting depth	Potential rooting depth describes the minimum and maximum depths to a layer that may impede root extension.	Very deep	1.2-1.5 m
		Deep	0.9-1.19 m
		Moderately deep	0.6-0.89 m
		Slightly deep	0.45-0.59 m
		Shallow	0.25-0.44 m
		Very shallow	0.15-0.24 m
		Very high	>250 mm

Profile available water (PAW)	A classification of profile total available water for the soil profile depth of 0.9 m (or to the potential rooting depth).	High	150-249 mm
		Moderately high	90-149 mm
		Moderate	60-89 mm
		Low	30-59 mm
		Very low	0-29 mm
Macroporosity class	Macroporosity expresses the air-filled porosity of the soil at ‘field capacity’ for the soil profile depth of 0-0.6 m.	Very high	>15 %
		High	10-14.9 %
		Moderate	7.5-9.9 %
		Low	5-7.4 %
		Very low	0-4.9 %

Soil Drainage classification

Drainage class	Depth below A horizon (cm)	Depth from surface (cm)	Low chroma on ped or cut surfaces (%)	High Chroma Redox mottles (%)
Very poor[1]	1	≤10	≥50	
Poor	≤15	≤30	≥50	
Imperfect	≤15	≤30	≤50	and/or ≥2
	>15	30–90	≥50	
Moderately well		30–90		≥2
		60–90	≥50	
Well		<90		<2

[1] To qualify for very poorly drained, the profile must have an O horizon in place of an A horizon and a lack of distinct topsoil.

Appendix D

Table D.1: Ramiha silt loam soil profile description.

Location	40° 21' 28.2174" S 175° 44' 23.9220" E	
Elevation	355 m	
Depth (cm)	**Notation**	**Description**
3 – 0		Thatch
0 – 4	Ap1	Dark brown (10YR 4/3); silt loam; very friable; slightly sticky; plastic; moderate fine nut and coarse crumb structure; abundant fine roots, gradational boundary.
4 – 20	Ap2	Dark brown (10YR 4/3); silty clay loam; friable; slightly sticky; plastic; well-developed fine nut and moderate coarse crumb structure; many fine roots; gradational boundary.
20 – 37	ABw	Dark brown (10YR 4/3) and yellowish brown (10YR 5/4) earthworm mottled, distinct medium mottles; silty clay loam; friable; sticky and plastic; moderately developed fine nut and moderate coarse crumb structure; many fine roots; gradational boundary.
37 – 65	Bw1	Yellowish brown (10YR 5/4); silty clay loam; friable; sticky and plastic; moderately developed fine nut and moderate coarse crumb structure; few fine roots; gradational boundary.
65 – 72	Bw2	Yellowish brown (10YR 5/4); sandy clay loam; glassy; friable; slightly sticky and plastic; weakly developed fine nut and moderate coarse crumb structure; few fine roots; gradational boundary.
72 – 84	2Bw3	Kawakawa Tephra. Light brown (7.5YR 6/5) with strong brown (7.5YR 4/6) coatings on cracks and peds; sandy loam (tephra); brittle; non sticky and non-plastic; greasy; massive breaking to weak coarse crumb structure; lower 2cm is white (10 YR 8/2) fine sandy loam; massive; gradational boundary.
84 – 102	3Bw4	Yellowish brown (10YR 5/4-5/5); silty clay loam; firm; sticky and plastic; weak medium block structure; no roots; gradational boundary.
102 – 150+	3Bw5	Brown (7.5YR 5/4); silty clay loam; firm; sticky and plastic; weak fine block and nut structure; no roots.
		Greywacke not struck.

Table D.2: Ramiha silt loam soil bulk density measurements.

Depth (cm)	**Bulk density (g/cm^3)**
5 – 10	0.94
24 – 29	1.12
50 – 55	1.17
72 – 77	0.86
90 – 95	1.38

Figure D.1: Ramiha silt loam – 1 m soil profile.

Table D.3: Shannon silt loam soil profile description.

Location	40° 20’ 52.4790” S 175° 44’ 04.0578” E	
Elevation	244 m	
Depth (cm)	**Notation**	**Description**
0 – 13	Ap	Dark greyish brown (10YR 4/2-4/3); silt loam; friable; slightly sticky and plastic; moderate fine nut and moderate medium crumb structure; many fine roots; gradational boundary.
13 – 20	ABw	Dark yellowish brown (10YR4/4), 40% yellowish brown (10YR 5/4) 5% yellowish brown (10YR 5/8) medium distinct earthworm mottles; silty clay loam; friable; sticky and plastic; moderate fine nut breaking to moderate coarse crumbs; many fine roots; gradational boundary.
20 – 41	Bg1	40% light brownish grey (2.5Y 6/3), 40% yellowish brown (10YR 5/4), 20% yellowish brown (10YR 5/8) medium distinct mottles; silty clay loam; firm; sticky and very plastic; moderate medium block structure; few fine roots; gradational boundary.
41 – 70	Bg2	40% light grey (2.5Y 6/2-7/2), 60% strong brown (7.5YR 5/8) coarse distinct mottles; silty clay loam grading down to sandy clay loam; firm; sticky and very plastic; moderate medium block structure; thin pale brownish grey clay coatings on peds; few fine roots; gradational boundary.
70 – 86	2Bg3	80% light grey (2.5Y 7/2), 20% strong brown (7.5YR 5/8) coarse distinct mottles; a 5cm grey band dips 15* towards NW across the pit; medium sandy loam with a few subangular chert fragments up to 5cm; firm; slightly sticky and plastic; no roots; sharp boundary.
86 – 105	2Bg4	Brownish yellow (10YR 6/8) with a few (2%) light grey (2.5Y 7/2-7/3) fine distinct mottles; a few dark reddish-brown concretions up to 1cm diameter; a few light grey gammations up to 2cm wide; sandy clay loam with a few chips of angular greywacke and chert up to 3cm; firm; sticky and plastic; massive; no roots.
		Sand continues to at least 2 m depth.

Table D.4: Shannon silt loam soil bulk density measurements.

Depth (cm)	Bulk density (g/cm^3)
5 – 10	1.28
30 – 35	1.46
50 – 55	1.57
70 – 75	1.60
92 – 97	1.67

Figure D.2: Shannon silt loam – 1 m soil profile.

Table D.5: Tokomaru silt loam soil profile description.

Location	40° 19’ 54.7032” S 175° 44’ 43.6080” E	
Elevation	102 m	
Depth (cm)	**Notation**	**Description**
0 – 8	Ap1	Dark greyish brown (10YR 4/2-4/3); a few dark reddish-brown mottles down root channels; silt loam; friable; slightly sticky and plastic; medium fine nut and medium coarse crumb structure; abundant fine roots; gradational boundary.
8 – 17	Ap2	Dark greyish brown (10YR 4/2); silt loam; firm; sticky and plastic; moderate fine block and moderate medium crumb structure; many fine roots; gradational boundary.
17 – 27	ABgc	20% dark greyish brown (10YR 4/2), 60% light brownish grey (2.5Y 6/2), 20% strong brown (7.5YR 5/8-4/6); silty clay loam; common dark reddish brown to black Fe/Mn concretions up to 5mm diameter; firm; sticky and plastic; moderate fine blocky structure; common fine roots; gradational boundary.
27 – 66	Bgt1	50% light brownish grey (2.5Y 6/2), 50% strong brown (7.5YR 5/8) coarse prominent mottles; common light brownish grey (2.5Y 6/3) clay coatings on peds and root channels; silty clay loam; firm; sticky and very plastic; well-developed coarse blocky structure; few fine roots; gradational boundary.
66 – 84	Bgt2	60% light grey (2.5Y 7/2-8/2), 40% strong brown (7.5YR 5/8) coarse prominent mottles; common light brownish grey (2.5Y 6/3) and a few darker organic rich clay coatings on peds and root channels; silty clay loam; firm; sticky and very plastic; moderately developed coarse blocky structure; few fine roots; gradational boundary.
84 – 105+	Bxg	50% light grey (5Y7/2), 50% strong brown (7.5YR 5/8) coarse prominent mottles; silt loam; very firm (fragipan); sticky and very plastic; light grey vertical gammations with orange selvedges; columnar structure breaking to moderate coarse blocks; no roots.

Table D.6: Tokomaru silt loam soil bulk density measurements.

Depth (cm)	**Bulk density (g/cm^3)**
5 – 10	1.23
20 – 25	1.60
40 – 45	1.62
60 – 65	1.59
88 – 93	1.64

Figure D.3: Tokomaru silt loam – 1 m soil profile.

Appendix E

Redox probe installation information

A SWAP Instruments® ORP-80-4-D soil redox probe was installed at each study site to monitor soil redox potential (*Eh*) over time. These probes were pre-calibrated, ready to be installed in the field. First, measurements were made to ensure the depth of the probe will be at the appropriate depth in the soil (Figure E.1). Second, a pre-drill auger is used to pre-form a hole ready for the probe to be inserted into (Figure E.2). Third, the redox probe was gently hammered into the pre-drilled hole to the appropriate depth below the ground (Figure E.3). Wiring connections were then completed to the data logger. Final site set ups are shown in Figure E.4, Figure E.5 and Figure E.6.

Figure E.1: Soil redox probe next to tape measure and pre-drill auger. The ORP-80-4-D soil redox probe has four platinum electrodes at 20, 40, 60 and 80 cm, but drilled 10 cm below the ground surface to a depth of 30, 50, 70 and 90 cm as shown in the photo. The plastic cap with electrolyte fluid was removed just prior to installation.

Figure E.2: Pre-drill is used to prepare a hole for the soil redox probe, drilled to the appropriate depth 10 cm below the surface.

Figure E.3: Redox probe is gently hammered into the pre-drilled hole, 10 cm below the ground surface. Inset photo shows depth after being hammered in and subsequently covered over.

Figure E.4: Ramiha silt loam site set up. Soil description pit was dug adjacent to the monitoring pen. A wind turbine is present in the background.

Figure E.5: Shannon silt loam site set up. Soil description pit was dug adjacent to the monitoring pen.

Figure E.6: Tokomaru silt loam site set up. Soil description pit was dug adjacent to the monitoring pen.

Appendix F

Table F.1: Wastewater discharge loads (t yr^{-1}) in the Horizons region (Cox et al., 2022).

Discharge	NO_3^--N t yr^{-1}	NO_2^--N t yr^{-1}	NH_4^+-N t yr^{-1}	*SIN* t yr^{-1}
AFFCO Fielding at Industrial Wastewater	15.21	6.97	11.41	33.6
Dannevirke STP at microfiltered oxpond	9.16	2.44	28.25	39.85
Eketahuna STP at Secondary oxpond waste	0.07	0.02	1.67	1.76
Feilding STP at Secondary oxpond waste	159.52	5.46	180.82	345.8
Foxton STP at Secondary oxpond waste	0.04	0.04	9.3	9.37
Halcombe at Secondary oxpond	0.02	< 0.01	0.92	0.95
Hunterville STP at Microfiltration Plant	0.26	< 0.01	0.06	0.32
Kimbolton STP at oxpond waste	0.9	0.01	0.38	1.29
Marton STP at Rock filtered oxpond waste	2.89	0.3	7.89	11.08
National Park STP at Secondary oxpond	0.09	0.01	0.72	0.82
Norsewood STP at oxpond waste	0.11	0.01	0.18	0.30
Ohakune STP at Secondary oxpond waste	1.59	0.25	17.63	19.47
Ormondville STP at 2nd oxpond waste	0.01	< 0.01	0.05	0.07
Pahiatua STP at Tertiary oxpond waste	0.31	0.12	1.99	2.42
PNCC STP at Tertiary Treated Effluent	4.12	7.00	349.58	360.71
Pongaroa STP at 2nd oxpond waste	0.04	0.01	0.29	0.34
PPCS Oringi STP at oxpond waste	0.16	< 0.01	< 0.01	0.17
Raetihi STP at Secondary oxpond waste	0.07	0.02	2.09	2.18
Rangataua STP at Secondary oxpond waste	< 0.01	< 0.01	0.13	0.13
Ratana STP at Secondary oxpond waste	0.04	0.03	0.38	0.45
Riverlands at Industrial wastewater	10.48	2.3	20.52	33.3
Rongotea STP at Secondary oxpond waste	0.12	0.01	1.61	1.75
Sanson STP at Secondary oxpond waste	0.04	0.01	3.07	3.12
Taihape STP at oxpond waste	0.42	0.11	3.16	3.69
Taumarunui STP at Tertiary treated waste	3.85	0.85	12.45	17.14
Tokomaru at oxpond waste	0.05	< 0.01	0.25	0.3
Waiouru STP at oxpond waste	3.00	0.06	0.49	3.54
Winstone Pulp WWTP at oxpond waste	0.14	0.56	3.42	4.12
Woodville STP at Secondary oxpond waste	0.52	0.09	3.09	3.69

Appendix G

Table G.1: Observed and predicted average annual river *SIN* loads (t yr^{-1}) with initial AF_N values.

Monitoring site	Observed *SIN* load (t yr^{-1})	Predicted *SIN* load (t yr^{-1})	Error (t yr^{-1})	Error (%)
Tokomaru River at Horseshoe bend	8	29	21	256
Whakapapa at Footbridge	8	30	22	263
Mangapapa at Troup Road	12	36	24	195
Kumeti at Te Rehunga	15	13	-2	-16
Mangatainoka at Larsons Road	19	47	28	150
Ohau at Gladstone Reserve	19	45	26	136
Hautapu at Alabasters	24	81	57	244
Tokiahuru at Junction	28	48	20	73
Raparapawai at Jackson Road	29	75	46	159
Hautapu at Papakai Road Bridge	31	81	50	161
Rangitīkei at Pukeokahu	36	318	282	785
Owahanga at Branscombe Bridge	39	217	178	454
Mangawhero at Pakihi Rd Bridge	61	116	55	90
Hautapu at US Rangitīkei River Conf	62	119	57	92
Pohangina at Mais Reach	81	255	174	214
Mangatoro at Mangahei Road	82	106	24	29
Mangawhero at Raupiu Road	104	367	263	253
Mangahao at Ballance	113	177	65	58
Oroua at Almadale Slackline	115	250	136	119
Makuri at Tuscan Hills	121	68	-53	-44
Manawatū at Weber Road	259	504	245	94
Turakina at ONeills Bridge	264	291	27	10
Tiraumea at Ngaturi	317	126	-191	-60
Whanganui at Cherry Grove	338	354	16	5
Mangatainoka at Brewery	346	657	312	90
Rangitīkei at Mangaweka	364	834	470	129
Oroua at Awahuri Bridge	370	867	497	134
Manawatū at Hopelands	482	1146	664	138
Whangaehu at Kauangaroa	549	806	257	47
Ongarue at Taringamotu	605	589	-17	-3
Rangitīkei at Onepuhi	640	1039	399	62
Whanganui at Te Maire	1155	1042	-113	-10
Rangitīkei at McKelvies	1300	1552	252	19
Manawatū at Upper Gorge	1770	2386	615	35
Manawatū at Teachers College	1892	2855	963	51
Manawatū at Opiki Bridge	2226	3422	1196	54
Whanganui at Pipiriki	2735	2115	-620	-23
Whanganui at Te Rewa	3864	2165	-1699	-44

Table G.2: Observed and predicted average annual river *SIN* loads (t yr^{-1}) with calibrated AF_N values.

Monitoring site	Observed *SIN* load (t yr^{-1})	Predicted *SIN* load (t yr^{-1})	Error (t yr^{-1})	Error (%)
Tokomaru River at Horseshoe bend	8	28	20	243
Whakapapa at Footbridge	8	31	23	277
Mangapapa at Troup Road	12	36	23	191
Kumeti at Te Rehunga	15	13	-2	-15
Mangatainoka at Larsons Road	19	46	27	144
Ohau at Gladstone Reserve	19	43	24	128
Hautapu at Alabasters	24	78	54	230
Tokiahuru at Junction	28	46	18	63
Raparapawai at Jackson Road	29	74	46	158
Hautapu at Papakai Road Bridge	31	78	47	150
Rangitīkei at Pukeokahu	36	322	286	796
Owahanga at Branscombe Bridge	39	196	157	400
Mangawhero at Pakihi Rd Bridge	61	96	35	58
Hautapu at US Rangitīkei River Conf	62	110	48	78
Pohangina at Mais Reach	81	241	160	196
Mangatoro at Mangahei Road	82	92	10	13
Mangawhero at Raupiu Road	104	300	196	189
Mangahao at Ballance	113	176	63	56
Oroua at Almadale Slackline	115	230	115	100
Makuri at Tuscan Hills	121	66	-56	-46
Manawatū at Weber Road	259	486	227	88
Turakina at ONeills Bridge	264	263	-1	0
Tiraumea at Ngaturi	317	82	-234	-74
Whanganui at Cherry Grove	338	365	27	8
Mangatainoka at Brewery	346	652	306	88
Rangitīkei at Mangaweka	364	809	445	122
Oroua at Awahuri Bridge	370	826	456	123
Manawatū at Hopelands	482	1125	642	133
Whangaehu at Kauangaroa	549	677	128	23
Ongarue at Taringamotu	605	608	3	0
Rangitīkei at Onepuhi	640	990	351	55
Whanganui at Te Maire	1155	1076	-79	-7
Rangitīkei at McKelvies	1300	1490	190	15
Manawatū at Upper Gorge	1770	2299	529	30
Manawatū at Teachers College	1892	2748	856	45
Manawatū at Opiki Bridge	2226	3307	1081	49
Whanganui at Pipiriki	2735	2128	-606	-22
Whanganui at Te Rewa	3864	2154	-1709	-44

Table G.3: Observed and predicted average annual river *SIN* loads (t yr^{-1}) with calibrated AF_N values for the Manawatū catchment.

Monitoring site	Observed *SIN* load (t yr^{-1})	Predicted *SIN* load (t yr^{-1})	Error (t yr^{-1})	Error (%)
Tokomaru River at Horseshoe bend	8	27	19	230
Mangapapa at Troup Road	12	34	21	174
Kumeti at Te Rehunga	15	11	-4	-24
Mangatainoka at Larsons Road	19	43	25	130
Raparapawai at Jackson Road	29	69	40	139
Pohangina at Mais Reach	81	223	142	174
Mangatoro at Mangahei Road	82	81	-1	-1
Mangahao at Ballance	113	162	49	44
Oroua at Almadale Slackline	115	216	101	88
Makuri at Tuscan Hills	121	52	-70	-57
Manawatū at Weber Road	259	429	170	66
Tiraumea at Ngaturi	317	47	-269	-85
Mangatainoka at Brewery	346	607	261	76
Oroua at Awahuri Bridge	370	805	435	118
Manawatū at Hopelands	482	999	517	107
Manawatū at Upper Gorge	1770	2038	268	15
Manawatū at Teachers College	1892	2456	564	30
Manawatū at Opiki Bridge	2226	3009	783	35

Table G.4: Observed and predicted average annual river *SIN* loads (t yr^{-1}) with calibrated AF_N values for the Rangitīkei catchment.

Monitoring site	Observed *SIN* load (t yr^{-1})	Predicted *SIN* load (t yr^{-1})	Error (t yr^{-1})	Error (%)
Hautapu at Alabasters	24	68	44	187
Hautapu at Papakai Road Bridge	31	68	37	118
Rangitīkei at Pukeokahu	36	281	245	682
Hautapu at US Rangitīkei River Conf	62	98	36	59
Rangitīkei at Mangaweka	364	712	348	95
Rangitīkei at Onepuhi	640	877	238	37
Rangitīkei at McKelvies	1300	1367	67	5

Table G.5: Observed and predicted average annual river *SIN* loads (t yr^{-1}) with calibrated AF_N values for the Whanganui catchment.

Monitoring site	Observed *SIN* load (t yr^{-1})	Predicted *SIN* load (t yr^{-1})	Error (t yr^{-1})	Error (%)
Whakapapa at Footbridge	8	38	29	355
Whanganui at Cherry Grove	338	435	97	29
Ongarue at Taringamotu	605	714	109	18
Whanganui at Te Maire	1155	1271	116	10
Whanganui at Pipiriki	2735	2702	-33	-1
Whanganui at Te Rewa	3864	2806	-1057	-27

Appendix H

Tables of each monitoring site containing a breakdown of the rock types, drainage class and *LSNAI* categories.

Table H.1: Hautapu at Alabasters

Rock types

	Area (km^2)	Percent
Volcanic ash over Sandstone	138.1	49.3
Sandstone	57.5	20.5
Mudstone	54.1	19.3
Volcanic ash	14.2	5.1
Volcanic ash over Mudstone	9.1	3.2
Volcanic deposits over Volcanic ash	5.4	1.9
Alluvium	1.8	0.7
Volcanic deposits over Sandstone	0.0	0.0
Total	**280.2**	**100.0**

Drainage Class

	Area (km^2)	Percent
Well	205.1	73.2
Moderately well	75.1	26.8
Total	**280.2**	**100.0**

LSNAI

	Area (km^2)	Percent
Medium	75.1	26.8
Low	205.1	73.2
Total	**280.2**	**100.0**

Table H.2: Hautapu at Papakai Road Bridge

Rock types

	Area (km^2)	Percent
Volcanic ash over Sandstone	138.1	49.3
Sandstone	57.5	20.5
Mudstone	54.1	19.3
Volcanic ash	14.2	5.1
Volcanic ash over Mudstone	9.1	3.2
Volcanic deposits over Volcanic ash	5.4	1.9
Alluvium	1.8	0.7
Volcanic deposits over Sandstone	0.0	0.0
Total	**280.2**	**100.0**

Drainage Class

	Area (km^2)	Percent
Well	205.1	73.2
Moderately well	75.1	26.8
Total	**280.2**	**100.0**

LSNAI

	Area (km^2)	Percent
Medium	75.1	26.8
Low	205.1	73.2
Total	**280.2**	**100.0**

Table H.3: Hautapu at US Rangitīkei River Conf

Rock types

	Area (km^2)	Percent
Volcanic ash over Sandstone	140.4	37.1
Sandstone	139.8	36.9
Mudstone	66.0	17.4
Volcanic ash	14.2	3.8
Volcanic ash over Mudstone	9.1	2.4
Volcanic deposits over Volcanic ash	5.4	1.4
Alluvium	3.3	0.9
Volcanic deposits over Sandstone	0.0	0.0
Total	**378.3**	**100.0**

Drainage Class

	Area (km^2)	Percent
Well	226.3	59.8
Moderately well	137.7	36.4
Imperfect	14.2	3.8
Total	**378.3**	**100.0**

LSNAI

	Area (km^2)	Percent
Medium	151.9	40.2
Low	226.3	59.8
Total	**378.3**	**100.0**

Table H.4: Kumeti at Te Rehunga

Rock types

	Area (km²)	Percent
Greywacke	7.4	59.8
Alluvium over Gravels	2.4	19.2
Gravels	1.2	9.7
Loess over Gravels	0.5	4.0
Loess over Sandstone	0.4	3.6
Peat over Greywacke	0.3	2.5
Alluvium	0.1	1.1
Total	**12.4**	**100.0**

Drainage Class

	Area (km²)	Percent
Well	7.9	63.9
Moderately well	3.5	28.3
Poor	1.0	7.8
Total	**12.4**	**100.0**

LSNAI

	Area (km²)	Percent
High	1.0	7.8
Low	4.5	36.5
Very low	6.9	55.7
Total	**12.4**	**100.0**

Table H.5: Makuri at Tuscan Hills

Rock types

	Area (km^2)	Percent
Limestone	73.7	44.4
Mudstone	37.0	22.3
Sandstone	32.3	19.5
Gravels	13.3	8.0
Greywacke	6.4	3.8
Alluvium	3.2	1.9
Total	**165.9**	**100.0**

Drainage Class

	Area (km^2)	Percent
Well	110.5	66.6
Moderately well	38.3	23.1
Poor	8.8	5.3
Imperfect	8.3	5.0
Total	**165.9**	**100.0**

LSNAI

	Area (km^2)	Percent
High	8.8	5.3
Medium	46.0	27.8
Low	104.7	63.1
Very low	6.4	3.8
Total	**165.9**	**100.0**

Table H.6: Manawatū at Hopelands

Rock types

	Area (km^2)	Percent
Sandstone	249.8	20.3
Greywacke	181.2	14.7
Loess over Gravels	178.8	14.5
Mudstone	151.5	12.3
Loess over Unconsolidated sediments	97.7	7.9
Gravels	95.7	7.8
Unconsolidated sediments	80.7	6.6
Limestone	68.2	5.5
Alluvium	48.0	3.9
Argillite	39.9	3.2
Alluvium over Gravels	23.1	1.9
Loess over Sandstone	9.6	0.8
Gravels over Sandstone	5.2	0.4
Peat over Greywacke	1.6	0.1
Total	**1230.8**	**100.0**

Drainage Class

	Area (km^2)	Percent
Well	784.2	63.7
Imperfect	257.2	20.9
Moderately well	154.4	12.5
Poor	34.9	2.8
Total	**1230.8**	**100.0**

LSNAI

	Area (km^2)	Percent
High	42.6	3.5
Medium	336.5	27.3
Low	673.8	54.7
Very low	177.9	14.5
Total	**1230.8**	**100.0**

Table H.7: Manawatū at Opiki Bridge

Rock types

	Area (km^2)	Percent
Sandstone	897.4	21.5
Greywacke	825.9	19.8
Mudstone	569.6	13.7
Alluvium	384.3	9.2
Loess over Gravels	284.5	6.8
Gravels	268.4	6.4
Unconsolidated sediments	170.8	4.1
Loess over Unconsolidated sediments	162.7	3.9
Limestone	162.3	3.9
Loess	143.2	3.4
Loess over Sandstone	93.9	2.3
Argillite	72.7	1.7
Loess over Greywacke	55.0	1.3
Alluvium over Gravels	40.8	1.0
Loess over Mudstone	13.5	0.3
Gravels over Sandstone	9.0	0.2
Loess over Alluvium	8.8	0.2
Peat over Greywacke	5.7	0.1
Total	**4168.5**	**100.0**

Drainage Class

	Area (km^2)	Percent
Well	2051.3	49.2
Moderately well	894.3	21.5
Imperfect	854.9	20.5
Poor	368.0	8.8
Total	**4168.5**	**100.0**

LSNAI

	Area (km^2)	Percent
High	446.3	10.7
Medium	1162.3	27.9
Low	1779.9	42.7
Very low	779.9	18.7
Total	**4168.4**	**100.0**

Table H.8: Manawatū at Teachers College

Rock types

	Area (km^2)	Percent
Sandstone	897.4	23.3
Greywacke	784.7	20.3
Mudstone	569.6	14.8
Alluvium	318.2	8.2
Loess over Gravels	277.7	7.2
Gravels	267.5	6.9
Unconsolidated sediments	168.0	4.4
Limestone	162.3	4.2
Loess over Unconsolidated sediments	137.6	3.6
Argillite	72.7	1.9
Loess	63.1	1.6
Loess over Sandstone	50.2	1.3
Alluvium over Gravels	35.0	0.9
Loess over Greywacke	25.9	0.7
Loess over Mudstone	13.5	0.4
Gravels over Sandstone	9.0	0.2
Peat over Greywacke	5.7	0.1
Total	**3858.0**	**100.0**

Drainage Class

	Area (km^2)	Percent
Well	2004.5	52.0
Moderately well	823.7	21.4
Imperfect	772.7	20.0
Poor	257.2	6.7
Total	**3858.0**	**100.0**

LSNAI

	Area (km^2)	Percent
High	287.7	7.5
Medium	1103.3	28.6
Low	1721.3	44.6
Very low	745.7	19.3
Total	**3857.9**	**100.0**

Table H.9: Manawatū at Upper Gorge

Rock types

	Area (km^2)	Percent
Sandstone	702.8	22.3
Greywacke	564.5	17.9
Mudstone	561.6	17.8
Loess over Gravels	263.1	8.3
Gravels	248.7	7.9
Alluvium	247.7	7.9
Limestone	162.2	5.1
Loess over Unconsolidated sediments	128.7	4.1
Unconsolidated sediments	86.1	2.7
Argillite	72.7	2.3
Loess over Sandstone	39.7	1.3
Alluvium over Gravels	32.9	1.0
Loess over Mudstone	12.5	0.4
Loess	11.5	0.4
Gravels over Sandstone	9.0	0.3
Loess over Greywacke	6.3	0.2
Peat over Greywacke	1.6	0.0
Total	**3151.6**	**100.0**

Drainage Class

	Area (km^2)	Percent
Well	1716.1	54.5
Imperfect	638.4	20.3
Moderately well	623.2	19.8
Poor	174.0	5.5
Total	**3151.6**	**100.0**

LSNAI

	Area (km^2)	Percent
High	191.6	6.1
Medium	924.3	29.3
Low	1484.7	47.1
Very low	551.0	17.5
Total	**3151.5**	**100.0**

Table H.10: Manawatū at Weber Road

Rock types

	Area (km^2)	Percent
Sandstone	167.7	24.4
Mudstone	128.5	18.7
Loess over Gravels	88.8	12.9
Greywacke	64.4	9.4
Limestone	57.9	8.4
Unconsolidated sediments	50.2	7.3
Loess over Unconsolidated sediments	45.9	6.7
Argillite	39.9	5.8
Gravels	29.0	4.2
Alluvium	10.5	1.5
Alluvium over Gravels	2.3	0.3
Loess over Sandstone	1.3	0.2
Total	**686.4**	**100.0**

Drainage Class

	Area (km^2)	Percent
Well	433.3	63.1
Imperfect	154.8	22.5
Moderately well	94.3	13.7
Poor	4.1	0.6
Total	**686.4**	**100.0**

LSNAI

	Area (km^2)	Percent
High	4.5	0.7
Medium	232.5	33.9
Low	385.6	56.2
Very low	63.8	9.3
Total	**686.4**	**100.0**

Table H.11: Mangahao at Ballance

Rock types

	Area (km^2)	Percent
Greywacke	189.2	68.7
Gravels	36.6	13.3
Loess over Gravels	12.6	4.6
Alluvium	10.9	3.9
Sandstone	9.3	3.4
Loess over Unconsolidated sediments	7.2	2.6
Loess over Sandstone	4.0	1.5
Loess over Greywacke	3.3	1.2
Loess	1.3	0.5
Mudstone	0.7	0.3
Unconsolidated sediments	0.0	0.0
Total	**275.2**	**100.0**

Drainage Class

	Area (km^2)	Percent
Well	121.6	44.2
Moderately well	110.7	40.2
Imperfect	42.1	15.3
Poor	0.9	0.3
Total	**275.2**	**100.0**

LSNAI

	Area (km^2)	Percent
High	10.3	3.7
Medium	1.3	0.5
Low	83.9	30.5
Very low	179.8	65.3
Total	**275.2**	**100.0**

Table H.12: Mangapapa at Troup Road

Rock types

	Area (km^2)	Percent
Greywacke	9.3	35.4
Alluvium	5.7	21.7
Loess over Sandstone	4.1	15.4
Loess	3.4	13.0
Sandstone	2.7	10.1
Mudstone	1.0	3.9
Loess over Gravels	0.1	0.5
Total	**26.3**	**100.0**

Drainage Class

	Area (km^2)	Percent
Well	18.4	70.1
Poor	5.7	21.7
Imperfect	2.2	8.2
Total	**26.3**	**100.0**

LSNAI

	Area (km^2)	Percent
High	5.7	21.7
Medium	2.2	8.2
Low	9.1	34.6
Very low	9.3	35.4
Total	**26.3**	**100.0**

Table H.13: Mangatainoka at Brewery

Rock types

	Area (km^2)	Percent
Greywacke	119.5	28.1
Sandstone	71.4	16.8
Gravels	64.9	15.3
Alluvium	63.3	14.9
Loess over Gravels	42.5	10.0
Mudstone	39.8	9.4
Loess over Mudstone	12.5	2.9
Gravels over Sandstone	3.8	0.9
Limestone	2.6	0.6
Loess over Unconsolidated sediments	2.4	0.6
Loess over Sandstone	1.1	0.3
Unconsolidated sediments	1.0	0.2
Total	**424.7**	**100.0**

Drainage Class

	Area (km^2)	Percent
Well	287.7	67.8
Moderately well	91.8	21.6
Poor	33.7	7.9
Imperfect	11.5	2.7
Total	**424.7**	**100.0**

LSNAI

	Area (km^2)	Percent
High	33.7	7.9
Medium	26.1	6.2
Low	245.4	57.8
Very low	119.4	28.1
Total	**424.7**	**100.0**

Table H.14: Mangatainoka at Larsons Road

Rock types

	Area (km^2)	Percent
Greywacke	54.2	81.1
Sandstone	5.8	8.7
Gravels	3.1	4.6
Alluvium	3.0	4.4
Loess over Gravels	0.7	1.1
Total	**66.9**	**100.0**

Drainage Class

	Area (km^2)	Percent
Moderately well	47.2	70.6
Well	17.6	26.3
Imperfect	2.1	3.1
Total	**66.9**	**100.0**

LSNAI

	Area (km^2)	Percent
Medium	1.2	1.8
Low	11.4	17.1
Very low	54.2	81.1
Total	**66.9**	**100.0**

Table H.15: Mangatoro at Mangahei Road

Rock types

	Area (km^2)	Percent
Sandstone	71.4	31.3
Mudstone	65.1	28.5
Limestone	39.5	17.3
Greywacke	22.6	9.9
Argillite	20.2	8.8
Gravels	9.2	4.0
Alluvium over Gravels	0.4	0.2
Alluvium	0.1	0.0
Total	**228.5**	**100.0**

Drainage Class

	Area (km^2)	Percent
Well	102.3	44.8
Imperfect	73.9	32.3
Moderately well	52.3	22.9
Total	**228.5**	**100.0**

LSNAI

	Area (km^2)	Percent
Medium	121.0	53.0
Low	85.0	37.2
Very low	22.6	9.9
Total	**228.5**	**100.0**

Table H.16: Mangawhero at Pakihi Rd Bridge

Rock types

	Area (km^2)	Percent
Volcanic ash over Volcanic deposits	77.7	47.1
Volcanic ash over Sandstone	56.8	34.4
Sandstone	11.0	6.6
Volcanic ash	7.7	4.7
Volcanic ash over Mudstone	5.3	3.2
Alluvium over Volcanic ash	3.6	2.2
Alluvium	2.7	1.6
Volcanic deposits over Sandstone	0.3	0.2
Total	**165.0**	**100.0**

Drainage Class

	Area (km^2)	Percent
Moderately well	131.0	79.4
Well	28.2	17.1
Poor	5.9	3.6
Total	**165.0**	**100.0**

LSNAI

	Area (km^2)	Percent
High	5.7	3.4
Medium	131.0	79.4
Low	28.4	17.2
Total	**165.0**	**100.0**

Table H.17: Mangawhero at Raupiu Road

Rock types

	Area (km^2)	Percent
Mudstone	185.5	28.5
Volcanic ash over Volcanic deposits	141.9	21.8
Volcanic ash over Sandstone	125.5	19.3
Sandstone	125.4	19.3
Volcanic ash	32.8	5.0
Volcanic ash over Mudstone	19.7	3.0
Alluvium	11.4	1.8
Volcanic deposits over Sandstone	5.3	0.8
Alluvium over Volcanic ash	3.6	0.6
Volcanic deposits	0.3	0.0
Total	**651.7**	**100.0**

Drainage Class

	Area (km^2)	Percent
Moderately well	503.5	77.3
Well	135.2	20.8
Poor	7.3	1.1
Imperfect	5.6	0.9
Total	**651.7**	**100.0**

LSNAI

	Area (km^2)	Percent
High	7.1	1.1
Medium	509.1	78.1
Low	135.5	20.8
Total	**651.7**	**100.0**

Table H.18: Ohau at Gladstone Reserve

Rock types

	Area (km^2)	Percent
Greywacke	90.0	86.9
Loess over Greywacke	6.2	6.0
Loess	2.9	2.8
Alluvium over Gravels	2.8	2.7
Gravels	1.7	1.7
Total	**103.6**	**100.0**

Drainage Class

	Area (km^2)	Percent
Moderately well	62.5	60.3
Well	39.1	37.7
Imperfect	2.1	2.0
Total	**103.6**	**100.0**

LSNAI

	Area (km^2)	Percent
Low	13.6	13.1
Very low	90.0	86.9
Total	**103.6**	**100.0**

Table H.19: Ohura at Tokorima

Rock types

	Area (km^2)	Percent
Sandstone	297.8	44.2
Mudstone	201.6	29.9
Volcanic ash over Mudstone	58.1	8.6
Alluvium	41.1	6.1
Volcanic ash over Sandstone	36.8	5.5
Volcanic ash	26.8	4.0
Volcanic deposits	10.9	1.6
Volcanic ash over Volcanic deposits	0.3	0.0
Total	**673.5**	**100.0**

Drainage Class

	Area (km^2)	Percent
Well	558.7	83
Moderately well	114.8	17
Total	**673.5**	**100**

LSNAI

	Area (km^2)	Percent
Medium	114.8	17
Low	558.7	83
Total	**673.5**	**100**

Table H.20: Ongarue at Taringamotu

Rock types

	Area (km^2)	Percent
Volcanic ash over Volcanic deposits	281.7	25.7
Volcanic ash over Mudstone	205.5	18.8
Volcanic ash	186.8	17.1
Volcanic ash over Greywacke	132.0	12.1
Volcanic ash over Sandstone	128.2	11.7
Volcanic deposits	88.8	8.1
Sandstone	49.8	4.5
Greywacke	12.4	1.1
Mudstone	8.5	0.8
Alluvium	0.6	0.1
Total	**1094.4**	**100.0**

Drainage Class

	Area (km^2)	Percent
Well	1089.8	99.6
Moderately well	4.5	0.4
Total	**1094.4**	**100.0**

LSNAI

	Area (km^2)	Percent
Medium	4.5	0.4
Low	1077.4	98.5
Very low	12.4	1.1
Total	**1094.3**	**100.0**

Table H.21: Oroua at Almadale Slackline

Rock types

	Area (km^2)	Percent
Sandstone	87.2	27.2
Greywacke	82.3	25.6
Alluvium	37.8	11.8
Loess over Gravels	32.3	10.1
Loess	29.5	9.2
Unconsolidated sediments	24.4	7.6
Loess over Sandstone	18.2	5.7
Alluvium over Gravels	5.0	1.5
Gravels	3.9	1.2
Loess over Greywacke	0.4	0.1
Loess over Alluvium	0.1	0.0
Total	**321.0**	**100.0**

Drainage Class

	Area (km^2)	Percent
Moderately well	174.7	54.4
Well	86.6	27.0
Imperfect	42.8	13.3
Poor	16.9	5.3
Total	**321.0**	**100.0**

LSNAI

	Area (km^2)	Percent
High	19.9	6.2
Medium	143.5	44.7
Low	81.5	25.4
Very low	76.1	23.7
Total	**321.0**	**100.0**

Table H.22: Oroua at Awahuri Bridge

Rock types

	Area (km^2)	Percent
Sandstone	171.6	23.6
Loess over Gravels	127.4	17.5
Loess	106.0	14.6
Alluvium	102.5	14.1
Greywacke	82.3	11.3
Loess over Sandstone	67.8	9.3
Unconsolidated sediments	33.4	4.6
Mudstone	18.4	2.5
Alluvium over Gravels	12.7	1.8
Gravels	3.9	0.5
Loess over Greywacke	0.4	0.1
Loess over Alluvium	0.1	0.0
Total	**726.4**	**100.0**

Drainage Class

	Area (km^2)	Percent
Moderately well	323.2	44.5
Imperfect	158.7	21.9
Well	141.1	19.4
Poor	103.3	14.2
Total	**726.4**	**100.0**

LSNAI

	Area (km^2)	Percent
High	150.6	20.7
Medium	357.1	49.2
Low	142.6	19.6
Very low	76.1	10.5
Total	**726.4**	**100.0**

Table H.23: Owahanga at Branscombe Bridge

Rock types

	Area (km²)	Percent
Mudstone	200.0	47.0
Argillite	93.2	21.9
Sandstone	67.7	15.9
Alluvium	34.6	8.1
Greywacke	27.2	6.4
Limestone	2.0	0.5
Windblown sands	0.5	0.1
Total	**425.2**	**100.0**

Drainage Class

	Area (km²)	Percent
Well	199.8	47.0
Imperfect	98.5	23.2
Moderately well	95.2	22.4
Poor	31.7	7.5
Total	**425.2**	**100.0**

LSNAI

	Area (km²)	Percent
Very high	0.4	0.1
High	31.3	7.5
Medium	190.5	45.6
Low	168.7	40.4
Very low	27.1	6.5
Total	**418.1**	**100.0**

Table H.24: Pohangina at Mais Reach

Rock types

	Area (km^2)	Percent
Sandstone	136.0	41.2
Unconsolidated sediments	63.7	19.3
Greywacke	57.6	17.5
Alluvium	28.1	8.5
Loess over Gravels	13.0	3.9
Gravels	10.9	3.3
Loess over Sandstone	7.3	2.2
Mudstone	3.8	1.2
Loess	3.8	1.2
Alluvium over Gravels	2.1	0.6
Loess over Greywacke	1.6	0.5
Loess over Mudstone	1.0	0.3
Loess over Unconsolidated sediments	0.8	0.2
Total	**329.8**	**100.0**

Drainage Class

	Area (km^2)	Percent
Well	158.9	48.2
Moderately well	98.1	29.7
Imperfect	62.8	19.1
Poor	10.0	3.0
Total	**329.8**	**100.0**

LSNAI

	Area (km^2)	Percent
High	12.3	3.7
Medium	131.2	39.8
Low	133.3	40.4
Very low	53.0	16.1
Total	**329.8**	**100.0**

Table H.25: Rangitīkei at Mangaweka

Rock types

	Area (km^2)	Percent
Sandstone	736.5	27.9
Volcanic ash over Greywacke	468.4	17.8
Volcanic ash over Sandstone	451.9	17.1
Greywacke	379.0	14.4
Mudstone	167.0	6.3
Volcanic deposits over Volcanic ash	141.7	5.4
Volcanic ash	92.4	3.5
Volcanic deposits over Greywacke	63.6	2.4
Alluvium	38.6	1.5
Volcanic deposits over Sandstone	19.8	0.8
Alluvium over Gravels	14.8	0.6
Volcanic deposits	14.3	0.5
Gravels	13.9	0.5
Volcanic ash over Mudstone	12.0	0.5
Loess over Sandstone	7.9	0.3
Loess over Gravels	7.4	0.3
Loess over Mudstone	1.9	0.1
Loess	1.5	0.1
Volcanic ash over Limestone	1.5	0.1
Volcanic deposits over Alluvium	1.4	0.1
Total	**2635.4**	**100.0**

Drainage Class

	Area (km^2)	Percent
Well	1968.7	74.7
Moderately well	508.2	19.3
Imperfect	144.3	5.5
Poor	14.2	0.5
Total	**2635.4**	**100.0**

LSNAI

	Area (km^2)	Percent
High	32.9	1.2
Medium	449.4	17.1
Low	1790.7	68.0
Very low	362.3	13.7
Total	**2635.3**	**100.0**

Table H.26: Rangitīkei at McKelvies

Rock types

	Area (km^2)	Percent
Sandstone	1022.5	26.9
Volcanic ash over Greywacke	468.4	12.3
Volcanic ash over Sandstone	453.7	11.9
Greywacke	379.0	10.0
Mudstone	290.8	7.7
Loess	230.5	6.1
Volcanic deposits over Volcanic ash	141.7	3.7
Loess over Sandstone	138.4	3.6
Alluvium over Gravels	129.8	3.4
Loess over Gravels	118.6	3.1
Alluvium	116.9	3.1
Volcanic ash	92.4	2.4
Volcanic deposits over Greywacke	63.6	1.7
Windblown sands	54.9	1.4
Volcanic deposits over Sandstone	19.8	0.5
Gravels	18.9	0.5
Unconsolidated sediments	15.9	0.4
Volcanic deposits	14.3	0.4
Volcanic ash over Mudstone	12.0	0.3
Loess over Unconsolidated sediments	6.7	0.2
Loess over Mudstone	1.9	0.0
Gravels over Sandstone	1.8	0.0
Volcanic ash over Limestone	1.5	0.0
Volcanic deposits over Alluvium	1.4	0.0
Loess over Alluvium	1.3	0.0
Loess over Windblown sands	1.1	0.0
Alluvium over Mudstone	0.6	0.0
Total	**3798.4**	**100.0**

Drainage Class

	Area (km^2)	Percent
Well	2290.7	60.3
Moderately well	744.1	19.6
Imperfect	456.6	12.0
Poor	307.0	8.1
Total	**3798.4**	**100.0**

LSNAI

	Area (km^2)	Percent
Very high	54.9	1.4
High	419.2	11.0
Medium	868.0	22.9
Low	2093.9	55.1
Very low	362.3	9.5
Total	**3798.4**	**100.0**

Table H.27: Rangitīkei at Onepuhi

Rock types

	Area (km²)	Percent
Sandstone	926.0	28.8
Volcanic ash over Greywacke	468.4	14.6
Volcanic ash over Sandstone	453.7	14.1
Greywacke	379.0	11.8
Mudstone	290.1	9.0
Volcanic deposits over Volcanic ash	141.7	4.4
Loess over Gravels	93.7	2.9
Volcanic ash	92.4	2.9
Alluvium	79.2	2.5
Loess over Sandstone	74.4	2.3
Volcanic deposits over Greywacke	63.6	2.0
Loess	30.5	0.9
Alluvium over Gravels	25.1	0.8
Volcanic deposits over Sandstone	19.8	0.6
Gravels	18.9	0.6
Unconsolidated sediments	15.9	0.5
Volcanic deposits	14.3	0.4
Volcanic ash over Mudstone	12.0	0.4
Loess over Unconsolidated sediments	6.7	0.2
Loess over Mudstone	1.9	0.1
Volcanic ash over Limestone	1.5	0.0
Volcanic deposits over Alluvium	1.4	0.0
Gravels over Sandstone	0.6	0.0
Alluvium over Mudstone	0.6	0.0
Loess over Alluvium	0.3	0.0
Total	**3211.6**	**100.0**

Drainage Class

	Area (km²)	Percent
Well	2157.5	67.2
Moderately well	674.4	21.0
Imperfect	310.4	9.7
Poor	69.2	2.2
Total	**3211.6**	**100.0**

LSNAI

	Area (km²)	Percent
High	121.9	3.8
Medium	746.8	23.3
Low	1980.6	61.7
Very low	362.3	11.3
Total	**3211.5**	**100.0**

Table H.28: Rangitīkei at Pukeokahu

Rock types

	Area (km^2)	Percent
Volcanic ash over Greywacke	303.3	40.0
Greywacke	132.4	17.4
Volcanic ash over Sandstone	130.4	17.2
Sandstone	109.4	14.4
Volcanic ash	64.0	8.4
Mudstone	6.0	0.8
Gravels	4.8	0.6
Volcanic deposits over Greywacke	4.6	0.6
Volcanic deposits	3.2	0.4
Alluvium	0.6	0.1
Total	**758.6**	**100.0**

Drainage Class

	Area (km^2)	Percent
Well	738.6	97.4
Moderately well	19.4	2.6
Poor	0.6	0.1
Total	**758.6**	**100.0**

LSNAI

	Area (km^2)	Percent
High	0.6	0.1
Medium	19.4	2.6
Low	606.2	79.9
Very low	132.4	17.4
Total	**758.6**	**100.0**

Table H.29: Raparapawai at Jackson Road

Rock types

	Area (km^2)	Percent
Loess over Gravels	15.7	34.6
Greywacke	9.5	21.0
Sandstone	5.8	12.9
Alluvium	5.4	11.9
Loess over Sandstone	3.8	8.4
Loess over Unconsolidated sediments	2.9	6.3
Gravels	2.1	4.7
Alluvium over Gravels	0.1	0.2
Unconsolidated sediments	0.0	0.0
Total	**45.4**	**100.0**

Drainage Class

	Area (km^2)	Percent
Well	25.2	55.5
Imperfect	12.3	27.2
Poor	5.5	12.2
Moderately well	2.3	5.1
Total	**45.4**	**100.0**

LSNAI

	Area (km^2)	Percent
High	10.1	22.2
Medium	7.4	16.3
Low	19.0	41.9
Very low	8.9	19.6
Total	**45.4**	**100.0**

Table H.30: Tiraumea at Ngaturi

Rock types

	Area (km^2)	Percent
Mudstone	316.9	43.0
Sandstone	214.9	29.2
Limestone	80.2	10.9
Alluvium	42.9	5.8
Argillite	32.8	4.5
Gravels	28.5	3.9
Greywacke	13.0	1.8
Alluvium over Gravels	7.1	1.0
Total	**736.3**	**100.0**

Drainage Class

	Area (km^2)	Percent
Well	258.2	35.1
Imperfect	249.5	33.9
Moderately well	188.9	25.7
Poor	39.7	5.4
Total	**736.3**	**100.0**

LSNAI

	Area (km^2)	Percent
High	39.7	5.4
Medium	426.5	57.9
Low	257.0	34.9
Very low	13.0	1.8
Total	**736.3**	**100.0**

Table H.31: Tokiahuru at Junction

Rock types

	Area (km^2)	Percent
Volcanic ash over Volcanic deposits	114.7	58.3
Volcanic deposits over Volcanic ash	45.6	23.2
Volcanic deposits	13.6	6.9
Volcanic ash	8.1	4.1
Volcanic ash over Sandstone	7.7	3.9
Volcanic ash over Alluvium	5.0	2.6
Alluvium	1.9	1.0
Total	**196.7**	**100.0**

Drainage Class

	Area (km^2)	Percent
Well	147.6	75.1
Moderately well	43.6	22.2
Poor	5.5	2.8
Total	**196.7**	**100.0**

LSNAI

	Area (km^2)	Percent
High	3.4	1.7
Medium	43.6	22.2
Low	149.7	76.1
Total	**196.7**	**100.0**

Table H.32: Tokomaru River at Horseshoe bend

Rock types

	Area (km^2)	Percent
Greywacke	44.3	80.2
Loess over Greywacke	8.0	14.5
Loess	2.1	3.7
Gravels	0.8	1.4
Alluvium	0.1	0.1
Alluvium over Gravels	0.0	0.0
Total	**55.3**	**100.0**

Drainage Class

	Area (km^2)	Percent
Well	25.1	45.4
Moderately well	24.8	44.9
Imperfect	5.3	9.6
Poor	0.1	0.1
Total	**55.3**	**100.0**

LSNAI

	Area (km^2)	Percent
High	1.2	2.2
Low	10.8	19.6
Very low	43.3	78.3
Total	**55.3**	**100.0**

Table H.33: Turakina at ONeills Bridge

Rock types

	Area (km^2)	Percent
Sandstone	424.2	44.9
Mudstone	272.1	28.8
Alluvium	67.4	7.1
Loess	60.3	6.4
Loess over Sandstone	33.1	3.5
Unconsolidated sediments	23.6	2.5
Volcanic ash over Sandstone	21.4	2.3
Volcanic ash over Mudstone	18.0	1.9
Windblown sands	10.2	1.1
Loess over Gravels	9.4	1.0
Alluvium over Mudstone	3.4	0.4
Volcanic ash	1.9	0.2
Total	**945.1**	**100.0**

Drainage Class

	Area (km^2)	Percent
Well	385.1	40.7
Moderately well	244.0	25.8
Imperfect	199.0	21.1
Poor	117.0	12.4
Total	**945.1**	**100.0**

LSNAI

	Area (km^2)	Percent
Very high	10.2	1.1
High	142.3	15.1
Medium	416.2	44.0
Low	376.4	39.8
Total	**945.1**	**100.0**

Table H.34: Whakapapa at Footbridge

Rock types

	Area (km^2)	Percent
Volcanic ash	63.5	56.5
Volcanic deposits over Volcanic ash	31.7	28.3
Volcanic deposits	9.8	8.7
Volcanic ash over Volcanic deposits	4.1	3.7
Sandstone	2.2	2.0
Volcanic ash over Sandstone	1.0	0.9
Total	**112.4**	**100.0**

Drainage Class

	Area (km^2)	Percent
Well	112.4	100
Total	**112.4**	**100**

LSNAI

	Area (km^2)	Percent
Low	112.4	100
Total	**112.4**	**100**

Table H.35: Whangaehu at Kauangaroa

Rock types

	Area (km^2)	Percent
Mudstone	479.1	26.7
Sandstone	399.7	22.3
Volcanic ash over Volcanic deposits	281.9	15.7
Volcanic ash over Sandstone	197.9	11.0
Volcanic deposits over Volcanic ash	125.0	7.0
Volcanic ash	70.1	3.9
Alluvium	56.5	3.1
Unconsolidated sediments	50.4	2.8
Volcanic deposits	47.9	2.7
Volcanic ash over Mudstone	42.2	2.4
Volcanic deposits over Sandstone	21.5	1.2
Sandstone over Mudstone	6.6	0.4
Volcanic ash over Alluvium	5.0	0.3
Loess	4.6	0.3
Alluvium over Volcanic ash	3.6	0.2
Volcanic ash over Unconsolidated sediments	0.9	0.0
Total	**1792.9**	**100.0**

Drainage Class

	Area (km^2)	Percent
Moderately well	1089.6	60.8
Well	594.8	33.2
Imperfect	70.5	3.9
Poor	38.1	2.1
Total	**1792.9**	**100.0**

LSNAI

	Area (km^2)	Percent
High	35.8	2.0
Medium	1158.8	64.6
Low	598.4	33.4
Total	**1792.9**	**100.0**

Table H.36: Whanganui at Cherry Grove

Rock types

	Area (km^2)	Percent
Volcanic ash	246.3	28.3
Volcanic ash over Mudstone	167.8	19.3
Volcanic ash over Volcanic deposits	118.8	13.6
Volcanic ash over Sandstone	114.8	13.2
Volcanic deposits	101.3	11.6
Volcanic ash over Greywacke	53.0	6.1
Volcanic deposits over Volcanic ash	36.5	4.2
Greywacke	13.1	1.5
Sandstone	10.3	1.2
Alluvium	6.6	0.8
Mudstone	1.2	0.1
Peat over Volcanic deposits	0.7	0.1
Total	**870.4**	**100.0**

Drainage Class

	Area (km^2)	Percent
Well	852.7	98.0
Poor	15.4	1.8
Moderately well	2.3	0.3
Imperfect	0.0	0.0
Total	**870.4**	**100.0**

LSNAI

	Area (km^2)	Percent
High	15.4	1.8
Medium	2.3	0.3
Low	839.5	96.5
Very low	13.1	1.5
Total	**870.4**	**100.0**

Table H.37: Whanganui at Pipiriki

Rock types

	Area (km^2)	Percent
Sandstone	2126.6	36.2
Volcanic ash over Mudstone	834.5	14.2
Volcanic ash	602.9	10.3
Volcanic ash over Sandstone	597.4	10.2
Mudstone	563.2	9.6
Volcanic ash over Volcanic deposits	511.1	8.7
Volcanic deposits	268.4	4.6
Volcanic ash over Greywacke	185.0	3.1
Alluvium	102.8	1.8
Volcanic deposits over Volcanic ash	36.5	0.6
Greywacke	25.6	0.4
Volcanic ash over Alluvium	7.9	0.1
Volcanic deposits over Mudstone	4.0	0.1
Volcanic deposits over Sandstone	3.2	0.1
Sandstone over Mudstone	1.5	0.0
Peat over Volcanic deposits	0.7	0.0
Volcanic ash over Gravels	0.7	0.0
Total	**5871.9**	**100.0**

Drainage Class

	Area (km^2)	Percent
Well	5195.6	88.5
Moderately well	613.0	10.4
Poor	41.3	0.7
Imperfect	22.0	0.4
Total	**5871.9**	**100.0**

LSNAI

	Area (km^2)	Percent
High	39.0	0.7
Medium	635.0	10.8
Low	5172.2	88.1
Very low	25.6	0.4
Total	**5871.7**	**100.0**

Table H.38: Whanganui at Te Maire

Rock types

	Area (km^2)	Percent
Volcanic ash over Mudstone	451.9	21.6
Volcanic ash	434.8	20.7
Volcanic ash over Volcanic deposits	417.7	19.9
Volcanic ash over Sandstone	243.8	11.6
Volcanic deposits	204.3	9.7
Volcanic ash over Greywacke	185.0	8.8
Sandstone	69.0	3.3
Volcanic deposits over Volcanic ash	36.5	1.7
Greywacke	25.6	1.2
Mudstone	15.9	0.8
Alluvium	9.7	0.5
Volcanic ash over Alluvium	1.5	0.1
Peat over Volcanic deposits	0.7	0.0
Total	**2096.4**	**100.0**

Drainage Class

	Area (km^2)	Percent
Well	2073.0	98.9
Poor	15.4	0.7
Moderately well	8.0	0.4
Imperfect	0.0	0.0
Total	**2096.4**	**100.0**

LSNAI

	Area (km^2)	Percent
High	15.4	0.7
Medium	8.0	0.4
Low	2047.4	97.7
Very low	25.6	1.2
Total	**2096.3**	**100.0**

Table H.39: Whanganui at Te Rewa

Rock types

	Area (km^2)	Percent
Sandstone	2574.3	39.8
Volcanic ash over Mudstone	853.7	13.2
Mudstone	648.9	10.0
Volcanic ash over Sandstone	627.5	9.7
Volcanic ash	604.2	9.4
Volcanic ash over Volcanic deposits	511.1	7.9
Volcanic deposits	269.6	4.2
Volcanic ash over Greywacke	185.0	2.9
Alluvium	105.8	1.6
Volcanic deposits over Volcanic ash	36.5	0.6
Greywacke	25.6	0.4
Volcanic ash over Alluvium	7.9	0.1
Volcanic deposits over Mudstone	4.0	0.1
Volcanic deposits over Sandstone	3.2	0.0
Loess	1.7	0.0
Sandstone over Mudstone	1.5	0.0
Peat over Volcanic deposits	0.7	0.0
Volcanic ash over Gravels	0.7	0.0
Total	**6461.6**	**100.0**

Drainage Class

	Area (km^2)	Percent
Well	5504.7	85.2
Moderately well	888.9	13.8
Poor	45.9	0.7
Imperfect	22.0	0.3
Total	**6461.6**	**100.0**

LSNAI

	Area (km^2)	Percent
High	43.6	0.7
Medium	910.8	14.1
Low	5481.4	84.8
Very low	25.6	0.4
Total	**6461.3**	**100.0**

Table H.40: Whanganui at Wades Landing

Rock types

	Area (km^2)	Percent
Volcanic ash over Mudstone	752.5	20.5
Sandstone	595.6	16.2
Volcanic ash	471.0	12.8
Volcanic ash over Sandstone	459.1	12.5
Volcanic ash over Volcanic deposits	423.6	11.6
Mudstone	385.9	10.5
Volcanic deposits	249.4	6.8
Volcanic ash over Greywacke	185.0	5.0
Alluvium	70.1	1.9
Volcanic deposits over Volcanic ash	36.5	1.0
Greywacke	25.6	0.7
Volcanic ash over Alluvium	7.9	0.2
Volcanic deposits over Mudstone	4.0	0.1
Peat over Volcanic deposits	0.7	0.0
Sandstone over Mudstone	0.0	0.0
Total	**3666.8**	**100.0**

Drainage Class

	Area (km^2)	Percent
Well	3463.0	94.4
Moderately well	183.5	5.0
Poor	17.9	0.5
Imperfect	2.3	0.1
Total	**3666.8**	**100.0**

LSNAI

	Area (km^2)	Percent
High	17.9	0.5
Medium	185.8	5.1
Low	3437.4	93.7
Very low	25.6	0.7
Total	**3666.7**	**100.0**

Appendix I

Table I.1: Estimated instream *SIN* uptake (t yr^{-1}), estimated root zone *SIN* losses (t yr^{-1}) and the estimated instream uptake as a proportion of root zone losses for all monitoring sites.

Monitoring site	**Instream *SIN* uptake (t yr^{-1})**	**Root zone *SIN* losses (t yr^{-1})**	**Instream uptake as a % of root zone losses**
Kumeti at Te Rehunga	0.1	17.5	0.7
Mangatainoka at Larsons Road	0.8	59.8	1.3
Mangapapa at Troup Road	0.8	47.6	1.6
Oroua at Almadale Slackline	8.1	418.0	1.9
Raparapawai at Jackson Road	1.9	102.4	1.9
Ohau at Gladstone Reserve	1.2	55.1	2.2
Tokomaru River at Horseshoe bend	0.8	36.2	2.2
Mangahao at Ballance	7.1	241.8	2.9
Pohangina at Mais Reach	13.9	411.9	3.4
Rangitikei at Pukeokahu	39.8	504.0	7.9
Oroua at Awahuri Bridge	68.4	851.3	8.0
Mangawhero at Pakihi Rd Bridge	17.2	213.9	8.1
Ongarue at Taringamotu	113.8	1003.9	11.3
Mangawhero at Raupiu Road	92.5	814.6	11.4
Hautapu at US Rangitikei River Conf	30.3	237.9	12.7
Rangitikei at Mangaweka	196.6	1551.4	12.7
Mangatainoka at Brewery	130.1	997.8	13.0
Hautapu at Alabasters	22.2	161.8	13.7
Hautapu at Papakai Road Bridge	22.2	161.8	13.7
Whanganui at Te Maire	276.0	1854.8	14.9
Whangaehu at Kauangaroa	302.6	1920.9	15.8
Tokiahuru at Junction	16.5	103.0	16.0
Rangitikei at Onepuhi	338.5	2091.8	16.2
Rangitikei at McKelvies	496.3	2880.2	17.2
Whanganui at Cherry Grove	120.0	672.7	17.8
Whanganui at Wades Landing	646.8	3608.6	17.9
Ohura at Tokorima	150.0	779.4	19.2
Whakapapa at Footbridge	12.7	61.1	20.8
Manawatu at Hopelands	505.6	2229.6	22.7
Whanganui at Pipiriki	1191.8	4878.1	24.4
Owahanga at Branscombe Bridge	137.5	547.7	25.1
Manawatu at Opiki Bridge	1690.4	6519.9	25.9
Manawatu at Teachers College	1591.3	6137.6	25.9
Manawatu at Weber Road	287.2	1110.8	25.9
Whanganui at Te Rewa	1429.0	5370.5	26.6
Manawatu at Upper Gorge	1538.1	5386.7	28.6
Turakina at ONeills Bridge	261.4	841.4	31.1
Mangatoro at Mangahei Road	104.7	320.8	32.7
Makuri at Tuscan Hills	75.2	215.7	34.8
Tiraumea at Ngaturi	538.2	1033.6	52.1
Mean			**16.1**

Appendix J

Licencing and publishing agreements for:

- Chapter 3: publication
- Chapter 4: publication

Licence to Publish

SPRINGER NATURE

Licensee:	Springer Nature Switzerland AG	(the 'Licensee')
Journal Name:	Environmental Monitoring and Assessment	(the 'Journal')
Manuscript Number:	f07f1054-16f3-4d6f-8d93-00721f5e3a46	
Proposed Title of Article:	Assessment of spatial variability and temporal stability of groundwater redox conditions in New Zealand	(the 'Article')
Author(s) [Please list all named Authors]:	Stephen B. Collins, Ranvir Singh, Stuart R. Mead, David J. Horne, Jon K. F. Roygard	(the 'Author')
Corresponding Author Name:	Stephen B. Collins	

1 Grant of Rights

a) For good and valuable consideration, the Author hereby grants to the Licensee the perpetual, exclusive, world-wide, assignable, sublicensable and unlimited right to: publish, reproduce, copy, distribute, communicate, display publicly, sell, rent and/ or otherwise make available the article identified above, including any supplementary information and graphic elements therein (e.g. illustrations, charts, moving images) (the "Article") in any language, in any versions or editions in any and all forms and/or media of expression (including without limitation in connection with any and all end-user devices), whether now known or developed in the future. Without limitation, the above grant includes: (i) the right to edit, alter, adapt, adjust and prepare derivative works; (ii) all commercial use, advertising, and marketing rights, including without limitation graphic elements on the cover of the journal and in relation to social media; (iii) rights for any training, educational and/or instructional purposes; (iv) the right to add and/or remove links or combinations with other media/works; and (v) the right to create, use and/or license and/or sublicense content data or metadata of any kind in relation to the Article (including abstracts and summaries) without restriction. The above rights are granted in relation to the Article as a whole or any part and with or in relation to any other works.

b) Without limiting the rights granted above, Licensee is granted the rights to use the Article for the purposes of analysis, testing, and development of publishing- and research-related workflows, systems, products, projects, and services; to confidentially share the Article with select third parties to do the same; and to retain and store the Article and any associated correspondence/files/forms to maintain the historical record, and to facilitate research integrity investigations. The grant of rights set forth in this clause (b) is irrevocable.

c) The Licensee will have the right, but not the obligation, to exercise any or all of the rights granted herein. If the Licensee elects not to publish the Article for any reason, all publishing rights under this Agreement as set forth in clause 1.a) above will revert to the Author.

2 Copyright

Ownership of copyright in the Article will be vested in the name of the Author. When reproducing the Article or extracts from it, the Author will acknowledge and reference first publication in the Journal.

3 Use of Article Versions

a) For purposes of this Agreement: (i) references to the "Article" include all versions of the Article; (ii) "Submitted Manuscript" means the version of the Article as first submitted by the Author; (iii) "Accepted Manuscript" means the version of the Article accepted for publication, but prior to copy-editing and typesetting; and (iv) "Version of Record" means the version of the Article published by the Licensee, after copy-editing and typesetting. Rights to all versions of the Manuscript are granted on an exclusive basis, except for the Submitted Manuscript, to which rights are granted on a non-exclusive basis.

b) The Author may make the Submitted Manuscript available at any time and under any terms (including, but not limited to, under a CC BY licence), at the Author's discretion. Once the Article has been published, the Author will include an acknowledgement and provide a link to the Version of Record on the publisher's website: "This preprint has not undergone peer review (when applicable) or any post-submission improvements or corrections. The Version of Record of this article is published in [insert journal title], and is available online at https://doi.org/[insert DOI]".

c) The Licensee grants to the Author (i) the right to make the Accepted Manuscript available on their own personal, self-maintained website immediately on acceptance, (ii) the right to make the Accepted Manuscript available for public release on any of the following twelve (12) months after first publication (the "Embargo Period"): their employer's internal website; their institutional and/or funder repositories. Accepted Manuscripts may be deposited in such repositories immediately upon acceptance, provided they are not made publicly available until after the Embargo Period.

The rights granted to the Author with respect to the Accepted Manuscript are subject to the conditions that (i) the Accepted Manuscript is not enhanced or substantially reformatted by the Author or any third party, and (ii) the Author includes on the Accepted Manuscript an acknowledgement in the following form, together with a link to the published version on the publisher's website: "This version of the article has been accepted for publication, after peer review (when applicable) but is not the Version of Record and does not reflect post-acceptance improvements, or any corrections. The Version of Record is available online at: http://dx.doi.org/[insert DOI]. Use of this Accepted Version is subject to the publisher's Accepted Manuscript terms of use https://www.springernature.com/gp/open-research/policies/accepted-manuscript-terms". Under no circumstances may an Accepted Manuscript be shared or distributed under a Creative Commons or other form of open access licence.

d) The Licensee grants to the Author the following non-exclusive rights to the Version of Record, provided that, when reproducing the Version of Record or extracts from it, the Author acknowledges and references first publication in the Journal according to current citation standards. As a minimum, the acknowledgement must state: "First published in [Journal name, volume, page number, year] by Springer Nature".

i. to reuse graphic elements created by the Author and contained in the Article, in presentations and other works created by them;

ii. the Author and any academic institution where they work at the time may reproduce the Article for the purpose of course teaching (but not for inclusion in course pack material for onward sale by libraries and institutions);

iii. to reuse the Version of Record or any part in a thesis written by the same Author, and to make a copy of that thesis available in a repository of the Author(s)' awarding academic institution, or other repository required by the awarding academic institution. An acknowledgement should be included in the citation: "Reproduced with permission from Springer Nature"; and

iv. to reproduce, or to allow a third party to reproduce the Article, in whole or in part, in any other type of work (other than thesis) written by the Author for distribution by a publisher after an embargo period of 12 months.

For clarity, where any graphic element is used on the cover of the Journal all intellectual property rights in any compilation constituting the cover will be vested solely in the Licensee, and the Author is not entitled to make or authorise any other person to make use of any such compilation without the prior written consent of the Licensee.

4 Warranties & Representations

Author warrants and represents that:

a)

i. the Author is the sole copyright owner or has been authorised by any additional copyright owner(s) to grant the rights defined in clause 1,

ii. the Article does not infringe any intellectual property rights (including without limitation copyright, database rights or trade mark rights) or other third party rights and no licence from or payments to a third party are required to publish the Article,

iii. the Article has not been previously published or licensed, nor has the Author committed to licensing any version of the Article under a licence inconsistent with the terms of this Agreement,

iv. if the Article contains materials from other sources (e.g. illustrations, tables, text quotations), Author has obtained written permissions to the extent necessary from the copyright holder(s), to license to the Licensee the same rights as set out in clause 1 but on a non-exclusive basis and without the right to use any graphic elements on a stand-alone basis and has cited any such materials correctly;

b) all of the facts contained in the Article are according to the current body of research true and accurate;

c) nothing in the Article is obscene, defamatory, violates any right of privacy or publicity, infringes any other human, personal or other rights of any person or entity or is otherwise unlawful and that informed consent to publish has been obtained for any research participants;

d) nothing in the Article infringes any duty of confidentiality owed to any third party or violates any contract, express or implied, of the Author;

e) all institutional, governmental, and/or other approvals which may be required in connection with the research reflected in the Article have been obtained and continue in effect;

f) all statements and declarations made by the Author in connection with the Article are true and correct; and

g) the signatory who has signed this agreement has full right, power and authority to enter into this agreement on behalf of all of the Authors.

5 Cooperation

a) The Author will cooperate fully with the Licensee in relation to any legal action that might arise from the publication of the Article, and the Author will give the Licensee access at reasonable times to any relevant accounts, documents and records within the power or control of the Author. The Author agrees that any Licensee affiliate through which the Licensee exercises any rights or performs any obligations under this Agreement is intended to have the benefit of and will have the right to enforce the terms of this Agreement.

b) Author authorises the Licensee to take such steps as it considers necessary at its own expense in the Author’s name(s) and on their behalf if the Licensee believes that a third party is infringing or is likely to infringe copyright in the Article including but not limited to initiating legal proceedings.

6 Author List

Changes of authorship, including, but not limited to, changes in the corresponding author or the sequence of authors, are not permitted after acceptance of a manuscript.

7 Post Publication Actions

The Author agrees that the Licensee may remove or retract the Article or publish a correction or other notice in relation to the Article if the Licensee determines that such actions are appropriate from an editorial, research integrity, or legal perspective.

8 Controlling Terms

The terms of this Agreement will supersede any other terms that the Author or any third party may assert apply to any version of the Article.

9 Governing Law

This Agreement will be governed by, and construed in accordance with, the laws of Switzerland. The courts of Zug, Switzerland will have exclusive jurisdiction.

Signed for and on behalf of the Author(s)
Corresponding Author: Stephen B. Collins
Email: s.collins1@massey.ac.nz
IP Address: 150.107.172.248

Time Stamp: 2024-11-25 11:54:14

Springer Nature Switzerland AG, Gewerbestrasse 11, 6330 Cham, Switzerland
v.4.0.8 - (08_2024)-SNS AG

ELSEVIER

Publishing Agreement

Elsevier Ltd

Modelling and Mapping of Subsurface Nitrate-Attenuation Index in Agricultural Landscapes

Corresponding author	Mr Stephen B. Collins
E-mail address	s.collins1@massey.ac.nz

Journal	Journal of Environmental Management
Article number	125628
Our reference	YJEMA_125628
PII	S0301-4797(25)01604-4

Your Status

- I am one author signing on behalf of all co-authors of the manuscript and I am duly authorized to do so by all co-authors of the manuscript

The License Agreement

The authors have created the article identified above which, together with any tables, illustrations or other material submitted for publication as part of the article, is referred to in this License Agreement as the "Article". The authors wish Elsevier Ltd to publish and distribute the Article and to protect the rights granted under this License Agreement. To enable Elsevier Ltd to do so, each author grants Elsevier Ltd the rights set out in this License Agreement.

Copyright ownership of the Article

Each author retains their copyright in the Article. Except for the license of the Article as set out below, this License Agreement does not transfer any rights in patents, trademarks or other intellectual property rights to Elsevier Ltd. Elsevier Ltd shall publish and distribute the Article with an appropriate copyright notice.

Authors' rights in the Article

Each author retains the right to re-use the Article for their own commercial and non-commercial purposes, as well as to create derivative works, without permission from Elsevier Ltd or payment to Elsevier Ltd. Each author shall, in connection with any such re-use of the Article, fully acknowledge and attribute the original publication of the Article.

Nothing in this License Agreement shall limit the re-use rights of authors.

By way of illustrative examples of re-use, each author retains the right to:

- make copies of the Article (or part of the Article) to promote companies or products they own, whether or not such promotion is commercial;
- include the Article in a thesis or dissertation;
- extend the Article to a book, include the Article in a subsequent compilation of their own work, or re-use portions, excerpts, and their own figures, tables and images from the Article in their own new works (which in each case may be published with Elsevier or with a third party commercial or non-commercial publisher, at the author's discretion);
- use and share the Article for scholarly purposes, including for classroom teaching, in conferences, and for Massive Open Online Courses;
- create translations of the Article and authorize others to do so for scholarly collaborations and sharing;
- publicly share the Article on commercial or non-commercial websites, such as institutional repositories; and
- post the Article on commercial scholarly collaboration websites for any purpose.

Each author acknowledges the importance of the integrity, authenticity and permanence of the scholarly record and agrees that the version of the Article that appears or will appear in the journal and embodies all value-adding publisher activities (including duplicate publication of the Article in violation of publishing ethics principles, as further described below.

Author’s grant of rights in the Article

Each author hereby grants to Elsevier Ltd the following rights, effective from the date on which the Article is accepted for publication:

a. the non-exclusive right to publish, reproduce, display, distribute and otherwise use the Article, or any part of the Article, for any purpose, in print, electronic and all other media (whether now known or later developed), and to prepare derivative works, in any form, in all languages, throughout the world, for the full term of copyright;
b. the non-exclusive right to license third parties to exercise all or any of the rights granted herein for commercial or non-commercial purposes; and
c. the right to enforce the rights granted herein against third parties.

In addition, each author has selected the Creative Commons Attribution Works 4.0 International License (“the CC BY License”) and grants Elsevier Ltd the right to apply the CC BY License to the Article where the Article is published in the journal on Elsevier Ltd’s and/or the publisher’s online platforms on an Open Access basis. Full details of the CC BY License are available at https://creativecommons.org/licenses/by/4.0/.

Supplemental Materials and Research Data

“Supplemental Materials” shall mean materials published as a supplemental part of the Article, including but not limited to graphical, illustrative, video and audio material.

“Research Data” shall mean the result of observations or experimentation that validate research findings and that are published separate to the Article, which can include but are not limited to raw data, processed data, software, algorithms, protocols and methods.

With respect to any Supplemental Materials and/or Research Data that an author submits, that author retains all rights in such Supplemental Materials and/or Research Data and hereby grants Elsevier Ltd a perpetual worldwide, non-exclusive right and license to publish, extract, reformat, adapt, build upon, index, redistribute, link to and otherwise use all or any part of the Supplemental Materials and/or Research Data in all forms and media (whether now known or later developed), and permit others to do so.

Where Elsevier Ltd and/or the publisher publish the Article on their online platforms on an Open Access basis and publish the Supplemental Materials with the Article, Elsevier Ltd and/or the publisher shall apply the same end user license to the Supplemental Materials as to the Article. Where an author has selected a specific end user license under which the Research Data is to be made available on a site or through a service, Elsevier Ltd and/or the publisher shall apply that end user license to the Research Data on that site or service.

Reversion of rights

Articles may sometimes be accepted for publication but later rejected in the publication process, even in some cases after public posting in “Articles in Press” form, in which case all rights granted to Elsevier Ltd under this License Agreement will revert to the author (see https://www.elsevier.com/about/policies-and-standards/article-withdrawal).

Revisions and addenda

This License Agreement may not be varied unless such variation is in writing and signed by Elsevier Ltd and the corresponding author. This License Agreement supersedes any previous agreements entered into between each author and Elsevier Ltd in relation to the Article from the date hereof.

Author Representations/Ethics and Disclosure

Each author affirms the Author Representations noted below and confirm that they have reviewed and complied with the relevant Instructions to Authors, Ethics in Publishing policy, Declarations of Interest disclosure, and information for authors from countries affected by sanctions. Please note that some journals may require that all co-authors sign and submit Declarations of Interest disclosure forms. Each author is also aware of Elsevier Ltd’s and/or the publisher’s policies with respect to retractions and withdrawal (https://www.elsevier.com/about/policies-and-standards/article-withdrawal). For further information see the publishing ethics page at http://www.elsevier.com/publishingethics and the journal home page. For further information on sanctions, see: https://www.elsevier.com/about/policies-and-standards/trade-sanctions.

Author Representations

- The Article submitted to the journal for review is original, has been written by the stated authors and has not been previously published.

- The Article was not submitted for review to another journal while under review by this journal and will not be submitted to any other journal.
- The Article, the Supplemental Materials and the Research Data do not infringe any copyright, violate any other intellectual property, privacy or other rights of any person or entity, or contain any libelous or other unlawful matter.
- All necessary written permissions have been obtained from the copyright owners of any excerpts from copyrighted works that are included in the Article, the Supplemental Materials, and/or the Research Data, and all such third parties have been correctly and appropriately credited.
- Except as expressly set out in this License Agreement, the stated author(s) are the legal and beneficial owners of the rights granted herein and the Article is not subject to any prior rights or licenses.
- Each author confirms that they are not identified as a Specially Designated National ("SDN") and if any of the authors reside in Russia, Belarus, Iran, Cuba or Syria the Article has been prepared in a personal, academic or research capacity and not as an official representative or otherwise on behalf of the relevant government or institution.
- If any personal details or images of patients, research subjects or other individuals have been used, all written and fully informed consents required by applicable law have been obtained and evidence of such consents has been retained, and the authors have complied with Elsevier Ltd's and/or the publisher's policies relating to the use of such materials. See https://www.elsevier.com/about/policies-and-standards/patient-consent for further information.
- Any software contained in the Supplemental Materials is free from viruses, contaminants and worms.

Corresponding Author's Representation

If the Article or any of the Supplemental Materials were prepared jointly with other authors, I (as corresponding author) have informed all co-author(s) of the terms of this License Agreement and have duly obtained their authorization to sign this License Agreement as their agent.

Governing Law and Jurisdiction

This License Agreement will be governed by and construed in accordance with the laws of the country or state in which Elsevier Ltd is incorporated ("the Governing State"), without regard to conflict of law principles, and the parties irrevocably consent to the exclusive jurisdiction of the courts of the Governing State.

☑ **I have read and agree to the terms of the License Agreement.**

Appendix K

Statements of Contribution

MASSEY UNIVERSITY
TE KUNENGA KI PŪREHUROA
UNIVERSITY OF NEW ZEALAND

GRADUATE RESEARCH SCHOOL

STATEMENT OF CONTRIBUTION
DOCTORATE WITH PUBLICATIONS/MANUSCRIPTS

We, the student and the student's main supervisor, certify that all co-authors have consented to their work being included in the thesis and they have accepted the student's contribution as indicated below in the Statement of Originality.

Student name:	Stephen Collins
Name and title of main supervisor:	Professor Ranvir Singh
In which chapter is the manuscript/published work?	Chapter 3

Describe the contribution that the student and members of the supervisory team have made to the manuscript/published work:[1]

Stephen B. Collins: Conceptualisation, Methodology, Formal analysis, Data curation, Writing – Original draft, Visualisation; Ranvir Singh: Conceptualisation, Methodology, Writing – Review & editing, Supervision; Stuart R. Mead: Methodology, Validation; David J. Horne: Conceptualisation, Writing – Review & editing; Jon K. F. Roygard: Conceptualisation.

Please select one of the following three options:

(●) **The manuscript/published work is published or in press**

Please provide the full reference of the research output:
Collins, S.B., Singh, R., Mead, S.R., Horne, D.J., Roygard, J.K.F., 2025. Assessment of spatial variability and temporal stability of groundwater redox conditions in New Zealand. Environ. Monit. Assess. 197, 58. https://doi.org/10.1007/s10661-024-13427-y

( ) **The manuscript is currently under review for publication**

Please provide the name of the journal:

( ) **It is intended that the manuscript will be published, but it has not yet been submitted to a journal**

Student's signature:	Stephen Collins — Digitally signed by Stephen Collins Date: 2025.10.08 10:00:28 +13'00'	Main supervisor's signature:	Ranvir Singh — Digitally signed by Ranvir Singh DN: cn=Ranvir Singh, c=NZ, email=r.singh.ranvir@gmail.com Date: 2025.10.08 11:00:10 +13'00'

This form should be placed at the beginning of each relevant thesis chapter.

[1] Refer to the Massey University Publishing and Authorship guidelines (OneMassey for staff, Stream for students) and/ or Contributor Roles Taxonomy (CRediT) guidelines for guidance.

MASSEY UNIVERSITY
TE KUNENGA KI PŪREHUROA
UNIVERSITY OF NEW ZEALAND

GRADUATE RESEARCH SCHOOL

STATEMENT OF CONTRIBUTION
DOCTORATE WITH PUBLICATIONS/MANUSCRIPTS

We, the student and the student's main supervisor, certify that all co-authors have consented to their work being included in the thesis and they have accepted the student's contribution as indicated below in the Statement of Originality.			
Student name:	Stephen Collins		
Name and title of main supervisor:	Professor Ranvir Singh		
In which chapter is the manuscript/published work?		Chapter 4	
Describe the contribution that the student and members of the supervisory team have made to the manuscript/published work:[1] Stephen B. Collins: Writing – original draft, Visualization, Methodology, Formal analysis, Data curation, Conceptualization. Ranvir Singh: Writing – review & editing, Supervision, Methodology, Conceptualization. Stuart R. Mead: Validation, Methodology, Supervision. David J. Horne: Writing – review & editing, Conceptualization, Supervision.			
Please select one of the following three options:			
◉	**The manuscript/published work is published or in press** Please provide the full reference of the research output: Collins, S.B., Singh, R., Mead, S.R., Horne, D.J., 2025. Modelling and mapping of subsurface nitrate-attenuation index in agricultural landscapes. J. Environ. Manage. 384, 125628. https://doi.org/10.1016/j.jenvman.2025.125628		
○	**The manuscript is currently under review for publication** Please provide the name of the journal:		
○	**It is intended that the manuscript will be published, but it has not yet been submitted to a journal**		
Student's signature:	Stephen Collins — Digitally signed by Stephen Collins Date: 2025.10.08 10:04:43 +13'00'	Main supervisor's signature:	Ranvir Singh — Digitally signed by Ranvir Singh DN: cn=Ranvir Singh, c=NZ, email=r.singh.ranvir@gmail.com Date: 2025.10.08 11:02:16 +13'00'
This form should be placed at the beginning of each relevant thesis chapter.			

[1] Refer to the Massey University Publishing and Authorship guidelines (OneMassey for staff, Stream for students) and/ or Contributor Roles Taxonomy (CRediT) guidelines for guidance.

MASSEY UNIVERSITY
TE KUNENGA KI PŪREHUROA
UNIVERSITY OF NEW ZEALAND

GRADUATE RESEARCH SCHOOL

STATEMENT OF CONTRIBUTION DOCTORATE WITH PUBLICATIONS/MANUSCRIPTS

We, the student and the student's main supervisor, certify that all co-authors have consented to their work being included in the thesis and they have accepted the student's contribution as indicated below in the Statement of Originality.

Student name:	Stephen Collins
Name and title of main supervisor:	Professor Ranvir Singh
In which chapter is the manuscript/published work?	Chapter 6

Describe the contribution that the student and members of the supervisory team have made to the manuscript/published work:[1]

Stephen B. Collins: Writing – original draft, Visualization, Methodology, Formal analysis, Data curation, Conceptualization. Ranvir Singh: Writing – review & editing, Supervision, Methodology, Conceptualization. Stuart R. Mead: Methodology, Supervision. David J. Horne: Writing – review & editing, Conceptualization, Supervision.

Please select one of the following three options:

○ **The manuscript/published work is published or in press**

Please provide the full reference of the research output:

○ **The manuscript is currently under review for publication**

Please provide the name of the journal:

◉ **It is intended that the manuscript will be published, but it has not yet been submitted to a journal**

Student's signature:	Stephen Collins Digitally signed by Stephen Collins Date: 2025.10.08 10:07:15 +13'00'	Main supervisor's signature:	Ranvir Singh Digitally signed by Ranvir Singh DN: cn=Ranvir Singh, c=NZ, email=r.singh.ranvir@gmail.com Date: 2025.10.08 11:01:29 +13'00'

This form should be placed at the beginning of each relevant thesis chapter.

[1] Refer to the Massey University Publishing and Authorship guidelines (OneMassey for staff, Stream for students) and/ or Contributor Roles Taxonomy (CRediT) guidelines for guidance.